

ORGANIC AEROSOL COMPOSITION IN THE SOUTHEASTERN UNITED STATES AND THE ROLE OF LOW-MOLECULAR-WEIGHT ORGANIC ACIDS

A Dissertation
Presented to
The Academic Faculty

by

Yunle Chen

In Partial Fulfillment
of the Requirements for the Degree
Doctorate of Philosophy in the
School of Earth and Atmospheric Sciences

Georgia Institute of Technology
August 2020

COPYRIGHT © 2020 BY YUNLE CHEN

ORGANIC AEROSOL COMPOSITION IN THE SOUTHEASTERN UNITED STATES AND THE ROLE OF LOW-MOLECULAR-WEIGHT ORGANIC ACIDS

Approved by:

Dr. Nga L. Ng, Advisor
School of Chemical and Biomolecular
Engineering, School of Earth and
Atmospheric Sciences, and School of Civil
and Environmental Engineering
Georgia Institute of Technology

Dr. Rodney J. Weber
School of Earth and
Atmospheric Sciences
Georgia Institute of Technology

Dr. L. Greg Huey
School of Earth and
Atmospheric Sciences
Georgia Institute of Technology

Dr. Armistead G. Russell
School of Civil and Environmental
Engineering
Georgia Institute of Technology

Dr. Pengfei Liu
School of Earth and
Atmospheric Science
Georgia Institute of Technology

Date Approved: July 10, 2020

In Loving Memory of

Yongxian Zhong

ACKNOWLEDGEMENTS

First I would like to express my sincere gratitude to my advisor, Dr. Sally Ng, for her tremendous support through my doctoral study. She introduced me to the world of atmospheric science, trained me to be a good researcher, and taught me how to enjoy every challenge. I would especially thank her for having great confidence in me in the moments I myself fail to do so. Her passion and perseverance will always inspire me.

It has been an honor and pleasure to work with Dr. Rodney Weber, Dr. Greg Huey, Dr. Ted Russell, and David Tanner. I am truly thankful for their always prompt response, generous help, and unreserved guidance. Their expertise and insights not only enriched my research, but also broadened my horizons of other interesting fields in atmospheric science. I am also thankful to Dr. Pengfei Liu for being on my dissertation committee.

I have been fortunate to have many excellent colleagues. Special acknowledgements to Dr. Lu Xu for being a wonderful mentor, and to Dr. Gamze Eris, Taekyu Joo, Masayuki Takeuchi, and Dr. Wing-Yin Tuet for being great lab mates and friends. I am also grateful to other Ng group members and collaborators: Dr. Chris Boyd, Javier Sanchez, Dr. Hongyu Guo, Dr. Thomas Berkemeier, Dr. Fobang Liu, Gabriela Saavedra, Dr. Jean Rivera Rios, Dr. Yuchen Wang, Dr. Weiqi Xu, Dr. Dao Huang, Dr. Theodora Nah, Dr. Sandra Blair, Athena Xu, Sabrina Westgate, James Rowe, Laura Yang, Yi Ji, Ziqi Gao, Dr. Ting Fang, Dr. Qian Zhang, Dr. Dong Gao, Justin Min, and Linghan Zeng. I will always remember our time together with fondness.

Finally I would like to thank my family and friends for their company. All these would not be possible without their unvarying love, trust, and support.

TABLE OF CONTENTS

ACKNOWLEDGEMENTS	iv
LIST OF TABLES	ix
LIST OF FIGURES	x
LIST OF SYMBOLS AND ABBREVIATIONS	xvi
SUMMARY	xx
CHAPTER 1. Introduction	1
1.1 Atmospheric Organic Aerosols	1
1.1.1 Why Study Organic Aerosols	1
1.1.2 Source Apportionment for Organic Aerosols	2
1.2 Atmospheric Organic Acids	3
1.2.1 Organic Acids as Gases and in Aerosols	3
1.2.2 Secondary Production of Organic Acids	4
1.2.3 Importance of Organic Acids in a Changing Climate	5
1.3 Thesis Overview	5
CHAPTER 2. Chemical Characterization of Secondary Organic Aerosol at a Rural Site in the Southeastern U. S.: Insights from Simultaneous HR-ToF-AMS and FIGAERO-CIMS Measurements	7
2.1 Background	7
2.2 Methods	10
2.2.1 Site Description	10
2.2.2 Instrumentation	10
2.2.3 Source Apportionment Methods	13
2.2.4 Estimating Mass Concentration of Organic Nitrate Functionality from AMS Measurements	14
2.3 Results and Discussion	15
2.3.1 Campaign Overview and OA Bulk Properties	15
2.3.2 Overview of Organic Compounds Detected by FIGAERO-CIMS	16
2.3.3 AMS OA Factors	19
2.3.4 FIGAERO-CIMS OA Factors	21
2.3.5 Tracer Species Detected by FIGAERO-CIMS and Their Implications	29
2.3.6 Correlations between AMS OA Factors and FIGAERO-CIMS OA Factors	30
2.3.7 Change of the Abundance of Biogenic VOC and AMS OA Factors in a Transitional Period	32
2.4 Conclusions	34
CHAPTER 3. Low-Molecular-Weight Organic Acids in the Southeastern U. S.: Formation, Partitioning, and Implications for Organic Aerosol Aging	55
3.1 Background	55

3.2	Methods	57
3.2.1	Site Description	57
3.2.2	Instrumentation	58
3.2.3	OA Source Apportionment Analysis	59
3.2.4	Liquid Water Content (LWC) and pH Calculation	59
3.3	Results and Discussion	60
3.3.1	Overview of LMWOA Measured at Yorkville	60
3.3.2	Possible Secondary Formation Mechanisms of Different LMWOA	61
3.3.3	Unexpectedly High Particle-Phase Fraction of LMW Monocarboxylic Acids and Possible Explanations	67
3.3.4	Links between Particulate LMWOA and MO-OOA	69
3.4	Conclusions	73
CHAPTER 4. Low-Molecular-Weight Organic Acids Production in BVOC Photooxidation under ambient relevant conditions		91
4.1	Background	91
4.2	Methods	92
4.2.1	Chamber Experiments	92
4.2.2	Instrumentation	93
4.2.3	Measurements of FA and AA	94
4.3	Results and Discussion	94
4.3.1	FA and AA Production in “Clean” Chamber	94
4.3.2	FA and AA Production in BVOC Photooxidation Experiments	95
4.3.3	Potential Mechanism of FA and AA Formation Enhanced by Water	96
4.4	Conclusions	98
CHAPTER 5. Summary and Future Works		106
5.1	Summary	106
5.2	Future Works	107
5.2.1	OA Characterization Aided by Instrument Improvements	107
5.2.2	Sources of Aged SOA	108
5.2.3	Conducting Laboratory Experiments under Ambient-Relevant Conditions	108
APPENDIX A. Response of the Aerodyne Aerosol Mass Spectrometer to Inorganic Sulfates and Organosulfur Compounds: Applications in Field and Laboratory Measurements		110
A.1	Background	110
A.2	Methods	112
A.2.1	Laboratory Characterization of Standard Compounds	112
A.2.2	Characterization of Chamber-Generated Biogenic SOA and Ambient OA	114
A.2.3	Sulfate Apportionment Method	116
A.3	Results and Discussion	124
A.3.1	Sulfate Apportionment for Laboratory-Generated Binary Mixtures	124
A.3.2	Effect of Particle Acidity on AS Fragmentation Pattern	125
A.3.3	Sulfate Apportionment for Chamber-Generated Isoprene SOA	127
A.3.4	Application to Field Measurements for OS Estimation	128
A.3.5	Application to Field Measurements for MSA Estimation	130

A.4	Conclusions	132
	REFERENCES	152

LIST OF TABLES

Table 2-1	Effective Molecular Composition of FIGAERO Factors.	36
Table 3-1	Campaign-average concentrations of LMWOA.	75
Table 3-2	Correlation coefficients (Pearson's R^2) of both-phase formic, acetic, oxalic, malonic, succinic acids and selected tracer species. LMWOA are in the unit of $\mu\text{g m}^{-3}$, and tracer species are in the unit of Hz.	76
Table 3-3	Correlation coefficients (Pearson's R^2) of particulate LMWOA (by PILS-IC) and OA factors (by AMS). All concentrations are particle-phase measurements in the unit of $\mu\text{g m}^{-3}$.	77
Table 4-1	Summary of experimental conditions.	100
Table A-1	Standard Compounds.	134
Table A-2	Sulfate Fragmentation Table.	136
Table A-3	Normalized Sulfate Fragments for Pure Compounds from GT AMS.	137

LIST OF FIGURES

Figure 2-1	Correlation between FIGAERO total OA signals and AMS total OA mass concentration.	37
Figure 2-2	Study mean diurnal trends of elemental ratios measured by AMS (red) and FIGAERO-CIMS (blue). The AMS O:C and N:C with and without including $\text{NO}_{3,\text{org}}$ are in shaded area (with $\text{NO}^+/\text{NO}_2^+$ ratio of 5 and 10) and in dashed line, respectively.	38
Figure 2-3	Study mean (a) FIGAERO mass spectra, (b) fraction of pOC and pON compounds plotted as a function of time of a day, (c) and (d) fraction of ions of different carbon numbers (grouped as C_{1-5} , C_{6-10} , C_{11-15} , and $\text{C}_{>15}$) in pOC and pON, and (e) and (f) fraction of C_{1-5} , C_{6-10} , C_{11-15} , and $\text{C}_{>15}$ compounds in pOC and pON plotted as a function of time of day.	39
Figure 2-4	Normalized mass spectra of pOC ions measured by FIGAERO-CIMS, grouped by carbon atom number.	40
Figure 2-5	Normalized mass spectra of pON ions measured by FIGAERO-CIMS, grouped by carbon atom number.	41
Figure 2-6	(a) Time series, (b) mass fraction, (c) normalized mass spectra, and (d) diurnal profiles of AMS OA factors resolved by PMF.	42
Figure 2-7	(a) comparison of Isoprene-OA profile resolved by PMF and ME-2 (a-value 0), (b) average mass concentration for the three factors for the model runs, and (c) correlations R (Pearson) between the time series of selected factors and the time series of external data as a function of the model runs.	43
Figure 2-8	(a) Time Series, and study mean (b) mass fraction, (c) normalized mass spectra, and (d) diurnal profiles (standard deviations in shaded areas) of AMS OA factors resolved by ME-2.	44
Figure 2-9	Time series (daily averaged) of the mass fraction of Isoprene-OA in total OA (fIsoprene-OA) and temperature. Time series (daily averaged) of the mass fraction of Isoprene-OA in total OA (fIsoprene-OA) and temperature.	45
Figure 2-10	Diagnostic plots of PMF analysis on FIGAERO-CIMS measurements.	46

Figure 2-11	Scatter plots of pairs of highly-correlated ions, error bars representing estimated errors by simple Poisson statistics (left column) and after scaling by a factor of 10 (right column).	47
Figure 2-12	Diagnostic plots of PMF analysis on FIGAERO-CIMS measurements. Note that the input errors estimated from Poisson estimates were increased by a factor of 10 when performing PMF analysis.	48
Figure 2-13	(a) Time series, and study mean (b) fraction, (c) normalized mass spectra, and (d) diurnal profiles (standard deviations in shaded areas) of FIGAERO OA factors resolved by PMF.	49
Figure 2-14	Fraction of pOC and pON ions of different carbon numbers (grouped as C ₁₋₅ , C ₆₋₁₀ , C ₁₁₋₁₅ , and C _{>15}) in each FIGAERO OA factor.	50
Figure 2-15	Thermograms of (a) C ₅ H ₉ NO ₇ , (b) C ₃ H ₄ O ₅ , and (c) C ₃ H ₄ O ₄ ions measured by FIGAERO-CIMS.	51
Figure 2-16	Diurnal data of selected tracer species for isoprene and monoterpene SOA. (a) C ₅ H ₉ NO ₇ (isoprene+NO ₃ ·, isoprene+OH·+NO _x); (b) C ₅ H ₁₂ O ₄ (isoprene+OH·, IEPOX uptake); (c) C ₅ H ₁₀ O ₅ (isoprene+OH·, non-IEPOX pathway); (d) C ₁₀ H ₁₅ NO ₈ (α-/β-pinene+NO ₃ ·, α-/β-pinene+OH·+NO _x); (e) C ₉ H ₁₄ O ₄ (fresh monoterpene SOA); (f) C ₈ H ₁₂ O ₆ (aged monoterpene SOA).	52
Figure 2-17	Comparison between AMS daytime factors and FIGAERO-CIMS daytime factors ((a), (b)), and AMS nighttime factor and FIGAERO-CIMS nighttime factor ((c), (d)).	53
Figure 2-18	Main biogenic VOC and AMS factor concentrations as a function of temperature. The data points are grouped in temperature bins of 2 °C increment and colored by time of day, where afternoon (12:00 – 16:00) measurements are in red and night (00:00 – 04:00) measurements are in black. The mid-point line, lower and upper boxes, lower and upper whiskers, represent median, 25th percentiles, 75th percentiles, 10th percentiles, and 90th percentiles, respectively.	54
Figure 3-1	(a) Time series of and (b) correlations between aerosol water content associated with organics (W _o) and inorganics (W _i).	78

Figure 3-2	(a) Particle-phase concentrations, (b) gas-phase concentrations, and (c) both-phase concentrations of formic, acetic, oxalic, malonic, and succinic acids.	79
Figure 3-3	Diurnal profiles of (a) formic acid, (b) acetic acid, (c) oxalic acid, (d) malonic acid, and (e) succinic acid in the gas, particle, and both phases.	80
Figure 3-4	Diurnal profiles of temperature, O _x mixing ratio, solar radiation, inorganic water content, relative humidity, and aerosol pH.	81
Figure 3-5	Diurnal profiles of (a) gas-, particle-, and both-phase formic-to-acetic (FA / AA) ratio, and (b) both-phase fraction of dicarboxylic acids in total LMWOA.	82
Figure 3-6	The both-phase concentrations of formic, acetic, LMW dicarboxylic acids (oxalic + malonic + succinic), and fraction of LMW dicarboxylic acids in total LMWOA plotted against odd oxygen, LWC, and LWC fraction ($f(\text{LWC}) = \text{LWC} / (\text{LWC} + \text{OA} + \text{sulfate} + \text{ammonium} + \text{nitrate})$), respectively. Data points are colored by sunlight intensity to distinguish day and night. The mid-point line, lower and upper boxes, lower and upper whiskers, represent median, 25th percentiles, 75th percentiles, 10th percentiles, and 90th percentiles, respectively.	83
Figure 3-7	The both-phase fraction of LMW dicarboxylic acids as a function of isoprene mixing ratio. Data points are colored by inorganic water fraction.	84
Figure 3-8	Analytically calculated S curves and ambient data plotted against ISORROPIA-predicted particle pH of (a) formic acid and (c) acetic acid (adapted from Nah, et al. ³⁰); ambient (b) $\varepsilon(\text{HCOO}^-)$ and (d) $\varepsilon(\text{CH}_3\text{COO}^-)$ plotted against their corresponding both-phase concentrations. Data points in (a) and (c) are colored by the corresponding both-phase concentrations, in (b) and (d) are colored by isoprene mixing ratio. The black line is the S curve calculated using the selected time period's average temperature (23.4 ± 4.0 °C) and W_i (1.6 ± 1.7 $\mu\text{g m}^{-3}$). The grey lines are S curves calculated using 1 standard deviation from the average temperature and W_i (i.e., temperature = 27.4 °C and $W_i = 0.5$ $\mu\text{g m}^{-3}$ for dotted grey line; temperature = 19.4 °C and $W_i = 3.3$ $\mu\text{g m}^{-3}$ for solid grey line).	85
Figure 3-9	Analytically calculated S curves and ambient data plotted against ISORROPIA-predicted particle pH of oxalic acid (adapted from Nah et al. (2018a)). Data points were colored by the both-phase oxalic acid concentration. The black line is the S	86

curve calculated using the selected time period's average temperature (23.4 ± 4.0 °C) and W_i (1.6 ± 1.7 $\mu\text{g m}^{-3}$). The grey lines are S curves calculated using 1 standard deviation from the average temperature and W_i (i.e., temperature = 27.4 °C and $W_i = 0.5$ $\mu\text{g m}^{-3}$ for dotted grey line; temperature = 19.4 °C and $W_i = 3.3$ $\mu\text{g m}^{-3}$ for solid grey line).

Figure 3-10	The particle-phase fraction of LMW monocarboxylic acids (formic + acetic, in the form of formate and acetate, respectively) in total LMWOA plotted against isoprene mixing ratio. Data points are colored by NVC / LMWOA charge ratio.	87
Figure 3-11	(a) Time series and (b) correlations of AMS MO-OOA factor and PILS-IC total particulate LMWOA.	88
Figure 3-12	BL MO-OOA concentration as a function of BL height.	89
Figure 3-13	Diurnal profiles of (a) observed and modeled BL MO-OOA concentration; (b) simulated contributions from different processes to the total mass of MO-OOA in the boundary layer.	90
Figure 4-1	FA and AA time series in photooxidation experiments in humidified “clean” chamber.	101
Figure 4-2	Summary of formic and acetic acid molar yields under different conditions.	102
Figure 4-3	Time Series of (a) FA, (b) AA, and tracer compounds: (c) CH_4O_3 (g), (d) gaseous $\text{C}_5\text{H}_8\text{O}_4$, (e) $\text{C}_5\text{H}_{12}\text{O}_4$ (p), and (f) $\text{C}_5\text{H}_{12}\text{O}_6$ (p) in isoprene photooxidation experiments. The yellow shade indicates UV lights were on, while grey shade indicates UV lights were off. Note that $\text{C}_5\text{H}_{12}\text{O}_4$ (p) and $\text{C}_5\text{H}_{12}\text{O}_6$ (p) signals in experiment with MSSA seed (yellow) were scaled by a factor of 1/10.	103
Figure 4-4	Time Series of (a) FA, (b) AA, and tracer compound (c) $\text{C}_{10}\text{H}_{18}\text{O}_3$ (g) in α -pinene photooxidation experiments, and (d) difference between normalized particle mass spectra 50% RH, WAS experiment and 50% RH, DAS experiment. In (a)(b)(c), the yellow shade indicates UV lights were on in all experiments, and blue shade indicates that UV lights were off in three humid experiments but still on in the dry experiment, while grey shade indicates UV lights were off in the dry experiment. In (d), positive values mean ions have a higher abundance in 50% RH WAS experiment, while negative values mean ions have a higher abundance in 50% RH DAS experiment.	105

Figure A-1	Fractions of organosulfur fragments produced by standard organosulfur compounds in the AMS as a function of the molecular weight of carbon backbones. The data points are colored by their carbon backbone structures and bonding types.	138
Figure A-2	Peak fit of main sulfate fragments for OS-10.	139
Figure A-3	Peak fit of main sulfate fragments and CH_3SO_2^+ for MSA.	140
Figure A-4	Peak fit of main sulfate fragments for Centreville measurements.	141
Figure A-5	(a) Typical normalized sulfate mass spectra of organosulfur compounds (OS; OS-10 refers to sodium benzyl sulfate in Table A-1), ammonium sulfate (AS), methanesulfonic acid (MSA), and sodium sulfate (SS), not including water fragments. (b) Mass fraction of main family HSO ions. (c) $f_{\text{H}_2\text{SO}_4}$ vs. f_{HSO_3} for standard compounds. For OS, the shown f_{HSO_3} and $f_{\text{H}_2\text{SO}_4}$ are averages for all 15 OS. OS and SS standard calibrations were only performed with the GT AMS, while MSA and AS standard calibrations were performed with multiple AMS.	142
Figure A-6	RIE_{SO_4} calibration results for MSA and sodium ethyl sulfate (OS-2). The collection efficiency (CE) of 1 was applied to AMS data considering that atomized organosulfur particles were liquid droplets. The slope is acquired with intercept forced through zero.	143
Figure A-7	(a) “MSA sulfate” to “AS sulfate” ratio calculated by sulfate apportionment method as a function of MSA / AS molar ratio in particles. (b) “OS sulfate” to “AS sulfate” ratio calculated by sulfate apportionment method as a function of OS / AS molar ratio in particles for OS-15 / AS mixture. The slopes and intercepts are obtained by orthogonal distance regression (ODR). The Pearson’s R is obtained by linear least-squares fit.	144
Figure A-8	(a) $f_{\text{H}_2\text{SO}_4}$ vs. f_{HSO_3} for standard compounds and the strong SO_2 plume (average data) during the WINTER aircraft campaign. Both f_{HSO_3} and $f_{\text{H}_2\text{SO}_4}$ are normalized to those of AS from the specific AMS, so that AS would always be at (1,1) (b) Evolution of f_{HSO_3} and $f_{\text{H}_2\text{SO}_4}$ (normalized to pure AS), pH, and AMS species in a power plant plume in WINTER aircraft campaign. Acidic AS is 1:1 mixture of ammonium sulfate and sulfuric acid.	145

Figure A-9	Reaction profile of the chamber isoprene photooxidation experiment. The fAS and fOS refer to fraction of “AS sulfate” and “OS sulfate”, respectively, in total sulfate.	146
Figure A-10	$f_{H_2SO_4}$ vs. f_{HSO_3} for ambient measurements and time series of “AS sulfate”, “OS/SS sulfate” and “MSA sulfate” for (a) Centreville; (b) Mace Head; (c) Polarstern. OS and SS standard calibrations are from GT AMS, while MSA and AS standard calibrations are from the AMS that was used for the corresponding ambient measurements.	147
Figure A-11	(a) Comparison of AMS total sulfate and AMS “AS sulfate” (calculated by sulfate apportionment method) with PM ₁ inorganic sulfate (measured by PILS-IC). (b) Time series of total sulfate (measured by the AMS), “OS sulfate” (calculated by sulfate apportionment method), sulfate functionality concentration of main organosulfur compounds (measured by offline HILIC–TQD), and isoprene-OA factor (resolved by PMF). (c) Comparison of “OS sulfate” with isoprene-OA. The Pearson’s R is obtained by linear least-squares fit.	148
Figure A-12	Comparison of “OS sulfate” with (a) LO-OOA factor; (b) MO-OOA factor; (c) BBOA factor for Centreville measurements. The AMS factor time series are from (Xu et al., 2015a; Xu et al., 2015b) The Pearson’s R is obtained by linear least-squares fit.	149
Figure A-13	Comparison of MSA mass concentration estimated by sulfate apportionment method and signature fragments method for (a) Mace Head measurements and (b) Polarstern measurements. The Pearson’s R is obtained by linear least-squares fit.	151

LIST OF SYMBOLS AND ABBREVIATIONS

$\varepsilon(\text{HCOO}^-)$	Particle phase fraction of formic acid
$\varepsilon(\text{CH}_3\text{COO}^-)$	Particle phase fraction of acetic acid
κ	Hygroscopicity parameter
$\overline{\text{OS}}_c$	Carbon oxidation state
2-MGA	2-methylglyceric acid
2-MT	2-methyltetrol
AA	Acetic acid
AFTN-LO	Afternoon less-oxidized factor
AS	Ammonium sulfate
BBOA	Biomass burning organic aerosol
BL	Boundary layer
BVOC	Biogenic volatile organic compounds
CCN	Cloud condensation nuclei
CE	Collection efficiency
CIMS	Chemical ionization mass spectrometer
CMAQ	Community Multiscale Air Quality model
CPC	Condensation particle counter
DAS	Effloresced ammonium sulfate
Day-MO	Daytime more-oxidized factor
Day-ONRich	Daytime organic-nitrate-rich factor
DMA	Differential mobility analyzer
EC	Elemental carbon
$f(\text{LWC})$	Fraction of liquid water content in PM ₁ submicron aerosol
FA	Formic acid
FIGAERO	Filter Inlet for Gases and AEROsols
GC-FID	Gas chromatography-flame ionization detector
GTEC	Georgia Tech Environmental Chamber
H:C	Hydrogen-to-carbon ratio

H ₂ O ₂	Hydrogen peroxide
HMHP	Hydroxymethyl hydroperoxide
HMML	Hydroxymethyl-methyl-lactone
HOA	Hydrocarbon-like organic aerosol
HOMs	Highly oxygenated molecules
HPIC	High-pressure ion chromatography
HR-ToF-AMS	High-resolution time-of-flight aerosol mass spectrometer
IC	Ion chromatograph
IEPOX	Isoprene epoxydiol
IEPOX-SOA	IEPOX-derived SOA via IEPOX uptake
ISOP(OOH) ₂	isoprene dihydroxy dihydroperoxide
ISOPOOH	Isoprene hydroxy hydroperoxide
ISOPOOH-SOA	ISOPOOH-derived SOA via non-IEPOX pathways
Isoprene-OA	Isoprene-derived organic aerosol
LMWOA	Low-molecular-weight organic acids
LO-OOA	Less-oxidized oxygenated organic aerosol
LV-OOA	Low-volatility oxygenated organic aerosol
LWC	Liquid water content
MAE	Methacrylic acid epoxide
MBTCA	3-methyl-1,2,3-butanetricarboxylic acid
MCA	Multiple component analysis
ME-2	Multilinear engine
MO-OOA	More-oxidized oxygenated organic aerosol
MRN-LO	Morning less-oxidized factor
MSA	Methanesulfonic acid
MSSA	1:2 magnesium sulfate + sulfuric acid
MTA	Methyltartaric acids
MW	Molecular weight
N:C	Nitrogen-to-carbon ratio
NGT-ONRich	Nighttime organic-nitrate-rich factor
NO _{3,org}	Organic nitrate functionality measured in the HR-ToF-AMS

NO ₃ ·	Nitrate radical
NO _x	Nitrogen oxides
NR	Non-refractory
NVC	Nonvolatile cations
O:C	Oxygen-to-carbon ratio
O ₃	Ozone
OA	Organic aerosol
OC	Organic carbon
OH·	Hydroxyl radical
OOA	Oxygenated organic aerosol
OS	Organosulfur compounds
O _x	Odd oxygen (O ₃ + NO ₂)
PALMS	Particle Ablation by Laser Mass Spectrometry
PILS	Particle-into-liquid sampler
PM ₁	Submicron aerosol
PMF	Positive matrix factorization
POA	Primary organic aerosol
pOC	Particulate organic compound not containing nitrogen
pON	Particulate organic nitrates
PTFE	Perfluorotetrafluoroethylene
RH	Relative humidity
RIE	Relative ionization efficiency
RV	Research vessel
SCI	Stabilized Criegee intermediates
SEARCH	South Eastern Aerosol Research and Characterization
SF ₆ ⁻	Sulfur hexafluoride ions
SMPS	Scanning mobility particle sizer
SO ₂	Sulfur dioxide
SOA	Secondary organic aerosol
SOAS	Southern Oxidant and Aerosol Study
SS	Sodium sulfate

SV-OOA	Semi-volatile oxygenated organic aerosol
T_{\max}	Maximum desorption temperature
TOC	Total organic carbon
VOC	Volatile organic compounds
WAS	Deliquesced ammonium sulfate
W_i	Particle water uptake by inorganic species
WINTER	Wintertime Investigation of Transport, Emissions, and Reactivity aircraft campaign
W_o	Particle water uptake by organic species
WRF	Weather Research and Forecasting model
WSOC	Water-soluble organic compounds

SUMMARY

Particulate matter (PM) is important component of atmosphere, which can affect the planetary energy budget, visibility, and public health. While atmospheric PM can be complex mixtures of inorganic and organic components from a variety of sources, organic aerosols (OA) represent a significant fraction (20-90%) of tropospheric submicron PM. Therefore, a better understanding of atmospheric organic aerosols is essential for reliable evaluation of their impacts and effective regulations. The southeastern United States is known for its large biogenic volatile organic compounds (VOC) emissions from both conifer and deciduous forests, among which isoprene and monoterpenes are the most dominant biogenic VOC and SOA precursors, and thus attract substantial interests.

Our knowledge of OA compositions advances with the development of measurement techniques in the past two decades. This thesis presents two-month measurements conducted at a rural site in the southeastern United States, with a focus on the comparison of data acquired by two mass spectrometers with different measuring capabilities, a high-resolution time-of-flight aerosol mass spectrometer (HR-ToF-AMS, Aerodyne) and a chemical ionization mass spectrometer equipped with a Filter Inlet for Gases and AEROSols (FIGAERO-CIMS, Aerodyne). We found FIGAERO-CIMS data with molecular-level information provides new perspective to the interpretation of AMS OA factors that have been identified in the southeastern United States for over a decade. Specifically, while the AMS Isoprene-OA factor has been largely attributed to isoprene epoxydiols (IEPOX) uptake in previous studies, more pathways of isoprene oxidation were identified. Notable isoprene particulate organic nitrates (pON) formation and ISOPOOH-

SOA (isoprene hydroxy hydroperoxide oxidation products via non-IEPOX pathways) was observed; both pathways have not been resolved by AMS analysis before. AMS less-oxidized oxygenated OA factor (LO-OOA) correlated well with nighttime ON-rich factor (NGT-ONRich) resolved by FIGAERO-CIMS, which contained a series of monoterpene SOA tracers, consolidating that monoterpene SOA composes a large fraction of LO-OOA in the southeastern United States. Nonetheless, the non-negligible isoprene-derived pON in NGT-ONRich factor also related it to nocturnal isoprene chemistry, which was not identified by previous AMS analysis. Molecular-based mass spectrometry is proven to be a good supplement to AMS factorization analysis, which together provide more insights into the nature of OA.

In addition to the comprehensive characterization of OA in the southeastern United States, this thesis puts more focus on low-molecular-weight organic acids (LMWOA). Organic acids are ubiquitous atmospheric components, contributing to atmospheric acidity, affecting particle acidity, and directly participating in particle-phase reactions. LMWOA are normally end products of photochemical oxidation and linked to OA aging. Recent studies showed secondary formation from biogenic VOC oxidation is a largely underestimated source of LMWOA. In this study, the sources and partitioning of five most abundant LMWOA at a rural site in the southeastern United States were investigated. We propose that for formic and acetic acids, their gas and particle phases were largely decoupled; the majority of the gas-phase formic and acetic acids were formed rapidly and in situ through biogenic VOC photooxidation, while their particle-phase counterparts were likely from transport. For LMW dicarboxylic acids, their formation was more related to aqueous chemistry than gas-phase reactions, and their gas-particle partitioning was in

thermodynamic equilibrium. Through the links between LMWOA and aged SOA, transport and local OA processing were identified as sources for aged SOA in this work, while the diurnal pattern of aged SOA was dominantly driven by boundary layer dynamics.

Following up the findings that gas-phase formic and acetic acids were dominantly formed through biogenic VOC photooxidation, a series of chamber experiments were conducted to investigate formic and acetic acid formation in the photooxidation of isoprene and α -pinene, two of most abundant biogenic VOC in the southeastern United States. Chamber experiments were performed under different relative humidity (RH), using both effloresced and deliquesced ammonium sulfate seed particles to study the role of water vapor and aerosol water. We found the introduction of both gaseous and particulate water in general enhanced formic and acetic acids formation. Given the relatively high RH in the southeastern United States, tropospheric water would be a non-negligible factor affecting LMWOA formation, and including it in current modeling frameworks may improve simulations and help explain the large measurement-model discrepancies of formic and acetic acids observed in previous studies.

CHAPTER 1. INTRODUCTION

1.1 Atmospheric Organic Aerosols

1.1.1 *Why Study Organic Aerosols*

The atmospheric aerosols are minute solid and liquid particles suspended in the air. Aerosols can affect the planetary energy budget by directly absorbing and scattering radiation and indirectly serving as cloud condensation nuclei (CCN) to affect cloud properties (Kanakidou et al., 2005;Kroll and Seinfeld, 2008;Shrivastava et al., 2017). In addition to their role in climate, aerosols also have important impact on visibility and public health. Epidemiological studies have revealed associations between exposure to ambient aerosols with mortality and damaging effects on the respiratory and cardiovascular systems (Dockery et al., 1993;Kanakidou et al., 2005;Facchini et al., 2008). While atmospheric aerosols are complex mixtures of inorganic and organic components from a variety of sources, organic aerosol (OA) represents a significant fraction (20-90%) of tropospheric submicron aerosols (Kanakidou et al., 2005;Zhang et al., 2007a;Kroll and Seinfeld, 2008). Therefore, a better understanding of atmospheric organic aerosols is essential for reliable evaluation of their impacts and effective regulations.

There are two types of OA, primary OA (POA), which is directly emitted to atmosphere, and secondary OA (SOA), which is formed by the oxidation of volatile organic compounds (VOC). A simplified mechanism of SOA formation from precursor VOC can be described as the formation of functionalized, less volatile products from the oxidation of organic molecules by atmospheric oxidants (e.g., hydroxyl radical (OH \cdot), ozone (O $_3$),

and nitrate radical ($\text{NO}_3\cdot$). Products of sufficiently low volatility will condense into the particle phase (Seinfeld and Pandis, 2016), and in the particle phase, organic molecules can undergo further reactions. Many studies consistently showed that SOA dominates OA burden (Goldstein and Galbally, 2007; Zhang et al., 2007a). However, due to the variety of oxidizable organics in the atmosphere and the complexity of processes these compounds undergoing, many uncertainties exist regarding SOA formation and degradation (Hallquist et al., 2009).

1.1.2 Source Apportionment for Organic Aerosols

A lot of efforts have been made to understand OA sources. Lim and Turpin (2002) used elemental carbon (EC) as primary organic carbon (OC) tracer and estimated that ~46% OC was secondary in Atlanta, and the fraction ranged up to 88% on short timescale. Based on the measurement of fine-particle organic compounds soluble in water (WSOC), Weber et al. (2007) showed that 70–80% of the carbon in summertime WSOC is of biogenic origin in Atlanta, while the formation of SOA was also controlled by anthropogenic sources. With the wide use of Aerodyne Aerosol Mass Spectrometer (AMS) to quantitatively characterize the chemical composition of submicron non-refractory (NR) species (DeCarlo et al., 2006; Canagaratna et al., 2007), several techniques have been developed to deconvolved AMS OA mass spectra, e.g. multiple component analysis (MCA) (Zhang et al., 2007a), positive matrix factorization (PMF) (Ulbrich et al., 2009), and multilinear engine (ME-2) (Canonaco et al., 2013). At most sites, the OA can be separated into oxygenated OA (OOA), hydrocarbon-like OA (HOA), and some other components depending on location and season, e.g. isoprene- or IEPOX-derived OA (Isoprene-OA), and biomass burning OA (BBOA) (Jimenez et al., 2009; Ng et al., 2010; Hu

et al., 2015;Xu et al., 2015a). OOA factor can be further divided into more-oxidized OOA (MO-OOA, characterized by higher O:C ratio) and less-oxidized OOA (LO-OOA, characterized by lower O:C ratio) (Setyan et al., 2012;Xu et al., 2015a), which have been named as low-volatility OOA (LV-OOA) and semi-volatile OOA (SV-OOA), respectively, in some studies (Ng et al., 2010;Jimenez et al., 2009). While HOA factor has been considered as a good surrogate for combustion POA (Zhang et al., 2005;Jimenez et al., 2009;Ulbrich et al., 2009), multiple studies showed that OOA factor is secondary, and in general LO-OOA corresponds to fresh SOA, MO-OOA to aged SOA (Zhang et al., 2005;Zhang et al., 2007a;Jimenez et al., 2009;Ng et al., 2010). The two OOA factor together dominates submicron OA (Jimenez et al., 2009), but the sources of LO-OOA and MO-OOA are still under debate. One aim of this thesis is to provide a better understanding on LO-OOA and MO-OOA compositions.

1.2 Atmospheric Organic Acids

1.2.1 Organic Acids as Gases and in Aerosols

Organic acids are ubiquitous in both gas and particle phase. They are major contributors of atmospheric acidity (Keene and Galloway, 1984), especially in unpolluted areas, and can play a critical role on aerosol chemistry through their effects on particle acidity (Millet et al., 2015). Organic acids are also known to be sinks for hydroxyl radical and stabilized Criegee intermediates (SCI) (Jacob, 1986), and thus affect atmospheric radical budgets. Meanwhile, they also directly participate in particle-phase reactions like esterification to form low volatile compounds.

Sources of organic acids include direct emissions from terrestrial vegetation, soil, biomass burning, secondary photochemical production, and aqueous phase chemistry (Chebbi and Carlier, 1996;Khare et al., 1999;Paulot et al., 2011;Millet et al., 2015;Malecha and Nizkorodov, 2016;Sorooshian et al., 2007). Recent studies showed that the concentration of these small acids are largely underestimated by models and secondary formation from biogenic emissions could be an underrated sources (Paulot et al., 2011;Millet et al., 2015). Small monocarboxylic acid, e.g. formic acid and acetic acid, are dominant in the gas phase, while the most abundant organic acid in the particle phase is normally oxalic acid followed by succinic and/or malonic acid (Kawamura and Bikkina, 2016;Chebbi and Carlier, 1996). Dicarboxylic acids generally dominate aerosol phase, because their vapor pressures are 2 to 4 orders of magnitude lower than corresponding monocarboxylic acids (Chebbi and Carlier, 1996). Meanwhile, organic acids formed in the gas phase can partition to condensed phase, and vice versa. This process is mainly driven by pH (Facchini et al., 1992). while salt ions can also have an impact (Häkkinen et al., 2014).

1.2.2 Secondary Production of Organic Acids

Multiple studies showed that secondary formation, especially from biogenic emissions, can be an important yet underestimated source for atmospheric organic acids (Paulot et al., 2011;Millet et al., 2015). Ozonolysis and OH-oxidation of a variety of VOC (e.g. isoprene, MACR, MVK, and monoterpenes) leads to low-molecular-weight organic acids (LMWOA) formation (Millet et al., 2015;Jacob and Wofsy, 1988). Oxalic acid is considered a tracer for aqueous processing (Chebbi and Carlier, 1996;Carlton et al., 2007), and can be formed in aqueous aromatics, glyoxal photooxidation (Carlton et al., 2007). The

reaction of dissolved formaldehyde in aqueous phase with OH radicals in cloud droplets produce formic acid (Chameides and Davis, 1983). Small organic acids can also be formed by the oxidation of larger acids (Carlton et al., 2006b), and photodegradation of SOA (Malecha and Nizkorodov, 2016).

1.2.3 Importance of Organic Acids in a Changing Climate

Recent studies showed that particle pH is related to toxicity (Fang et al., 2017). It is of great interest that the abundance of organic acids in the atmosphere and their role in influencing particle pH, especially when the emission of sulfur dioxide (SO₂) and nitrogen oxides (NO_x) have been continuously decreasing in the United States, and how organic acids partitioning will be influenced by the ongoing changes of acid-base balance, and in return affect aerosol concentrations and compositions, is also a hot topic. Specifically, small organic acids are normally end products of photochemical oxidation and linked to OA aging. Previous studies have shown good correlations between AMS CO₂⁺ (or *m/z* 44) signal, a widely used marker for oxygenated OA, with either individual organic acids or ensembles of organic acids (Takegawa et al., 2007; Sorooshian et al., 2010; Yatavelli et al., 2015). Organic acids can be a proxy for a better understanding of MO-OOA formation and aged OA sources.

1.3 Thesis Overview

This thesis includes both field measurements and laboratory chamber studies, aiming to expand our knowledge of OA sources and formation mechanism in the southeastern United States with the advances of instruments, with a special focus on the sources and chemistry of LMWOA. Chapter 2 presents two-month measurements at a rural site in the

southeastern United States, where factorization analysis and molecular-level measurements were combined for a more comprehensive characterization of ambient OA. Chapter 3 presents more analysis about LMWOA formation and partitioning in the same field study, which also provides more insights to aged SOA sources in the southeastern United States. Chapter 4 presents a laboratory study investigating LMWOA formation in biogenic VOC photooxidation. Chapter 5 summarizes the findings and provides suggestions for future work.

CHAPTER 2. CHEMICAL CHARACTERIZATION OF SECONDARY ORGANIC AEROSOL AT A RURAL SITE IN THE SOUTHEASTERN U. S.: INSIGHTS FROM SIMULTANEOUS HR-TOF-AMS AND FIGAERO-CIMS MEASUREMENTS

2.1 Background

The southeastern United States is known for its large biogenic VOC emissions from both conifer and deciduous forests, under the influence of intensive anthropogenic activities (Weber et al., 2007; Xu et al., 2015a). Isoprene and monoterpenes (α -pinene, β -pinene, and limonene) are the most dominant biogenic VOC and SOA precursors in the southeastern United States and there is substantial interest in these compounds. For isoprene-derived SOA, isoprene epoxydiols (IEPOX) uptake followed by subsequent condensed-phase reactions (Surratt et al., 2010; Lin et al., 2012; Paulot et al., 2009b) is known to be the major pathway in the southeastern United States, approximately contributing 18 – 36 % to total OA in warm seasons (Budisulistiorini et al., 2013; Hu et al., 2015; Xu et al., 2015a; Xu et al., 2015b). Isoprene organic nitrates formed from both photooxidation and nitrate radical oxidation have been characterized in ambient measurements and included in models (Lee et al., 2016; Bates and Jacob, 2019), as well as non-IEPOX SOA formed from hydroxy hydroperoxide (ISOPOOH) oxidation (Krechmer et al., 2015; Nagori et al., 2019). Monoterpene nocturnal reactions have been shown to be an important source of particulate organic nitrates in the southeastern United States (Xu et al., 2015a; Xu et al., 2015b; Pye et al., 2015), while more recent studies have demonstrated that monoterpenes are also the prominent source of total OA in the southeastern United

States given the large fraction of non-nitrogen-containing monoterpene-derived species (Zhang et al., 2018a; Xu et al., 2018a).

A better understanding of OA composition is aided by advances in state-of-art real-time aerosol instrumentation in the past two decades. Each instrument, with its unique capabilities, provides one piece of information to the SOA puzzle. The high-resolution time-of-flight aerosol mass spectrometer (HR-ToF-AMS, Aerodyne; henceforth referred to as AMS) (DeCarlo et al., 2006; Canagaratna et al., 2007), for example, has been widely used in both laboratory experiments and field measurements. Designed to quantitatively characterize chemical composition of submicron non-refractory (NR-PM₁) aerosol, the AMS produces ensemble average mass spectra for organic and inorganic species. Different methods have been used to deconvolve AMS OA mass spectra, e.g., multiple component analysis (Zhang et al., 2007a), positive matrix factorization (PMF) (Ulbrich et al., 2009; Canonaco et al., 2013). Oxygenated OA (OOA) is a subgroup, or factor, that has been ubiquitously resolved by AMS factorization analysis and normally used as a surrogate for SOA, while other OA factors can be more regional and seasonal, e.g., isoprene-derived OA (Isoprene-OA) and biomass burning OA (BBOA) (Jimenez et al., 2009; Ng et al., 2010; Hu et al., 2015; Xu et al., 2015a; Cubison et al., 2011). OOA can be further divided into more-oxidized OOA (MO-OOA, characterized by higher O:C ratio) and less-oxidized OOA (LO-OOA, characterized by lower O:C ratio) (Setyan et al., 2012; Xu et al., 2015a), which have also been named as low-volatility OOA (LV-OOA) and semi-volatile OOA (SV-OOA), respectively, in some studies (Ng et al., 2010; Jimenez et al., 2009). In general, LO-OOA corresponds to fresh SOA and MO-OOA corresponds to aged SOA (Zhang et al., 2005; Zhang et al., 2007a; Jimenez et al., 2009; Ng et al., 2010). The two OOA factors

account for a large fraction of submicron OA worldwide (Jimenez et al., 2009), but the sources of LO-OOA and MO-OOA at different locations are still largely unknown. The Chemical Ionization Mass Spectrometer (henceforth referred to as CIMS) is a well-established technique for online measurements of gaseous species (Huey, 2007), and the recent combination of a Filter Inlet for Gases and AEROSols (henceforth referred to as FIGAERO) to the CIMS (henceforth referred to as FIGAERO-CIMS) allows for the application of CIMS in aerosol molecular composition characterization (Lopez-Hilfiker et al., 2014). Source apportionment analysis has been performed on CIMS gas- and particle-phase measurements in previous studies in a similar manner to that of AMS measurements (Yan et al., 2016; Massoli et al., 2018; Lee et al., 2018). Compared to traditional AMS source apportionment, FIGAERO-CIMS can provide more information on the identity of each factor, e.g., chemical formulae of tracer molecules and the location of the maximum desorption signal in temperature space (T_{\max}), by which enthalpy of sublimation and compound vapor pressure can be evaluated (Lopez-Hilfiker et al., 2014). The FIGAERO-CIMS is highly complementary to the AMS and could substantially expand our knowledge of the AMS OA factors that have been known for over a decade.

Here, we present results from two-month measurements at Yorkville, GA, a rural site in the southeastern United States, during a transitional season from summer to fall. Along with a suite of additional instrumentation (Nah et al. (2018a;2018b)), AMS and FIGAERO-CIMS were deployed, and factorization analysis was applied to measurements from both instruments, in an effort to gain new insights into established AMS OA factors. By combining AMS and FIGAERO-CIMS measurements, we show that isoprene and monoterpenes were dominant OA precursors during both day and night. We also identify

notable isoprene oxidation pathways, besides IEPOX uptake, and their contribution to particulate organic nitrates, which was less recognized by previous AMS measurements.

2.2 Methods

2.2.1 Site Description

The ambient measurements took place from mid-August to mid-October 2016 at the South Eastern Aerosol Research and Characterization (SEARCH) field site at Yorkville, Georgia (33.92833 N, 85.04555 W, 394 masl). The instruments were housed in an air-conditioned trailer. The Yorkville site was a long-term field site located in a rural environment approximately 55 km northwest of Atlanta, immediately surrounded by forests and open pastures for cattle grazing. Compared to previous measurements at this site (Xu et al., 2015a;2015b), the sampling period of this study was characterized by a transition from warmer to colder season, which had a direct influence on biogenic VOC emissions, e.g. isoprene mixing ratio decreased from more than 2 ppb at the beginning of campaign to below 1 ppb at the end (daily average). More details of this 2016 Yorkville campaign have been presented in recent publications by Nah et al. (2018a;2018b).

2.2.2 Instrumentation

An AMS (DeCarlo et al., 2006;Canagaratna et al., 2007) was used to characterize the composition of NR-PM₁. Ambient air was sampled through a URG PM₁ cyclone at 16.7 L min⁻¹ to remove coarse particles. A nafion dryer was placed upstream of the AMS to dry the particles (RH < 20 %) in order to eliminate the influence of RH on particle collection efficiency (CE) in the AMS (Matthew et al., 2008;Middlebrook et al., 2012).

Measurements were taken every minute and post-averaged to a 5-minute time interval. Gas-phase interference was eliminated by subtracting the signals when the AMS sampled through a HEPA filter. Ionization efficiency (IE) calibrations were performed with 300 nm ammonium nitrate particles, and sulfate relative ionization efficiency (RIE) calibrations were performed with 300 nm ammonium sulfate particles. Both calibrations were conducted on a weekly basis. AMS data were analyzed using the data analysis toolkit SQUIRREL (v1.57) and PIKA (v1.16G) within the Igor Pro software (v6.37, Wavemetrics, Portland, OR). The organics data matrix and error matrix for source apportionment analysis were also generated from PIKA v1.16G. Elemental ratios, including oxygen-to-carbon ratio (O:C), hydrogen-to-carbon ratio (H:C), and nitrogen-to-carbon ratio (N:C), were obtained using the method outlined by Canagaratna et al. (2015). By comparing AMS with parallel particle-into-liquid sampler (PILS) coupled to ion chromatograph (IC) and filter measurements, a constant CE of 0.9 was applied to AMS measurements (Nah et al., 2018a).

An iodide-adduct FIGAERO-CIMS was used to characterize particle-phase multifunctional organic species, given the advantage of its high selectivity towards highly-polarizable species, such as carboxylic acids and polyols. A detailed description of FIGAERO-CIMS can be found in Lopez-Hilfiker et al. (2014), while a detailed description of the iodide ionization mechanisms can be found in Huey et al. (1995) and Lee et al. (2014). In brief, ambient air was sampled through a URG PM₁ cyclone and PM₁ particles were collected on a perfluorotetrafluoroethylene (PTFE) filter (2 µm pore size Zefluor™, Pall Corporation) in the FIGAERO unit for 25 minutes at a flow rate of 16.7 L min⁻¹. To prevent potential positive artefact arising from gases sticking onto the filter during sampling, a 30-cm long parallel plate activated carbon denuder (Eatough et al., 1993) was

installed upstream of the FIGAERO inlet. After collection, particles were immediately desorbed off the PTFE filter by heated N₂ flowing through the filter. The thermal desorption process took 35 minutes, during which the temperature was increased from room temperature (~ 25 °C) to ~200 °C in 15 minutes, held at ~200 °C for another 15 minutes, and cooled for 5 minutes. One filter background measurement was taken for every five cycles by keeping the filter on the desorption line. Raw data were saved every second and were pre-averaged to a 10-second time interval before data processing. The data were analyzed using the data analysis toolkit Tofware (v2.5.11, Tofwerk, Thun, Switzerland and Aerodyne, Billerica, MA) within the Igor Pro software (v6.37, Wavemetrics, Portland, OR). The FIGAERO-CIMS particle data matrix was also generated from Tofware v2.5.11. The signals reported for particles in later discussion were integrations over the thermal desorption process, with background subtracted. The signals are in counts per second (Hz), if not specified in the following discussion, which implies a uniform sensitivity assumption for FIGAERO-CIMS measurements. Due to the nature of iodide reagent ion, which has a higher sensitivity towards oxygenated organic compounds (Lee et al., 2014), the importance of more oxidized compounds will be over-emphasized while less oxidized compounds under-emphasized. Nevertheless, a good correlation (R = 0.84) between total OA measured by AMS and FIGAERO-CIMS (Figure 2-1) suggests that the assumption of uniform sensitivity to some extent could be reasonable in this study. When we compared the FIGAERO-CIMS measurements with AMS measurements, the FIGAERO-CIMS signals were converted to mass concentrations by multiplying ion signals in Hz with the molecular weight (MW) of each ion, and the new unit is g mol⁻¹ s⁻¹. This conversion allows for an easier cross-instrument comparison between AMS and FIGAERO-CIMS. We are

aware that the unit $\text{g mol}^{-1} \text{s}^{-1}$ is not an actual mass concentration; rather it is a scalar of the ion signal based on MW.

This study focuses on AMS and FIGAERO-CIMS measurements. Other co-located instruments included PILS-ICs to measure water-soluble inorganic and organic acid species, CIMSs to measure gaseous species, PILS and mist chambers coupled to a total organic carbon (TOC) analyzer to measure particle- and gas-phase water-soluble organic carbon, and gas chromatography-flame ionization detector (GC-FID) with a Markes focusing trap to measure hourly resolved VOC, and a chemiluminescence monitor to measure NO and NO₂.

2.2.3 *Source Apportionment Methods*

As organic measurements from the AMS and FIGAERO-CIMS are comprised of hundreds of species, source apportionment methods were applied to both measurements for a better understanding of OA sources and composition. Two widely used source apportionment methods, positive matrix factorization (PMF) and the multilinear engine (ME-2) algorithm, were used here. PMF is the most commonly used source apportionment method for AMS data (Lanz et al., 2007; Ulbrich et al., 2009; Jimenez et al., 2009; Ng et al., 2010; Zhang et al., 2011). It is a least-squares approach based on a receptor-only multivariate factor analytic model to solve bilinear unmixing problems. PMF deconvolves the observed data matrix as a linear combination of various factors with constant mass spectra but varying concentrations across the dataset. The model solution of PMF is not unique due to rotational ambiguity. The ME-2 solver works in a similar manner to PMF. The difference between PMF and ME-2 is that ME-2 allows users to introduce *a priori*

information, in the form of a known factor time series and / or a factor profile, as inputs to the model to constrain the solution (Canonaco et al., 2013). In the following discussion, we applied PMF analysis to both AMS and FIGAERO-CIMS datasets, respectively. For the AMS dataset, we found that unconstrained PMF runs failed to identify reasonable solutions, i.e., the contribution from Isoprene-OA was largely overestimated, likely due to interferences as measurements were conducted during transition in seasons (isoprene emissions), which will be discussed later. Therefore we performed ME-2 analysis on the AMS dataset and constrained it with a fixed Isoprene-OA factor profile. The constraining method was known as a-value approach (Canonaco et al., 2013; Crippa et al., 2014), where the a-value (ranging from 0 to 1) determines how much a factor profile is allowed to vary from the input source profile. The Isoprene-OA factor profile (anchor profile) we used to constrain the ME-2 analysis was previously resolved by PMF from Centreville, Alabama, during the SOAS campaign (Xu et al., 2015a; Xu et al., 2015b). A description of our ME-2 analysis is provided in Section 3.

2.2.4 Estimating Mass Concentration of Organic Nitrate Functionality from AMS Measurements

The mass concentration of organic nitrate functionality ($NO_{3,org}$) was calculated based on NO^+/NO_2^+ from AMS measurements (Farmer et al., 2010), by eq. 2.1-2.2.

$$NO_{2,org} = \frac{NO_{2,meas} \times (R_{meas} - R_{AN})}{R_{ON} - R_{AN}} \quad (2.1)$$

$$NO_{3,org} = NO_{2,org} \times (R_{ON} + 1) \quad (2.2)$$

where R_{meas} is the $\text{NO}^+/\text{NO}_2^+$ ratio from field measurements; R_{AN} is the $\text{NO}^+/\text{NO}_2^+$ ratio of pure ammonium nitrate; and R_{ON} is the $\text{NO}^+/\text{NO}_2^+$ ratio of pure organic nitrates. Note that $\text{NO}_{3,\text{org}}$ refers to the mass concentration of nitrate functionality only ($-\text{ONO}_2$). In this study, an R_{AN} of 3 (average value from three IE calibrations of ammonium nitrate throughout the field measurements) was adopted for $\text{NO}_{3,\text{org}}$ calculation. For R_{ON} , two values, an upper bound of 10 and a lower bound of 5, derived from β -pinene+ $\text{NO}_3\cdot$ and isoprene+ $\text{NO}_3\cdot$ systems, respectively, were adopted to acquire a $\text{NO}_{3,\text{org}}$ range for field measurements (Bruns et al., 2010; Boyd et al., 2015a; Xu et al., 2015b).

2.3 Results and Discussion

2.3.1 Campaign Overview and OA Bulk Properties

The meteorological data of the campaign have already been discussed in detailed in Nah et al. (2018a). Briefly, the two-month measurements were characterized by moderate temperature (average 24.0 ± 4.0 °C) and high RH (average 68.9 ± 17.9 %). Isoprene was the most abundant VOC (average 1.21 ± 1.08 ppb), followed by propane (average 0.84 ± 0.39 ppb), α -pinene (average 0.37 ± 0.40 ppb), and β -pinene (average 0.32 ± 0.29 ppb), making biogenic VOC the predominant OA precursors at Yorkville. A clear decreasing trend was observed for isoprene concentration as temperature decreased throughout the campaign, which is consistent with the seasonal variation of isoprene emission (Seinfeld and Pandis, 2016). The Yorkville site is located in a rural environment with low but non-negligible NO_x level, with an average NO and NO_2 concentrations of 0.15 ± 0.35 ppb and 2.2 ± 1.8 ppb, respectively. NO was probably transported from roadways, peaking at around 9 am.

Organic species were the dominant component of NR-PM₁ (average $5.0 \pm 2.3 \mu\text{g m}^{-3}$), contributing 75 % to the total NR-PM₁ aerosol mass measured by AMS. The study mean diurnal trends of OA elemental ratios measured by both the AMS and FIGAERO-CIMS are shown in Figure 2-2. Since the nitrate functionality of organic nitrates largely fragments into NO⁺ and NO₂⁺ in the AMS (Farmer et al., 2010) and will result in underestimated O:C and N:C values for OA, the nitrogen mass and oxygen mass from NO_{3,org} have been added back in AMS O:C and N:C analysis. Compared to the OA measured by AMS, the OA measured by FIGAERO-CIMS was more oxidized, with a lower H:C (by 0.08 compared to AMS H:C) and a higher O:C (by 0.17 compared to original AMS O:C, and by 0.10 compared to the upper bound of AMS O:C after including oxygen atoms from NO_{3,org}). This difference can be explained by the selective sensitivity of the iodide reagent ion, which has a higher sensitivity towards oxygenated organic compounds (Lee et al., 2014). After including NO_{3,org} in the AMS N:C calculation, the AMS N:C measurements fell into the range of the FIGAERO N:C measurements (average of 0.017 from FIGAERO; average of 0.006 to 0.025 from AMS). Both AMS and FIGAERO-CIMS measurements consistently showed O:C peaked in the afternoon while N:C peaked at night, suggesting that OA at Yorkville was more oxidized in the afternoon and organic nitrates accounted for a larger OA fraction at night.

2.3.2 Overview of Organic Compounds Detected by FIGAERO-CIMS

Figure 2-3(a) shows the normalized spectra (signals in mixing ratio) of FIGAERO-CIMS measurements. In total, 769 multifunctional organic compounds possessing 1 – 18 carbons have been identified in this study, of which 423 were CHO species (pOC, containing at least one carbon atom, at least one oxygen atom, and an even number of

hydrogen atoms), and 346 were nitrogen-containing CHON species that match the formula of a particulate organic nitrate (pON, containing one nitrogen atom, at least one carbon atom, three or more oxygen atoms, and an odd number of hydrogen atoms). Compounds not attached to an iodide ion were excluded, as their ionization mechanisms were uncertain. Organic nitrates containing two or more nitrogen atoms were not included in the discussion given they are much less abundant compared to organic mononitrates. Since FIGAERO-CIMS cannot distinguish compounds of the same molecular formula but with different molecular structures, the detected organic nitrate compounds can be peroxy nitrates or multifunctional alkyl nitrates.

On average, pOC and pON contributed $87.7 \pm 10.8 \%$ and $12.3 \pm 10.8 \%$, respectively, to total FIGAERO-CIMS signals (Table 2-1), while pOC and pON showed distinct diurnal patterns. pON had a higher contribution at night (Figure 2-3(b)), consistent with our observations of higher N:C at night, which was reported by previous FIGAERO-CIMS studies at other sites (Lee et al., 2016; Huang et al., 2019). A 10 am peak was also observed for pON fraction, following NO peak which happened around 9 am, likely due to enhanced ON formation as NO level increased. The pON fraction was also estimated using AMS nitrate measurements, where we calculated lower and upper bound of $\text{NO}_{3,\text{org}}$ using a $\text{NO}^+/\text{NO}_2^+$ ratio of 10 and 5, respectively, and then applied an average MW of 220 g mol^{-1} (effective MW of all pON measured by FIGAERO-CIMS) to convert AMS $\text{NO}_{3,\text{org}}$ to mass concentration of organic nitrates (sum of mass of both organic and nitrate functionalities of the organic nitrates). The resulting pON fraction ($\text{pON}/(\text{Org} + \text{NO}_{3,\text{org}})$, 5 – 18 %) was comparable to FIGAERO-CIMS measurements and also agreed with previous studies in the southeastern United States (Xu et al., 2015b; Ng et al., 2017). For a

group of pON or pOC with the same carbon atom number, a bell-shaped distribution was observed as a function of oxygen atom number (Figure 2-4 and Figure 2-5), similar to observations from previous field measurements (Lee et al., 2016; Lee et al., 2018; Huang et al., 2019).

The average effective formulae of pOC and pON are $C_{6.4}H_{9.0}O_{5.3}N_0$ and $C_{7.5}H_{11.6}O_{6.5}N_1$, respectively. A series of small organic compounds ($MW < 80 \text{ g mol}^{-1}$) were detected by FIGAERO-CIMS in this study, some of which were in high abundance, e.g., CH_2O_2 and $C_2H_4O_3$. These ions should not be detected in the particle phase due to expected high volatility and were likely thermal decomposition products of less-volatile molecules, not uncommon in FIGAERO thermograms (Stark et al., 2017; Schobesberger et al., 2018). The presence of these ions biased effective formulae and MWs calculations, thus the values reported in Table 2-1 could be smaller than the actual molecules. Meanwhile, these small but highly-oxidized fragments may also have a higher carbon oxidation state and bias the AMS elemental ratio calculation as well. pON molecules on average had around one more carbon than pOC molecules, meaning pON was composed of larger molecules compared to pOC. In Figure 2-3, to better illustrate the difference between pOC and pON composition, we grouped pOC and pON species into four subgroups based on the carbon atom number, C_{1-5} , C_{6-10} , C_{11-15} , and $C_{>15}$. For both pOC and pON, compounds with fewer than 15 carbon atoms accounted for majority of total signals ($99.8 \pm 0.1 \%$ for pOC and $99.6 \pm 0.2 \%$ for pON), with C_{6-10} being the most dominant subgroup ($53.4 \pm 33.3 \%$ in pOC and $65.8 \pm 5.4 \%$ in pON), followed by C_{1-5} ($42.4 \pm 33.8 \%$ in pOC and $26.9 \pm 5.3 \%$ in pON), and C_{11-15} ($4.0 \pm 0.7 \%$ in pOC and $7.0 \pm 1.1 \%$ in pON) (Figure 2-3(c) and (d)). pON contained a higher fraction from C_{6-10} while

pOC contained a higher fraction from C₁₋₅, explaining the difference in their average formulae. Each subgroup showed distinct diurnal patterns, while the same subgroup exhibited similar trends in pOC and pON (Figure 2-3(e) and (f)). Specifically, C₁₋₅ species had a larger contribution during the daytime while C₆₋₁₀ species were more dominant during the night. This is consistent with emission of their potential precursors, where C₁₋₅ were more likely to arise from isoprene oxidation while C₆₋₁₀ were more likely to arise from monoterpenes, though contributions from other sources, fragmentation of monoterpene products, and dimer formation in isoprene oxidation are also possible. There was a lack of a clear day-night contrast for C₁₁₋₁₅ species, likely due to their low concentrations, low instrument sensitivity, and/or formation from various sources.

2.3.3 AMS OA Factors

We started our analysis with unconstrained PMF runs using the Solution Finder (SoFi 6.4) software. Three factors can be resolved by unconstrained runs, which are Isoprene-OA, LO-OOA, and MO-OOA. This three-factor solution was consistent with previous AMS measurements conducted in summer at Yorkville (Xu et al., 2015a; Xu et al., 2015b), in which no primary OA factor was resolved. However, the contribution from Isoprene-OA appeared to be largely overestimated in our unconstrained PMF runs. The campaign-average Isoprene-OA fraction was 45 ± 15 % (Figure 2-6) and the fraction was as high as 90 % at the beginning of the campaign, when the emission of isoprene was higher. However, previous measurements at the same site showed that Isoprene-OA only accounted for 32.5 % of total OA in July (Xu et al., 2015a; Xu et al., 2015b). Meanwhile, the $f_{C_5H_6O}$ ($C_5H_6O^+/OA$, a tracer for isoprene-derived SOA (Hu et al., 2015)) of the resolved Isoprene-OA was 7.0 ‰ (Figure 2-6(c)), while in previous studies Isoprene-OA had an

$f_{C_{5H_6O}}$ of around 20 % (Hu et al., 2015; Xu et al., 2015b). These discrepancies indicated that the Isoprene-OA factor resolved by unconstrained PMF likely included interferences from other types of OA as measurements were conducted during transition in seasons (isoprene emissions), and that unconstrained PMF alone was not sufficient to identify the correct solution for this dataset. Therefore, we applied constraints in form of Isoprene-OA profile. In previous studies, only the POA profile, rather than SOA, has been fixed in ME-2 analysis (Crippa et al., 2014; Elser et al., 2016). However, as Isoprene-OA is a commonly resolved biogenic SOA in the southeastern United States during summertime (Xu et al., 2015a; Xu et al., 2015b; Hu et al., 2015; Budisulistiorini et al., 2016; Rattanavaraha et al., 2016) and its profile shows consistency in different studies (Hu et al., 2015), we constrained the Isoprene-OA profile with a “clean” Isoprene-OA profile resolved in the southeastern United States during summer 2013 SOAS measurements at Centreville (Xu et al., 2015a; Xu et al., 2015b). The rotations were explored using the a-value approach (Lanz et al., 2008; Canonaco et al., 2013; Crippa et al., 2014). We tested five a-values for the Isoprene-OA profile, from 0 to 0.8, with an increment of 0.2. The determination of a final solution was guided by three criteria: mass fraction of each factor (Figure 2-7(b)), correlation between factor time series with external tracers, and the $f_{C_{5H_6O}}$ of resolved Isoprene-OA (Figure 2-7(c)). Different external tracers were also used for identifying OA factors. 2-methyltetrol is the ring-opening product of IEPOX and can be measured by I-CIMS (Surratt et al., 2010; Lin et al., 2012; Hu et al., 2015). Lopez-Hilfiker et al. (2016) showed that the 2-methyltetrol signal detected in FIGAERO-CIMS may be derived from thermal decomposition of accretion products or other organics of lower volatility, but IEPOX uptake is still the major source for this fragment. Here, we still used the 2-

methyltetrol ($C_5H_{12}O_4$) signal measured by FIGAERO-CIMS as a tracer species for Isoprene-OA. Previous studies showed that organic nitrates made up a substantial portion of LO-OOA in the southeastern United States, correlating well with LO-OOA (Xu et al., 2015a), and used LO-OOA as a surrogate for pON-derived aerosol (Pye et al., 2015). Thus, in this work we used organic nitrate functionality as an external tracer for LO-OOA.

Based on the above criteria, a three-factor solution with an a -value of 0 was chosen for the AMS dataset. The chosen three-factor solution gave the best correlations between Isoprene-OA and $C_5H_{12}O_4$ signal ($R = 0.85$), LO-OOA and $NO_{3,org}$ ($R = 0.84$), and the highest $f_{C_5H_6O}$ (23 %) (Figure 2-7). The mass spectra and time series for the factors are shown in Figure 2-8. With ME-2 analysis, the fraction of Isoprene-OA was lower compared to unconstrained PMF. On average, Isoprene-OA, LO-OOA, and MO-OOA contributed $17 \pm 5 \%$, $33 \pm 15 \%$, and $50 \pm 13 \%$ to total OA, respectively. Over the course of the campaign, the fraction of Isoprene-OA in total OA decreased from 26% to 8% (daily averages), consistent with the decreasing temperature during season transition (Figure 2-9). Similar to previous measurements at the same site (Xu et al., 2015a;2015b), MO-OOA was characterized by a wide afternoon peak, likely related to strong daytime photochemistry, while LO-OOA had a nighttime enhancement, which can arise from changes in boundary layer height, temperature-driven partitioning, as well as nocturnal OA formation such as nitrate radical oxidation of biogenic VOC. The diurnal trend of Isoprene-OA also showed an afternoon enhancement, but the day-night contrast was less pronounced compared to MO-OOA. MO-OOA had the highest O:C (0.91), followed by Isoprene-OA (0.63) and LO-OOA (0.49).

2.3.4 FIGAERO-CIMS OA Factors

The integration of each thermogram, with background subtracted, was taken as the total particle-phase signal (255 desorption cycles were measured in total). The factorization analysis was performed on the integrated total particle-phase signals in the Igor Pro based PMF Evaluation Tool (version 2.06). Initially, the errors of integrated signals were estimated using Poisson statistics as follows:

$$\sigma = \sqrt{I} \quad (2.3)$$

where I is the integrated ion signal in the unit of ions. However, we noticed that the σ values estimated by Poisson statistics only provide a lower limit for the real noise, probably due to unaccounted variabilities introduced by thermogram integration, which can be subjected to overlapping peaks and fragmented ions. As a consequence, the Q/Q_{exp} from the PMF analyses is $\gg 1$ (Figure 2-10), indicating that the estimated errors were underrepresented (Ulbrich et al., 2009). Given the complexity of uncertainties associated with the thermal desorption processes and a lack of well-developed methods to estimate these uncertainties, we developed an empirical scaling factor by comparing the time series of several pairs of highly-correlated ions (Figure 2-11). Figure 2-11(a), for example, shows a scatter plot of two ions that are highly correlated as a function of time. The Poisson uncertainties for each data point, calculated according to eq. 1.3, are also shown. The measured scatter does not have any clear trend with time and is clearly much larger than the calculated Poisson uncertainties. Thus, the uncertainties input into the PMF analysis were empirically increased by a factor of 10 to better account for the observed scatter. This empirical scaling factor of 10 was applied to all errors, which gives more reasonable Q/Q_{exp} values (Figure 2-12) and now only requires one factor to explain the highly-correlated ions. As discussed above, thermal decomposition processes could result in the production of a

series of small organic compounds ($MW < 80 \text{ g mol}^{-1}$). We included these small ions in the PMF analysis, since their time variations reflected those of their parent compounds, but including them will likely result in overestimation of the carbon oxidation state and underestimation of the effective MWs of the factors in later discussion.

Carbon oxidation state of each FIGAERO-CIMS factor was calculated using a formula modified from that in Kroll et al. (2011) to include organic nitrate contributions, where a group oxidation state of -1 was applied to -ONO₂ functionality:

$$\overline{OS}_c = 2 \times (\text{O:C} - 3 \times \text{N:C}) - \text{H:C} + \text{N:C} \quad (2.4)$$

which can be rewritten as

$$\overline{OS}_c = 2 \times \text{O:C} - \text{H:C} - 5 \times \text{N:C} \quad (2.5)$$

As mentioned above, iodide reagent ion has a higher sensitivity towards oxygenated organic compounds. Meanwhile, the small and highly-oxidized organic compounds formed in potential thermal decomposition may have a higher carbon oxidation state than their parent molecules. Thus, the average carbon oxidation states calculated for FIGAERO-CIMS factors could be higher than the actual values.

Five FIGAERO-CIMS OA factors were resolved (Figure 2-13). Two factors showing clearly higher N:C (0.028 and 0.032) were distinguished by their diurnal trends and thus denoted as Day-ONRich (daytime ON-rich) factor and NGT-ONRich (nighttime ON-rich) factor. For the remaining three daytime factors with lower N:C (0.008, 0.009, and 0.011), one showed a significantly higher \overline{OS}_c and was denoted as Day-MO (daytime more-oxidized, $\overline{OS}_c = 0.50$) factor, while the other two were distinguished by their diurnal

trends and thus denoted as MRN-LO (morning less-oxidized) factor and AFTN-LO (afternoon less-oxidized) factor. Day-MO, Day-ONRich, MRN-LO, AFTN-LO, and NGT-ONRich factors accounted for 25 ± 15 %, 12 ± 10 %, 21 ± 13 %, 23 ± 16 %, and 18 ± 13 % of total signals measured by FIGAERO-CIMS, respectively. The average effective formulae and MWs were calculated for each factor, as well as for their pOC and pON components, and are shown in Table 2-1. Similar to the discussion in Section 3.2, the pOC and pON species of each factor were grouped into and discussed as C₁₋₅, C₆₋₁₀, C₁₁₋₁₅, and C_{>15} subgroups (Figure 2-14). The concentration of C_{>15} subgroup was negligible, so we excluded them from the following discussion. Below, we evaluate and discuss tracer ions for each FIGAERO-CIMS OA factor, based on both their absolute abundance (i.e., ions of the highest signal in the mass spectrum of each factor) and their fractional abundance (i.e., ions dominantly presented in a certain factor).

NGT-ONRich had the largest MW (193.4 g mol^{-1}), highest effective carbon atom number (7.0), and lowest $\overline{\text{OS}}_c$ (0.13), meaning this factor was composed of larger and less oxidized molecules. This feature can be seen more clearly in Figure 2-14. Compared to the other four factors, both pOC and pON of NGT-ONRich had a larger fraction from C₆₋₁₀ and C₁₁₋₁₅ subgroups, and a smaller fraction from C₁₋₅ subgroup. NGT-ONRich also had the highest effective nitrogen atom number (0.22), meaning one in every five molecules was an organic nitrate. The most abundant pON species in NGT-ONRich were C₃H₉NO₇ and C₁₀H₁₅NO₈, accounting for 7.8 and 3.5 % of pON signals in this factor, respectively. C₁₀H₁₅NO₈ has been characterized in multiple chamber studies as major products of α -/ β -pinene/limonene+NO₃ \cdot and α -/ β -pinene photooxidation with the presence of NO_x (Nah et al., 2016; Lee et al., 2016; Faxon et al., 2018; Takeuchi and Ng, 2019). At Yorkville, the

majority of $C_{10}H_{15}NO_8$ was presented in NGT-ONRich, implying that nocturnal chemistry is its most important source. Besides $C_{10}H_{15}NO_8$, a series of $C_{9,10}$ pON ($C_9H_9,11,13NO_{8,9,10}$ and $C_{10}H_{13,15,17}NO_{8,9,10}$) were also dominantly presented in NGT-ONRich, which were similar to fingerprint ions reported by Massoli et al. (2018) for gaseous terpene nitrate factor at Centreville during the SOAS campaign. The NGT-ONRich we resolved here is likely the particle-phase counterpart of that gaseous terpene nitrate factor. $C_5H_9NO_7$ was not solely present in NGT-ONRich. Instead, it contributed an even higher fraction to Day-ONRich, suggesting that both daytime and nighttime pathways were critical for $C_5H_9NO_7$ at Yorkville. This is consistent with $C_5H_9NO_7$ being detected in previous laboratory studies on isoprene+ $NO_3\cdot$ and isoprene photooxidation in the presence of NO_x (Ng et al., 2008; Lee et al., 2016). Both $C_5H_9NO_7$ and $C_{10}H_{15}NO_8$ have also been identified at Centreville in rural Alabama, United States, during SOAS, among the top ten most abundant pON species (Lee et al., 2016). In another field study at the boreal forest research station SMEAR II located in Hyytiälä, southern Finland, $C_{10}H_{15}NO_8$ has been suggested to be a fingerprint molecule for a daytime factor measured with NO_3^- -based CI-APi-TOF (Yan et al., 2016), but in this study it was more abundant at night. The pOC tracer of NGT-ONRich was $C_8H_{12}O_5$, likely corresponding to 2-hydroxyterpenylic acid, which was proposed to be an α -pinene SOA tracer formed from further oxidation of terpenylic acid (Eddingsaas et al., 2012a; Kahnt et al., 2014a; Kahnt et al., 2014b; Sato et al., 2016). Taken together, the high contribution from C_{6-10} subgroup and the presence of quite a few monoterpene SOA tracers in NGT-ONRich strongly related this factor to monoterpene chemistry, with a non-negligible contribution from isoprene organic nitrates. NGT-ONRich also contained the highest fraction of C_{11-15} group. While most signals were from C_{11} ions, we also observed

some C₁₄ and C₁₅ compounds, e.g., pOC C₁₄H₁₈₋₂₂O₅₋₇ and C₁₅H₂₀₋₂₄O₅₋₇, pON C₁₄H₂₁₋₂₅NO₇ and C₁₅H₂₃₋₂₇NO₇, which possibly originated from sesquiterpene oxidation, though more fundamental laboratory studies are needed to further constrain this.

Day-ONRich had an effective nitrogen atom number of 0.16, lower compared to NGT-ONRich, but still significantly higher than other daytime factors. 23 % of Day-ONRich pON signals was from C₅H₉NO₇, implying isoprene as the crucial precursor of Day-ONRich, even considering half of C₅H₉NO₇ signal may arise from fragmentation of other larger molecules (Figure 2-15(a)). The second highest pON ion, C₅H₇NO₇, was also likely from isoprene. The high signals from C₅H₇NO₇ and C₅H₉NO₇ made the C₁₋₅ ON subgroup as prevalent as the C₆₋₁₀ ON subgroup, which was a distinctive feature for Day-ONRich (Figure 2-14). Meanwhile, the pOC of Day-ONRich also contained noticeably more C₁₋₅ ions than other factors, probably due to fragmentation process being a favored pathway under high-NO conditions (Kroll and Seinfeld, 2008). As a result, Day-ONRich had the lowest effective MW (164.5 g mol⁻¹) and the lowest effective carbon number (5.6). The most abundant pOC species of Day-ONRich were C₃H₄O₅, C₄H₆O₅, and C₅H₈O₅. The formula of C₃H₄O₅ implied dicarboxylic acid and it has been reported in aqueous processes (Lim et al., 2010). However, the average thermogram of C₃H₄O₅ showed two peaks (Figure 2-15(b)), where the first peak (T_{max} = 74.3 °C) roughly matched the volatility of C₃ dicarboxylic acids and the second peak (T_{max} = 113.2 °C) likely came from thermal decomposition of molecules of lower volatility. Similar multiple-peak behavior was observed for C₃H₄O₄, a tracer compound for Day-MO (Figure 2-15(c)). C₄H₆O₅, possibly malic acid, has been reported as a higher-generation product of unsaturated fatty acids photochemistry (Kawamura et al., 1996), but has also been found in isoprene SOA in

several studies, including particle-phase reactions in isoprene photooxidation in the presence of NO_x, non-IEPOX pathway via ISOPOOH+OH· reaction (ISOPOOH-SOA), and isoprene ozonolysis (Nguyen et al., 2010; Xu et al., 2014; Krechmer et al., 2015). One isomer of C₅H₈O₅, 3-hydroxyglutaric acid, has been used as a tracer for α-/β-pinene photooxidation SOA (Claeys et al., 2007), while other studies have identified C₅H₈O₅ in isoprene SOA when the IEPOX pathway was suppressed (Nguyen et al., 2011; Krechmer et al., 2015; Liu et al., 2016). C₅H₈O₅ was also found in the oxidation of 1,3,5-trimethylbenzene (Praplan et al., 2014), toluene (Kleindienst et al., 2007), and levoglucosan (Zhao et al., 2014). There was no sign of prevalent anthropogenic emissions or biomass burning events during the measurements, so the presence of C₅H₈O₅ was more likely linked to monoterpene photooxidation and/or non-IEPOX isoprene chemistry.

Day-MO was dominated by pOC signals (accounting for 95 % of signals) and characterized by the highest \overline{OS}_c (0.50) of all factors. The tracer ions of Day-MO were C₄H₄O₆, C₅H₆O₆, and C₅H₈O₆. Given their lower degree of saturation and considerably high O:C, these compounds were likely carboxylic acids, particularly di- or even tri-carboxylic acids. For instances, C₄H₄O₆, likely 2-hydroxy-3-oxosuccinic acid, was identified in OH· initiated oxidation of aqueous succinic and tartaric acids (Chan et al., 2014; Cheng et al., 2016). C₅H₈O₆ was likely 2,3-dihydroxy-2-methylsuccinic acid, a product of aqueous cross photoreaction of glycolic and pyruvic acids (Xia et al., 2018), or methyltartaric acids (MTA), tracers of aged isoprene SOA (Jaoui et al., 2019). However, we cannot rule out the possibility that they were fragments from thermal decomposition of larger molecules. Techniques without thermal desorption processes will be beneficial in understanding the nature of highly-oxidized OA molecules in future studies.

Similar to Day-MO, pOC accounted for more than 90% of total signals in MRN-LO and AFTN-LO. These two factors had similar fractions from each subgroup (Figure 2-14), though they were dominated by different ions. For MRN-LO, the dominating ions were $C_8H_{12}O_5$ and $C_3H_4O_4$, while $C_7H_{10}O_5$ also stood out. $C_8H_{12}O_5$, as discussed above, was related to α -/ β -pinene SOA, and $C_7H_{10}O_5$ also likely corresponded to an α -pinene SOA tracer, i.e., 3-acetylpentanedioic acid (Kleindienst et al., 2007). $C_3H_4O_4$ could correspond to malonic acid or its isomers, but given its high desorption temperature (Figure 2-15(c)), $C_3H_4O_4$ was more likely fragments of larger molecules. For AFTN-LO, the most prominent ions were $C_4H_4O_6$, $C_5H_{10}O_{4,5}$, and $C_9H_{14}O_{4,5}$. $C_4H_4O_6$, as discussed above, was likely related to aqueous processing. $C_9H_{14}O_4$, likely pinic acid (Seinfeld and Pandis, 2016), was a well-established fresh α -pinene SOA tracer, and $C_9H_{14}O_5$ was probably related to α -/ β -pinene SOA (Kahnt et al., 2014a;Kahnt et al., 2014b;Sato et al., 2016). $C_5H_{10}O_5$ has been shown to be a dominant product of ISOPOOH-SOA (Krechmer et al., 2015;D'Ambro et al., 2017), but has also been detected in isoprene ozonolysis and isoprene photooxidation under high-NO (Jaoui et al., 2019). It is interesting that a non-IEPOX isoprene SOA product was found to be one of the prominent tracers for an afternoon low-NO fresh SOA factor in our study. Previous factorization analysis of AMS measurements alone suggested that ISOPOOH-SOA accounted for only ~2 % of ambient OA at Centreville during summer 2013 SOAS measurements (Krechmer et al., 2015). If the $C_5H_{10}O_5$ we observed in AFTN-LO was dominantly from ISOPOOH+OH \cdot reaction via non-IEPOX pathway, ISOPOOH-SOA may account for a more considerable fraction of fresh isoprene SOA in our study compared to that reported in Centreville. Thus, the initial difficulty we encountered when resolving Isoprene-OA, which is believed to form mainly via the IEPOX pathway, from

PMF analysis of AMS data may be explained to some extent. Taken together, although both MRN-LO and AFTN-LO were relatively fresh SOA, MRN-LO had more contribution from monoterpenes, while AFTN-LO was more dominated by isoprene SOA.

2.3.5 *Tracer Species Detected by FIGAERO-CIMS and Their Implications*

As discussed in Section 3.4, a series of biogenic SOA tracers, mostly from isoprene and monoterpenes, has established their importance in more than one FIGAERO-CIMS OA factor. To better understand the OA formation mechanisms, we selected six isoprene and monoterpene SOA tracers to represent different oxidation pathways and examined their distributions in the five FIGAERO-CIMS OA factors (Figure 2-16).

For isoprene SOA, $C_5H_9NO_7$ was chosen here as pON tracer, $C_5H_{12}O_4$ as IEPOX uptake tracer, and $C_5H_{10}O_5$ as non-IEPOX tracer. Note that $C_5H_{10}O_5$ can form from isoprene oxidation under various conditions: while $C_5H_{10}O_5$ is a major product in $ISOPOOH+OH\cdot$ when the IEPOX uptake pathway is suppressed (Krechmer et al., 2015;D'Ambro et al., 2017), it also forms in $isoprene+O_3$ and $isoprene+ OH\cdot+NO_x$ (Jaoui et al., 2019). Most of the $C_5H_9NO_7$ signals were found in Day-ONRich (39 %) and NGT-ONRich (32 %), suggesting a non-negligible isoprene ON formation during both day and night. The efficient nocturnal isoprene oxidation is possibly via the reaction with nitrate radicals rather than with ozone (Ng et al., 2008;Brown et al., 2009;Schwantes et al., 2015;Fry et al., 2018). In addition, the recent work by Fry et al. (2018) suggested a substantially longer nighttime peroxy radical lifetime in ambient air versus under chamber conditions, which allows for the formation of lower-volatility products and thus higher SOA yields from isoprene nocturnal chemistry. $C_5H_{12}O_4$ was only noticeable in daytime,

non-ON-Rich factors, consistent with its low-NO photochemistry origin. $C_5H_{10}O_5$ was also only present in daytime factors. However, different from $C_5H_{12}O_4$, a noticeable fraction of its signal was in Day-ONRich, implying that $C_5H_{10}O_5$ can also be formed under high-NO conditions. One interesting observation was that while $C_5H_{12}O_4$ is an early-generation product of isoprene oxidation, it had a larger fraction in Day-MO (expected to be aged SOA) than in AFTN-LO (expected to be fresh SOA). Here, we hypothesize that the Day-MO factor was closely related to particle-phase aqueous processes, and the presence of $C_5H_{12}O_4$ in Day-MO can be explained by that IEPOX uptake to the particle phase requires aerosol water. Aqueous chemistry can also explain the acid-like ions observed in large abundance in Day-MO.

For monoterpene SOA, $C_{10}H_{15}NO_8$ was used here as pON tracer, $C_9H_{14}O_4$, likely pinic acid (Seinfeld and Pandis, 2016), as fresh SOA tracer, and $C_8H_{12}O_6$, likely 3-methyl-1,2,3-butanetricarboxylic acid (MBTCA) (Szmigielski et al., 2007; Zhang et al., 2010b; Müller et al., 2012; Eddingsaas et al., 2012b), as an aged SOA tracer. $C_{10}H_{15}NO_8$ was prominently present in the nighttime factor NGT-ONRich, implying that nocturnal oxidation, likely by nitrate radicals, was its major source. The majority of $C_9H_{14}O_4$ signal was found in MRN-LO and AFTN-LO as expected, consolidating MRN-LO and AFTN-LO as daytime fresh SOA factors. $C_8H_{12}O_6$ was suggested to form from OH-initiated oxidation of pinonic acid in the gas phase (Müller et al., 2012; Szmigielski et al., 2007), but at Yorkville it was present in comparable abundance in MRN-LO, AFTN-LO, Day-MO, and NGT-ONRich, suggesting that complex aging pathways of fresh monoterpene SOA took place both day and night.

2.3.6 Correlations between AMS OA Factors and FIGAERO-CIMS OA Factors

To compare AMS OA factors with FIGAERO-CIMS OA factors, we first converted FIGAERO-CIMS signals (Hz) to mass concentration (Hz g mol^{-1}) by simply applying the effective MW to the time series of each factor, while still assuming uniform sensitivity for all compounds. The hourly averages were used for cross-instrument comparison and results are shown in Figure 2-17.

For both AMS and FIGAERO-CIMS measurements, only one nighttime factor was resolved, LO-OOA from AMS and NGT-ONRich from FIGAERO-CIMS. A good correlation ($R = 0.77$) in time series was observed between them (Figure 2-17(c) and (d)). As discussed above, the FIGAERO-CIMS measurements strongly related this factor to monoterpene chemistry, which was consistent with previous AMS measurements in the southeastern United States (Xu et al., 2015a; Xu et al., 2015b). NGT-ONRich also showed a prevalent contribution from organic nitrates, with one fourth of molecules being pON species. However, FIGAERO-CIMS also identified a non-negligible presence of isoprene-derived pON species in this factor, which the AMS was unable to resolve, implying the potential contribution from isoprene nocturnal organic nitrate formation. In a recent study, Xu et al. (2018a) showed that the major source of LO-OOA in the southeastern United States is from monoterpenes, but also includes contributions from sesquiterpene oxidation pathways. Our observation of a series of C_{14} and C_{15} species in NGT-ONRich is consistent with the presence of sesquiterpene SOA, though it cannot provide a further quantitative constraint.

Two daytime factors were resolved for AMS measurements, while four were resolved for FIGAERO-CIMS measurements. Strong correlation was observed for the summation of the AMS daytime factors (Isoprene-OA + MO-OOA) and the summation of the FIGAERO-CIMS daytime factors (Day-MO + Day-ONRich + MRN-LO + AFTN-LO), with $R = 0.89$ (Figure 2-17(a) and (b)). For daytime factors, the Day-ONRich factor was unique to FIGAERO-CIMS. In the AMS, the nitrate functionalities of pON fragmented into NO^+ and NO_2^+ ions, which were not included in

source apportionment analysis, and may explain the difficulty of resolving daytime ON-rich factors for AMS dataset. Both AMS and FIGAERO-CIMS resolved one daytime aged SOA factor, i.e., AMS MO-OOA factor and FIGAERO-CIMS Day-MO factor, and these two factors were mildly correlated ($R = 0.71$). For AMS MO-OOA, different theories regarding its sources and formation pathways have been proposed (which are not mutually exclusive), including photochemical aging of fresh OA (Jimenez et al., 2009;Ng et al., 2010;Bougiatioti et al., 2014), aqueous processes (Xu et al., 2017b), formation of highly oxygenated molecules (HOMs) (Ehn et al., 2014), long-range transport (Hayes et al., 2013), and entrainment of aged SOA from the residual layer (Nagori et al., 2019). In our previous discussion, we tentatively related FIGAERO-CIMS Day-MO, which correlated with AMS MO-OOA, to aqueous processes, but cannot rule out other processes. AMS resolved only one daytime fresh SOA factor, Isoprene-OA. Isoprene-OA was largely, but not entirely, attributed to IEPOX uptake (Xu et al., 2015a;Schwantes et al., 2015), and the enhanced signal at m/z 82 ($C_5H_6O^+$) may arise from methylfuran-like structures (Robinson et al., 2011;Budisulistiorini et al., 2013;Hu et al., 2015). FIGAERO-CIMS resolved two daytime fresh SOA factors, MRN-LO and AFTN-LO. The summation of MRN-LO and AFTN-LO showed good correlation with AMS isoprene-OA factor ($R = 0.76$). We observed various ions with high abundance in MRN-LO and AFTN-LO that were likely associated with isoprene organic nitrates, isoprene oxidation via non-IEPOX pathways, and monoterpene oxidation. Previous studies have shown that IEPOX-SOA was enhanced even under high-NO conditions (Jacobs et al., 2014;Schwantes et al., 2019) and that α -pinene SOA could interfere with AMS Isoprene-OA apportionment (Xu et al., 2018a). All these observations may suggest a more complex origin for the AMS Isoprene-OA factor (i.e., not just IEPOX uptake).

2.3.7 Change of the Abundance of Biogenic VOC and AMS OA Factors in a Transitional Period

This field campaign took place during the transition in seasons from summer to fall, where decreasing temperature led to changes in abundances of SOA precursors. Figure 2-18 shows the mixing ratios of major VOC (isoprene, α -pinene, and β -pinene) and mass concentrations of AMS OA factors as a function of temperature. The FIGAERO-CIMS factors were not discussed here because fewer data points were measured by FIGAERO-CIMS and were not sufficient to provide statistically reliable results. To eliminate the influence of daily meteorological variations, two sampling periods with relatively stable meteorological conditions were chosen to represent daytime (12:00 – 16:00, high temperature and boundary layer height, peak solar radiation) and nighttime (00:00 – 04:00, low temperature and boundary layer height, zero solar radiation), respectively. Isoprene mixing ratio showed a strong dependence on temperature in both day and night. The mixing ratios of α -pinene and β -pinene were moderately dependent on temperature when temperature was lower than 25 °C, and remained relatively constant when the temperature was higher than 25 °C, where most daytime data points resided. For AMS factors, Isoprene-OA increased with temperature, followed the trend of isoprene, as expected. This can be explained by the longer lifetime of aerosol compared to gas species, and Isoprene-OA showed a delayed response to temperature changes. The strong dependence of Isoprene-OA on temperature suggested isoprene as the dominant precursor of this factor, implying that Isoprene-OA resolved from AMS measurements is still a good surrogate of isoprene-derived SOA even with the potential interference from monoterpene SOA as discussed above. LO-OOA showed similar trends to monoterpenes, consistent with our discussion above and previous literature that monoterpenes are the dominant precursors to LO-OOA in this region. For MO-OOA, a mild dependence on temperature was observed, suggesting

that at least some of its sources were affected by temperature, e.g., through aging of isoprene-derived SOA (emission of isoprene is temperature dependent).

2.4 Conclusions

Two-months of measurements were performed at a rural site in the southeastern United States during a transition in seasons. AMS and FIGAERO-CIMS measurements were combined to provide a better understanding of OA sources, composition, and properties. Both instruments consistently identified more oxidized OA in the afternoon and enhanced pON formation during the night, although the OA measured by FIGAERO-CIMS was more oxidized than that by AMS, due to the nature of iodide reagent ion that was used in FIGAERO-CIMS. Similar AMS OA factors were resolved compared to previous summer measurements at the same site, which were Isoprene-OA, LO-OOA, and MO-OOA (and no HOA). The fraction of AMS Isoprene-OA in total OA decreased from 26 % to 8 % over the campaign, concurrent with decreasing isoprene mixing ratio, which was strongly dependent on temperature. For FIGAERO-CIMS, three daytime fresh OA factors with low N:C (MRN-LO, AFTN-LO, and Day-MO) each accounted for about one fourth of total signals measured by FIGAERO-CIMS, and two factors with high N:C (Day-ONRich and NGT-ONRich) together accounted for the rest. MRN-LO and AFTN-LO were likely fresh biogenic SOA, with MRN-LO more dominated by monoterpene SOA and AFTN-LO more dominated by isoprene SOA. Day-MO was hypothesized to be a mixture of aged and fresh SOA whose formation was possibly aided by aerosol water. NGT-ONRich was mostly from nocturnal monoterpene chemistry, while daytime isoprene oxidation under the effects of NO_x was more important to Day-ONRich. Lastly, a series of C₁₄ and C₁₅ compounds were identified by FIGAERO-CIMS, possibly originated from

sesquiterpene oxidation pathways. In this study, a uniform sensitivity was assumed for all species measured by FIGAERO-CIMS, resulting in some uncertainties in the overall elemental ratios and carbon numbers. Future studies are warranted to continue to characterize and optimize instrument sensitivity for further quantitative analysis.

Previous studies (Qi et al., 2019;Stefenelli et al., 2019) have shown that combinations of AMS and molecular based mass spectrometric information is a way forward to provide more insights into the nature of SOA in general. In this study, factor analysis of FIGAERO-CIMS data provided new insights into the sources and composition of the typical AMS OA factors observed in the southeastern United States. Specifically, while the AMS Isoprene-OA factor has been largely attributed to IEPOX uptake in previous studies, we identified more pathways of isoprene oxidation that contributed to isoprene SOA formation in addition to IEPOX uptake. Notable isoprene pON formation was observed, likely from photooxidation in the presence of NO_x and nitrate radical oxidation, as well as notable ISOPOOH-SOA (ISOPOOH oxidation products via non-IEPOX pathways); both pathways have not been resolved by AMS analysis before. AMS LO-OOA factor correlated well with NGT-ONRich factor resolved by FIGAERO-CIMS, which contained a series of monoterpene SOA tracers, consolidating that LO-OOA was mostly attributed to monoterpene SOA in the southeastern United States. Nonetheless, the non-negligible isoprene-derived pON in NGT-ONRich factor also related it to nocturnal isoprene chemistry, which was not identified by previous AMS factorization analysis.

Table 2-1 Effective Molecular Composition of FIGAERO Factors.

	Effective Formula	Effective MW (g/mol)	O:C	H:C	N:C	\overline{OS}_C	Marker Ions
Day-MO	$C_{6.1}H_{8.1}O_{5.7}N_{0.05}$	173.0	0.94	1.33	0.009	0.50	
Day-MO (pOC)	$C_{6.0}H_{8.0}O_{5.7}N_0$	171.4	0.94	1.33	0	0.56	$C_4H_4O_6$, $C_5H_6O_6$, $C_5H_8O_6$
Day-MO (pON)	$C_{6.9}H_{9.8}O_{6.0}N_1$	203.0	0.87	1.41	0.14	-0.39	
Day-ONRich	$C_{5.6}H_{8.1}O_{5.4}N_{0.16}$	164.5	0.96	1.43	0.028	0.35	
Day-ONRich (pOC)	$C_{5.5}H_{7.6}O_{5.1}N_0$	154.8	0.94	1.40	0	0.47	$C_3H_4O_5$, $C_4H_6O_5$, $C_5H_8O_5$
Day-ONRich (pON)	$C_{6.7}H_{10.4}O_{7.0}N_1$	216.7	1.05	1.56	0.15	-0.22	$C_5H_9NO_7$, $C_5H_7NO_7$
MRN-LO	$C_{6.6}H_{9.3}O_{5.2}N_{0.06}$	172.2	0.79	1.41	0.008	-0.13	
MRN-LO (pOC)	$C_{6.5}H_{9.1}O_{5.2}N_0$	170.2	0.80	1.40	0	0.19	$C_8H_{12}O_5$, $C_3H_4O_4$, $C_7H_{10}O_5$
MRN-LO (pON)	$C_{7.6}H_{11.7}O_{5.7}N_1$	207.0	0.75	1.55	0.13	-0.71	
AFTN-LO	$C_{6.7}H_{10.1}O_{5.4}N_{0.07}$	177.7	0.79	1.49	0.011	0.04	
AFTN-LO (pOC)	$C_{6.7}H_{9.8}O_{5.3}N_0$	174.5	0.80	1.48	0	0.12	$C_4H_4O_6$, $C_5H_{10}O_5$, $C_5H_{10}O_4$, $C_9H_{14}O_4$, $C_9H_{14}O_5$
AFTN-LO (pON)	$C_{7.8}H_{13.0}O_{6.0}N_1$	217.7	0.77	1.66	0.13	-0.76	
NGT-ONRich	$C_{7.0}H_{10.0}O_{6.0}N_{0.22}$	193.4	0.85	1.41	0.032	0.13	
NGT-ONRich (pOC)	$C_{6.9}H_{9.5}O_{5.7}N_0$	182.9	0.83	1.38	0	0.28	$C_8H_{12}O_5$
NGT-ONRich (pON)	$C_{7.7}H_{11.7}O_{7.0}N_1$	230.0	0.91	1.51	0.13	-0.35	$C_5H_9NO_7$, $C_{10}H_{15}NO_8$

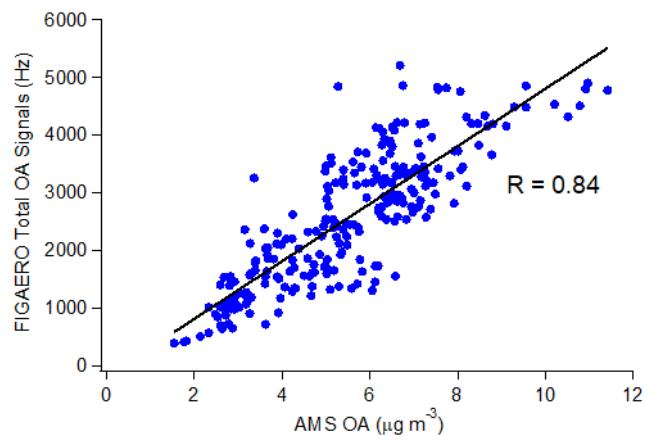


Figure 2-1 Correlation between FIGAERO total OA signals and AMS total OA mass concentration.

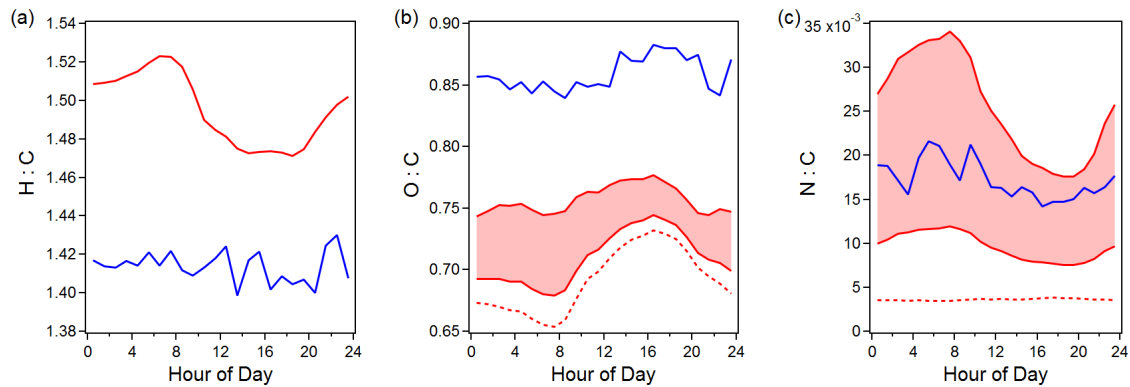


Figure 2-2 Study mean diurnal trends of elemental ratios measured by AMS (red) and FIGAERO-CIMS (blue). The AMS O:C and N:C with and without including $\text{NO}_{3,\text{org}}$ are in shaded area (with $\text{NO}^+/\text{NO}_2^+$ ratio of 5 and 10) and in dashed line, respectively.

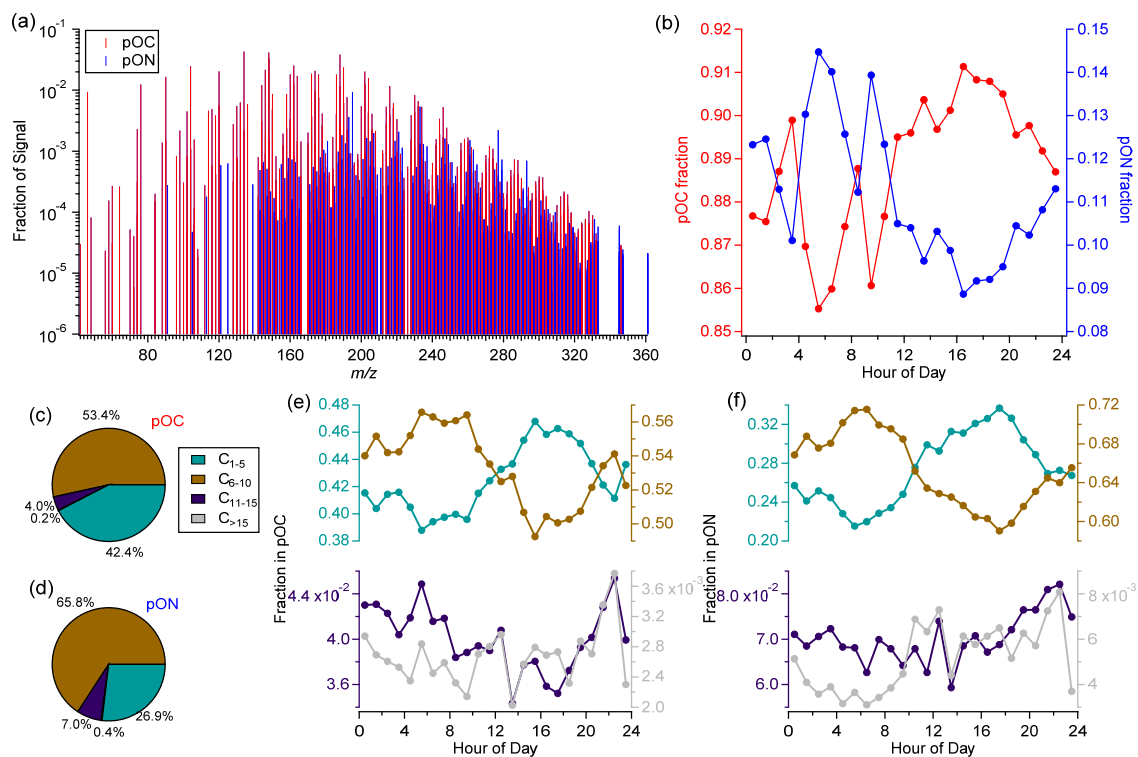


Figure 2-3 Study mean (a) FIGAERO mass spectra, (b) fraction of pOC and pON compounds plotted as a function of time of a day, (c) and (d) fraction of ions of different carbon numbers (grouped as C₁₋₅, C₆₋₁₀, C₁₁₋₁₅, and C_{>15}) in pOC and pON, and (e) and (f) fraction of C₁₋₅, C₆₋₁₀, C₁₁₋₁₅, and C_{>15} compounds in pOC and pON plotted as a function of time of day.

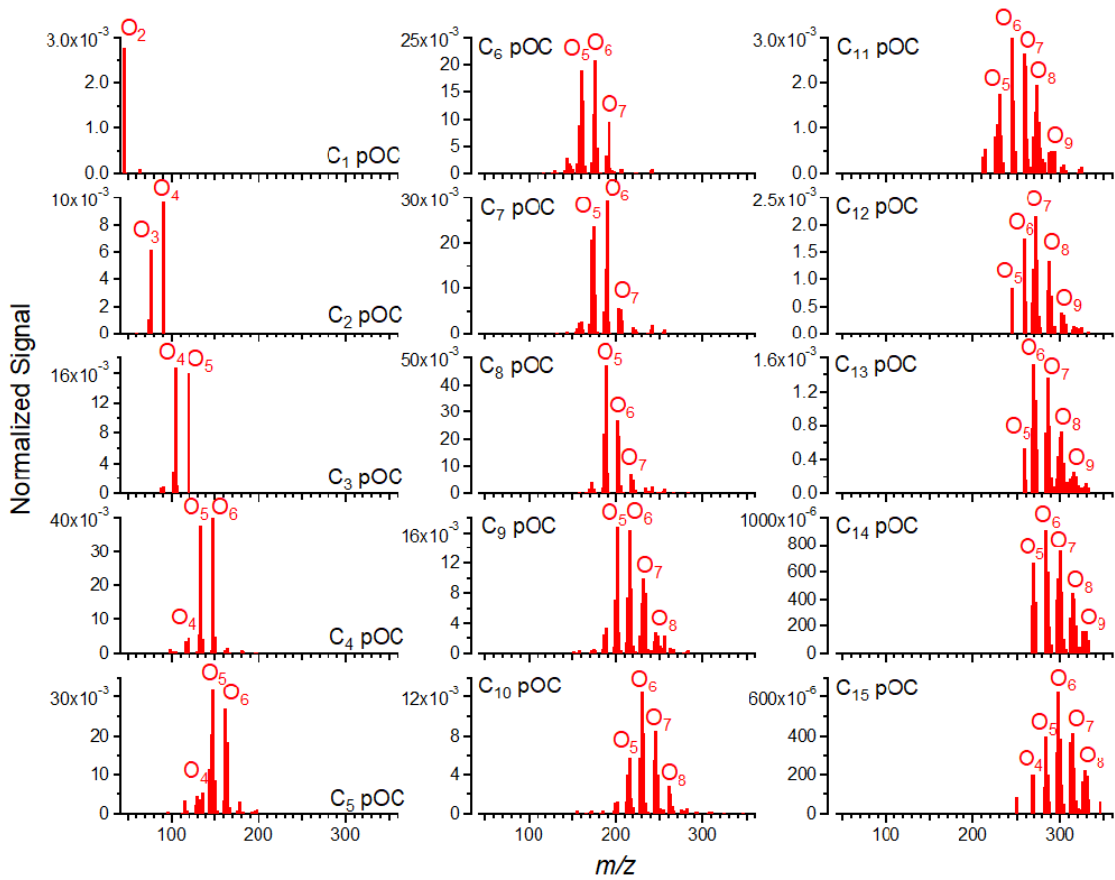


Figure 2-4 Normalized mass spectra of pOC ions measured by FIGAERO-CIMS, grouped by carbon atom number.

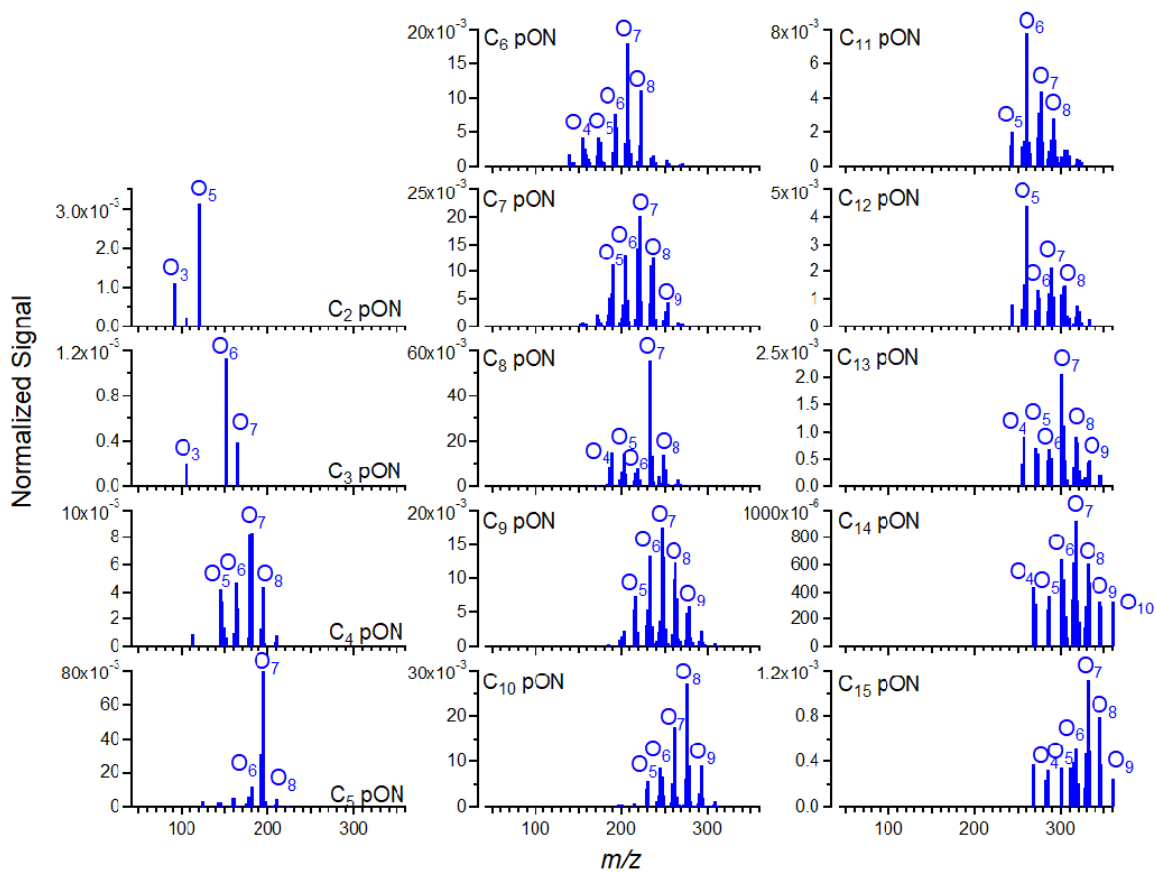


Figure 2-5 Normalized mass spectra of pON ions measured by FIGAERO-CIMS, grouped by carbon atom number.

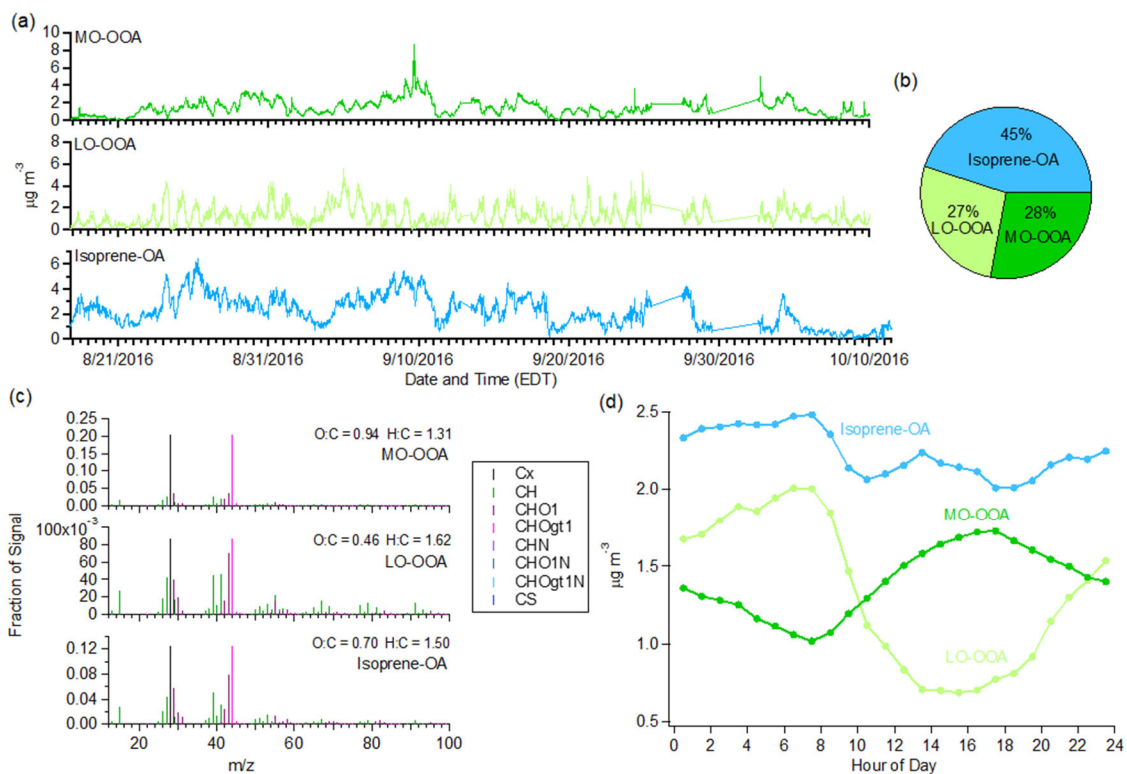


Figure 2-6 (a) Time series, (b) mass fraction, (c) normalized mass spectra, and (d) diurnal profiles of AMS OA factors resolved by PMF.

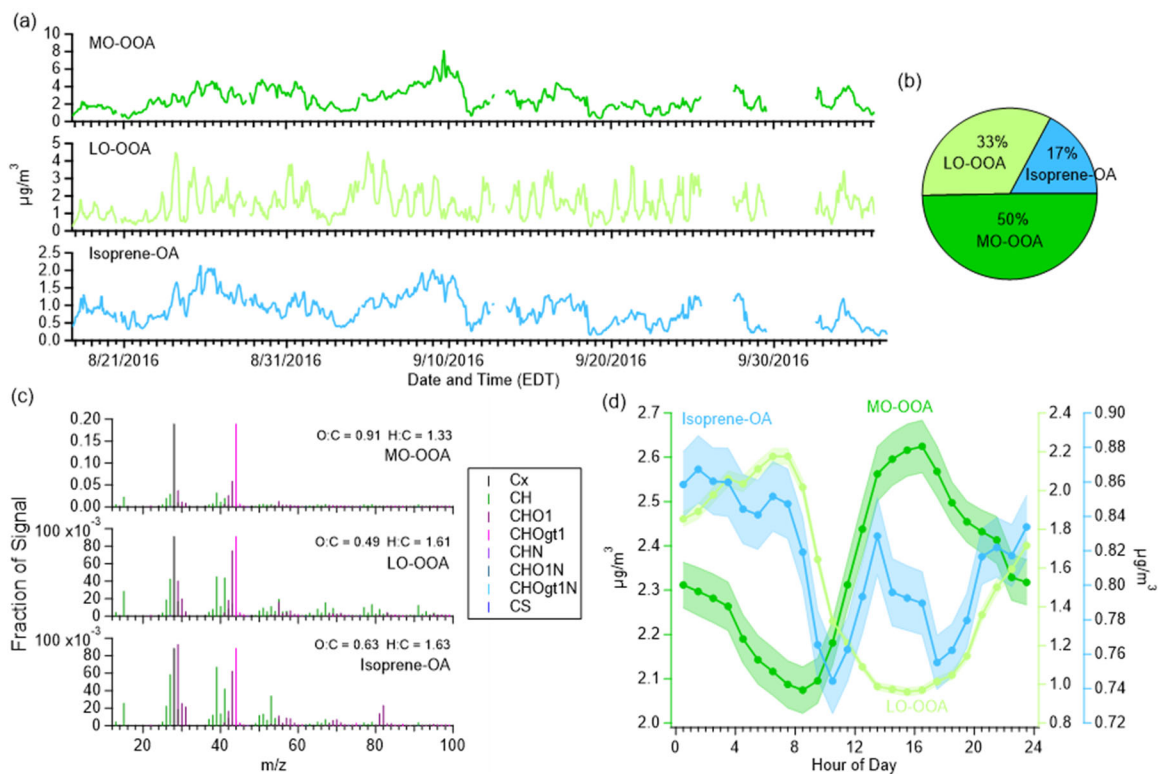


Figure 2-8 (a) Time Series, and study mean (b) mass fraction, (c) normalized mass spectra, and (d) diurnal profiles (standard deviations in shaded areas) of AMS OA factors resolved by ME-2.

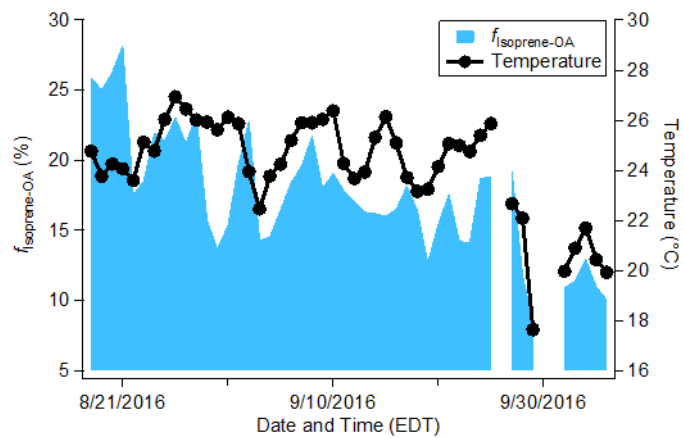


Figure 2-9 Time series (daily averaged) of the mass fraction of Isoprene-OA in total OA ($f_{\text{isoprene-OA}}$) and temperature.

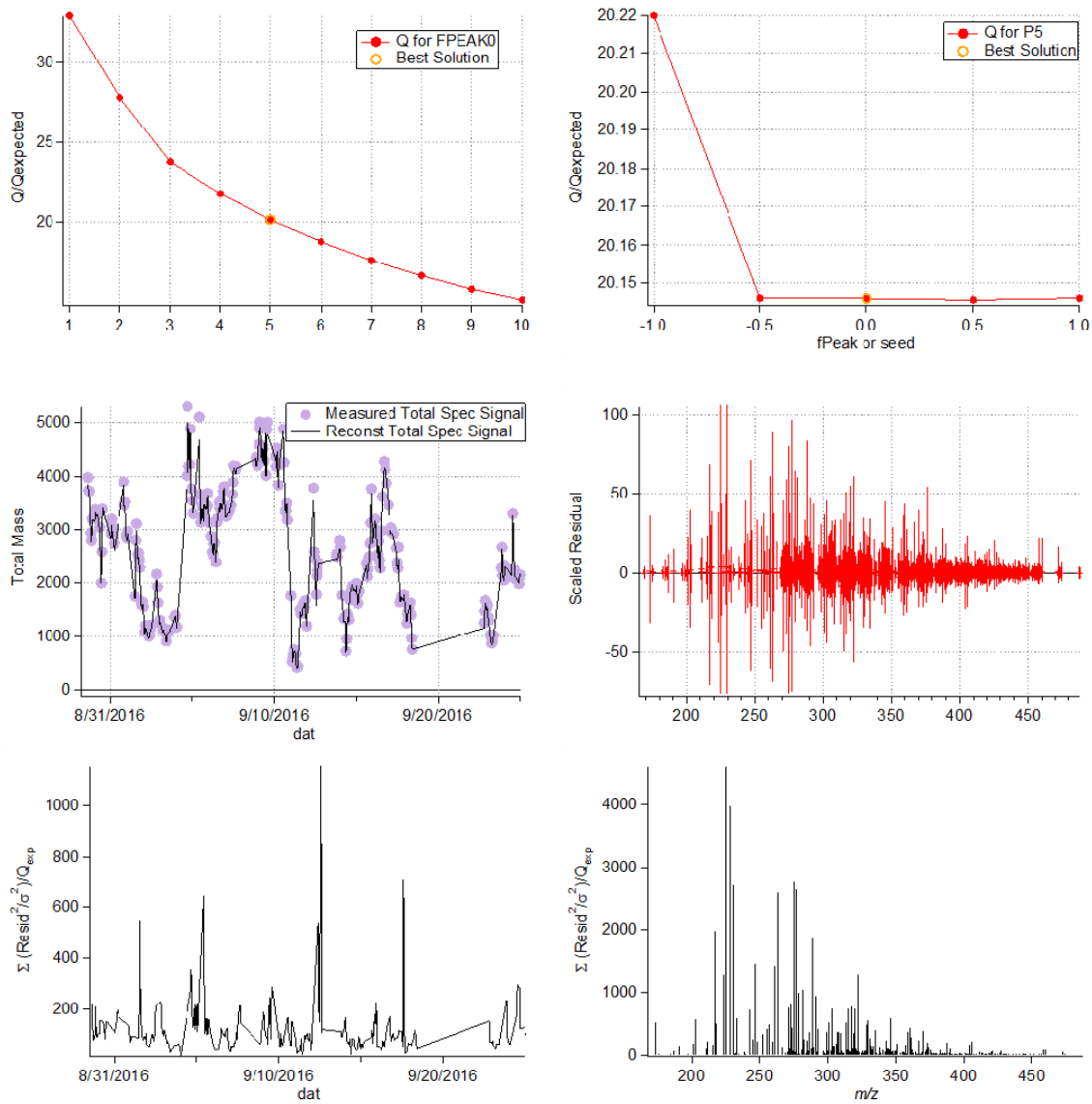


Figure 2-10 Diagnostic plots of PMF analysis on FIGAERO-CIMS measurements.

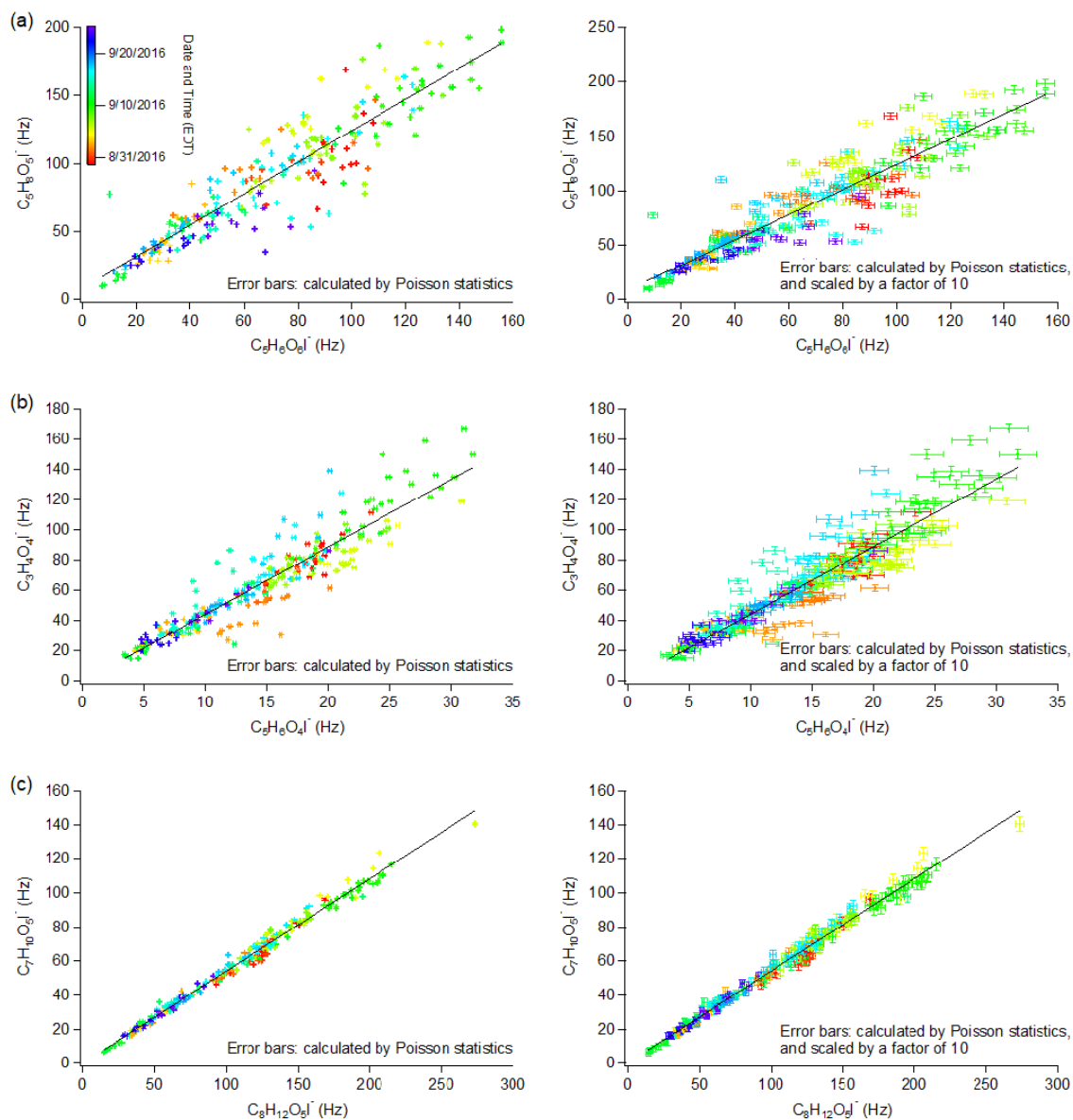


Figure 2-11 Scatter plots of pairs of highly-correlated ions, error bars representing estimated errors by simple Poisson statistics (left column) and after scaling by a factor of 10 (right column).

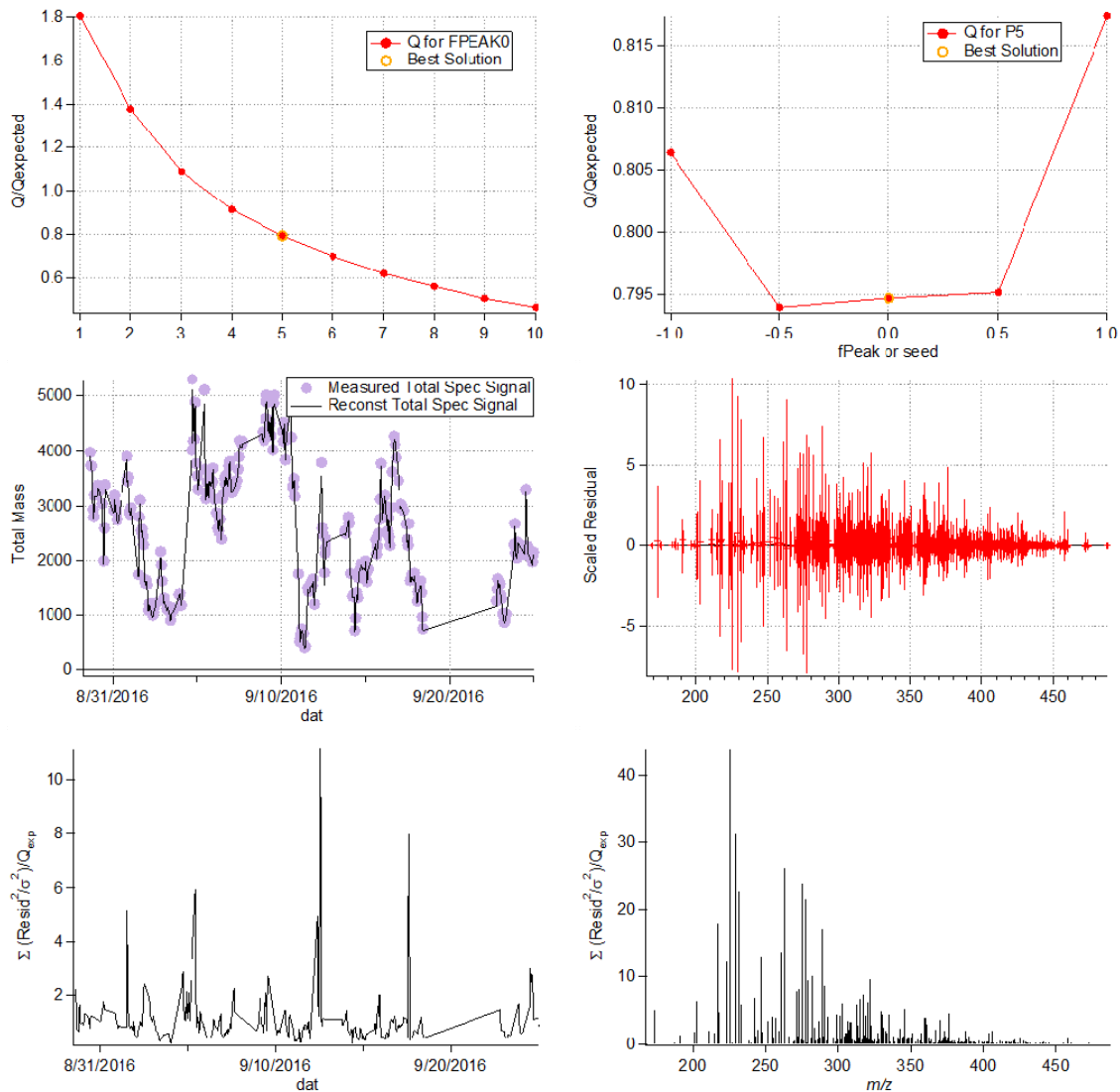


Figure 2-12 Diagnostic plots of PMF analysis on FIGAERO-CIMS measurements. Note that the input errors estimated from Poisson estimates were increased by a factor of 10 when performing PMF analysis.

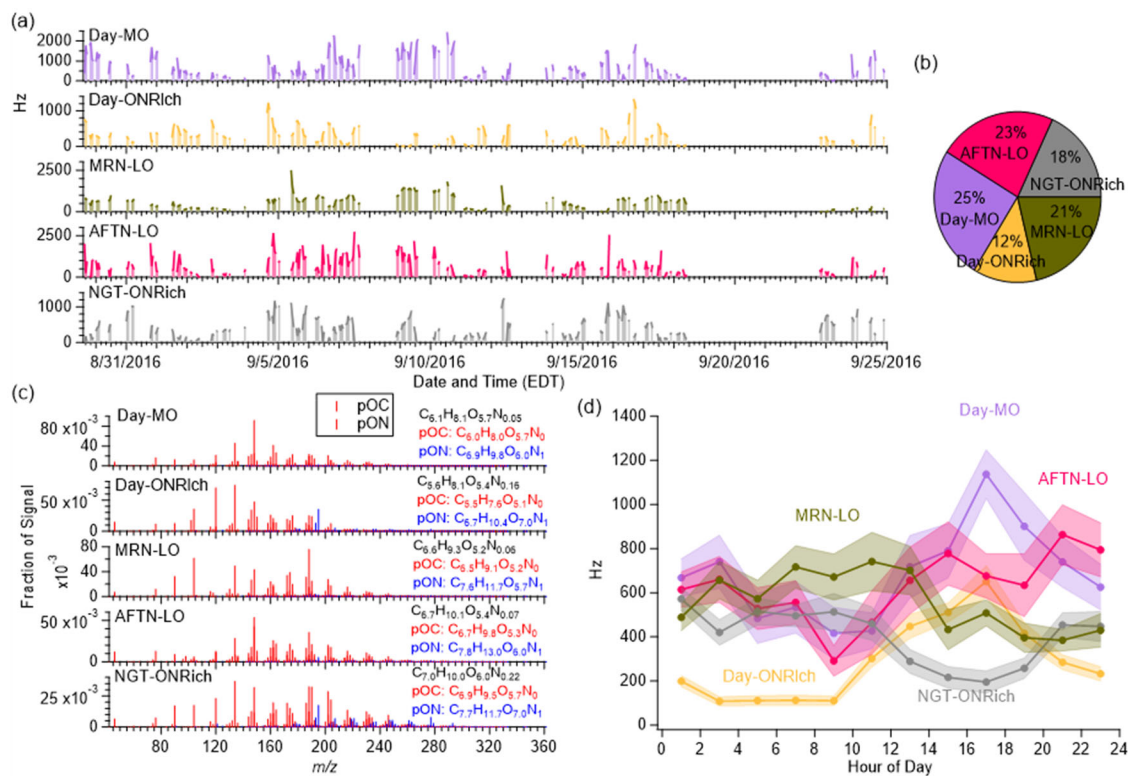


Figure 2-13 (a) Time series, and study mean (b) fraction, (c) normalized mass spectra, and (d) diurnal profiles (standard deviations in shaded areas) of FIGAERO OA factors resolved by PMF.

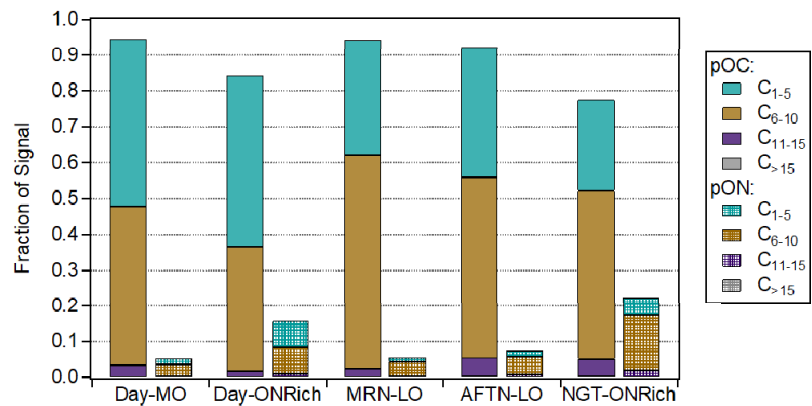


Figure 2-14 Fraction of pOC and pON ions of different carbon numbers (grouped as C₁₋₅, C₆₋₁₀, C₁₁₋₁₅, and C_{>15}) in each FIGAERO OA factor.

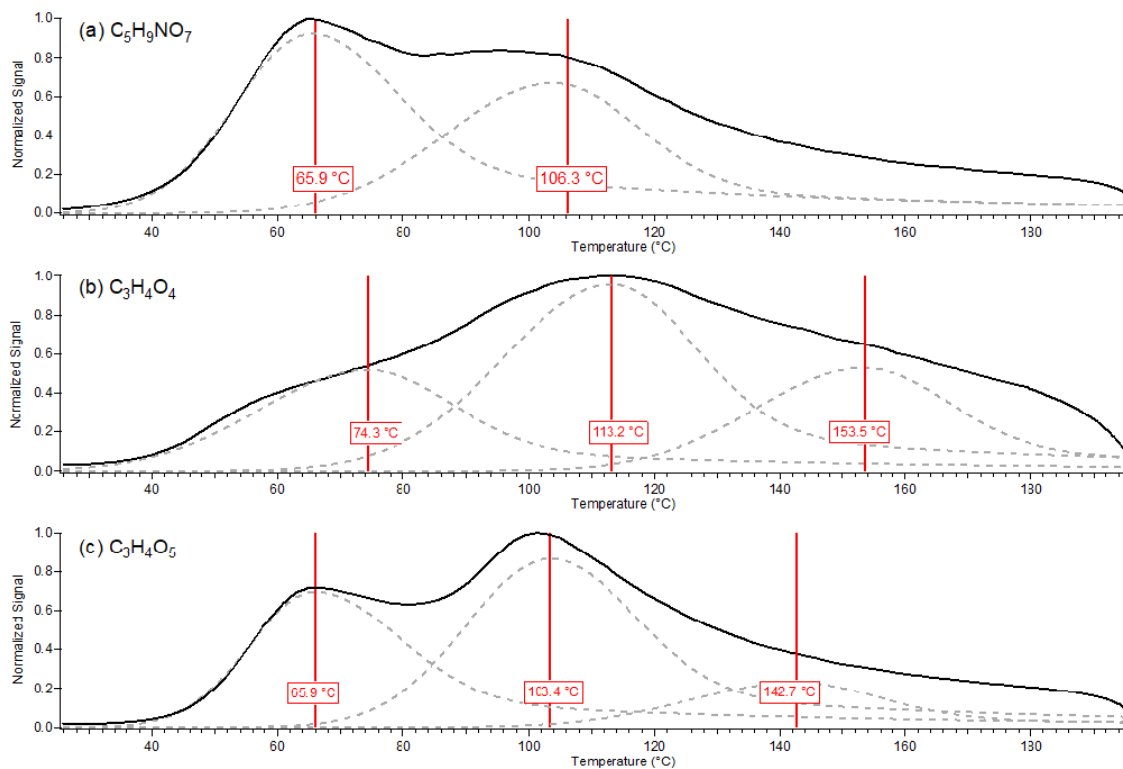


Figure 2-15 Thermograms of (a) $C_5H_9NO_7$, (b) $C_3H_4O_5$, and (c) $C_3H_4O_4$ ions measured by FIGAERO-CIMS.

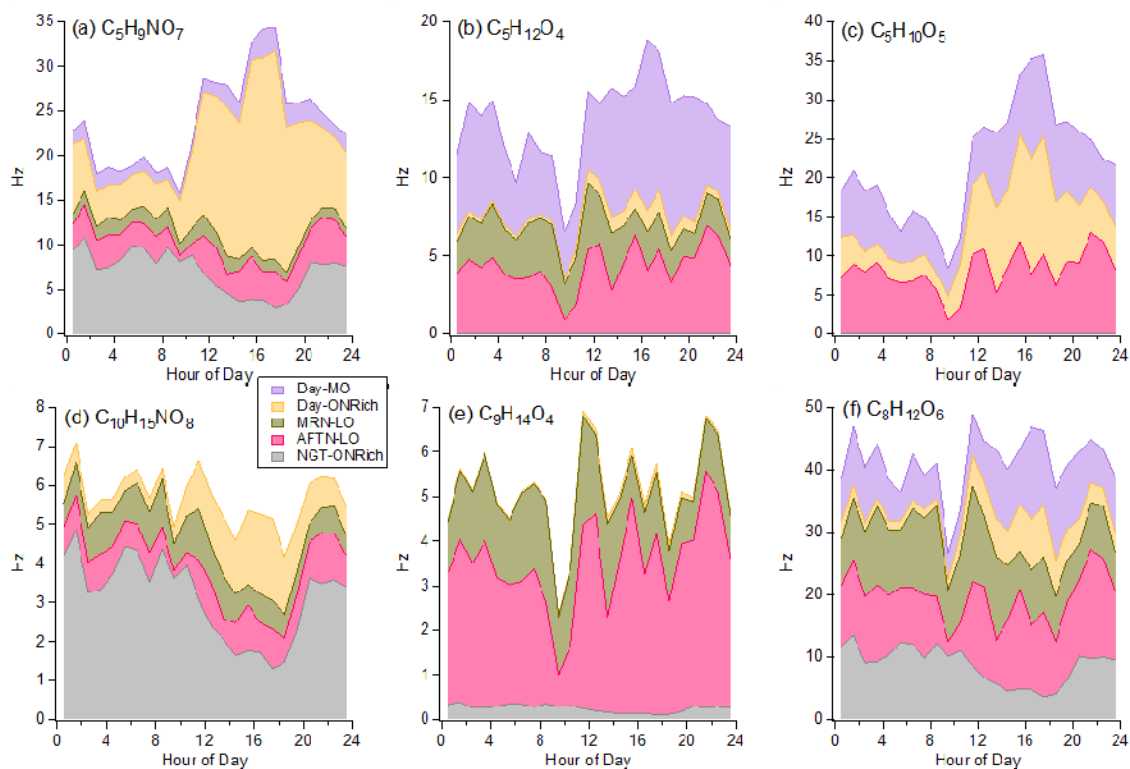


Figure 2-16 Diurnal data of selected tracer species for isoprene and monoterpene SOA. (a) $C_5H_9NO_7$ (isoprene+ $NO_3\cdot$, isoprene+ $OH\cdot$ + NO_x); (b) $C_5H_{12}O_4$ (isoprene+ $OH\cdot$, IEPOX uptake); (c) $C_5H_{10}O_5$ (isoprene+ $OH\cdot$, non-IEPOX pathway); (d) $C_{10}H_{15}NO_8$ (α -/ β -pinene+ $NO_3\cdot$, α -/ β -pinene+ $OH\cdot$ + NO_x); (e) $C_9H_{14}O_4$ (fresh monoterpene SOA); (f) $C_8H_{12}O_6$ (aged monoterpene SOA).

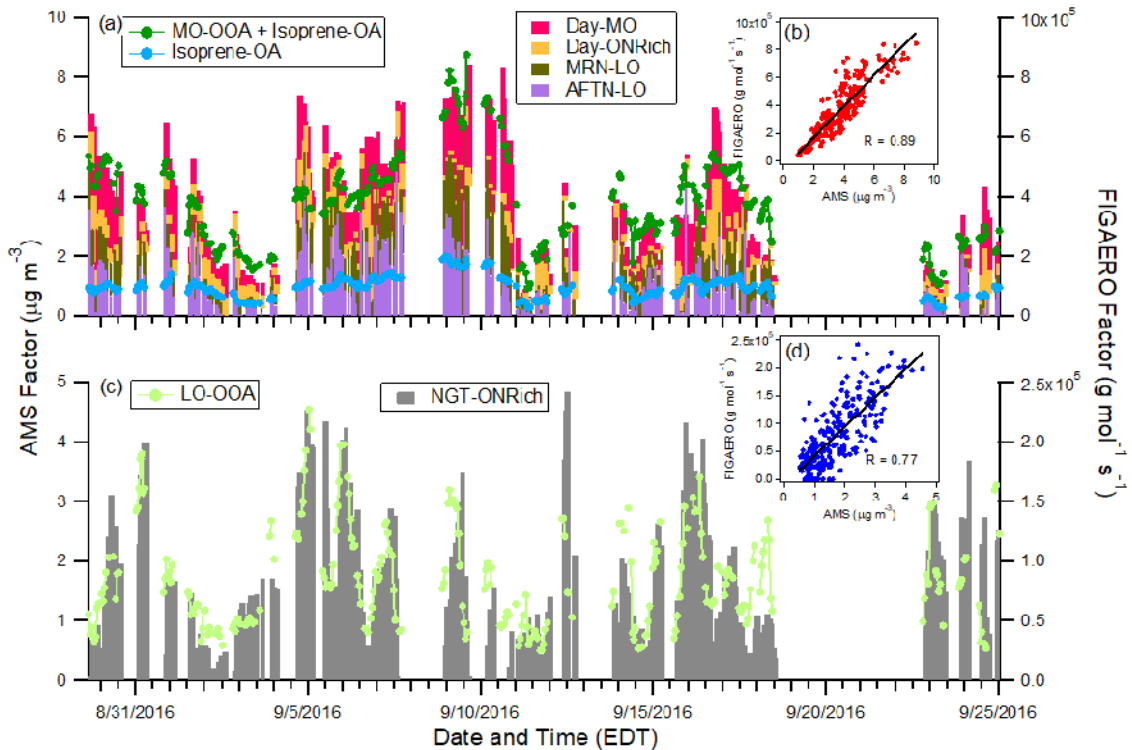


Figure 2-17 Comparison between AMS daytime factors and FIGAERO-CIMS daytime factors ((a), (b)), and AMS nighttime factor and FIGAERO-CIMS nighttime factor ((c), (d)).

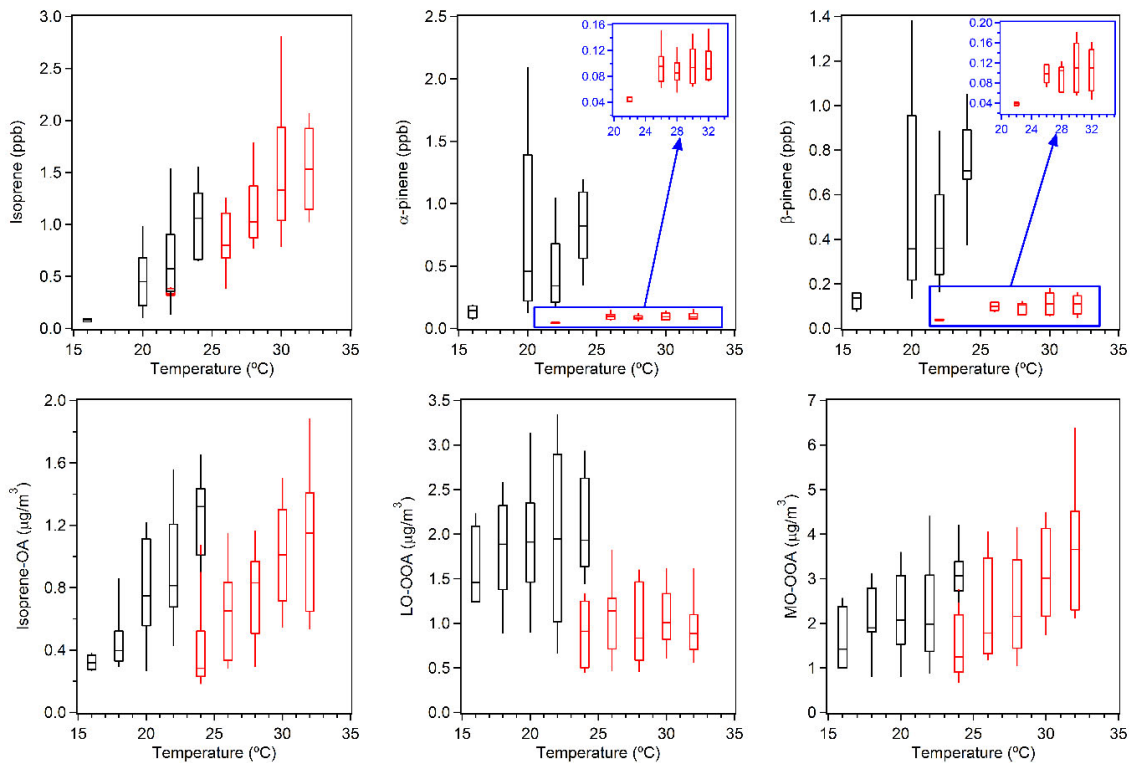


Figure 2-18 Main biogenic VOC and AMS factor concentrations as a function of temperature. The data points are grouped in temperature bins of 2 °C increment and colored by time of day, where afternoon (12:00 – 16:00) measurements are in red and night (00:00 – 04:00) measurements are in black. The mid-point line, lower and upper boxes, lower and upper whiskers, represent median, 25th percentiles, 75th percentiles, 10th percentiles, and 90th percentiles, respectively.

CHAPTER 3. LOW-MOLECULAR-WEIGHT ORGANIC ACIDS IN THE SOUTHEASTERN U. S.: FORMATION, PARTITIONING, AND IMPLICATIONS FOR ORGANIC AEROSOL AGING

3.1 Background

Organic acids are ubiquitous atmospheric components in the lower troposphere, abundant in both particle and gas phases. They are major contributors of atmospheric acidity in unpolluted areas (Keene and Galloway, 1984), and can play a critical role on aerosol chemistry through their effects on particle acidity (Millet et al., 2015) or by directly participating in particle-phase reactions (e.g. esterification) to form low volatile compounds. Organic acids are also known to be sinks for hydroxyl radical and stabilized Criegee intermediates (SCI) (Jacob, 1986), and thus affect atmospheric radical budgets. Sources of organic acids include direct emissions from terrestrial vegetation, soil, biomass burning, secondary photochemical production, and aqueous phase chemistry (Chebbi and Carlier, 1996; Khare et al., 1999; Sorooshian et al., 2007; Paulot et al., 2011; Millet et al., 2015; Malecha and Nizkorodov, 2016). Generally, formic and acetic acids are the most dominant organic acids in the gas phase, while the most abundant organic acids in the particle phase are normally oxalic acid followed by succinic and/or malonic acids (Chebbi and Carlier, 1996; Kawamura and Bikkina, 2016). Dicarboxylic acids generally have vapor pressures lower by a factor of 10^2 to 10^4 than that of corresponding monocarboxylic acids (Chebbi and Carlier, 1996), and are dominantly present in the particle phase.

The high-resolution time-of-flight aerosol mass spectrometer (HR-ToF-AMS, Aerodyne; henceforth referred to as AMS) (DeCarlo et al., 2006;Canagaratna et al., 2007) is a widely-used, sensitive, online instrument for quantitative characterization of submicron non-refractory (NR-PM₁) aerosol composition. In the AMS, the carboxylic acids can undergo decarboxylation processes and produce high intensity of CO₂⁺ (*m/z* 44) ion, which is the most reliable marker of oxygenated organic aerosol (Takegawa et al., 2007;Canagaratna et al., 2015). Through source apportionment analysis, e.g., multiple component analysis (Zhang et al., 2007a) and positive matrix factorization (PMF) (Ulbrich et al., 2009;Canonaco et al., 2013), AMS OA can be further deconvolved to different subgroups. One of a ubiquitously resolved subgroup, more-oxidized oxygenated OA (MO-OOA) (Jimenez et al., 2009;Ng et al., 2010;Cubison et al., 2011;Setyan et al., 2012;Xu et al., 2015a;Hu et al., 2015), or low-volatility oxygenated OA (LV-OOA) in some studies (Jimenez et al., 2009;Ng et al., 2010), is characterized by high *f*_{CO₂⁺} in AMS spectra. MO-OOA is normally interpreted as a surrogate for aged SOA (Zhang et al., 2011). Different theories regarding MO-OOA sources have been proposed (which are not mutually exclusive), including photochemical aging of fresh OA (Jimenez et al., 2009;Ng et al., 2010;Bougiatioti et al., 2014), aqueous processes (Xu et al., 2017b), formation of highly oxygenated molecules (HOMs) (Ehn et al., 2014), long-range transport (Hayes et al., 2013), and entrainment of aged SOA from the residual layer (Nagori et al., 2019).

A two-month field study has been conducted in Yorkville, Georgia, US, in fall 2016, with a set of state-of-art instruments deployed for comprehensive gas and aerosol measurements of organic species, as well as speciated measurements of low-molecular-weight organic acids (LMWOA) in both particle and gas phases. Related work from the

same campaign have been published elsewhere (Nah et al., 2018b; Nah et al., 2018a). In this study, we focus on understanding the sources and the determinant partitioning mechanisms for different LMWOA. In the following discussions, LMWOA will specifically refer to formic, acetic, oxalic, malonic, and succinic acids that were measured at Yorkville in this study. They are often the most abundant LMWOA in the lower troposphere. Meanwhile, through the links between LMWOA and MO-OOA, we aim to provide more insights into MO-OOA sources and organic aerosol aging pathways in the southeastern United States.

3.2 Methods

3.2.1 Site Description

The ambient measurements took place from mid-August to mid-October 2016 at the South Eastern Aerosol Research and Characterization (SEARCH) field site at Yorkville, Georgia (33.92833 N, 85.04555 W, 394 masl). The Yorkville site was approximately 55 km northwest of Atlanta, immediately surrounded by forests and agricultural land. All instruments were housed in an air-conditioned trailer. The sampling period of this study concurred with a transition from warmer to colder season, with moderate temperature (24.0 ± 4.0 °C, average \pm SE if not specified hereafter), high RH (68.9 ± 17.9 %). Isoprene was the most abundant volatile organic compounds (VOC, 1.21 ± 1.08 ppb), followed by propane (0.84 ± 0.39 ppb), α -pinene (0.37 ± 0.40 ppb), and β -pinene (0.32 ± 0.29 ppb), making biogenic VOC the predominant OA precursors at Yorkville. A clear decreasing trend was observed for isoprene as temperature decreased

throughout the campaign, which is consistent with the seasonal variation of isoprene emission (Seinfeld and Pandis, 2016).

3.2.2 Instrumentation

A Particle-into-Liquid Sampler was connected to a Dionex ICS-4000 capillary high-pressure ion chromatography (HPIC) system to measure water-soluble organic acids in the particle phase (Nah et al., 2018a), while another PILS was connected to two Dionex ICS-1500 ICs (Thermo Fisher Scientific) for the measurement of water soluble inorganic cation and anions. A custom-built quadrupole chemical ionization mass spectrometer (Q-CIMS) using sulfur hexafluoride ions (SF_6^-) as reagent ions was used to measure organic acids in the gas phase (Nah et al., 2018a; Nah et al., 2018b). An AMS (Aerodyne) was used to characterize the composition of NR- PM_{10} . A detailed description of AMS can be found in DeCarlo et al. (2006) and Canagaratna et al. (2007) A High Resolution Time-of-Flight Iodide-Adduct Chemical Ionization Mass Spectrometer coupled with a Filter Inlet for Gases and AEROsols (FIGAERO-HR-ToF-I-CIMS, Thun and Aerodyne, henceforth referred to as the FIGAERO-CIMS) was used to characterize both particle- (PM_{10}) and gas-phase multifunctional species. A detailed description of FIGAERO-CIMS can be found in Lopez-Hilfiker et al. (2014) while a detailed description of the iodide ionization mechanisms can be found in Huey et al. (1995) and Lee et al. (2014) Other co-located instruments included a gas chromatography-flame ionization detector (GC-FID) with a Markes focusing trap to measure hourly resolved VOC, and a chemiluminescence monitor to measure NO and NO_2 .

3.2.3 OA Source Apportionment Analysis

A widely used source apportionment method, multilinear engine (ME-2) algorithm, were used to deconvolve OA measured by FIGAERO-CIMS and AMS. The ME-2 solver is based on the least-squares approach based on a receptor-only multivariate factor analytic model to solve bilinear unmixing problems, which deconvolves the observed data matrix as a linear combination of various factors with constant mass spectra but varying concentrations across the dataset (Lanz et al., 2007;Ulbrich et al., 2009;Jimenez et al., 2009;Ng et al., 2010;Zhang et al., 2011). The ME-2 solver also allows users to introduce *a priori* information, in the form of a known factor time series and/or a factor profile, as inputs to the model to constrain the solution (Canonaco et al., 2013). In this study, we performed ME-2 analysis on AMS OA dataset with a fixed Isoprene-OA factor profile constrained. Details about source apportionment analysis for AMS OA can be found in Chen et al. (2020) Three OA factors have been resolved, isoprene-derived OA (Isoprene-OA), less-oxidized oxygenated OA (LO-OOA), and more-oxidized oxygenated OA (MO-OOA), indicating secondary formation from biogenic precursors was the most important OA source at Yorkville during the studied period. The MO-OOA factor, characterized by high f_{CO_2+} and a wide afternoon peak, was the most dominant factor that accounted for half of OA mass (50 ± 13 %). As a result, total OA concentration showed a good correlation with MO-OOA ($R^2 = 0.80$).

3.2.4 Liquid Water Content (LWC) and pH Calculation

The water uptake by inorganic species (W_i) and pH was calculated by ISORROPIA-II, (Fountoukis and Nenes, 2007) and details regarding the calculation can

be found in (Nah et al., 2018a). Hygroscopicity measurements for organic species were not available, a hygroscopic parameter (κ_{org}) of 0.126 (a typical value for biogenic SOA dominating rural southeastern United States (Guo et al., 2015)) was used for the calculation of water uptake by organic species (W_o). The results showed that W_o and W_i were correlated (Figure 3-1). In following discussions, ($W_o + W_i$) will be used as the LWC surrogate.

3.3 Results and Discussion

3.3.1 Overview of LMWOA Measured at Yorkville

The particle-phase (p), gas-phase (g), and both-phase (p+g) concentration time series and diurnal profiles of each LMWOA were shown in Figure 3-2 and Figure 3-3. Campaign-average concentrations of each LMWOA were listed in Table 3-1. Both-phase concentration was calculated as the summation of particle- and gas-phase concentrations. The most abundant LMWOA in the particle phase was oxalic acid ($74 \pm 48 \text{ ng m}^{-3}$, in the form of oxalate), followed by acetic ($64 \pm 25 \text{ ng m}^{-3}$, in the form of acetate), formic ($50 \pm 26 \text{ ng m}^{-3}$, in the form of formate), succinic ($48 \pm 27 \text{ ng m}^{-3}$, in the form of succinate), and malonic ($11 \pm 11 \text{ ng m}^{-3}$, in the form of malonate) acids. The most abundant LMWOA in the gas phase was formic acid ($2150 \pm 160 \text{ ng m}^{-3}$), followed by acetic ($1860 \pm 1340 \text{ ng m}^{-3}$), oxalic ($28 \pm 19 \text{ ng m}^{-3}$), succinic ($18 \pm 13 \text{ ng m}^{-3}$), and malonic ($5 \pm 3 \text{ ng m}^{-3}$) acids. An afternoon enhancement was observed for all five LMWOA, but the enhancement was less significant for particle-phase concentrations compared to their gas-phase counterparts. Higher temperature and lower aerosol pH in the afternoon (Figure 3-4), could account for some of this by suppressing gas-to-particle partitioning at that time. All five LMWOA gas-

phase and both-phase concentrations started to increase at ~08:00 and reached peak at ~20:00. The trends followed that of odd oxygen ($O_x = O_3 + NO_2$), a tracer of photochemical processing (Herndon et al., 2008), linking LMWOA to photochemical secondary formation. Compared to other LMWOA, acetic acid showed a higher rate of increasing from 18:00 to 20:00 and ended up with a more pronounced evening maximum, which was different from the smooth afternoon peaks observed for the rest LMWOA (Figure 3-3). Formic-to-acetic (FA / AA) ratio has been used to distinguish primary and secondary sources (Talbot et al., 1988;Khare et al., 1999), where a higher FA / AA ratio normally suggests secondary formation and a lower FA / AA ratio implies primary emissions. The greater-than-unit FA / AA ratio (1.56 ± 0.52) observed at Yorkville was comparable to previous studies (Talbot et al., 1988;Talbot et al., 1995;Khare et al., 1999;Millet et al., 2015;Baasandorj et al., 2015), which indicated secondary production predominated over primary emissions. Meanwhile, as a result of different diurnal patterns of formic and acetic acids, FA / AA ratio was the highest and also relatively constant from 10:00 to 18:00, but dropped suddenly from 18:00 to 20:00 (Figure 3-5 (a)), implying that primary sources, either from nearby agricultural emissions or traffic emissions from nearby roads, may be temporarily important in the evening.

3.3.2 Possible Secondary Formation Mechanisms of Different LMWOA

Both-phase concentrations, which were not affected by partitioning, were used to investigate the sources and formation pathways of LMWOA. Extraordinarily strong correlations were observed for oxalic, malonic, and succinic acids ($R^2 = 0.87-0.96$, Table 3-2), implying three LMW dicarboxylic acids likely formed simultaneously. The correlation between formic and acetic acids was not as strong as that between dicarboxylic

acids ($R^2 = 0.66$, Table 3-2). The correlation between acetic and dicarboxylic acids were even less significant ($R^2 = 0.41-0.47$, Table 3-2). The weaker correlation between acetic acid with the rest LMWOA was likely due to a larger contribution to acetic acid from primary sources as discussed above. Correlations between formic and dicarboxylic acids were also remarkable ($R^2 = 0.67-0.69$, Table 3-2), suggesting their secondary formation was from similar precursors or controlled by similar parameters.

How different processes affect LMWOA formation was explored by using O_x as a tracer of photochemical processing and LWC and $f(LWC)$ ($f(LWC) = LWC / (LWC + OA + sulfate + ammonium + nitrate)$) to track aqueous processing. Three dicarboxylic acids were highly correlated and thus categorized as one group. All LMWOA correlated positively with O_x , and considering all LMWOA both-phase concentrations were enhanced in the afternoon when the photochemical reactions were the strongest (Figure 3-3 and Figure 3-4), photochemical processing was undoubtedly a dominant source of LMWOA. Meanwhile, the dependence of formic and acetic acids on O_x were stronger compared to three LMW dicarboxylic acids (Figure 3-6). When it comes to aqueous processing, formic and acetic acids were clearly negatively correlated with LWC and $f(LWC)$, while LMW dicarboxylic acids showed little trend (Figure 3-6). The negative correlation between LMW monocarboxylic acids with LWC and $f(LWC)$ was probably due to the opposite diurnal profiles of LWC to that of O_x (Figure 3-4). O_x mixing ratio reached its nadir in the early morning at ~07:00, and started to increase soon after sunrise, peaking at ~18:00. LWC and relative humidity (RH) showed almost opposite trends, reaching peak at ~07:00 and nadir in the late afternoon. Since formic and acetic acids strongly dependent on atmospheric oxidant concentrations and photochemistry intensity, their time variations followed O_x and

thus opposite to LWC. LMW dicarboxylic acids, however, may form comparably through both photochemical and aqueous processing (which can happen both day and night), given their positive correlation with O_x but different dependences on LWC compared to formic and acetic acids. As a result, the both-phase fraction of LMW dicarboxylic acids (oxalic + malonic + succinic) in total LMWOA (formic + acetic + oxalic + malonic + succinic) evidently decreased with O_x and increased with LWC and $f(\text{LWC})$ (Figure 3-6). While we cannot rule out aqueous processing as an effective source for formic and acetic acids, it is clearly more important for oxalic, malonic, and succinic acid formation. Moreover, the both-phase fraction of LMW dicarboxylic acids was enhanced at night, peaking at ~08:00 (Figure 3-5(b)), suggesting appreciable LMW dicarboxylic acids nighttime formation, probably through aqueous processing (Altieri et al., 2008), which is not shared by LMW monocarboxylic acids.

Previous studies from the same campaign showed that isoprene and monoterpenes (α -pinene, β -pinene, and limonene) were the predominant SOA precursors at Yorkville during this season (Chen et al., 2020), and hence their connections to LMWOA were also investigated. A series of isoprene and monoterpene oxidation products was selected to represent different pathways and reaction generations. All tracer species were measured by FIGAERO-CIMS as clusters adducted to one iodide ion and in the unit of counts per second (Hz). The both-phase concentration was used for comparison, where particle-phase signals were integrations over the whole thermal desorption process, with sampling time and flow rate applied. For isoprene, the OH-initiated oxidation produces hydroxy hydroperoxide (ISOPOOH) and isoprene epoxydiols (IEPOX) under HO_2 -dominated conditions,^{37, 38} methacrylic acid epoxide (MAE) and hydroxymethyl-methyl-lactone (HMML) under NO-

dominated conditions (Nguyen et al., 2015a). $C_5H_{10}O_3I^-$, likely corresponding to both ISOPOOH and IEPOX, was selected to represent early-generation isoprene products under HO_2 -dominated conditions, and $C_4H_6O_3I^-$, likely corresponding to both MAE and HMML, was selected to represent early-generation isoprene products under NO-dominated conditions. IEPOX can undergo reactive uptake onto wet acidic aerosols, and produce 2-methyltetrol (2-MT) (Surratt et al., 2010; Lin et al., 2012; Hu et al., 2015; Paulot et al., 2009b), while HMML can form 2-methylglyceric acid (2-MGA) in the particle phase (Lin et al., 2013). $C_5H_{12}O_4I^-$, likely corresponding to 2-MT, and $C_4H_8O_4I^-$, likely corresponding to 2-MGA, were used to represent the two pathways. Besides IEPOX uptake, ISOPOOH can form SOA effectively through isomeric ISOPOOH, and $C_5H_{10}O_5I^-$ was selected as its tracer (Krechmer et al., 2015; D'Ambro et al., 2017; Liu et al., 2016). For monoterpenes, pinic acid ($C_9H_{14}O_4I^-$) (Seinfeld and Pandis, 2016) and 3-methyl-1,2,3-butanetricarboxylic acid (MBTCA, $C_8H_{12}O_6I^-$) (Szmigielski et al., 2007; Zhang et al., 2010b; Müller et al., 2012; Eddingsaas et al., 2012a) were used as fresh and aged monoterpene SOA tracers, respectively.

Formic acid showed strong correlation with MAE+HMML ($R^2 = 0.76$, Table 3-2) and ISOPOOH+IEPOX ($R^2 = 0.69$, Table 3-2), linking its formation to isoprene oxidation, especially under NO-dominated conditions. Acetic acid also correlated the best with MAE+HMML ($R^2 = 0.30$, Table 3-2) and ISOPOOH+IEPOX ($R^2 = 0.30$, Table 3-2) compared to other tracers, but the correlations were not as strong as formic acid, since primary emissions had a greater contribution to acetic acid than to formic acid as discussed above. Both MAE+HMML and ISOPOOH+IEPOX are early-generation gas-phase photochemical products of isoprene, implying that formic acid and secondary acetic acid

were photochemically and rapidly produced in the lower troposphere through gas-phase reactions. The observations were consistent with previous modeling study that photochemical production from biogenic precursors, particularly isoprene, was the largest source of formic and acetic acids (Paulot et al., 2011). For LMW dicarboxylic acids, their strong correlations with 2-MT ($R^2 = 0.71-0.80$, Table 3-2) stood out, while remarkable correlations were also observed for MBTCA ($R^2 = 0.64-0.68$, Table 3-2) and 2-MGA ($R^2 = 0.59-0.67$, Table 3-2). 2-MT and 2-MGA are derived from isoprene photooxidation and formed in the particle phase. Compared to formic and acetic acids which correlated the best with isoprene gas-phase oxidation products, the observations that LMW dicarboxylic acids were more associated with condensed-phase processing could to some extent explain why LWC had a greater impact on them than on formic and acetic acids. Previous studies have shown that aqueous processing of isoprene oxidation products, centering glyoxal, methylglyoxal, and pyruvic acid, lead to the formation of C₁ and C₂ organic acids including formic, acetic, and oxalic acids (Lim et al., 2005;Carlton et al., 2006b;Ervens et al., 2008;Paulot et al., 2009a;Perri et al., 2009;Nguyen et al., 2010;Carlton et al., 2006a). The formation pathways of larger organic acids, i.e. malonic and succinic acids, have not been fully explored yet to the best of our knowledge, but their formation has been observed in aqueous oxidation of intermediate isoprene oxidation products glycolaldehyde, methylglyoxal, and methyl vinyl ketone (Perri et al., 2009;Zhang et al., 2010a;Tan et al., 2012). Studies have shown that succinic acid can be formed in the aqueous phase from lower MW compounds, e.g. through esterification of smaller organic acids or radical-radical reactions (Wang et al., 2001;Altieri et al., 2008;Tan et al., 2012). Some of the reactions (e.g. esterification) can happen under dark conditions, pointing to nighttime

dicarboxylic acid formation. MBTCA was proposed as an aged monoterpene SOA tracer forming through gas-phase OH-initiated oxidation of pinonic acid (Zhang et al., 2010b; Müller et al., 2012). Due to its low volatility and high water-solubility, MBTCA tends to condense onto existing particles or partition into aerosol liquid water right after its formation (Müller et al., 2012; Aljawhary et al., 2016). In this study, a campaign-average particle-phase fraction of > 99.99% was observed for $C_8H_{12}O_6I^-$ ion through FIGAERO-CIMS measurements. Zhang et al. (2010b) have shown that the OH-initiated oxidation of pinonic acid is the rate-limiting step in the formation of MBTCA, and thus MBTCA may be a suitable tracer for photochemical aging initiated by hydroxyl radicals. LMW dicarboxylic acids, especially oxalic acid, have been suggested as an aqueous processing proxy. (Chebbi and Carlier, 1996; Ervens et al., 2011) We also mentioned above that their formation was more dependent on LWC abundance than LMW monocarboxylic acids. It is interesting that MBTCA, whose formation is independent of aerosol water, was closely correlated with these LMW dicarboxylic acids. While the mechanism has not been well explored, the photochemical degradation of larger organic acids like MBTCA may lead to the formation of LMWOA. Aljawhary et al. (2016) have shown that the aqueous phase OH-initiated oxidation of MBTCA produced LMWOA including oxalic and malonic acids. The good correlation between MBTCA and LMW dicarboxylic acids seen in our data is consistent with MBTCA residing in the LWC-rich phase, participating in aqueous processing and forming LMWOA.

While the correlations between LMWOA and biogenic SOA tracers implied isoprene to be the most important precursors for all LMWOA for the studied period, mono- and di-carboxylic acids responded differently to the instantaneous isoprene mixing ratio.

At lower isoprene abundance, both-phase LMW dicarboxylic acids accounted for a larger fraction of both-phase LMWOA (Figure 3-7). This shift was also favored under high LWC. One possible reason is the different time scale of mono- and di-carboxylic acid formation from isoprene. As discussed in the last section, formic and secondary acetic acids were likely formed rapidly through isoprene photooxidation, while the formation of LMW dicarboxylic acids, through aqueous reactions or even cloud-processing of later-generation product of isoprene oxidation, may take a longer time. Moreover, LMW dicarboxylic acids may have a greater variety of precursors than LMW monocarboxylic acids, e.g. through aqueous oxidation of monoterpene-derived products as discussed above, which also make them less dependent on isoprene availability.

3.3.3 Unexpectedly High Particle-Phase Fraction of LMW Monocarboxylic Acids and Possible Explanations

In a previous publication from the same campaign, Nah et al. (2018a) used thermodynamic models to explain the measured LMWOA gas-particle partitioning. While the measured oxalic acid gas-particle partitioning was in good agreement with the model prediction, the observed particle-phase fraction of formic and acetic acid concentrations were magnitudes higher than predictions. Figure 3-8(a) and (c) were adapted from Nah et al. (2018a) showing particle-phase fraction of formic (in the form of formate) and acetic (in the form of acetate) acids from measurements and ISORROPIA-II predictions as a function of aerosol pH. $\epsilon(\text{HCOO}^-)$ and $\epsilon(\text{CH}_3\text{COO}^-)$ are defined as the particle-phase molar concentration divided by the both-phase molar concentration. While the $\epsilon(\text{HCOO}^-)$ and $\epsilon(\text{CH}_3\text{COO}^-)$ were significantly underpredicted in the model, the largest deviations from predictions concurred with the lowest both-phase concentrations of formic and acetic acids.

When both-phase concentrations of formic and acetic acids were high, $\epsilon(\text{HCOO}^-)$ and $\epsilon(\text{CH}_3\text{COO}^-)$ tended to approach predictions. Similar trends were not observed for oxalic acid (Figure 3-9). Extremely high $\epsilon(\text{HCOO}^-)$ and $\epsilon(\text{CH}_3\text{COO}^-)$ only happened when formic and acetic acid both-phase concentrations were lower than $\sim 1 \mu\text{g m}^{-3}$, $\sim 10\%$ of their highest values. In addition, the high $\epsilon(\text{HCOO}^-)$ and $\epsilon(\text{CH}_3\text{COO}^-)$ also coincided with low isoprene abundance (Figure 3-8(b) and (d)), which was the major precursor of formic and secondary acetic acids based on our previous discussions. Therefore, the observed high $\epsilon(\text{HCOO}^-)$ and $\epsilon(\text{CH}_3\text{COO}^-)$ were possibly a combined result of decreasing local formation of formic and acetic acids due to the lack of precursors, and the remaining high particle-phase formic and acetic acid concentrations. In last section we showed that instantaneous isoprene mixing ratio had a larger impact on mono- than di-carboxylic acids, and a higher isoprene mixing ratio normally led to a larger both-phase fraction of LMW monocarboxylic acids in total LMWOA (Figure 3-7). In the particle phase, however, an opposite trend was observed that monocarboxylic acids accounted for a larger fraction of total particulate LMWOA when isoprene was less abundant (Figure 3-10). Since on average $> 95\%$ of formic and acetic acids resided in the gas phase, the good correlations between their both-phase concentrations with ISOPOOH+IEPOX and MAE+HMML were likely dominated by their gas-phase concentrations. Taken together, particle-phase formic and acetic acids seemed quite independent from the assumed precursor isoprene, and establishing no noticeable equilibrium with their gas-phase counterparts.

Water-soluble nonvolatile cations (NVC, e.g. Na^+ , K^+ , Mg^{2+} , Ca^{2+}), which generally present in larger quantities in coarse mode and to a lesser extent in fine mode, were also found to coexist with organic acids in previous studies (Lee et al.,

2002;Falkovich et al., 2004;Sullivan and Prather, 2007;Takahama et al., 2010). In particular, Lee et al. (2002) showed that 95% of mineral dust particles contained water-soluble organic acids in Atlanta based on single particle measurements. The formation of low-volatility organic acid salts with water-soluble NVC could be a possible explanation for particle-phase formate and acetate. In Figure 3-10, we colored the data points by NVC / LMWOA charge ratio, which was calculated as $([Na^+] + [K^+] + 2[Mg^{2+}] + 2[Ca^{2+}]) / ([HCOO^-] + [CH_3COO^-] + 2[C_2O_4^{2-}] + 2[CH_2(COO)_2^{2-}] + 2[C_2H_4(COO)_2^{2-}])$, and found that the higher fraction of LMW monocarboxylic acids in LMWOA in the particle phase concurred with higher NVC / LMWOA charge ratio. As NVC had no known local sources and was more likely transported from elsewhere, combined with the fact that a higher particle-phase fraction of LMW monocarboxylic acids in total LMWOA was also associated with lower isoprene emissions, we tentatively proposed that particle-phase formic and acetic acids were likely components of aged background OA (i.e. OA from long-range transport) and was bounded with NVC. For example, formic and acetic acids can be produced during biomass burning accompanied by abundant NVC (i.e. K^+) (Andreae, 2019), which allows the formation of nonvolatile formate and acetate salts.

3.3.4 *Links between Particulate LMWOA and MO-OOA*

In our previous discussions, we proposed that for formic and acetic acids, the gas and particle phases were largely decoupled; the majority of the gas-phase formic and acetic acids were formed rapidly and in situ through biogenic VOC photooxidation, while their particle-phase counterparts were likely from long-range transport, whereas LMW dicarboxylic acid formation was more related to aqueous chemistry than gas-phase reactions. We also proposed that the LMW monoacids in the gas and particle phases might

rarely interact, while the partitioning of LMW dicarboxylic acids (e.g. oxalic acid) was in thermodynamic equilibrium. In the particle phase, however, LMW monocarboxylic acid and LMW dicarboxylic acid concentrations showed substantially enhanced correlations compared to their both-phase concentrations ($R^2 = 0.41-0.69$ for both-phase concentrations, Table 3-2; $R^2 = 0.65-0.87$ for particle-phase concentrations, Table 3-3). All particulate LMWOA also correlated with total OA ($R^2 = 0.59-0.79$, Table 3-3), but the correlations between LMWOA with MO-OOA factor were noticeably stronger ($R^2 = 0.67-0.89$, Table 3-3). The best correlation was observed between total particulate LMWOA and MO-OOA ($R^2 = 0.90$, Table 3-3 and Figure 3-11). The AMS MO-OOA factor was characterized by high intensity of the CO_2^+ signal, a widely used marker for oxygenated OA. Good correlations between AMS CO_2^+ (or m/z 44) signal with either individual organic acids or ensembles of organic acids have been observed in different studies. (Takegawa et al., 2007; Sorooshian et al., 2010; Yatavelli et al., 2015) Takegawa et al. (2007) showed that oxalic acid is the largest contributor of AMS m/z 44, accounting for $10 \pm 4\%$ of the signal at an urban site at Tokyo. Yatavelli et al. (2015) estimated molecules with carboxylic acid functionality constitute on average 28% (range 10–50%) of northern hemispheric continental OA mass. In this study, we found that the five measured LMWOA accounted for $5.5 \pm 1.1\%$ of OA mass and $10.2 \pm 2.1\%$ of MO-OOA mass.

One thing intriguing is that different chemical reaction formation pathways appear to lead to the same destination. To investigate which process drove the correlations, a box model was constructed for MO-OOA following eq. 3.1 (Seinfeld and Pandis, 2016):

$$\frac{dc_i}{dt} = \frac{1}{H(t)}Q_i + R_i - \frac{1}{H(t)}v_{d_i}c_i + \frac{u}{\Delta x}(c_i^0 - c_i) + \frac{1}{H(t)}\frac{dH}{dt}\Big|_{\frac{dH}{dt}>0}(c_i^a - c_i) \quad (3.1)$$

where $H(t)$ is the boundary layer (BL) height, c_i is the BL concentration of species i , Q_i is the emission rate, R_i is the chemical production and loss rate, and v_{d_i} is the deposition velocity, c_i^0 is the background concentration of species i , c_i^a is the aloft concentration of species i , and u is the wind speed (with constant Δx direction). MO-OOA, as an aged SOA factor, should have no emission sources and, over multiple diel cycles (in this case 7), the net impact of horizontal advection is assumed small. Therefore the emission term and advection term are set to be zero. For the chemical production and loss term, the reaction between fresh SOA (Isoprene-OA and LO-OOA) with hydroxyl radicals is considered as MO-OOA sources, while the reaction between MO-OOA and hydroxyl radicals is considered as MO-OOA sinks. eq. 3.1 can be rewritten as:

$$\frac{d[M000A]}{dt} = (k_1[IsopOA] + k_2[L000A] - k_3[M000A])[OH] - \frac{1}{H(t)} v_{d_M} [M000A] + \frac{1}{H(t)} \frac{dH}{dt} \Big|_{\frac{dH}{dt} > 0} ([M000A]^a - [M000A]) \quad (3.2)$$

where the reaction rates k_1 , k_2 , and k_3 are tentatively set to be 5×10^{-12} , 1×10^{-12} , and $1 \times 10^{-13} \text{ cm}^3 \text{ mol}^{-1} \text{ s}^{-1}$, respectively. k_1 is set to be 5% of the isoprene+OH \cdot reaction, accounting for the volatility of Isoprene-OA. (Kostenidou et al., 2018) This is higher than that derived from Hu et al. (2016), though, as noted by Kostenidou et al. (2018), the volatility and loss of Isoprene-OA was uncertain and Hu et al. (2016) were considering IEPOX alone, so a high value is chosen to capture the maximum likely impact of local chemical formation of MO-OOA. The lifetime of Isoprene-OA using this rate constant is slightly over a day. k_3 is set to be 0.1% of the isoprene+OH \cdot reaction rate, and leads to a loss of about 2% per day, similar to, but more than, Malecha and Nizkorodov (2016). While Kostenidou et al. (2018) found MO-OOA to be relatively volatile than LO-OOA, we assume that the reaction

products are largely in other forms of MO-OOA (i.e. more oxidized components of MO-OOA), thus the net loss is small. k_2 is set to be 1% of the isoprene+OH· reaction rate, which accounts for its volatility, which was less than Isoprene-OA (Kostenidou et al., 2018), and its subsequent reaction to MO-OOA. The model is relatively insensitive to the reaction rates as currently set (particularly k_2 and k_3), and are included to assess the likely importance of local chemistry during a diel cycle. The maximum deposition velocity, v_{dM} , is set to be 0.3 cm s^{-1} , and is scaled by diurnal constraints as described in Nguyen et al. (2015b). The boundary layer heights are derived from the Weather Research and Forecasting model (WRF), and the OH· concentrations are taken from a Community Multiscale Air Quality model (CMAQ) simulation, both to the same period (Gao et al., 2020). The MO-OOA aloft concentration is considered to be a function of altitude, being fit to the observed MO-OOA concentration variation with BL height (Figure 3-12).

The model well captured the observed MO-OOA diurnal trend (Figure 3-13 (a)), and suggested that MO-OOA variation was dominantly driven by BL dynamics and aloft MO-OOA mixing down (Figure 3-13(b)). Given the strong correlations between LMWOA and MO-OOA, similar processes likely dominated particulate LMWOA variation likewise. In our previous discussion we attributed LMW dicarboxylic acids to the oxidation of local biogenic SOA, but as LMW dicarboxylic acids are often end products of photochemical oxidation, their accumulation in background OA was anticipated, if the thermodynamic conditions are right. We have proposed that particulate LMW monocarboxylic acids were likely from transport and part of background OA, to remain in the particle they are either externally mixed with the majority of the bulk PM_{10} (i.e., pH will be too low if internally mixed (Figure 3-10)), or they are stabilized by some other unknown process. For particulate

LMW dicarboxylic acids, though associations were observed between them and fresh SOA tracers, their formation was attributed to aqueous-phase processing, which can happen both in cloud droplets and aerosol water. Cloud processing was suggested to act as a significant source of LMW dicarboxylic acids (Yu et al., 2005;Bikkina et al., 2017;Yao et al., 2002;Ervens et al., 2004). In-cloud formed LMW dicarboxylic acids would mix down with background aged SOA as the BL rises, all the while maintain equilibrium between gas and particle phase component and with the majority of the partitioning favoring the particle phase (Figure 3-9). Taken together, MO-OOA was an ensemble of preexisting aged OA (e.g. from transport) and some contribution of more locally-formed SOA. The strong correlation between MO-OOA and particulate LMWOA is driven by the BL dynamics, but it does not contradict that they were formed from different precursors through different chemical processes.

3.4 Conclusions

In this study, we present real-time measurements of both particle- and gas-phase concentrations for five most commonly abundant low-molecular-weight organic acids (LMWOA) in a rural region in the southeastern United States during 2016 fall. Through comparison with secondary organic aerosol (SOA) tracers, we find that isoprene was the most important local precursor for all five LMWOA, but via different pathways. We propose that monocarboxylic acids (formic and acetic acids) were mainly formed through gas-phase photochemical reactions, while dicarboxylic acids (oxalic, malonic, and succinic acids) were more from aqueous processing. Unexpectedly high concentrations of particle-phase formic and acetic acids (in the form of formate and acetate, respectively) were observed and likely components of long-range transport OA, decoupled from their gas-

phase counterparts. In addition, extraordinary correlation was observed between particulate LMWOA and aged SOA, which we tentatively attributed to boundary layer dynamics.

Table 3-1 Campaign-average concentrations of LMWOA.

	Formic	Acetic	Oxalic	Malonic	Succinic
Gas-Phase (ng m⁻³)	2150 ± 160	1860 ± 1340	28 ± 19	5 ± 3	18 ± 13
Particle-Phase (ng m⁻³)	50 ± 26	64 ± 25	74 ± 48	11 ± 11	48 ± 27

Table 3-2 Correlation coefficients (Pearson's R²) of both-phase formic, acetic, oxalic, malonic, succinic acids and selected tracer species. LMWOA are in the unit of $\mu\text{g m}^{-3}$, and tracer species are in the unit of Hz.

	LMWOA (p+g)					Isoprene Oxidation Products (p+g)					Monoterpene Oxidation Products (p+g)	
	Formic	Acetic	Oxalic	Malonic	Succinic	ISOPOOH + IEPOX	2-MT	C ₅ H ₁₀ O ₅	MAE + HMML	2-MGA	Pinic Acid	MBTCA
Formic	1	0.66	0.68	0.67	0.69	0.69	0.35	0.54	0.76	0.45	0.07	0.20
Acetic		1	0.47	0.41	0.45	0.30	0.08	0.21	0.30	0.24	0.02	0.07
Oxalic			1	0.96	0.89	0.46	0.79	0.60	0.57	0.67	0.30	0.68
Malonic				1	0.87	0.41	0.71	0.62	0.59	0.64	0.31	0.64
Succinic					1	0.42	0.80	0.53	0.57	0.59	0.32	0.66
ISOPOOH + IEPOX						1	0.37	0.56	0.76	0.43	0.08	0.20
2-MT							1	0.43	0.42	0.60	0.27	0.56
C ₅ H ₁₀ O ₅								1	0.63	0.71	0.20	0.52
MAE + HMML									1	0.57	0.26	0.37
2-MGA										1	0.44	0.61
Pinic Acid											1	0.45
MBTCA												1

Table 3-3 Correlation coefficients (Pearson's R²) of particulate LMWOA (by PILS-IC) and OA factors (by AMS). All concentrations are particle-phase measurements in the unit of $\mu\text{g m}^{-3}$.

	Particulate LMWOA						OA and OA Factors			
	Formic	Acetic	Oxalic	Malonic	Succinic	Total LMWOA	OA	Isoprene-OA	LO-OOA	MO-OOA
Formic	1.00	0.69	0.87	0.81	0.65	0.90	0.73	0.54	0.11	0.78
Acetic		1.00	0.70	0.65	0.67	0.82	0.59	0.43	0.07	0.67
Oxalic			1.00	0.95	0.85	0.97	0.73	0.66	0.03	0.89
Malonic				1.00	0.80	0.93	0.65	0.62	0.01	0.86
Succinic					1.00	0.87	0.79	0.79	0.07	0.87
Total LMWOA						1.00	0.78	0.67	0.06	0.90
OA							1.00	0.83	0.34	0.80
Isoprene-OA								1.00	0.15	0.73
LO-OOA									1.00	0.03
MO-OOA										1.00

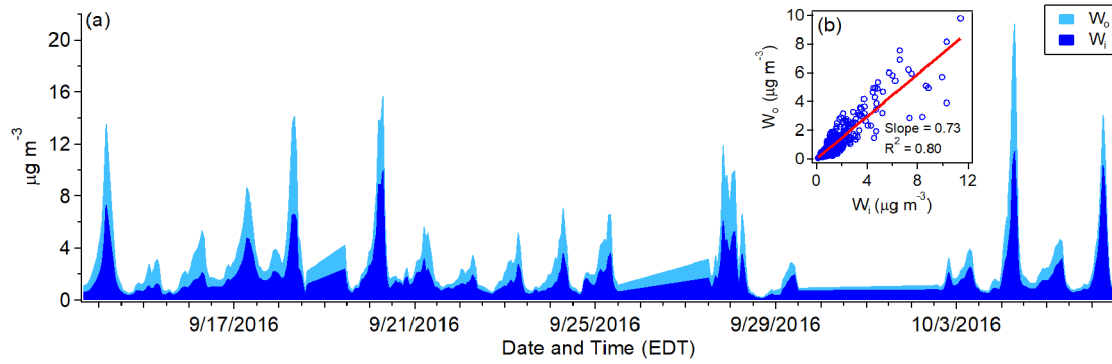


Figure 3-1 (a) Time series of and (b) correlations between aerosol water content associated with organics (W_o) and inorganics (W_i).

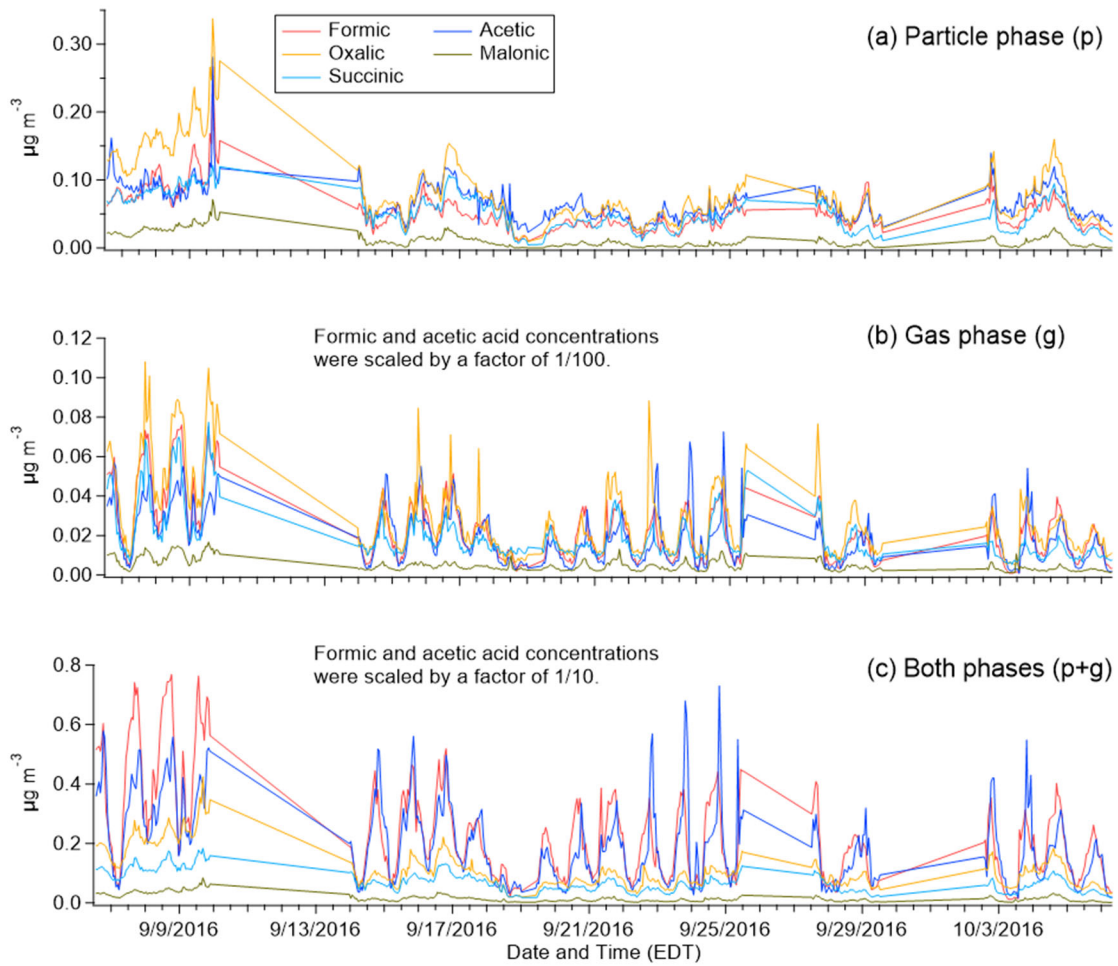


Figure 3-2 (a) Particle-phase concentrations, (b) gas-phase concentrations, and (c) both-phase concentrations of formic, acetic, oxalic, malonic, and succinic acids.

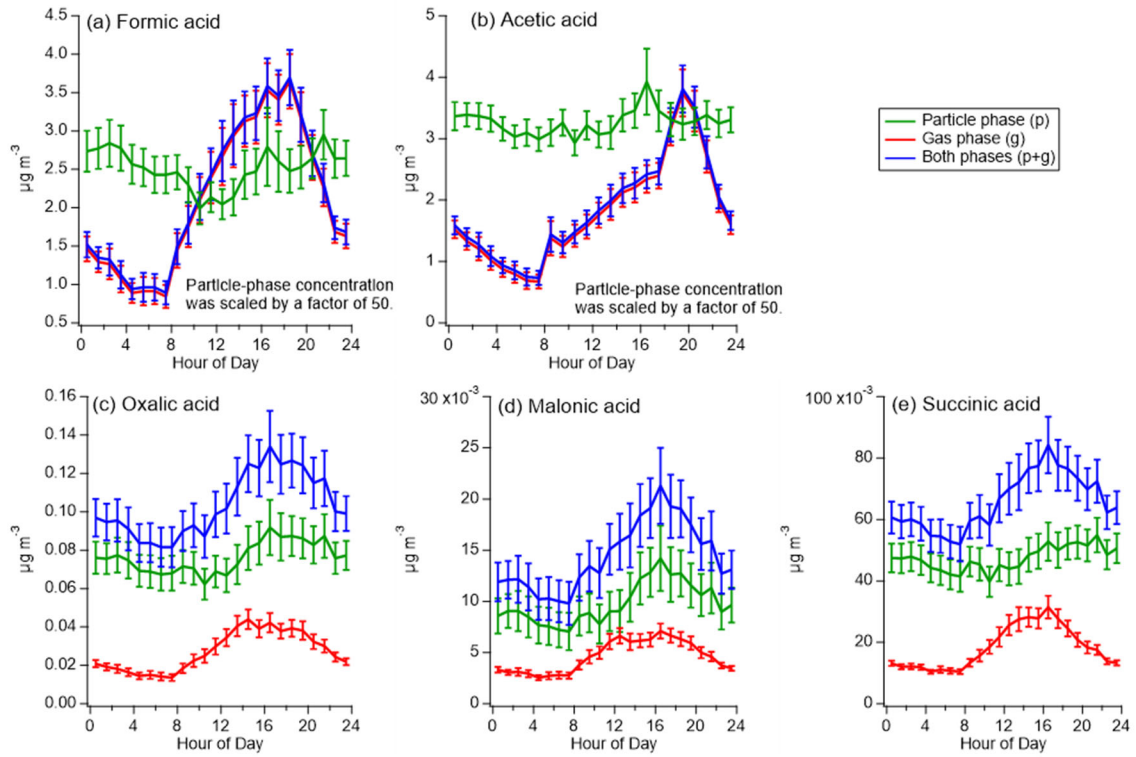


Figure 3-3 Diurnal profiles of (a) formic acid, (b) acetic acid, (c) oxalic acid, (d) malonic acid, and (e) succinic acid in the gas, particle, and both phases.

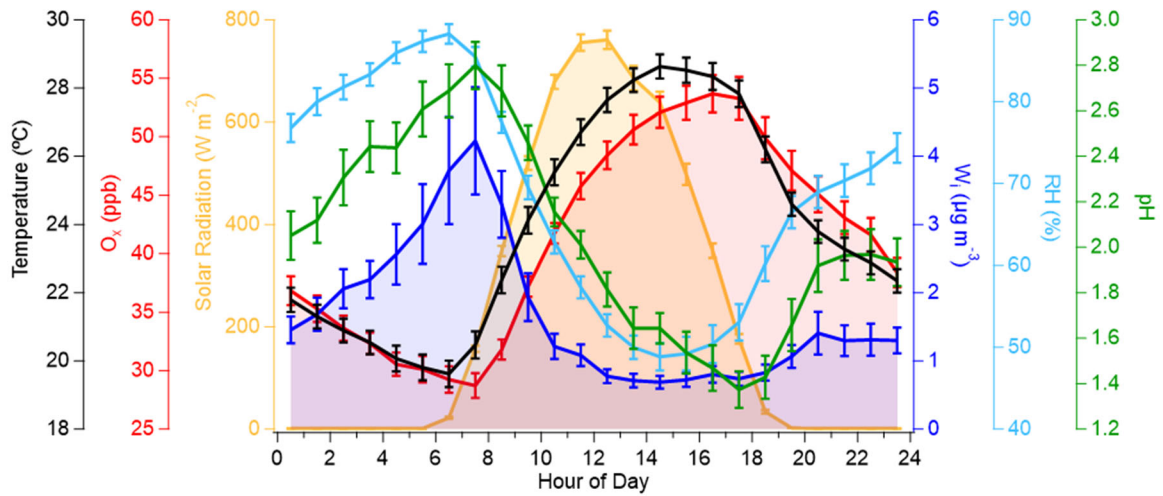


Figure 3-4 Diurnal profiles of temperature, O_x mixing ratio, solar radiation, inorganic water content, relative humidity, and aerosol pH.

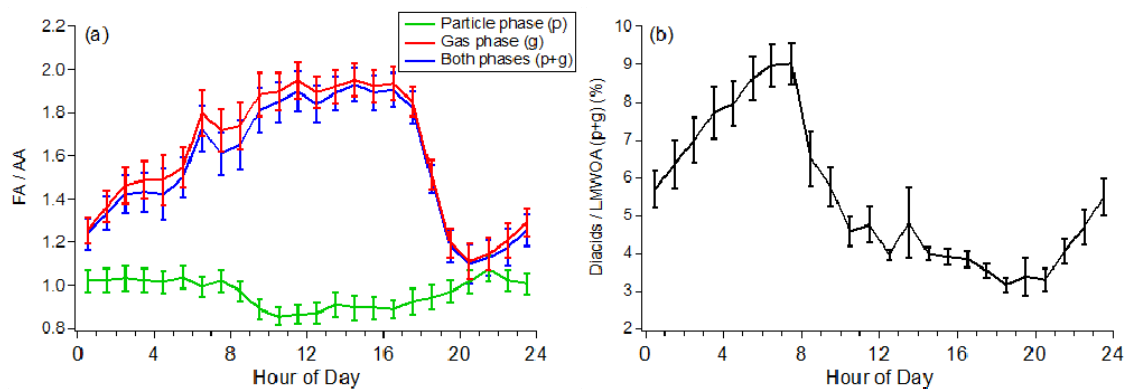


Figure 3-5 Diurnal profiles of (a) gas-, particle-, and both-phase formic-to-acetic (FA / AA) ratio, and (b) both-phase fraction of dicarboxylic acids in total LMWOA.

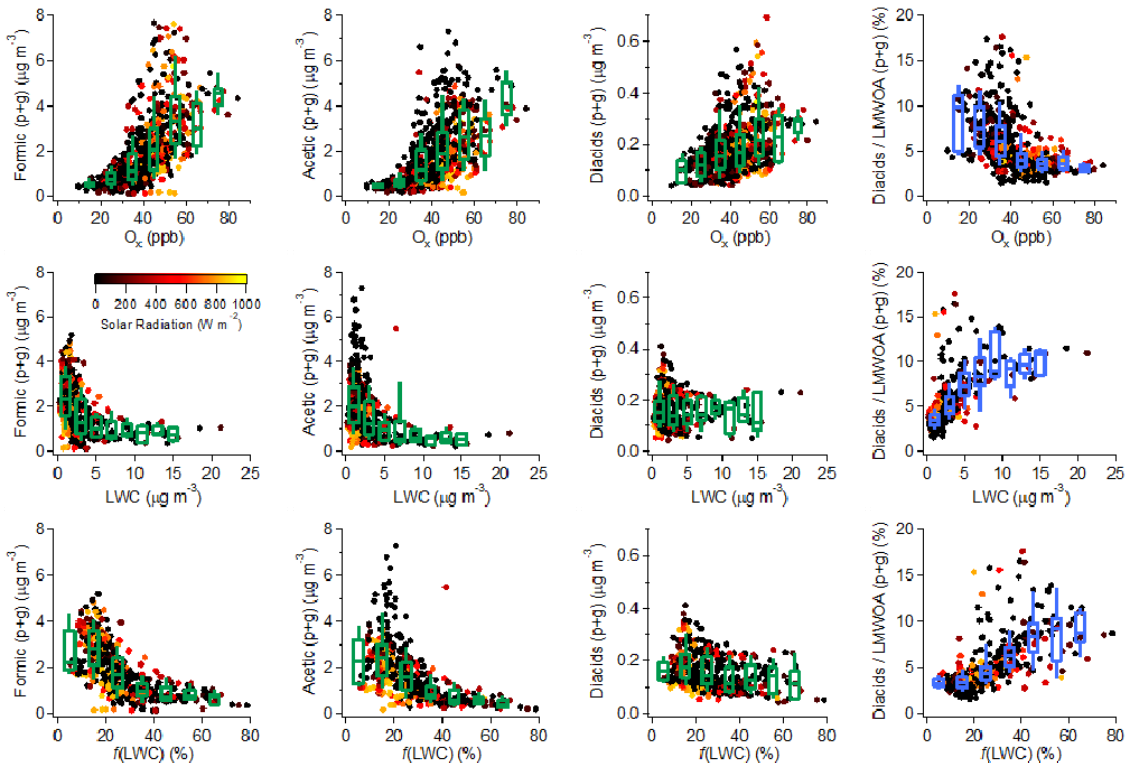


Figure 3-6 The both-phase concentrations of formic, acetic, LMW dicarboxylic acids (oxalic + malonic + succinic), and fraction of LMW dicarboxylic acids in total LMWVOA plotted against odd oxygen, LWC, and LWC fraction ($f(LWC) = LWC / (LWC + OA + \text{sulfate} + \text{ammonium} + \text{nitrate})$), respectively. Data points are colored by sunlight intensity to distinguish day and night. The mid-point line, lower and upper boxes, lower and upper whiskers, represent median, 25th percentiles, 75th percentiles, 10th percentiles, and 90th percentiles, respectively.

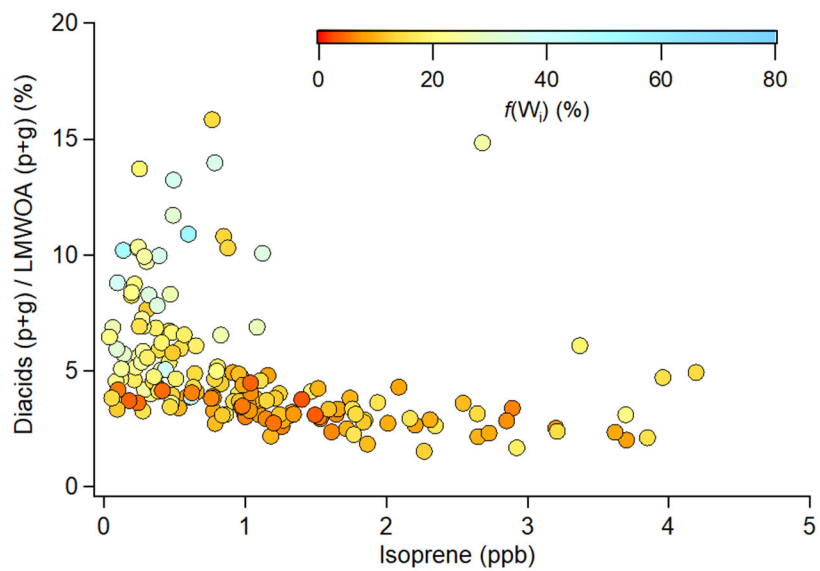


Figure 3-7 The both-phase fraction of LMW dicarboxylic acids as a function of isoprene mixing ratio. Data points are colored by inorganic water fraction.

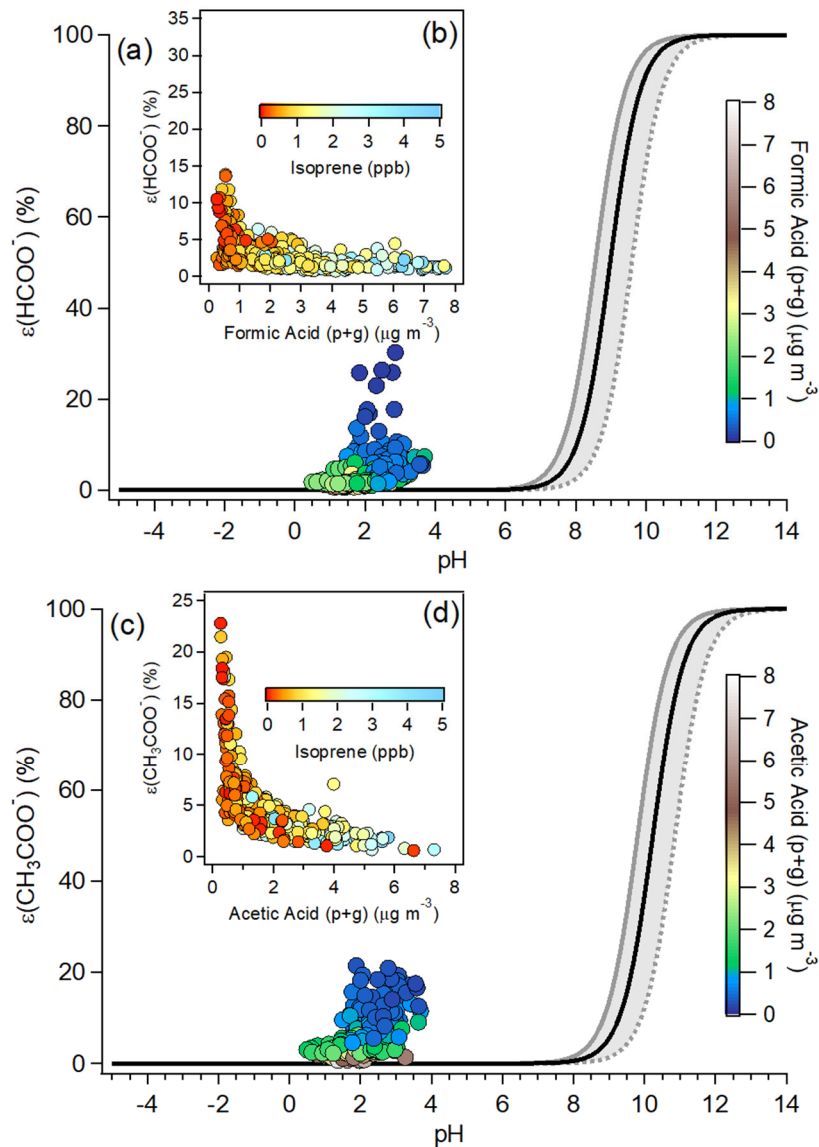


Figure 3-8 Analytically calculated S curves and ambient data plotted against ISORROPIA-predicted particle pH of (a) formic acid and (c) acetic acid (adapted from Nah, et al. ³⁰); ambient (b) $\epsilon(\text{HCOO}^-)$ and (d) $\epsilon(\text{CH}_3\text{COO}^-)$ plotted against their corresponding both-phase concentrations. Data points in (a) and (c) are colored by the corresponding both-phase concentrations, in (b) and (d) are colored by isoprene mixing ratio. The black line is the S curve calculated using the selected time period's average temperature ($23.4 \pm 4.0 \text{ }^\circ\text{C}$) and W_i ($1.6 \pm 1.7 \mu\text{g m}^{-3}$). The grey lines are S curves calculated using 1 standard deviation from the average temperature and W_i (i.e., temperature = $27.4 \text{ }^\circ\text{C}$ and $W_i = 0.5 \mu\text{g m}^{-3}$ for dotted grey line; temperature = $19.4 \text{ }^\circ\text{C}$ and $W_i = 3.3 \mu\text{g m}^{-3}$ for solid grey line).

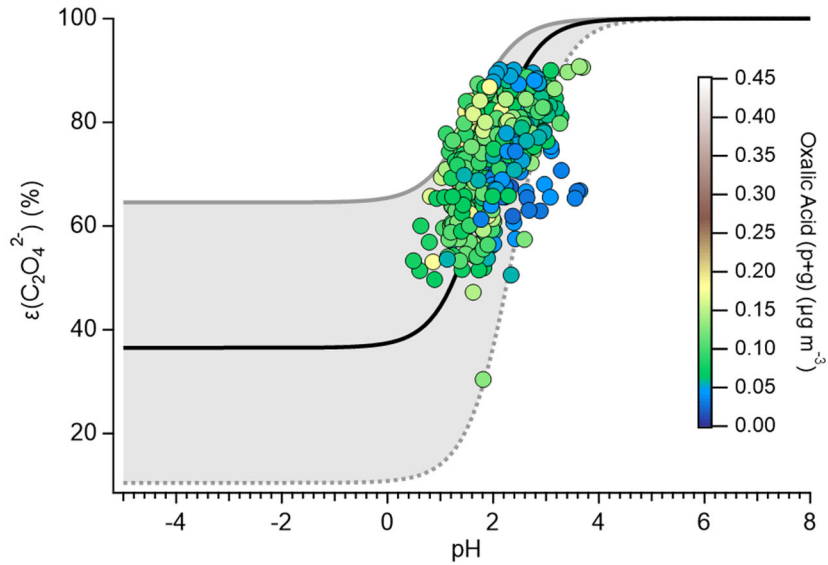


Figure 3-9 Analytically calculated S curves and ambient data plotted against ISORROPIA-predicted particle pH of oxalic acid (adapted from Nah et al. (2018a)). Data points were colored by the both-phase oxalic acid concentration. The black line is the S curve calculated using the selected time period's average temperature (23.4 ± 4.0 °C) and W_i (1.6 ± 1.7 $\mu\text{g m}^{-3}$). The grey lines are S curves calculated using 1 standard deviation from the average temperature and W_i (i.e., temperature = 27.4 °C and $W_i = 0.5$ $\mu\text{g m}^{-3}$ for dotted grey line; temperature = 19.4 °C and $W_i = 3.3$ $\mu\text{g m}^{-3}$ for solid grey line).

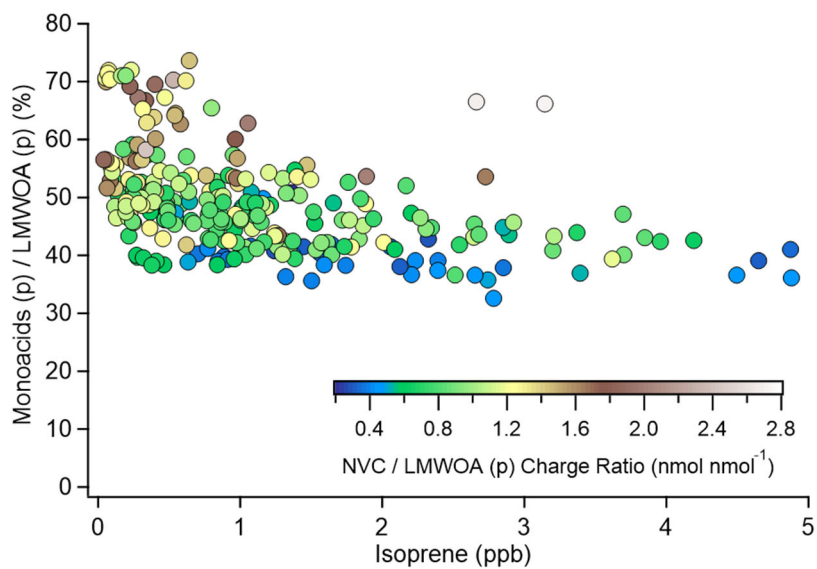


Figure 3-10 The particle-phase fraction of LMW monocarboxylic acids (formic + acetic, in the form of formate and acetate, respectively) in total LMWOA plotted against isoprene mixing ratio. Data points are colored by NVC / LMWOA charge ratio.

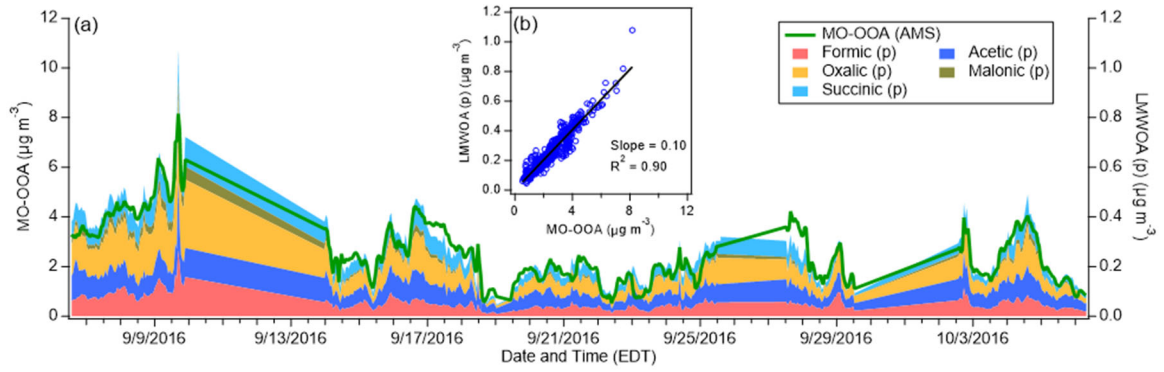


Figure 3-11 (a) Time series and (b) correlations of AMS MO-OOA factor and PILS-IC total particulate LMWOA.

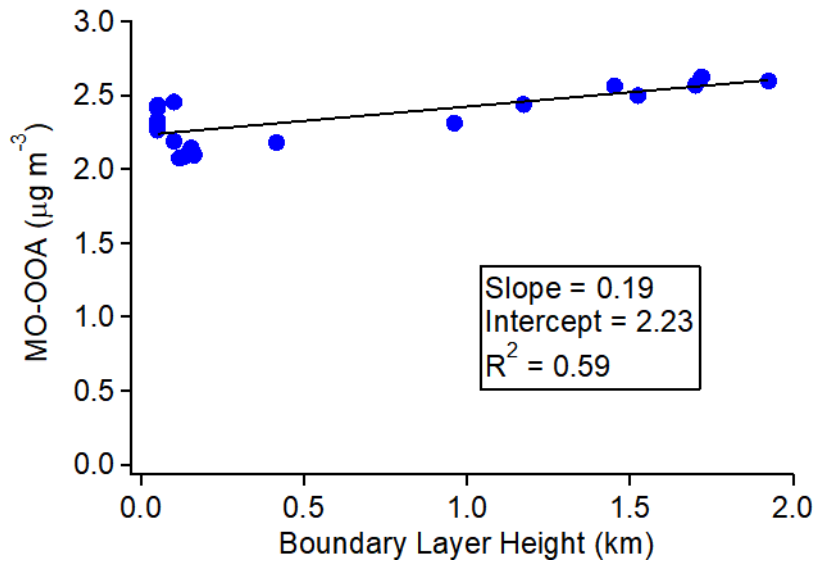


Figure 3-12 BL MO-OOA concentration as a function of BL height.

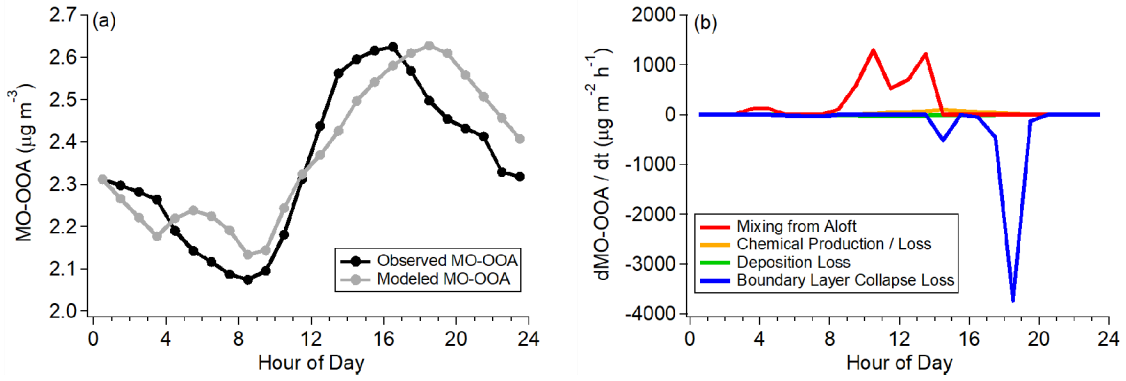


Figure 3-13 Diurnal profiles of (a) observed and modeled BL MO-OOA concentration; (b) simulated contributions from different processes to the total mass of MO-OOA in the boundary layer.

CHAPTER 4. LOW-MOLECULAR-WEIGHT ORGANIC ACIDS PRODUCTION IN BVOC PHOTOOXIDATION UNDER AMBIENT RELEVANT CONDITIONS

4.1 Background

Formic (HCOOH, FA) and acetic (CH₃COOH, AA) acids are ubiquitous atmospheric components. They are normally the most abundant organic acids in the gas phase (Chebbi and Carlier, 1996; Kawamura and Bikkina, 2016), and can also be pronounced in the aerosols (Liu et al., 2012; Yatavelli et al., 2014; Nah et al., 2018a). Sources of FA and AA include direct emissions from terrestrial vegetation, soil, biomass burning, secondary photochemical production, and aqueous phase chemistry (Chebbi and Carlier, 1996; Khare et al., 1999; Sorooshian et al., 2007; Paulot et al., 2011; Millet et al., 2015; Malecha and Nizkorodov, 2016). In recent studies, secondary photochemical production has been proposed to be a largely underestimated source for FA and AA (Paulot et al., 2011; Millet et al., 2015; Stavrou et al., 2011), which may explain the observed large measurement-model discrepancies, though the mechanism was still not well understood.

The presence of water vapor can change chemical mechanism, radical fates, and secondary organic aerosol (SOA) compositions (Jonsson et al., 2006; Nguyen et al., 2011; Boyd et al., 2015a; Hinks et al., 2018). In addition, aqueous phase photochemistry is known to be effective in organic acids production (Chameides and Davis, 1983; Ervens et al., 2008; Perri et al., 2009; Lee et al., 2011; Eugene et al., 2016). One gap to fill between measurements and models is that, most parameters used in models were obtained from

previous laboratory experiments performed under dry conditions, while the relative humidity (RH) of ambient environments can be fairly high in most regions. Therefore, in this study, we investigate the effects of both water vapor and aerosol liquid water on FA and AA formation in the photooxidation of isoprene and α -pinene, two of the most studied biogenic volatile compounds (BVOC). Chamber experiments are performed under both dry and high-RH conditions. Taking advantage of the property of ammonium sulfate seed particles, we investigate the role of aqueous phase chemistry by using effloresced or deliquesced ammonium sulfate seed to introduce different amount of aerosol liquid water (Faust et al., 2017).

4.2 Methods

4.2.1 Chamber Experiments

Chamber experiments were conducted in the Georgia Tech Environmental Chamber (GTEC) facility. Details of the facility have been described in Boyd et al. (Boyd et al., 2015b) Prior to the experiment, the Teflon chamber was flushed with zero air for ~24 h. Seed aerosol was first introduced by atomizing 15 mM ammonium sulfate solution (AS). Precursor BVOC, isoprene (99%, Sigma-Aldrich) or α -pinene (99 %, Sigma-Aldrich), was injected into a glass bulb and zero air was passed over the solution until it evaporated. H₂O₂ (50% aqueous solution, Sigma-Aldrich) was then injected as an OH precursor. Once the concentrations of all species stabilized, UV lights were turned on to initiate photooxidation. The photolysis of H₂O₂ yielded an OH concentration on the order of 10⁶ molecules/cm³ under low-NO conditions. In order to investigate the role of water vapor, experiments were performed at 22 °C under different RH conditions (~5%, ~50%, and ~70%) with same

precursor and H₂O₂ concentrations. For 50% RH experiments, both effloresced AS (DAS) and deliquesced AS (WAS) seed particles were used to investigate the role of aerosol water. For one isoprene experiment, 1:2 magnesium sulfate + sulfuric acid seed (MSSA, 8 mM magnesium sulfate + 16 mM sulfuric acid solution) was used to investigate the influence of acidic seed. For dry seed experiments, seed aerosols passed through a nafion dryer before entering the chamber. Experimental conditions are detailed in Table 4-1. In each experiment, after SOA formation reached peak growth, UV lights were turned off for 1 hour with all instruments still running.

4.2.2 Instrumentation

A custom-built quadrupole chemical ionization mass spectrometer (Q-CIMS) using sulfur hexafluoride ions (SF₆⁻) as reagent ions was used to measure organic acids in the gas phase. (Huey et al., 1995; Nah et al., 2018a; Nah et al., 2018b) A high resolution time-of-flight aerosol mass spectrometer (AMS, Aerodyne, Billerica, MA) was used to characterize the composition of NR-PM₁. (DeCarlo et al., 2006; Canagaratna et al., 2007) AMS data were analyzed using the data analysis toolkit SQUIRREL (v1.57) and PIKA (v1.16G) within the Igor Pro software (v6.37, Wavemetrics, Portland, OR). A High Resolution Time-of-Flight Iodide-Adduct Chemical Ionization Mass Spectrometer (Huey et al., 1995; Lee et al., 2014) coupled with a Filter Inlet for Gases and AEROSols (Lopez-Hilfiker et al., 2014) (FIGAERO-HR-ToF-I-CIMS, ToFwerk, Thun, Switzerland and Aerodyne, Billerica, MA, henceforth referred to as the FIGAERO-CIMS) was used to characterize both particle- (PM₁) and gas-phase multifunctional species. FIGAERO-CIMS data were analyzed using the data analysis toolkit 5 Tofware (v2.5.11, ToFwerk, Thun, Switzerland and Aerodyne, Billerica, MA) within the Igor Pro software (v6.37, Wavemetrics, Portland, OR). Aerosol

volume concentrations and distributions were measured using a scanning mobility particle sizer (SMPS; TSI) consisting of a differential mobility analyzer (DMA; TSI 3040) and a condensation particle counter (CPC; TSI 3775). A gas chromatography-flame ionization detector (GC-FID) with a Markes focusing trap to measure hourly resolved BVOC. Temperature and RH were monitored using a hydro-thermometer (Vaisala HMP110).

4.2.3 *Measurements of FA and AA*

FA and AA were detected in the deprotonated form HCOO^- (m/z 45) and CH_3COO^- (m/z 59), respectively. A 2 min background measurement was performed every 1 h during the experiments by passing the sampled air flow through an activated charcoal scrubber prior to delivery into the CIMS instrument. The scrubber can remove > 99% of the targeted species in ambient air. A 3 min FA calibration measurement was performed every 3 h during the experiments by adding standard FA to sample air flow, while AA calibration measurement was performed after experiments. The FA and AA calibration sources were permeation tubes (VICI Metronics) with emission rates of 66 and 97 nL min^{-1} , respectively.

Wall loss of formic acid was conducted under dry and 50% RH, by sending ~50 ppb formic acid to clean chamber. Over the experiment time (~ 6 h), formic acid wall loss is minor compared to total formic acid production. The loss is ~10% under humid conditions, and negligible under dry conditions

4.3 **Results and Discussion**

4.3.1 *FA and AA Production in “Clean” Chamber*

Blank experiments were conducted in “clean” Teflon chamber, in which only oxidant was introduced into the chamber (with or without seed particles) in the absence of BVOC precursors. While negligible FA and AA formation was observed under dry conditions, noticeable FA and AA was formed in “clean” chamber at 30% RH (Figure 4-1). Increasing RH from 30% to 70% or introducing seed particles had little effect on FA and AA production. In the following discussions, we took the average production of FA and AA in blank experiments as background, and subtracted it from BVOC photooxidation experiments that conducted under ~50% and ~ 70% RH. The formation of FA and AA in “clean” chamber may relate to the photooxidation and photolysis of the highly aged organic films on chamber walls (Malecha and Nizkorodov, 2016;Link et al., 2020), which can also be an underestimated sources of atmospheric FA and AA.

4.3.2 *FA and AA Production in BVOC Photooxidation Experiments*

The molar yields of FA and AA are shown in Figure 4-1. The yields were calculated as the ratio of FA (or AA) mixing ratio produced in the experiment when SOA reached peak growth, with background subtracted, with respect to the mixing ratio of reacted BVOC precursor. Limited by the time scale that can be achieved in the laboratory, FA and AA formation has not plateaued when the UV lights were turned off, and therefore the yields we reported here were only “instantaneous” yields, while the yields can be higher in real ambient environments. The reported FA and AA yield under dry conditions (16.8% FA and 10.4% AA in isoprene photooxidation, 12.3% FA and 10.7% AA in α -pinene photooxidation) were comparable to previous studies (Orlando et al., 2000;Paulot et al., 2009a;Lee et al., 2006). Water clearly affected FA and AA formation, but the influences are different in different BVOC systems.

In isoprene photooxidation, the addition of both water vapor and aerosol water enhanced FA formation. Under dry conditions, while acidic seed (MSSA) greatly changed the chemical pathways by enhancing isoprene epoxydiols (IEPOX) uptake followed by subsequent condensed-phase reactions (Surratt et al., 2010; Lin et al., 2012; Paulot et al., 2009b), the yields of FA and AA were comparable to experiments using DAS seed, implying that IEPOX-derived SOA was not a pronounced source of FA and AA in the time scale of ~ 6h in this study, though we cannot rule out the further processing of IEPOX-derived SOA can produce FA and AA effectively. Compared to dry experiments, FA formation was obviously enhanced under humid conditions and in the presence of aerosol water, implying that both gas-phase and particle-phase processes contribute to FA formation. FA molar yield increased by 150% (from 16.8% to 42.4%) under 70% RH with WAS seed compared to dry conditions. AA formation, however, was only enhanced when RH was higher than 70%, with yield doubled (from 10.4% to 20.9%) under 70% RH with WAS seed compared to dry conditions.

In α -pinene photooxidation, FA and AA showed consistent trends that water in both gas and particle phase substantially enhanced organic acid formation, with FA molar yield increased by 350% (from 12.3% to 55.2%) and AA yield increased by 230% (from 10.7% to 34.9%) under 70% RH with wet AS seed compared to dry conditions.

4.3.3 Potential Mechanism of FA and AA Formation Enhanced by Water

In both isoprene and α -pinene experiments, FA and AA formation stopped immediately once UV lights were turned off (Figure 4-3(a),(b) and Figure 4-4(a),(b)),

which implied photochemical reactions as predominant source of FA and AA in these experiments.

In isoprene photooxidation experiments, accompanying ceased FA formation (Figure 4-3(a)), CH_4O_3 (detected as the cluster adducted to one iodide ion if not specified hereafter), likely corresponding to hydroxymethyl hydroperoxide (HMHP), showed an immediate increase after UV was turned off under humid conditions, but no noticeable change was observed under dry conditions (Figure 4-3(c)). HMHP can be formed by the reaction between CH_2OO with water and the oxidation of formaldehyde by HO_2 radicals (Gäb et al., 1985; Su et al., 1979). The decomposition of HMHP leads to the formation of formic acid (Neeb et al., 1997), and studies have shown that water vapor can assist this process (Aplincourt and Ruiz-López, 2000). Therefore, the decomposition of HMHP may explain the substantial enhancement of FA formation in the presence of water vapor. Similarly, the enhanced AA formation under 70% RH was likely linked to $\text{C}_5\text{H}_8\text{O}_4$, since after UV was removed, the ceased AA formation under 70% RH was accompanied by $\text{C}_5\text{H}_8\text{O}_4$ increase (Figure 4-3(b) and (d)), which was not observed for other experiments. Paulot et al. (2009a) have proposed that decomposition of 2,4-dihydroxy-2-methyl-3-oxobutanal (one isomer of $\text{C}_5\text{H}_8\text{O}_4$) can be an effective source of acetic acid in isoprene photooxidation experiments. Our observation here may suggest that this process is of greater importance under high RH. It is noted that carbonyls like formaldehyde, glyoxal, and hydroxyacetone, which are known precursors of FA and AA, were not measured in this work. Future work is warranted to evaluate how their chemistry changes in the presence of water. Figure 4-2 also showed that under 50% RH, FA yield was higher in the experiment with wet AS (32.4%) compared to dry AS (25.9%), implying particle-phase

formation pathways of FA assisted by the aerosol water. In Figure 4-3 we showed the time series of two early-generation isoprene oxidation products, $C_5H_{12}O_4$ (2-methyltetrols) (Surratt et al., 2010; Surratt et al., 2007b), and $C_5H_{12}O_6$ (isoprene dihydroxy dihydroperoxides, or ISOP(OOH)₂ for short) in the particle phase (Figure 4-3(e) and (f)) (Krechmer et al., 2015; Liu et al., 2016; D'Ambro et al., 2017). For both $C_5H_{12}O_4$ and $C_5H_{12}O_6$ species, compared to experiments with dry AS seed, their partitioning to particle phase was obviously enhanced in experiments with wet AS seed, likely due to their hydrophilic nature. Meanwhile, compared to experiments under dry conditions, particulate $C_5H_{12}O_4$ and $C_5H_{12}O_6$ in humid experiments also decayed fast after reaching peak. Prior studies have shown that the degradation of fresh SOA can lead to the formation of FA and AA (Malecha and Nizkorodov, 2016).

The mechanism of FA and AA formation in α -pinene photooxidation were less studied. In our α -pinene photooxidation experiments, accompanying ceased FA and AA formation (Figure 4-4 (a) and (b)), we observed that gaseous $C_{10}H_{18}O_3$ showed immediate increase after UV was removed, and is probably linked to enhanced FA and AA formation under humid conditions (Figure 4-4 (c)), while the mechanism is not clear. In the particle phase, under same 50% RH, experiment using wet AS seed contains more small molecules compared to experiment using dry AS seed (Figure 4-4 (d)), indicating the presence of aerosol water favors fragmentation processes and produce small molecules, including FA and AA.

4.4 Conclusions

In this study, we quantitatively investigated the formation of FA and AA by isoprene and α -pinene photooxidation, with special focus on the effects of gaseous and particulate water. We found in general the presence of water, in both gas and particle phase, can enhance FA and AA formation. Under 70% RH with wet AS seed, which is relevant to wet seasons of the southeastern United States and Amazon rain forest, FA and AA formation yield can increase by 100-350% compared to dry conditions. This may help explain the measurement-model discrepancies observed in previous studies. In addition, we also noticed the formation of FA and AA in “clean” chamber, likely related to the photooxidation and photolysis of the highly aged organic films on chamber walls, which can also happen on surfaces in ambient environment and thus sources for FA and AA.

Table 4-1 Summary of experimental conditions.

No.	Precursor	[BVOC] ₀	RH (%)	Seed Type
1	Isoprene	49	3-6 (Dry)	effloresced (NH ₄) ₂ SO ₄ (DAS)
2	Isoprene	45	50-54 (50%RH)	effloresced (NH ₄) ₂ SO ₄ (DAS)
3	Isoprene	47	51-54 (50%RH)	deliquesced (NH ₄) ₂ SO ₄ (WAS)
4	Isoprene	46	67-70 (70%RH)	deliquesced (NH ₄) ₂ SO ₄ (WAS)
5	Isoprene	47	2-6 (Dry)	deliquesced MgSO ₄ /H ₂ SO ₄ (MSSA)
6	α-pinene	41	2-4 (Dry)	effloresced (NH ₄) ₂ SO ₄ (DAS)
7	α-pinene	43	49-52 (50%RH)	effloresced (NH ₄) ₂ SO ₄ (DAS)
8	α-pinene	43	50-54 (50%RH)	deliquesced (NH ₄) ₂ SO ₄ (WAS)
9	α-pinene	44	66-69 (70%RH)	deliquesced (NH ₄) ₂ SO ₄ (WAS)

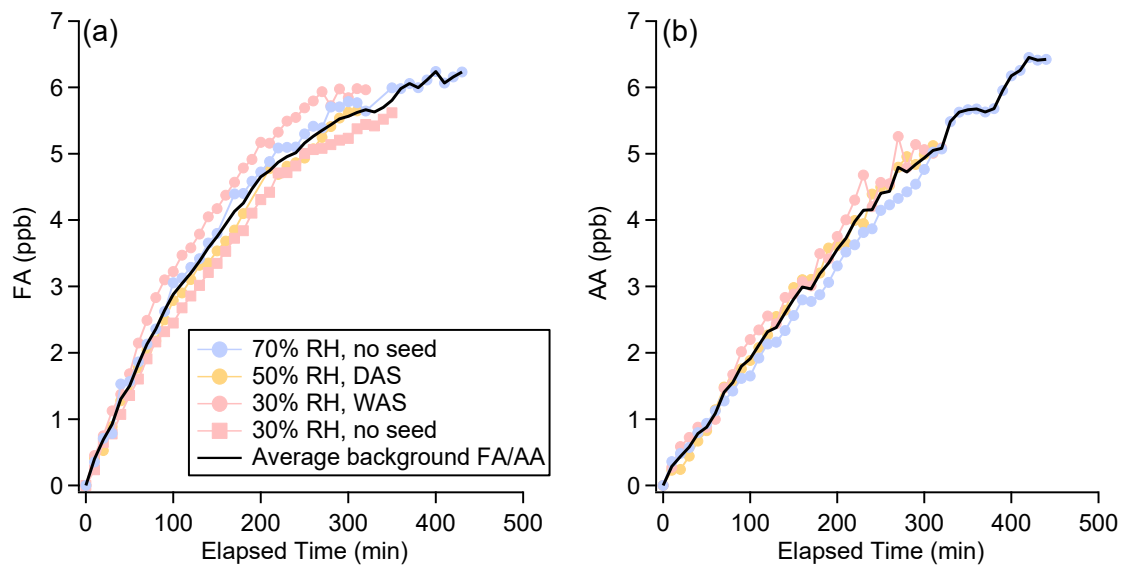


Figure 4-1 FA and AA time series in photooxidation experiments in humidified “clean” chamber.

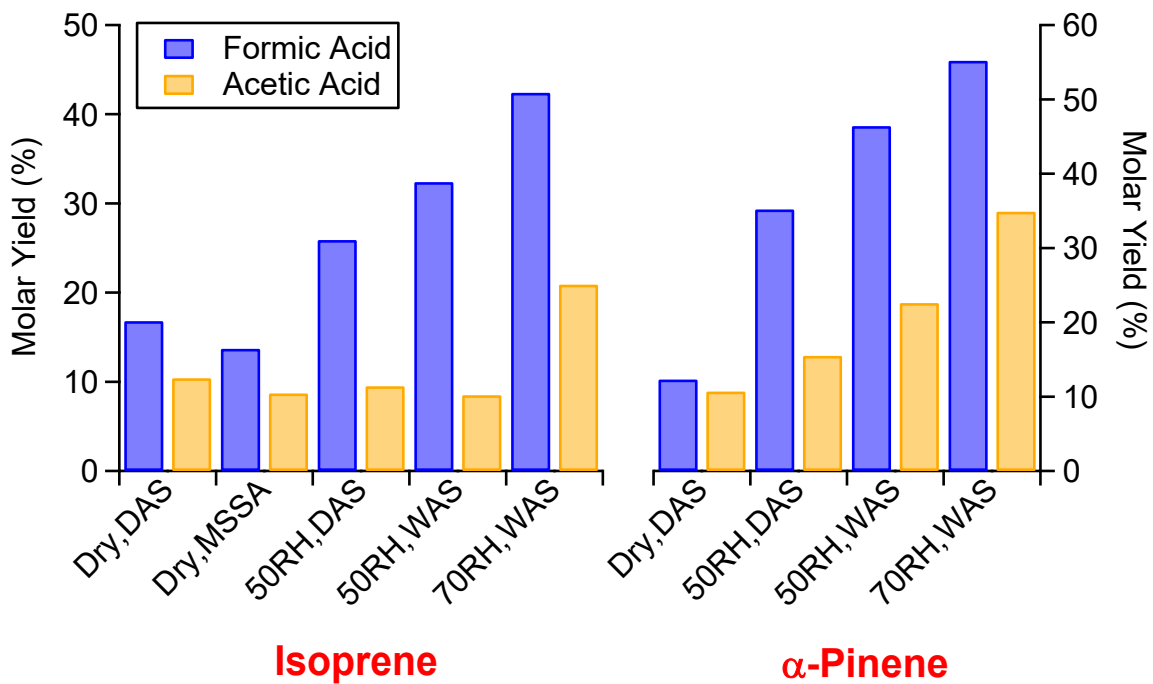


Figure 4-2 Summary of formic and acetic acid molar yields under different conditions.

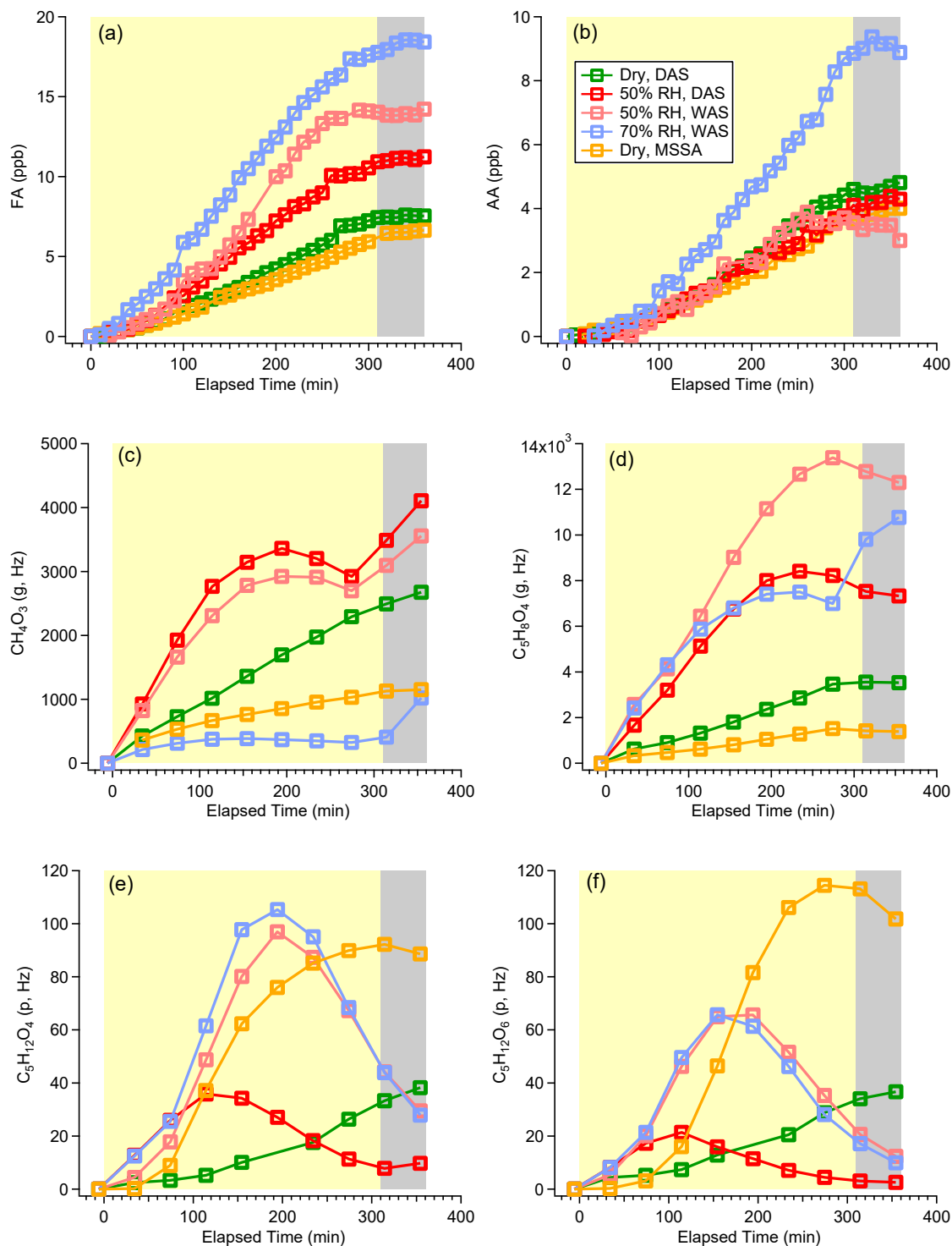


Figure 4-3 Time Series of (a) FA, (b) AA, and tracer compounds: (c) CH_4O_3 (g), (d) gaseous $\text{C}_5\text{H}_8\text{O}_4$, (e) $\text{C}_5\text{H}_{12}\text{O}_4$ (p), and (f) $\text{C}_5\text{H}_{12}\text{O}_6$ (p) in isoprene photooxidation experiments. The yellow shade indicates UV lights were on, while grey shade indicates UV lights were off. Note that $\text{C}_5\text{H}_{12}\text{O}_4$ (p) and $\text{C}_5\text{H}_{12}\text{O}_6$ (p) signals in experiment with

MSSA seed (yellow) were scaled by a factor of 1/10.

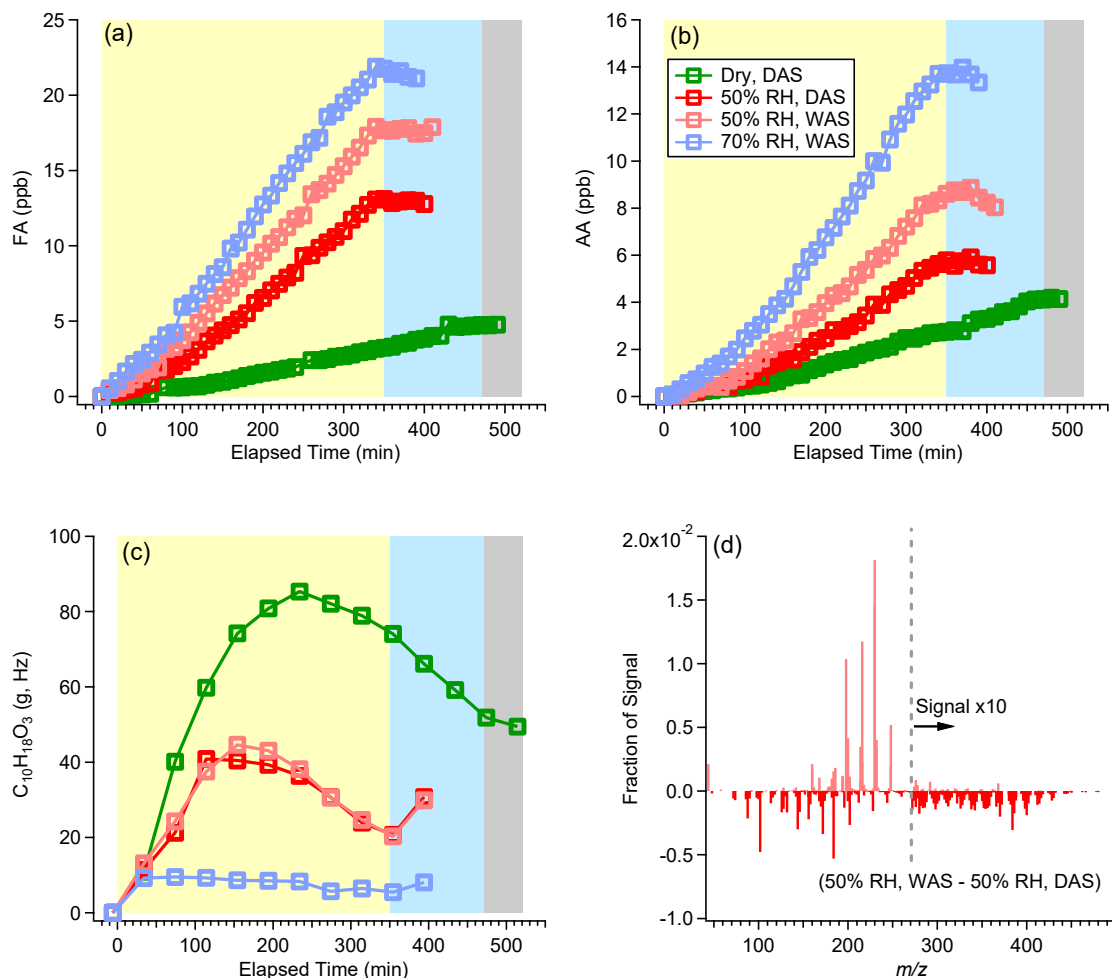


Figure 4-4 Time Series of (a) FA, (b) AA, and tracer compound (c) $C_{10}H_{18}O_3$ (g) in α -pinene photooxidation experiments, and (d) difference between normalized particle mass spectra 50% RH, WAS experiment and 50% RH, DAS experiment. In (a)(b)(c), the yellow shade indicates UV lights were on in all experiments, and blue shade indicates that UV lights were off in three humid experiments but still on in the dry experiment, while grey shade indicates UV lights were off in the dry experiment. In (d), positive values mean ions have a higher abundance in 50% RH WAS experiment, while negative values mean ions have a higher abundance in 50% RH DAS experiment.

CHAPTER 5. SUMMARY AND FUTURE WORKS

5.1 Summary

This thesis presents two-month measurements at Yorkville, GA, a rural site in the southeastern United States, during a season transition from summer to fall. The high-resolution molecular-based measurements by FIGAERO-CIMS well supplement the bulk-level measurements by AMS, and more chemical pathways have been identified to explain the AMS OA factors. Notable SOA formation was identified from isoprene and monoterpenes during both day and night. In addition to the well-recognized isoprene-derived SOA formation via IEPOX uptake, notable ISOPOOH-derived SOA via non-IEPOX pathways and abundant isoprene-derived organic nitrates was also observed. AMS LO-OOA factor has been mostly attributed to nighttime monoterpene SOA formation by previous AMS factorization analysis, while FIGAERO-CIMS measurements identified nocturnal isoprene chemistry also leads to the formation of LO-OOA.

The sources and partitioning of five most abundant LMWOA were further investigated for Yorkville, GA campaign. While these LMWOA can form in similar reactions and shared certain physicochemical properties, their formation and partitioning can be driven by quite different processes. For example, we found that the gas- and particle-phase formic and acetic acids were largely decoupled: the majority of the gas-phase formic and acetic acids were formed rapidly and in situ through biogenic VOC photooxidation, while their particle-phase counterparts were likely from transport and bonded to NVC, whereas the gas-particle partitioning of oxalic acid was in equilibrium and can be well captured by thermodynamic model. As LMWOA are normally end products of

photochemical oxidation and linked to OA aging, we also observed links between LMWOA and aged SOA. Particulate LMWOA showed strong correlation with MO-OOA, and can be a good tracer for aged SOA while their correlation was largely attributed to boundary layer dynamics.

A series of chamber experiments were conducted to quantitatively investigate formic and acetic acid formation in the photooxidation of isoprene and α -pinene, two most abundant biogenic VOC measured in Yorkville, GA campaign. We found the presence of both gaseous and particulate water in general enhanced formic and acetic acids formation. Given the relatively high RH in the southeastern United States, tropospheric gaseous and aerosol water would be a non-negligible factor affecting LMWOA formation. Including it in current modeling frameworks may help improve simulations and explain the large measurement-model discrepancies of formic and acetic acids observed in previous studies.

5.2 Future Works

5.2.1 OA Characterization Aided by Instrument Improvements

Chapter 2 presents field measurements using both HR-ToF-AMS and FIGAERO-CIMS, combining factorization analysis with molecular measurements for a better characterization of OA composition. The AMS has been developed for over two decades, and has been widely used in both ambient and laboratory studies. With limited resolution, the AMS only provide bulk-level chemical information, while factorization analysis takes full advantage of its measuring capability. Meanwhile, the wide usage of AMS allows for a well-established global database of AMS OA factors. The utilization of FIGAERO-CIMS for OA characterization is relatively new, but more information can be acquired with its

higher resolution. We show in Chapter 2 that FIGAERO-CIMS is a good supplement to AMS and brings more insights into the AMS factors that have been known for long. More parallel measurements using AMS and molecular-based online instruments would be worthwhile, which may allow a new interpretation of the AMS-based global OA distribution map. In addition, the fast advances of online mass spectrometry enable high time-resolution measurements of thousands of compounds. New data analysis techniques are needed to make full use of these large complex datasets.

5.2.2 *Sources of Aged SOA*

AMS MO-OOA factor, normally a surrogate of aged SOA, has been resolved ubiquitously and normally constitutes a considerable fraction of OA. Different theories have been proposed about MO-OOA sources. In Chapter 3, we show the five measured LMWOA strongly correlated with MO-OOA, but can only explain 10% of MO-OOA mass. It is still unclear what the majority of MO-OOA is. We also propose that the five LMWOA were of different origins, where particulate formate and acetate was from transport and oxalate was formed in aqueous processing of local biogenic SOA. Understanding how these different sources contribute to total MO-OOA would be helpful for future air pollution regulations.

5.2.3 *Conducting Laboratory Experiments under Ambient-Relevant Conditions*

In Chapter 4 we show that the presence of water can substantially change the yields of small organic acid formation from BVOC photooxidation. Traditionally, most chamber experiments have been conducted under dry conditions, while gaseous and particulate water is ubiquitous and abundant in ambient environment. Recent studies consistently

showed a large measurement-model discrepancies for formic and acetic acids, implying a missing source for these LMWOA. A gap to fill is that many parameters used in current model frameworks are from experiments conducted under dry conditions, and need to be updated. While increasing RH in chamber experiments introduces more uncertainties, e.g. background production of small molecules and wall loss of intermediate products, it is worth efforts to conduct experiments under more ambient-relevant conditions.

APPENDIX A. RESPONSE OF THE AERODYNE AEROSOL MASS SPECTROMETER TO INORGANIC SULFATES AND ORGANOSULFUR COMPOUNDS: APPLICATIONS IN FIELD AND LABORATORY MEASUREMENTS

A.1 Background

Organosulfur compounds have been identified in both laboratory-generated and ambient aerosols (Liggio and Li, 2006;Surratt et al., 2007a;Surratt et al., 2008;Riva et al., 2015;Stone et al., 2012;Tolocka and Turpin, 2012;Iinuma et al., 2007b;Iinuma et al., 2007a;Liao et al., 2015). It has been suggested that these compounds can comprise a substantial fraction of organic aerosol (OA) mass (Surratt et al., 2008;Tolocka and Turpin, 2012;Liao et al., 2015). Organosulfur compounds are generally of low volatility (Iinuma et al., 2007b;Iinuma et al., 2007a), and can be an important component of high molecular weight (MW) compounds in ambient aerosols. Due to their surface-active nature and chemical stability (Liggio and Li, 2006;Olson et al., 2011;Darer et al., 2011), organosulfur compounds can play a potentially important role in altering aerosol physicochemical properties (Stone et al., 2012;Tao et al., 2014;Estillore et al., 2016). Organosulfur compounds are also thought to be good tracers for aqueous particle-phase secondary OA (SOA) formation (McNeill et al., 2012). Given their importance, different methods have been explored to quantify organosulfur compounds in ambient aerosols. Offline methods such as Fourier transform infrared (FTIR) transmission spectroscopy have been used to measure C-O-S functional groups (Maria et al., 2003). The difference between total particulate sulfur measured by X-ray emission techniques and water soluble inorganic

sulfate measured by ion chromatography (IC) has been used to provide an upper-limit estimation of atmospheric organosulfur compounds (Surratt et al., 2008; Tolocka and Turpin, 2012; Sorooshian et al., 2015; Lukács et al., 2009). However, this method suffers uncertainties from instrument cross-calibrations (Lukács et al., 2009). Liquid chromatography-electrospray ionization-tandem mass spectrometry (LC-ESI-MS/MS) is widely used to identify and quantify organosulfur compounds (Stone et al., 2012), but the quantification of total organosulfur compounds is limited by the availability of authentic standards (Olson et al., 2011; Hettiyadura et al., 2015). For online methods, Particle Ablation by Laser Mass Spectrometry (PALMS) single particle mass spectrometer has been used to measure certain organosulfur compounds in single particles (Liao et al., 2015; Froyd et al., 2010), but as a single particle mass spectrometer, PALMS suffers from quantification issues (Murphy, 2007).

The high resolution time-of-flight aerosol mass spectrometer (HR-ToF-AMS, Aerodyne; henceforth referred to as AMS) has also been used to estimate the lower bound of ambient organosulfur compound concentrations based on the signal intensity of organosulfur ions ($C_xH_yO_zS^+$) and their fractional contributions in pure organosulfur compound standards (Huang et al., 2015). However, most sulfate and sulfonate functionalities in organosulfur compounds fragment to $H_xSO_y^+$ ions (Farmer et al., 2010; Huang et al., 2015). Meanwhile, $H_xSO_y^+$ ions in the AMS are often misinterpreted as arising only from inorganic sulfates in subsequent analysis. This potential misattribution can result in an underestimation of organic mass and a corresponding overestimation of inorganic sulfate mass, and it also causes underestimation of S/C. Docherty et al. (2011) have shown that when including the S content of organosulfates in elemental analysis

calculations, S/C can increase by a factor of 30 for an ambient study. Methanesulfonic acid, which is an important organosulfur compound in marine aerosols (Facchini et al., 2008;Ovadnevaite et al., 2014), has been quantified with the AMS based on their signature organosulfur fragments (sometimes complemented by PMF analysis) (Phinney et al., 2006;Zorn et al., 2008;Ge et al., 2012;Huang et al., 2015;Ovadnevaite et al., 2014;Huang et al., 2017;Willis et al., 2016), which are much more abundant due to the C-S bonding rather than C-O-S bonding, and the smaller size of methanesulfonic acid compared to other organosulfur compounds (Oae, 1991).

In this study, we developed a method to estimate the concentration of organosulfur compounds based on AMS-measured sulfate mass spectra. 16 standard organosulfur standards (including organosulfates, sulfonates, and sulfonic acids) were tested in the laboratory. Methanesulfonic acid was evaluated and discussed separately from other organosulfur compounds because of its distinctive mass spectrum. We applied this method to both chamber and ambient measurements and discussed their atmospheric implications. Four different AMSs were used in standard calibrations and chamber/ambient measurements, which will be referred hereafter as GT AMS (Georgia Institute of Technology group), Galway AMS (National University of Ireland Galway group), TROPOS AMS (Leibniz Institute for Tropospheric Research group), and Boulder AMS (University of Colorado-Boulder group) hereafter.

A.2 Methods

A.2.1 Laboratory Characterization of Standard Compounds

The fragmentation patterns of standard compounds were obtained by directly atomizing 10 - 140 μ M aqueous solutions of standard compounds into the AMS. The particles were generated by an ultrasonic nebulizer (U-5000AT, Cetac Technologies Inc., Omaha, Nebraska, USA), and passed through a nafion dryer to remove excess water prior to entering the AMS. In this study, 3 inorganic sulfates and 16 organosulfur compounds were tested with the GT AMS (Table A-1). The 3 inorganic sulfates are ammonium sulfate (AS), acidic AS (1:1 mixture of ammonium sulfate and sulfuric acid), and sodium sulfate (SS). The 16 organosulfur compounds include 4 linear alkyl organosulfate salts (sodium methyl sulfate, sodium ethyl sulfate, sodium n-heptyl sulfate, and sodium n-octyl sulfate), 2 oxygenated organosulfate salts, one containing a carboxylic acid functional group (potassium glycolic acid sulfate) and the other containing a carbonyl functional group (potassium hydroxyacetone sulfate), 6 aromatic organosulfate salts (potassium o-cresol sulfate, potassium p-cresol sulfate, potassium m-cresol sulfate, sodium benzyl sulfate, potassium 4-nitrophenyl sulfate, and potassium 4-hydroxy-3-methoxyphenylglycol sulfate), 2 sulfonate salts (sodium 1-butanesulfonate and sodium benzenesulfonate), and 2 sulfonic acids (methanesulfonic acid and ethanesulfonic acid). Pure sulfuric acid mass spectrum was acquired with the Boulder AMS. Methanesulfonic acid (MSA) will be discussed separately from other organosulfur compounds due to its unique fragmentation patterns in the AMS. Organosulfate, sulfonate, and sulfonic acid standards tested in this study but excluding MSA will be referred to as OS hereafter.

Structures of standard compounds are shown in Table A-1. Hydroxyacetone sulfate, glycolic acid sulfate, and benzyl sulfate were synthesized in the laboratory according to the method described in Hettiyadura et al. (2015); o-cresol sulfate, p-cresol sulfate, and m-

cresol sulfate were synthesized in the laboratory according to the method described in Staudt et al. (2014); the rest of organosulfur standards are commercially available. Among all OS standards evaluated in this work, glycolic acid sulfate (OS-3) is one of the most abundant atmospheric organosulfates quantified so far (Olson et al., 2011;Hettiyadura et al., 2015;Liao et al., 2015;Huang et al., 2018). Hydroxyacetone sulfate (OS-4), methyl sulfate (OS-1), o-cresol sulfate (OS-7), p-cresol sulfate (OS-8), m-cresol sulfate (OS-9), and benzylsulfate (OS-10) have also been detected in ambient aerosols in prior studies (Hettiyadura et al., 2015;Staudt et al., 2014).

A.2.2 Characterization of Chamber-Generated Biogenic SOA and Ambient OA

One isoprene photooxidation experiment under low-NO condition and four sets of field measurements conducted by different groups with different AMS were investigated in this study to probe the time variations and abundance of organosulfur compounds in well-controlled single VOC system and in different ambient environments, including biogenic VOC (BVOC) dominated southeastern US measurements (Centreville measurements), MSA abundant coastal and cruise measurements (Mace Head and Polarstern measurements), and high acidity aircraft measurements (WINTER measurements). Four different AMS are included in the discussions, GT AMS (chamber isoprene SOA and Centreville measurements), Galway AMS (Mace Head measurements), TROPOS AMS (Polarstern measurements), and Boulder AMS (WINTER measurements).

A.2.2.1 Chamber Experiment

Isoprene photooxidation SOA under low-NO condition were generated in the Georgia Tech Environmental Chamber (GTEC) facility. Details of the facility have been

described in Boyd et al. (2015a) and details of the experiment have been described in (Tuet et al., 2017). Briefly, the experiment was performed at 25 °C under dry (RH < 5 %) condition. Prior to the experiment, the chamber was flushed with zero air for ~24 h. Seed aerosol was first introduced by atomizing 15 mM AS solution and seed volume concentration was stabilized at ~ 25 $\mu\text{m}^3/\text{cm}^3$. Aerosol volume concentrations and distributions were measured using a scanning mobility particle sizer (SMPS; TSI) consisting of a differential mobility analyzer (DMA; TSI 3040) and a condensation particle counter (CPC; TSI 3775). Isoprene (99%, Sigma-Aldrich) was injected into a glass bulb and zero air was passed over the solution until it evaporated. The initial concentration of isoprene was 97 ppb. H_2O_2 (50% aqueous solution, Sigma-Aldrich) was then injected as an OH precursor. Once the concentrations of all species stabilized, UV lights were turned on to initiate photooxidation. The photolysis of H_2O_2 yielded an OH concentration on the order of 10^6 molecules/ cm^3 under low-NO conditions.

A.2.2.2 Field Measurements

The Centreville measurements were performed in Centreville, Alabama (USA), from 01 June to 15 July 2013 during the Southern Oxidant and Aerosol Study (SOAS) with the GT AMS (Xu et al., 2015a; Xu et al., 2015b). The Centreville site is a rural site located in a forested area, with high biogenic emissions, especially isoprene and monoterpenes. Biogenic volatile organic compounds (BVOC)-derived organosulfur species have been identified as an abundant contributor to total OA in the southeastern US (Surratt et al., 2008; Tolocka and Turpin, 2012), making this location ideal for organosulfur compound measurements.

The Mace Head measurements were performed at the Mace Head Global Atmosphere Watch research station, Ireland, from 12 July 2010 to 9 September 2010 with the Galway AMS (Ovadnevaite et al., 2014). This is a ground site located on the west coast of Ireland and facing westward to the northeast Atlantic, where clean marine air coming onshore can be perturbed by (mostly local) anthropogenic sources. In the summertime high oceanic biological activity results in abundant atmospheric MSA at this site.

The Polarstern measurements were performed on the German research vessel (RV) Polarstern during a cruise from Cape Town, Republic of South Africa to Bremerhaven, Germany, from 20 April to 20 May 2011 with the TROPOS AMS (Huang et al., 2017). The cruise took place during the autumn in the Southern hemisphere, when both dimethyl sulphide and MSA concentrations are expected to be relatively low, and spring in the Northern hemisphere, where phytoplankton blooms were often encountered, resulting in high MSA concentrations. This spatial contrast was reflected in the MSA concentration time series.

The Wintertime Investigation of Transport, Emissions, and Reactivity (WINTER) aircraft campaign took place out of the NASA Langley Research Center (Hampton, VA) from February 1 to March 15, 2015 aboard the National Center for Atmospheric Research (NCAR) C-130 aircraft, with the Boulder AMS (Schroder et al., 2018). One campaign objective was to look at the temporal evolution of power plant plumes under low temperature/stagnant conditions typical of the winter months in the northeastern United States.

A.2.3 Sulfate Apportionment Method

A.2.3.1 AMS Sulfate Mass Spectra of Standard Compounds

Organosulfates, sulfonates, and sulfonic acids predominantly fragment into separate organic ($C_xH_yO_z$) and sulfate fragments (SO_x) rather than organosulfur fragments ($C_xH_yO_zS$) in the AMS (Figure A-1), suggesting that most C-O-S (corresponding to organosulfates) and C-S (corresponding to sulfonates and sulfonic acids) bonds are not retained after vaporization and ionization. Sulfonate and sulfonic acid molecules do not contain a sulfate functional group, but the $H_xSO_y^+$ fragments they produce in the AMS would be counted as sulfate concentrations in standard data processing. Therefore, these $H_xSO_y^+$ fragments produced by sulfonates and sulfonic acids will still be referred to as “sulfate” fragments hereafter. For all OS tested in this study, organosulfur fragments only contribute 0.02 - 4% to the total signal, depending on the MW, structure, and bonding types (Figure A-1). Generally, OS with smaller MW of carbon backbones tend to produce a larger fraction of organosulfur fragments, but the structure of the carbon backbones and bonding types may also play a role. For instance, methyl sulfate (OS-1, $H_3C-O-SO_3^-$) and MSA ($H_3C-SO_3^-$) have the same carbon backbone, but MSA retains a much higher portion of organosulfur fragments (16%) because of the different bond types between sulfate/sulfonate groups and the carbon backbones. This difference becomes negligible when one more methyl group is added to the carbon backbone (Figure A-1, ethyl sulfate (OS-2) and ethanesulfonic acid (OS-15)). Phenyl sulfonates produce a higher fraction of organosulfur fragments compared to other OS with similar MW of carbon backbones (Figure A-1, benzenesulfonate (OS-14)), possibly due to the stabilization by resonance between benzene ring and sulfonate group.(Oae, 1991) Due to their small signals, the organosulfur fragments are subject to interference by stronger neighboring signals in the

most common V-mode resolution ($m/dm \sim 2500$) for the AMS when sampling complex matrices such as ambient aerosols, posing a barrier to estimating OS mass only by organosulfur fragments. In contrast, the major sulfate fragments have strong signals and can be well fitted (Figure A-2). Consequently, we focused on using the sulfate fragments to understand the fragmentation patterns of different inorganic sulfates and organosulfur compounds in the AMS.

The typical V-mode AMS high-resolution sulfate mass spectra of AS, MSA, SS, and an OS standard (sodium benzyl sulfate, OS-10) are shown in Figure A-5(a). The spectra obtained in this study show a very similar pattern to those reported elsewhere. (Zorn et al., 2008; Huang et al., 2015; Ge et al., 2012; Hogrefe et al., 2004) Among all the fragments produced by the fragmentation of these different sulfate/sulfonate-containing compounds, the main ions are SO^+ , SO_2^+ , SO_3^+ , HSO_3^+ , and H_2SO_4^+ (Canagaratna et al., 2007). Here, we referred to the sum of these five ions as ΣHSO and normalized each of the five ions to ΣHSO . The normalization can be expressed by eq.A.1-6:

$$\Sigma\text{HSO} = \text{SO}^+ + \text{SO}_2^+ + \text{SO}_3^+ + \text{HSO}_3^+ + \text{H}_2\text{SO}_4^+ \quad (\text{A.1})$$

$$f_{\text{SO}} = \frac{\text{SO}^+}{\Sigma\text{HSO}} \quad (\text{A.2})$$

$$f_{\text{SO}_2} = \frac{\text{SO}_2^+}{\Sigma\text{HSO}} \quad (\text{A.3})$$

$$f_{\text{SO}_3} = \frac{\text{SO}_3^+}{\Sigma\text{HSO}} \quad (\text{A.4})$$

$$f_{HSO_3} = \frac{HSO_3^+}{\Sigma HSO} \quad (A.5)$$

$$f_{H_2SO_4} = \frac{H_2SO_4^+}{\Sigma HSO} \quad (A.6)$$

The normalized SO^+ , SO_2^+ , SO_3^+ , HSO_3^+ , and $H_2SO_4^+$ abundance is shown in Figure A-5(b). For all standards, smaller ions like SO^+ , SO_2^+ and SO_3^+ , account for most of the ΣHSO signals, which can be explained by the extensive thermal decomposition during vaporization and fragmentation after electron impact (EI) ionization. Meanwhile, the HSO_3^+ fragment is only produced by MSA and AS (at different relative abundances), and $H_2SO_4^+$ fragment is exclusively produced by AS. These observations can be explained by their different chemical structures. For organosulfates, it takes less energy to break the O-S bond than the C-O bond, (Sanderson, 1971) so it is more likely for the organic part to retain the oxygen during fragmentation and result in small sulfate fragments with at most three oxygens. For MSA, the sulfur molecule is bonded to three oxygens so that the $H_2SO_4^+$ ion cannot be produced, while the HSO_3^+ ion can be produced by breaking the C-S bond. For ammonium sulfate, sulfate decomposes to either dehydrated SO_3 (+ H_2O) or intact H_2SO_4 , (Allan et al., 2004b) and the water signal produced due to the dehydration process is calculated based on an empirical sulfate fragmentation table (Table A-2). (Allan et al., 2004b) For the other sulfate/sulfonate-containing species discussed in this study (MSA, OS, and SS), there is no pathway to produce water fragments, therefore a sulfate fragmentation table without water fragments was used for these species (Table A-2).

The distinctive HSO_3^+ and $H_2SO_4^+$ ion fractions in different standard compounds provide the basis for our method of distinguishing different types of sulfate/sulfonate-

containing compounds. Figure A-5(c) shows the $f_{H_2SO_4}$ vs. f_{HSO_3} for all standard compounds. The four types of standards (AS, OS, SS, and MSA) together defined a triangle-shaped space, with OS and SS occupying indistinguishable regions in this space. There are some variations in f_{HSO_3} and $f_{H_2SO_4}$ among all OS (Table A-3), but the variations are small, thus the average value for all OS was used hereafter. Different types of inorganic sulfates and organosulfur compounds fall into different regions in this space and thus can be distinguished. The relative contribution from each type of sulfate/sulfonate-containing compounds can be estimated for any point in this space. The mass spectra of AS and MSA obtained by the Galway AMS, TROPOS AMS, and Boulder AMS are also shown in Figure A-5(c). The differences in the same type of compounds among different AMS likely arise from instrument-to-instrument and time-to-time variability. Therefore, when applying the apportionment method, calibrations with SS/OS, AS, and MSA standards to define the triangle region are required for the particular instrument and time period. In addition, calibrations of RIE for the standard species are required for accurate quantification.

A.2.3.2 Development of Sulfate Apportionment Method

Based on the different f_{HSO_3} and $f_{H_2SO_4}$ for different types of sulfate/sulfonate-containing compounds, we developed an approach to deconvolve total sulfate signals into components of inorganic and organic origins. Based on the f_{HSO_3} and $f_{H_2SO_4}$ values determined for pure standard compounds in the laboratory, the measured HSO_3^+ , $H_2SO_4^+$, and ΣHSO can be expressed as:

$$\begin{aligned} \text{HSO}_{3,\text{meas}} &= f_{\text{HSO}_3,\text{AS},\text{standard}} \times \Sigma\text{HSO}_{\text{AS}} + f_{\text{HSO}_3,\text{OS/SS},\text{standard}} \times \Sigma\text{HSO}_{\text{OS/SS}} \\ &+ f_{\text{HSO}_3,\text{MSA},\text{standard}} \times \Sigma\text{HSO}_{\text{MSA}} \end{aligned} \quad (\text{A.7})$$

$$\begin{aligned} \text{H}_2\text{SO}_{4,\text{meas}} &= f_{\text{H}_2\text{SO}_4,\text{AS},\text{standard}} \times \Sigma\text{HSO}_{\text{AS}} + f_{\text{H}_2\text{SO}_4,\text{OS/SS},\text{standard}} \times \Sigma\text{HSO}_{\text{OS/SS}} \\ &+ f_{\text{H}_2\text{SO}_4,\text{MSA},\text{standard}} \times \Sigma\text{HSO}_{\text{MSA}} \end{aligned} \quad (\text{A.8})$$

$$\Sigma\text{HSO}_{\text{meas}} = \Sigma\text{HSO}_{\text{AS}} + \Sigma\text{HSO}_{\text{OS/SS}} + \Sigma\text{HSO}_{\text{MSA}} \quad (\text{A.9})$$

The subscript “_{meas}” denotes the measured mass concentration of sulfate fragments, and the subscript “_{standard}” denotes measured fractions of standard compounds. $\Sigma\text{HSO}_{\text{AS}}$, $\Sigma\text{HSO}_{\text{OS/SS}}$, and $\Sigma\text{HSO}_{\text{MSA}}$ are ΣHSO for AS, OS or SS, and MSA, respectively, which can be solved by:

$$\begin{bmatrix} \Sigma\text{HSO}_{\text{AS}} \\ \Sigma\text{HSO}_{\text{OS/SS}} \\ \Sigma\text{HSO}_{\text{MSA}} \end{bmatrix} = \begin{bmatrix} f_{\text{HSO}_3,\text{AS},\text{standard}} & f_{\text{HSO}_3,\text{OS/SS},\text{standard}} & f_{\text{HSO}_3,\text{MSA},\text{standard}} \\ f_{\text{H}_2\text{SO}_4,\text{AS},\text{standard}} & f_{\text{H}_2\text{SO}_4,\text{OS/SS},\text{standard}} & f_{\text{H}_2\text{SO}_4,\text{MSA},\text{standard}} \\ 1 & 1 & 1 \end{bmatrix}^{-1} \begin{bmatrix} \text{HSO}_{3,\text{meas}} \\ \text{H}_2\text{SO}_{4,\text{meas}} \\ \Sigma\text{HSO}_{\text{meas}} \end{bmatrix} \quad (\text{A.10})$$

Afterwards, the fractions of ΣHSO in AMS total sulfate signals (i.e., $\left(\frac{\Sigma\text{HSO}}{\text{total sulfate}} \right)_{\text{standard}}$) acquired for each type of species during the calibrations will be used to convert ΣHSO signals from above calculations to total sulfate signals.

For OS and SS, they are indistinguishable in the f_{HSO_3} vs. $f_{\text{H}_2\text{SO}_4}$ space, but their relative contributions to total sulfate in ambient data can be highly dependent on the measurement locations. SS is considered as a refractory species and cannot be completely vaporized at 600 °C (default AMS vaporizer temperature) (Allan et al., 2004a). As a result,

for typical continental sites, SS signals may be a minor component compared to OS. For coastal and cruise measurements, SS cannot be neglected due to its abundance. In the following discussion, we will treat $\Sigma\text{HSO}_{\text{OS/SS}}$ resolved for a continental site (Centreville) as dominantly from OS (except for a short period of crustal events), and for coastal or marine measurements (Mace Head and Polarstern), we will treat OS and SS as one component, i.e., the summation of OS and SS.

A.2.3.3 Laboratory Calibration of Sulfate RIE

The sulfate RIE (relative ionization efficiency of the species of interest relative to nitrate) (Canagaratna et al., 2007) in the AMS (RIE_{SO_4}) can be calibrated with pure ammonium sulfate (Hu et al., 2017). The default RIE_{SO_4} of 1.2 was used for ammonium sulfate in this study because this calibration was not performed for the majority of the field studies discussed here. Our two-year records (2017 - 2018) of RIE_{SO_4} on the GT AMS is 1.20 ± 0.15 , validating that 1.2 is a good estimation. The RIE_{SO_4} of organosulfate compounds can be lower than that of ammonium sulfate, since during the fragmentation and ionization processes, the electronegative sulfate/sulfonate groups have a reduced tendency to retain the charge (Docherty et al., 2011; Aiken et al., 2007; Aiken et al., 2008). The RIE_{SO_4} was determined for two commercially available organosulfur compounds (MSA and ethyl sodium sulfate (OS-2)) with the GT AMS. Size-selected (300 nm) pure MSA (or OS-2) was atomized to the AMS and a condensation particle counter (CPC; TSI 3775) simultaneously. Sulfate concentration based on particle number was calculated by:

$$[\text{SO}_4]_{\text{CPC}} = \frac{n_{\text{CPC}} \pi \rho D_p^3}{6} f_{\text{SO}_4, \text{formula}} \quad (\text{A.11})$$

where n_{CPC} is the particle number concentration measured by CPC, ρ is the density of organosulfur compounds, D_p is the selected particle diameter, and $f_{SO_4, formula}$ is the sulfate functionality mass fraction according to the compound formula (e.g., 81/96 for MSA). The collection efficiency (CE) of 1 was applied to AMS data. Viscosity measurements of organosulfur compounds are lacking in literature. Here we assumed that MSA and OS-2 particles are of low viscosity given their low MW (Shiraiwa et al., 2017; DeRieux et al., 2018), while uncertainty regarding this assumption exists. A RIE_{SO_4} of 0.77 was calculated for MSA and a RIE_{SO_4} of 0.82 is calculated for OS-2 (Figure A-6). The reason for the lower RIE_{SO_4} for MSA is because a higher fraction of organosulfur fragments was produced in the fragmentation process of MSA compared to OS-2 (Figure A-1), and these fragments were not accounted in the sulfate concentration in eq. A.11. For the subsequent analysis, we tentatively applied an RIE of 0.8 to sulfate produced by organosulfur compounds. A default RIE of 1.2 was applied to “AS sulfate”.

A.2.3.4 Uncertainty Analysis

Recall that ΣHSO_{AS} , $\Sigma HSO_{OS/SS}$, and ΣHSO_{MSA} are calculated by eq. A.10 in the main text. Including the error of each term we can get:

$$\begin{bmatrix} \Sigma HSO_{AS} \pm \delta \Sigma HSO_{AS} \\ \Sigma HSO_{OS/SS} \pm \delta \Sigma HSO_{OS/SS} \\ \Sigma HSO_{MSA} \pm \delta \Sigma HSO_{MSA} \end{bmatrix} = \begin{bmatrix} (f_{HSO_3} \pm \delta f_{HSO_3})_{AS} & (f_{HSO_3} \pm \delta f_{HSO_3})_{OS/SS} & (f_{HSO_3} \pm \delta f_{HSO_3})_{MSA} \\ (f_{H_2SO_4} \pm \delta f_{H_2SO_4})_{AS} & (f_{H_2SO_4} \pm \delta f_{H_2SO_4})_{OS/SS} & (f_{H_2SO_4} \pm \delta f_{H_2SO_4})_{MSA} \\ 1 & 1 & 1 \end{bmatrix}^{-1} \begin{bmatrix} (HSO_3 \pm \delta HSO_3)_{meas} \\ (H_2SO_4 \pm \delta H_2SO_4)_{meas} \\ (\Sigma HSO \pm \delta \Sigma HSO)_{meas} \end{bmatrix}$$

(A.12)

For laboratory calibration of standard compounds, δf_{HSO_3} and $\delta f_{H_2SO_4}$ of pure standard compounds (AS and MSA) were calculated as the standard deviation during calibration when signals were stable, while δf_{HSO_3} and $\delta f_{H_2SO_4}$ of OS/SS were calculated as the standard deviation of all OS and SS compounds calibrated in this study. For uncertainties in the measured mass concentration of sulfate fragments, $\delta \Sigma HSO$ was calculated by error propagation:

$$\delta \Sigma HSO = \sqrt{(\delta SO^+)^2 + (\delta SO_2^+)^2 + (\delta SO_3^+)^2 + (\delta HSO_3^+)^2 + (\delta H_2SO_4^+)^2} \quad (A.13)$$

The uncertainties of apportionment results (ΣHSO_{AS} , $\Sigma HSO_{OS/SS}$, and ΣHSO_{MSA}) can be then assessed via Monte Carlo approach. For the scaling factor, $\left(\frac{\Sigma HSO}{\text{total sulfate}} \right)_{\text{standard}}$, used to convert ΣHSO signals from above calculations to total sulfate signals, the uncertainty was acquired from the standard calibration. The uncertainties of IE determination ($\sim 10\%$), CE determination ($\sim 30\%$), and RIE determination ($\sim 15\%$) were also encapsulated. (Bahreini et al., 2009)

A.3 Results and Discussion

A.3.1 Sulfate Apportionment for Laboratory-Generated Binary Mixtures

The sulfate apportionment method was first validated with laboratory-generated aerosols of known compositions. Two different types of standard compound solutions were pre-mixed and nebulized into an AMS (GT AMS). Particles with a mobility diameter of 300 nm were selected.

We first tested the mixture of AS with MSA. MSA and AS were dissolved in DI water in different molar ratios (3:1, 2:1, 1:1, 1:2, 1:3). The mixture solution was immediately nebulized into the AMS. After obtaining $\Sigma\text{HSO}_{\text{MSA}}$ and $\Sigma\text{HSO}_{\text{AS}}$ by eq. A.10, total sulfate signals by MSA (“MSA sulfate”) and AS (“AS sulfate”) were calculated by:

$$\text{SO}_{4,\text{MSA}} = \frac{\Sigma\text{HSO}_{\text{MSA}}}{\text{RIE}_{\text{SO}_4,\text{MSA}}} \left(\frac{\Sigma\text{HSO}}{\text{SO}_4} \right)_{\text{MSA,standard}} \quad (\text{A.14})$$

$$\text{SO}_{4,\text{AS}} = \frac{\Sigma\text{HSO}_{\text{AS}}}{\text{RIE}_{\text{SO}_4,\text{AS}}} \left(\frac{\Sigma\text{HSO}}{\text{SO}_4} \right)_{\text{AS,standard}} \quad (\text{A.15})$$

Figure A-7(a) shows “MSA sulfate” to “AS sulfate” molar ratio calculated by apportionment method as a function of MSA to AS molar ratio in the particles. The MSA to AS ratio in the particles was assumed to be the same as that in the solution (Matthew et al., 2008; Xu et al., 2017a; Xu et al., 2018b). MW of 98 g/mol and 81 g/mol are used for “AS sulfate” and “MSA sulfate”, respectively, to calculate their molar ratios. The calculated “MSA sulfate” to “AS sulfate” ratio agreed well with particle compositions (slope = 0.97 ± 0.02).

A similar binary mixture apportionment analysis was carried out for mixtures of AS and OS standards. The results of AS and ethanesulfonic acid (OS-15) mixtures are shown in Figure A-7(b). Similarly, the calculated sulfate produced by OS (“OS sulfate”) to “AS sulfate” ratio is highly correlated with particle composition. The slope is lower than 1 (0.88 ± 0.04) but still within the uncertainty of AMS measurements.

A.3.2 Effect of Particle Acidity on AS Fragmentation Pattern

Considering marine and stratospheric aerosols are rich in sulfuric acid (Ovadnevaite et al., 2014; Murphy et al., 2007), and the particle pH is low in the southeastern United States (Guo et al., 2015), we investigated the fragmentation pattern of acidic AS. Acidic sulfate (1:1 mixture of ammonium sulfate and sulfuric acid) was tested with the GT AMS, and pure sulfuric acid was tested with the Boulder AMS. The results are shown in Figure A-8(a). All f_{HSO_3} and $f_{H_2SO_4}$ are normalized to those of AS from the specific AMS to minimize the influence from instrument-to-instrument variability, so that AS would always be at point (1,1) in the $f_{H_2SO_4}$ vs. f_{HSO_3} space. Acidic AS shows a similar fragmentation pattern to AS, with a slightly higher production of HSO_3^+ and $H_2SO_4^+$ fragments (Table A-3 and Figure A-8(a)). However, pure sulfuric acid shows almost twice higher fractions of HSO_3^+ and $H_2SO_4^+$ fragments (Figure A-8(a)) compared to AS. We speculate that the reason is that a much larger fraction evaporates intact for pure sulfuric acid, compared to the fraction of the sulfate that evaporates as sulfuric acid for AS and acidic AS, and dehydration is more likely to happen for sulfate salts than sulfuric acid (Allan et al., 2004b; Drewnick et al., 2015). Since vaporization equilibrium between H_2SO_4 and $SO_3 + H_2O$ can shift with changing temperature, a precise temperature control of the AMS vaporizer and a MS tuning that favors a non-mass dependent response are necessary (Hu et al., 2017).

The Boulder AMS was also deployed in the WINTER aircraft campaign (Schroder et al., 2018), where it intercepted a strong coal-fired power plant plume (~ 50 ppb SO_2). As shown in Figure A-8(b), the estimated particle pH (calculated with the E-AIM model (Clegg et al., 1998; Wexler and Clegg, 2002; Clegg et al., 2003)) decreased rapidly to -1 in

the core of the plume. The highest f_{HSO_3} and $f_{H_2SO_4}$ values in the plume are 72% and 21% higher, respectively, compared to pure AS from the same AMS. In this strong plume, the sulfate concentration is an order of magnitude higher than ammonium, nitrate, and organics concentrations, thus the change in f_{HSO_3} and $f_{H_2SO_4}$ is attributed to the near sulfuric acid conditions and very high acidity. The shifts in f_{HSO_3} and $f_{H_2SO_4}$ to values outside the region defined by the OS/SS-AS-MSA triangle suggest that caution is needed when applying the apportionment method to data obtained under high acidity (near pure H_2SO_4 , molar ratio of $NH_4:SO_4 < 0.8$) conditions. Nevertheless, for ground studies the ambient particles are less acidic than pure sulfuric acid particles in most cases (Zhang et al., 2007b; Bougiatioti et al., 2016; Guo et al., 2017b; Liu et al., 2017; Guo et al., 2017a).

A.3.3 Sulfate Apportionment for Chamber-Generated Isoprene SOA

Organosulfates can be formed in isoprene photooxidation reactions (Surratt et al., 2007a; Surratt et al., 2010). Here, we applied the sulfate apportionment method to quantify OS formation in an isoprene photooxidation experiment (Tuet et al., 2017). The reaction profile is shown in Figure A-9. The increase in total sulfate concentration as SOA started to form is likely due to increase in collection efficiency (CE) with the condensation of organics (Docherty et al., 2013; Bahreini et al., 2005). We assumed all O-S bonds in C-O-S structures (corresponding to organosulfates) are broken. Thus no organosulfur fragments are produced, and sulfate/sulfonate functionality MW is 80 g/mol (corresponding to SO_3) for all OS. With these, we estimated that 7% of AS seed has become organosulfate as SOA reaches peak growth, and the “OS sulfate” could contribute to 7% of total SOA. $C_xH_yO_zS^+$ ions only account for 0.07% of total SOA, consolidating our assumption that almost all O-

S bonds in C-O-S structures are broken to form “OS sulfate”. Prior studies have shown that the formation of isoprene-epoxydiol (IEPOX) organosulfate (one of the abundant isoprene-derived organosulfates) is strongly enhanced in the presence of acidic sulfate seed (Surratt et al., 2007a; Surratt et al., 2010; Lin et al., 2012; Riedel et al., 2016; Zhang et al., 2018b; Cui et al., 2018). As our chamber experiment was conducted under dry conditions with ammonium sulfate seed, the contribution of organosulfates to total organic aerosols is expected to be lower than those under humid acidic conditions (Surratt et al., 2007a; Surratt et al., 2010).

A.3.4 Application to Field Measurements for OS Estimation

We applied the sulfate apportionment method to the SOAS data from Centreville to deconvolve sulfate from AS, OS, and MSA, respectively. The average “OS sulfate” mass is $0.12 \mu\text{g}/\text{m}^3$ for the whole campaign, which means that 4% of measured sulfate is from OS. We note that there are some negative values (6% of all the data) in the calculated “OS sulfate” concentration, which is due to data points falling outside the AS-MSA line in the triangle (Figure A-10(a)), as expected due to measurement noise. Our apportionment result is consistent with recent airborne and ground measurements in the same region. Liao et al. quantified IEPOX-sulfate using PALMS during flight measurements and determined that it accounted for ~5% of the total sulfate mass measured by AMS (Liao et al., 2015). Hu et al. (2015) also indicated that IEPOX-sulfate accounted for ~5% of total sulfate mass for SOAS measurements. Previous study by Guo et al. (2015) showed that AMS total sulfate is 20% higher than inorganic sulfate measured by particle-into-liquid-sampler coupled to an ion chromatograph (PILS-IC) during SOAS. After excluding the OS sulfate calculated

from our apportionment method, the resulting AMS “AS sulfate” shows a better agreement (slope = 0.97) with PM₁ inorganic sulfate measured by PILS-IC (Figure A-11(a)).

We also compare our OS with speciated organosulfur compounds quantified in PM_{2.5} filter samples collected at Centreville during SOAS, using offline hydrophilic interaction liquid chromatography (HILIC) and a triple quadrupole mass spectrometer (TQD MS) against authentic standards (Hettiyadura et al., 2017). We focus on OS compounds that are both used in the apportionment method development in this study and quantified in the filter analysis. The “OS sulfate” time series calculated by sulfate apportionment method is shown in Figure A-11(b), together with total sulfate measured by the AMS (Xu et al., 2015a; Xu et al., 2015b), methyl sulfate, glycolic acid sulfate and hydroxyacetone sulfate quantitatively measured by offline HILIC-TQD (Hettiyadura et al., 2017), and isoprene-OA resolved by PMF (Xu et al., 2015a; Xu et al., 2015b). The AMS “OS sulfate” shows a moderate correlation ($R = 0.52$) with speciated organosulfur compounds measured by offline HILIC-TQD. Two periods 6/17/2013 - 6/18/2013 and 6/24/2013 - 6/28/2013 are excluded when calculating the R value, because these two periods overlap with the crustal events when mineral cations are abundant and the contribution of SS is not negligible (Allen et al., 2015). For the “OS sulfate” spike on 6/26/2013, we speculated that it is due to the overlap of crustal event with strong isoprene-related OS formation. Further, we compared “OS sulfate” with AMS isoprene-OA factor under different isoprene-OA abundances to study the role of isoprene-derived OS at Centreville. As shown in Figure A-11(c), the correlation between “OS sulfate” and isoprene-OA is enhanced as the fraction of isoprene-OA in total OA increases. The improved correlation between “OS sulfate” and isoprene-OA as isoprene-OA fraction

increases is consistent with isoprene-derived OS being an important source of OS at Centreville in summer when isoprene is abundant (Hettiyadura et al., 2017). Such enhancement in correlation is not observed for other OA factors (Figure A-12), suggesting that even if other factors may contribute to OS, they are not the major sources.

A recent new study characterized 12 types of organosulfur compounds in filter samples of PM_{2.5} collected from SOAS (Hettiyadura et al., 2018). The sulfate mass associated with these 12 organosulfates over the studied period averaged 0.37 $\mu\text{g}/\text{m}^3$, with 2-methyltetrol sulfate accounting for 80% of the “OS sulfate” mass. These filter results imply that total “OS sulfate” could account for 16% of the total sulfate mass, which is higher than our estimation and prior studies by Liao et al. (2015) and Hu et al. (2015). Two instruments measuring particles of different sizes (PM₁ by the AMS and PM_{2.5} by filter) and uncertainties in different instrument/measurement techniques likely contribute to the different observations. In this study, we cannot exclude the possibility that the fragmentation pattern of 2-methyltetrol sulfate in the AMS is different from other OS standards. Future work is warranted to expand the analysis to encompass an even wider suite of OS standards as they become available and characterize OS sulfate measured by different techniques.

A.3.5 Application to Field Measurements for MSA Estimation

For measurements at coastal sites and from cruises, we focused on resolving MSA time variation for Mace Head and Polarstern measurements, in a similar manner to OS estimation, using 96 g/mol as MSA MW and 81 g/mol as sulfonic acid functionality MW.

Previous studies have reported the quantification of MSA with the AMS by a well-developed signature fragments method (Phinney et al., 2006; Zorn et al., 2008; Huang et al., 2015; Ovadnevaite et al., 2014; Huang et al., 2017) based on ions such as CH_3SO_2^+ , CH_4SO_3^+ , etc., which are almost solely produced by MSA. Based on the fragmentation pattern of the pure MSA standard, ambient MSA concentration can be calculated using the intensity of signature fragments and their relative contributions in pure MSA. Here, we compared MSA concentration calculated by the signature fragments method and sulfate apportionment method presented in this study. The results for Mace Head and the RV Polarstern measurements are shown in Figure A-13. For both datasets, the MSA concentration estimated by the two methods shows good correlation ($R^2 = 0.675$ for Mace Head data, and $R^2 = 0.710$ for Polarstern data). Compared to the signature fragments method, the average concentration estimated by sulfate apportionment method is higher by 30% for Mace Head measurements and 150% for Polarstern measurements. The reason is currently unknown, but a possible cause could be that the high acidity of submicron marine aerosols (Fridlind and Jacobson, 2000; Keene et al., 2004) affects sulfate fragmentation pattern as discussed above. For instance, for the Polarstern measurements, even accounting for the presence of large amount of sea salt sulfate, most data points have higher fractions of HSO_3^+ and H_2SO_4^+ fragments than the AS standard (Figure A-10(c)). Meanwhile, some data points fall outside the OS/SS-AS line in the triangle (Figure A-10(b), (c)), resulting in negative concentrations in MSA estimation (Figure A-13), which requires further investigation. Nevertheless, this shows that the sulfate apportionment method is capable of determining the presence of MSA and its approximate concentration, and of approximately separating the MSA contribution from that of AS and OS species.

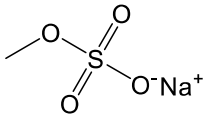
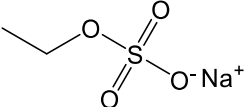
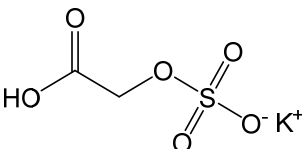
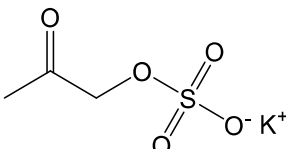
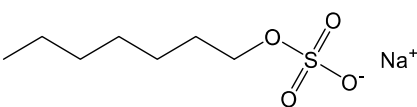
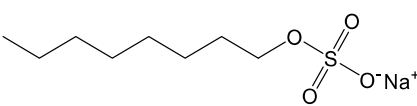
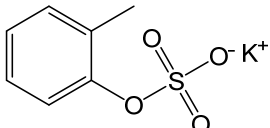
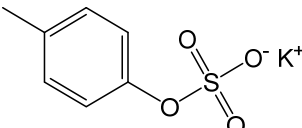
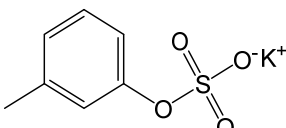
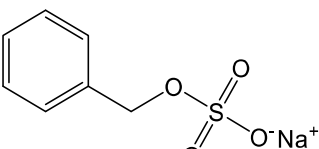
A.4 Conclusions

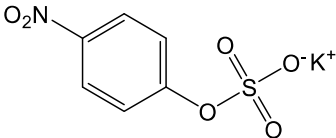
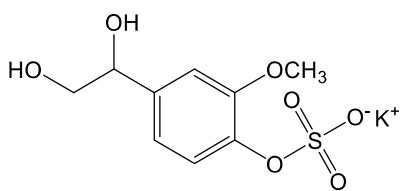
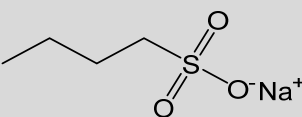
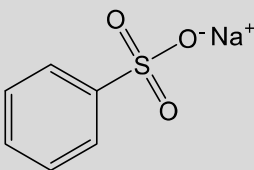
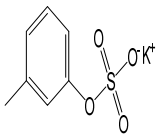
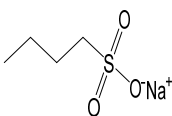
In this study, a novel sulfate apportionment method was developed for AMS analysis. We showed that sulfate fragments originated from organosulfur compounds can be resolved from those of inorganic sulfate based on their different sulfate fragmentation patterns, providing insights into the quantity and time variations of organosulfur compounds in the atmosphere. The advantage of this method is that the contribution of “AS sulfate”, “OS/SS sulfate”, and “MSA sulfate” can be directly estimated using AMS measurements with high time resolution. One thing to note is that the sulfate apportionment method only estimates the mass concentration of sulfate/sulfonate functionalities in organosulfur molecules. The estimation of total OS contribution can be dependent on a good estimation of OS MW.

We note that there are several limitations of this study. First, while we have considered an extensive set of atmospherically relevant OS standards, given the variety and complexity of atmospherically relevant organosulfur compounds, additional standards should be evaluated to explore the robustness of the fragmentation patterns of organosulfur compounds presented here. Second, we found that the sulfate fragmentation pattern can be very different under high acidity, making this method not directly applicable under near sulfuric acid conditions, though such extreme particle acidity is not common in typical continental surface measurements. Third, when data points fall outside the triangular region defined by OS/SS-AS-MSA, the estimated concentrations (either OS/SS, AS, or MSA, depending on where the data point falls) could be negative. As this will always occur to some degree due to the impact of random noise, averaging of longer data periods may be more meaningful under low concentration conditions.

Currently, the AMS sulfate is often misinterpreted as being entirely inorganic sulfate. Here, we applied the sulfate apportionment method to both chamber and ambient measurements. Our apportionment results clearly demonstrate that organosulfur compounds could be a non-negligible source of sulfate fragments in the AMS. Future studies need to take this into account when reporting organic and inorganic mass concentrations from AMS measurements. Overall, quantitative measurements of organosulfur compounds with high-time resolution will allow for improved constraints of their abundance in different environments and help advance the understanding of organosulfur compounds formation and related chemical processes in the atmosphere.

Table A-1 Standard Compounds.

Compound	Molecular Structure	Family	Source
Sodium methyl sulfate (OS-1)		Organosulfate	Commercial (99%)
Sodium ethyl sulfate (OS-2)		Organosulfate	Commercial (96.31%)
Potassium glycolic acid sulfate (OS-3)		Organosulfate	Lab Synthesized ^a (> 98%)
Potassium hydroxyacetone sulfate (OS-4)		Organosulfate	Lab Synthesized ^a (> 98%)
Sodium n-heptyl sulfate (OS-5)		Organosulfate	Commercial (99%)
Sodium n-octyl sulfate (OS-6)		Organosulfate	Commercial (> 95%)
Potassium o-cresol sulfate (OS-7)		Organosulfate	Lab Synthesized ^b (> 98%)
Potassium p-cresol sulfate (OS-8)		Organosulfate	Lab Synthesized ^b (> 98%)
Potassium m-cresol sulfate (OS-9)		Organosulfate	Lab Synthesized ^b (> 98%)
Sodium benzyl sulfate (OS-10)		Organosulfate	Lab Synthesized ^b (> 98%)

Potassium 4-nitrophenyl sulfate (OS-11)		Organosulfate	Commercial (> 98%)
Potassium 4-hydroxy-3-methoxyphenylglycol sulfate (OS-12)		Organosulfate	Commercial (> 98%)
Sodium 1-butanesulfonate (OS-13)		Sulfonate	Commercial (> 99%)
Sodium benzenesulfonate (OS-14)		Sulfonate	Commercial (97%)
Methanesulfonic acid (MSA)		Sulfonic Acid	Commercial (> 99%)
Ethanesulfonic acid (OS-15)		Sulfonic Acid	Commercial (95%)
Ammonium Sulfate (AS)	$(\text{NH}_4)_2\text{SO}_4$	Inorganic Sulfate	Commercial (> 99%)
Sodium Sulfate (SS)	Na_2SO_4	Inorganic Sulfate	Commercial (> 99%)

^a Hettiyadura et al. (2015).

^b Staudt et al. (2014).

Table A-2 Sulfate Fragmentation Table.

Ion	HR_frag_sulfate (AS)	HR_frag_sulfate (MSA, OS, SS)
O	0.04*HR_frag_sulfate[H2O]	-
HO	0.25*HR_frag_sulfate[H2O]	-
j18O	0.00205499*HR_frag_sulfate[O]	-
H2O	0.67*HR_frag_sulfate[SO2], 0.67*HR_frag_sulfate[SO]	-
Hj18O	0.00205499*HR_frag_sulfate[HO]	-
H2j18O	0.00205499*HR_frag_sulfate[H2O]	-
S	0.21*HR_frag_sulphate[SO2], 0.21*HR_frag_sulphate[SO], 0.068*HR_frag_sulphate[HSO3], 0.068*HR_frag_sulphate[H2SO4]	0.21*HR_frag_sulphate[SO2], 0.21*HR_frag_sulphate[SO], 0.068*HR_frag_sulphate[HSO3], 0.068*HR_frag_sulphate[H2SO4]
j33S	0.00789557*HR_frag_sulphate[S]	0.00789557*HR_frag_sulphate[S]
j34S	0.0447416*HR_frag_sulphate[S]	0.0447416*HR_frag_sulphate[S]

Table A-3 Normalized Sulfate Fragments for Pure Compounds from GT AMS.

Name	f_{SO}	f_{SO_2}	f_{SO_3}	f_{HSO_3}	$f_{\text{H}_2\text{SO}_4}$
OS-1	0.3760	0.6014	0.0215	0.0010	0.0000
OS-2	0.3821	0.5620	0.0528	0.0028	0.0003
OS-3	0.3686	0.6139	0.0174	0.0000	0.0002
OS-4	0.3755	0.6060	0.0184	0.0001	0.0000
OS-5	0.3655	0.5976	0.0364	0.0004	0.0000
OS-6	0.3864	0.5453	0.0671	0.0009	0.0002
OS-7	0.3772	0.5790	0.0433	0.0004	0.0001
OS-8	0.3735	0.5922	0.0336	0.0005	0.0002
OS-9	0.3754	0.5931	0.0310	0.0005	0.0000
OS-10	0.3664	0.6037	0.0285	0.0012	0.0002
OS-11	0.3684	0.5983	0.0333	0.0000	0.0000
OS-12	0.3807	0.5705	0.0481	0.0006	0.0001
OS-13	0.3754	0.6167	0.0061	0.0017	0.0001
OS-14	0.3712	0.6171	0.0044	0.0072	0.0001
OS-15	0.3796	0.6115	0.0021	0.0068	0.0000
MSA	0.4040	0.5358	0.0014	0.0587	0.0001
AS	0.3338	0.4223	0.1596	0.0546	0.0297
Acidic AS	0.3494	0.4667	0.0949	0.0567	0.0324
SS	0.3773	0.5914	0.0294	0.0013	0.0006

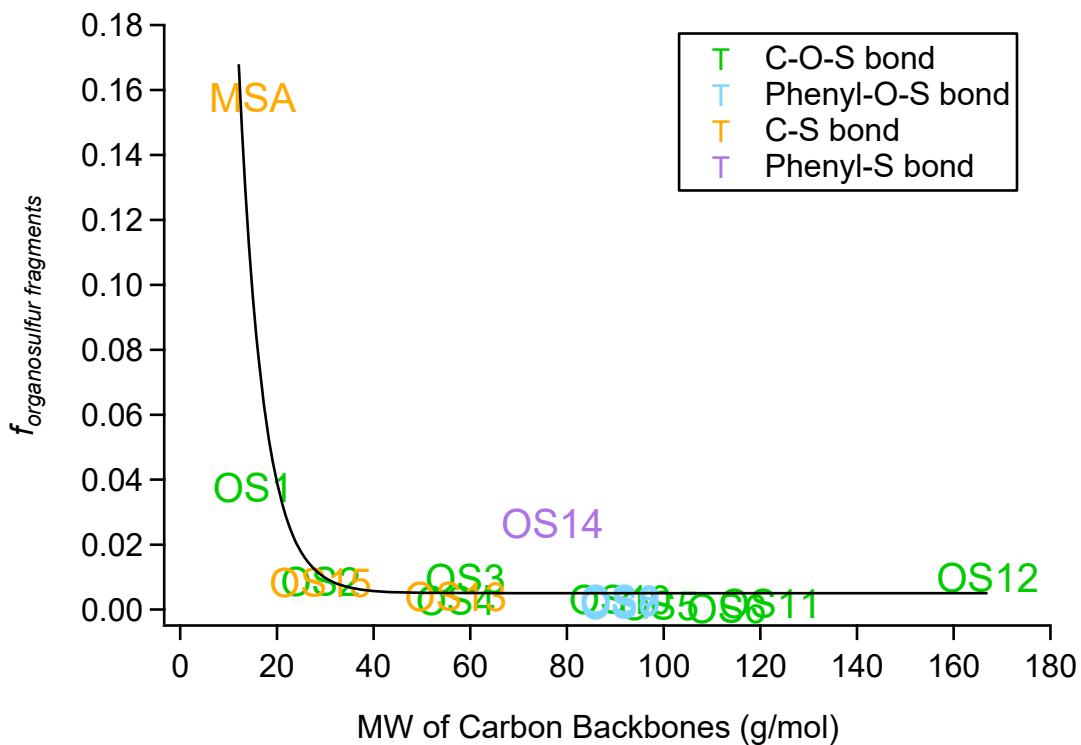


Figure A-1 Fractions of organosulfur fragments produced by standard organosulfur compounds in the AMS as a function of the molecular weight of carbon backbones. The data points are colored by their carbon backbone structures and bonding types.

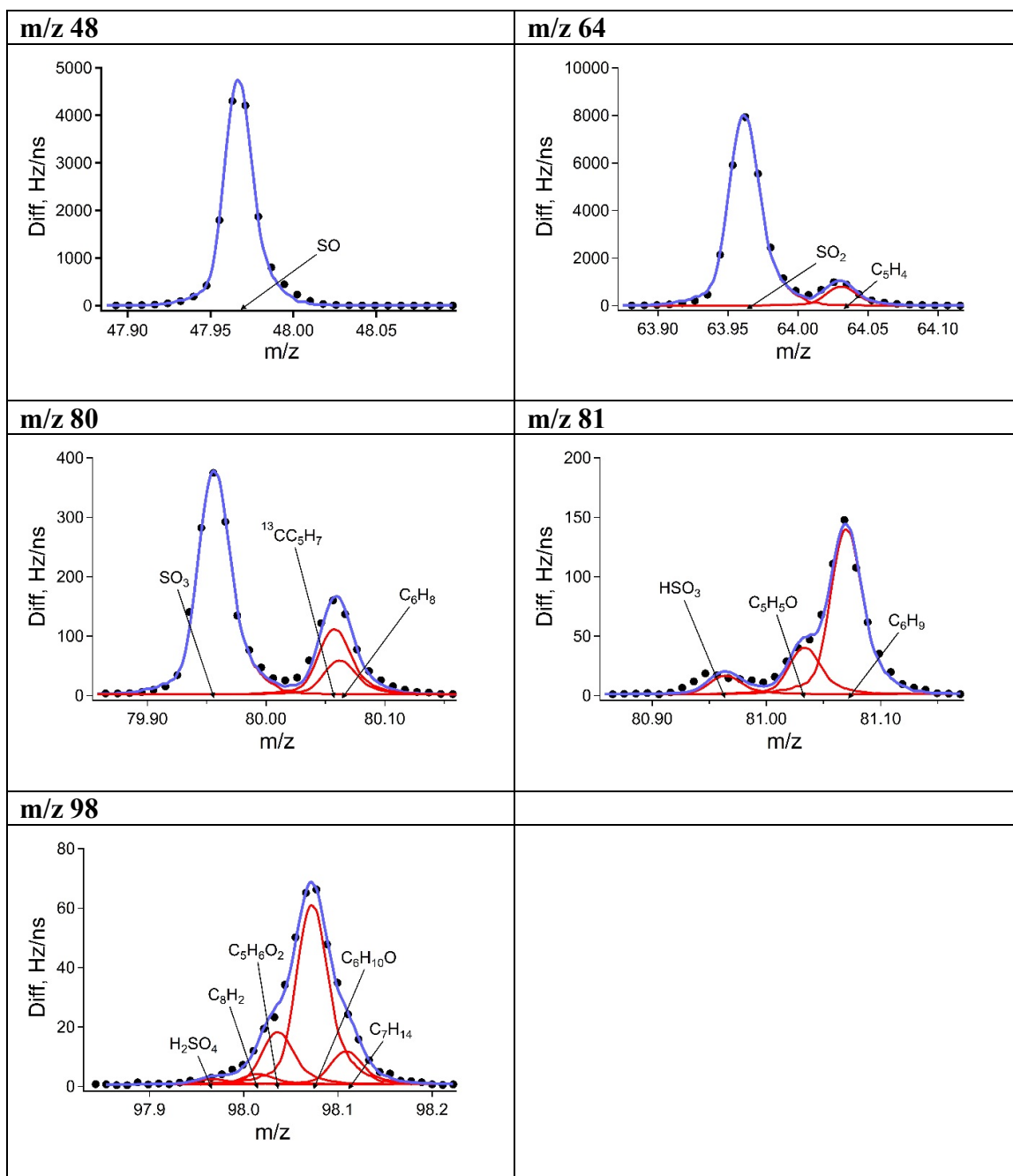


Figure A-2 Peak fit of main sulfate fragments for OS-10.

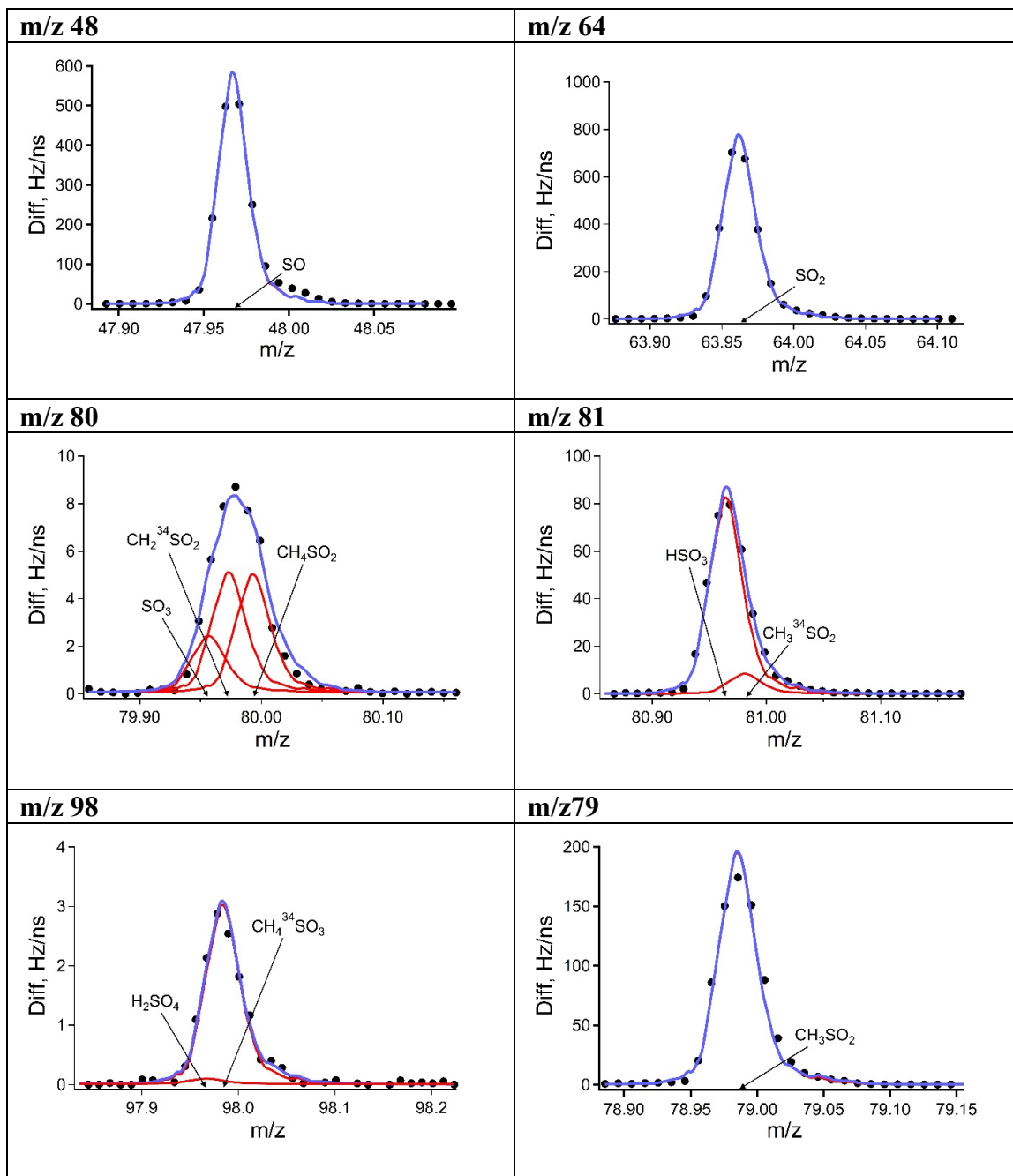


Figure A-3 Peak fit of main sulfate fragments and CH_3SO_2^+ for MSA.

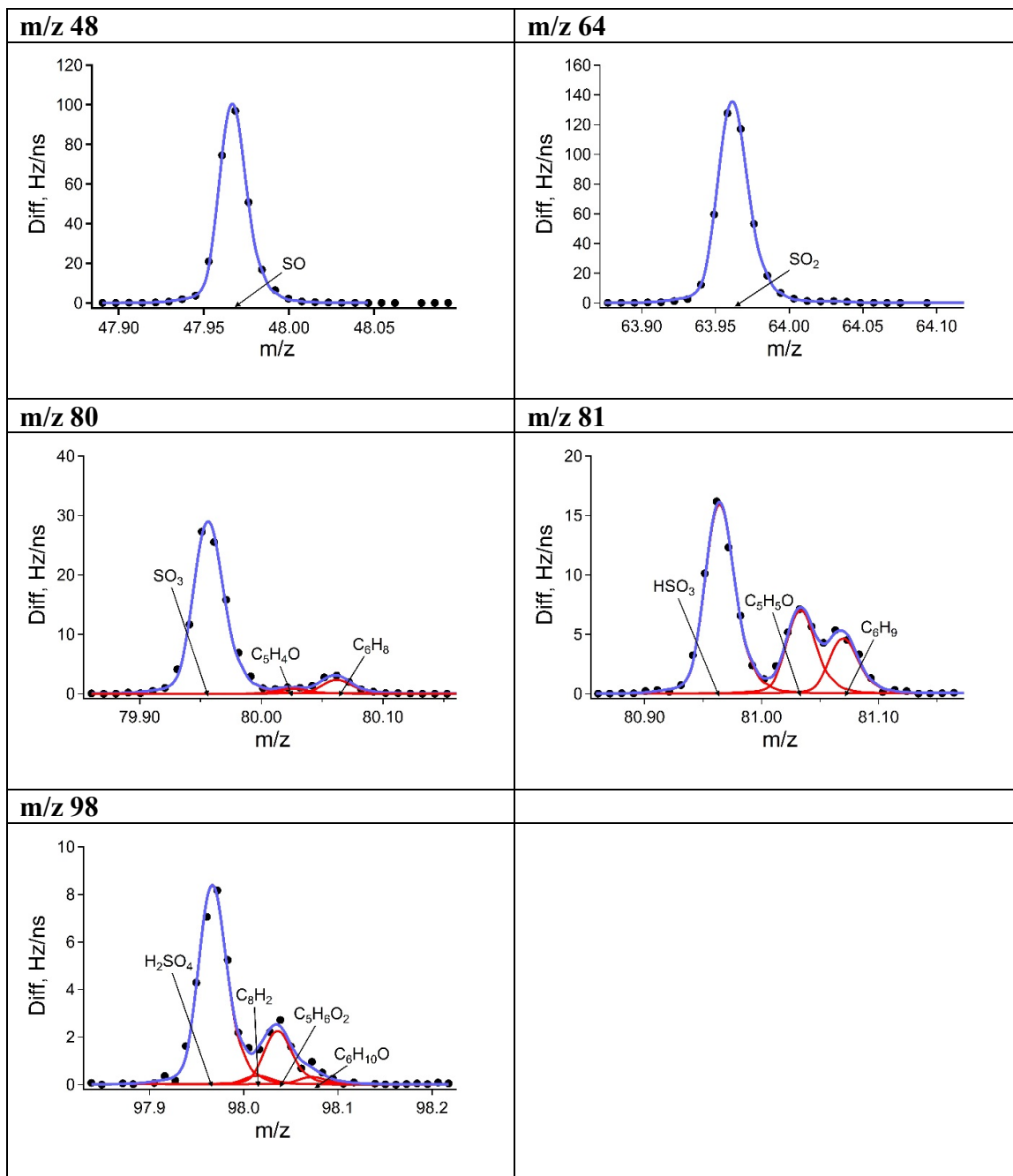


Figure A-4 Peak fit of main sulfate fragments for Centreville measurements.

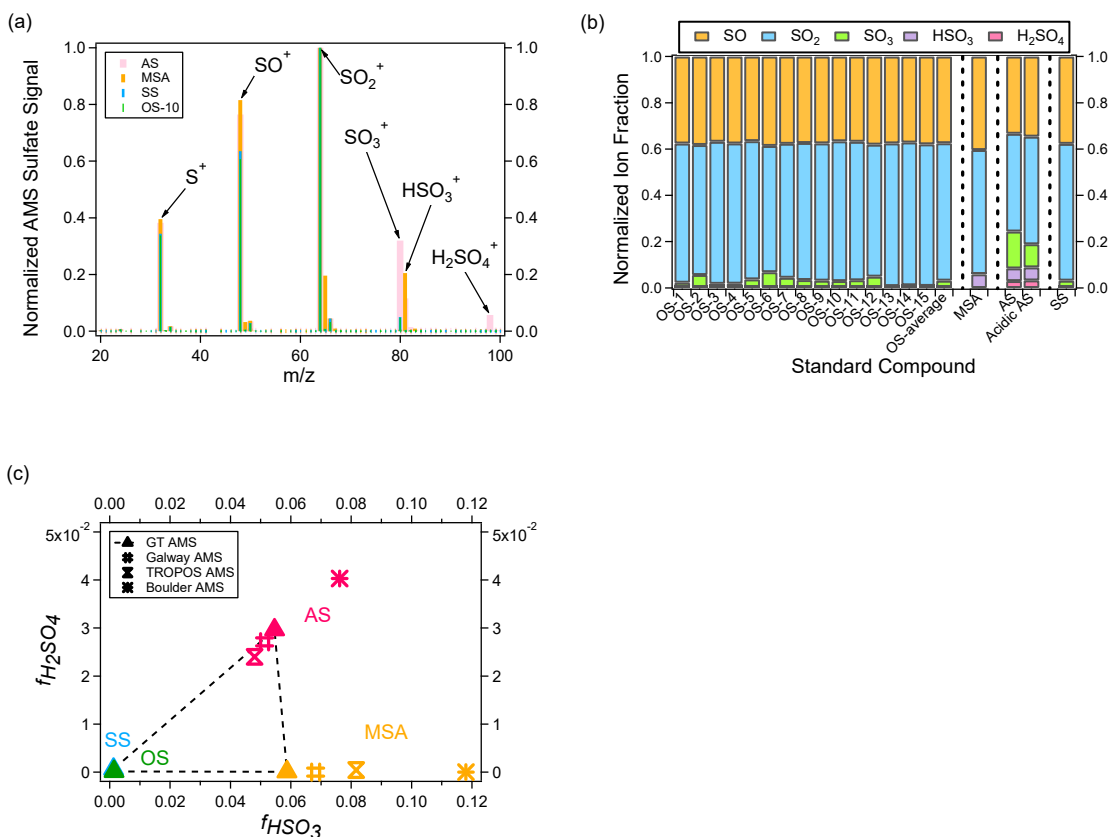


Figure A-5 (a) Typical normalized sulfate mass spectra of organosulfur compounds (OS; OS-10 refers to sodium benzyl sulfate in Table A-1), ammonium sulfate (AS), methanesulfonic acid (MSA), and sodium sulfate (SS), not including water fragments. (b) Mass fraction of main family HSO ions. (c) $f_{H_2SO_4}$ vs. f_{HSO_3} for standard compounds. For OS, the shown f_{HSO_3} and $f_{H_2SO_4}$ are averages for all 15 OS. OS and SS standard calibrations were only performed with the GT AMS, while MSA and AS standard calibrations were performed with multiple AMS.

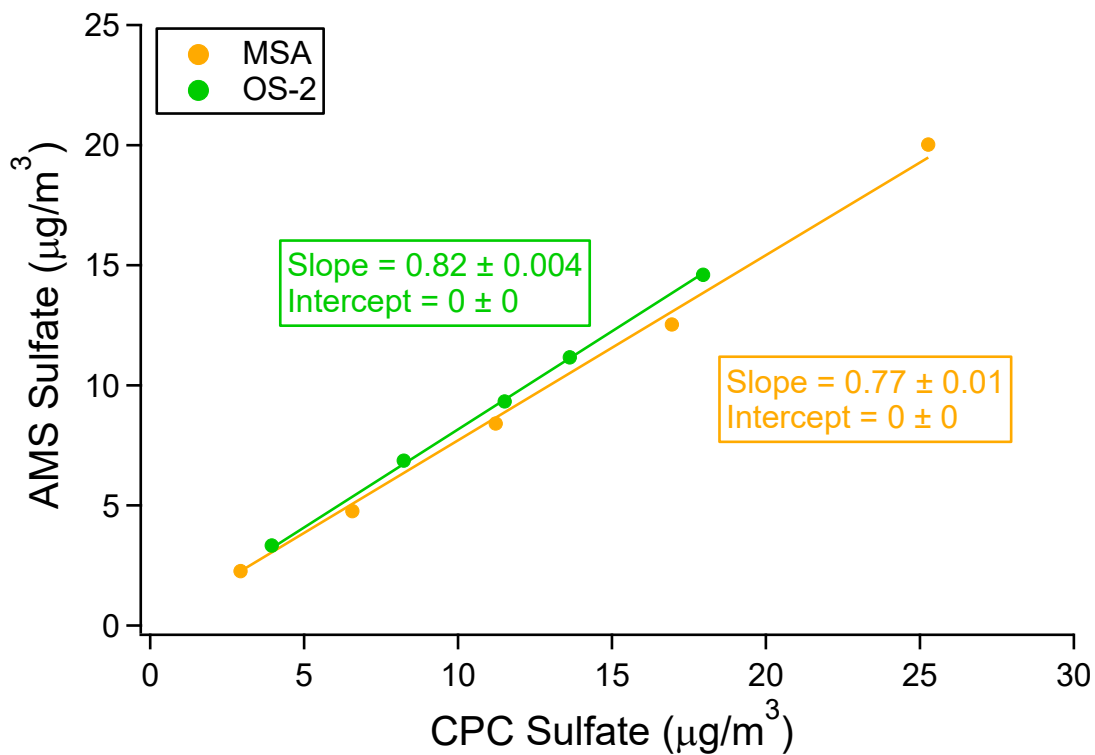


Figure A-6 RIE_{SO4} calibration results for MSA and sodium ethyl sulfate (OS-2). The collection efficiency (CE) of 1 was applied to AMS data considering that atomized organosulfur particles were liquid droplets. The slope is acquired with intercept forced through zero.

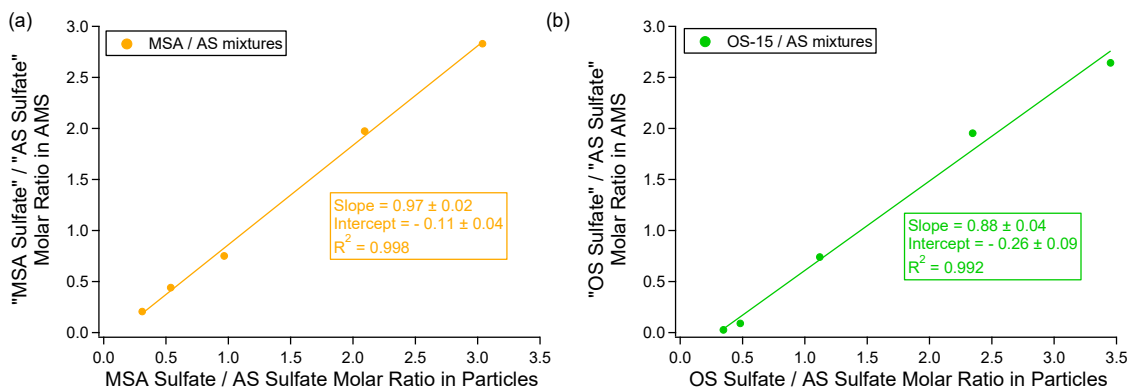


Figure A-7 (a) “MSA sulfate” to “AS sulfate” ratio calculated by sulfate apportionment method as a function of MSA / AS molar ratio in particles. (b) “OS sulfate” to “AS sulfate” ratio calculated by sulfate apportionment method as a function of OS / AS molar ratio in particles for OS-15 / AS mixture. The slopes and intercepts are obtained by orthogonal distance regression (ODR). The Pearson’s R is obtained by linear least-squares fit.

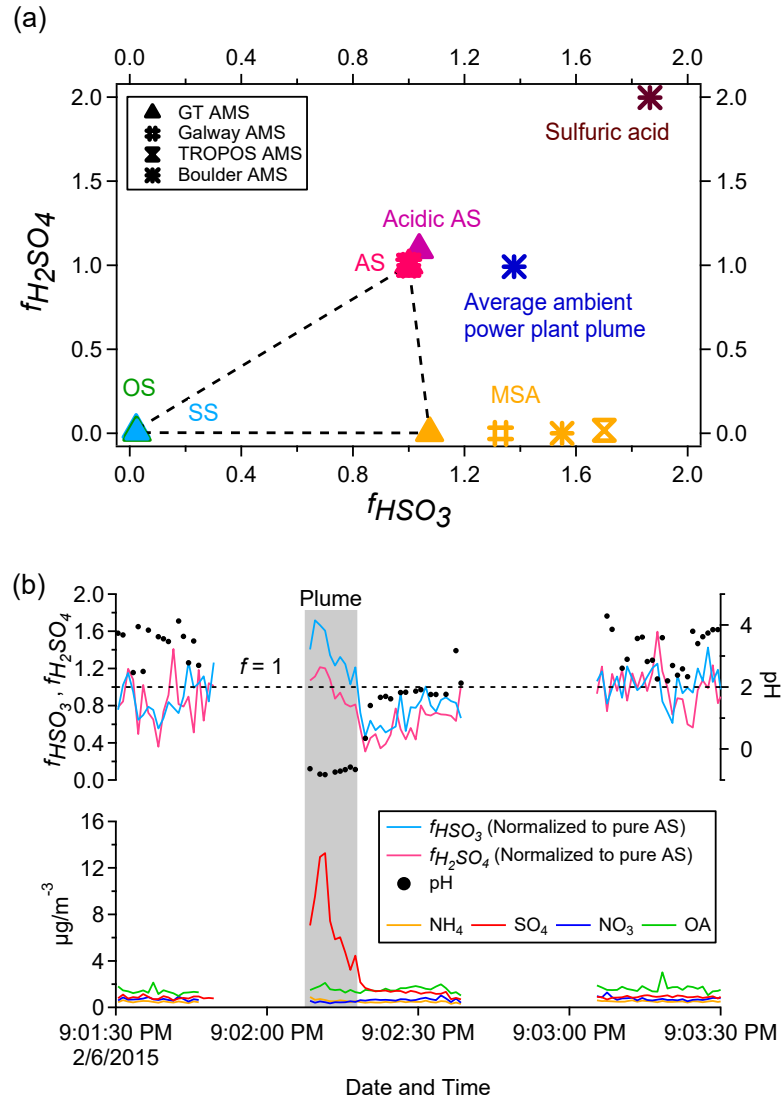


Figure A-8 (a) $f_{H_2SO_4}$ vs. f_{HSO_3} for standard compounds and the strong SO_2 plume (average data) during the WINTER aircraft campaign. Both f_{HSO_3} and $f_{H_2SO_4}$ are normalized to those of AS from the specific AMS, so that AS would always be at (1,1) (b) Evolution of f_{HSO_3} and $f_{H_2SO_4}$ (normalized to pure AS), pH, and AMS species in a power plant plume in WINTER aircraft campaign. Acidic AS is 1:1 mixture of ammonium sulfate and sulfuric acid.

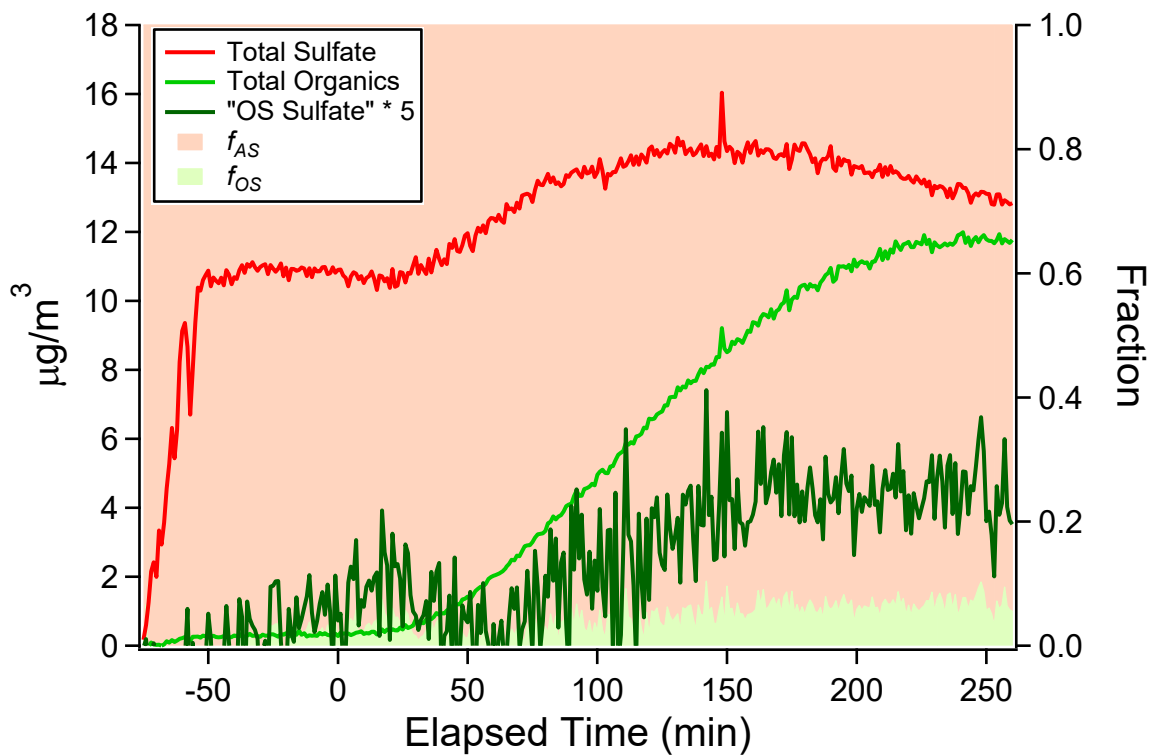


Figure A-9 Reaction profile of the chamber isoprene photooxidation experiment. The f_{AS} and f_{OS} refer to fraction of “AS sulfate” and “OS sulfate”, respectively, in total sulfate.

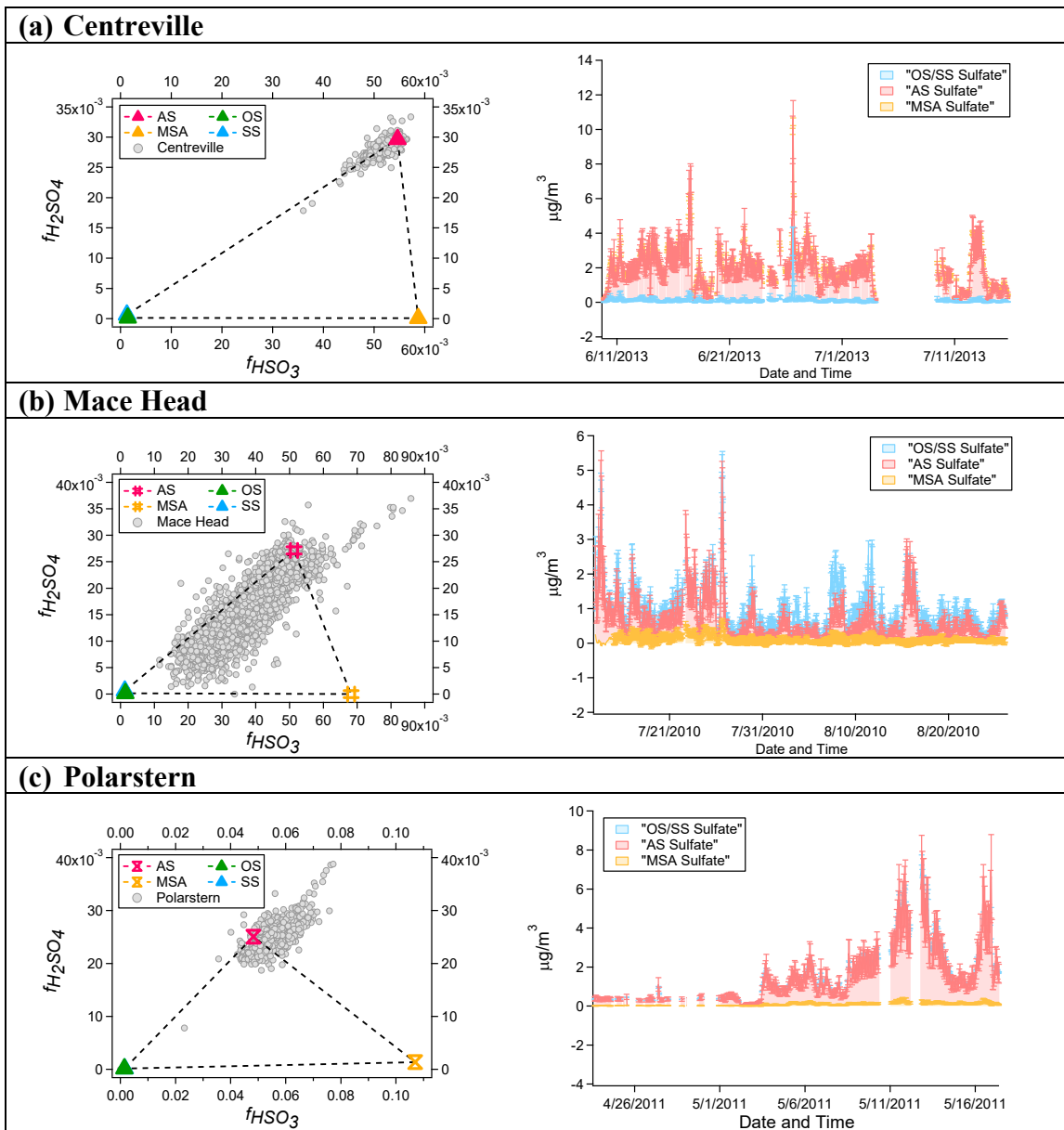


Figure A-10 $f_{H_2SO_4}$ vs. f_{HSO_3} for ambient measurements and time series of “AS sulfate”, “OS/SS sulfate” and “MSA sulfate” for (a) Centreville; (b) Mace Head; (c) Polarstern. OS and SS standard calibrations are from GT AMS, while MSA and AS standard calibrations are from the AMS that was used for the corresponding ambient measurements.

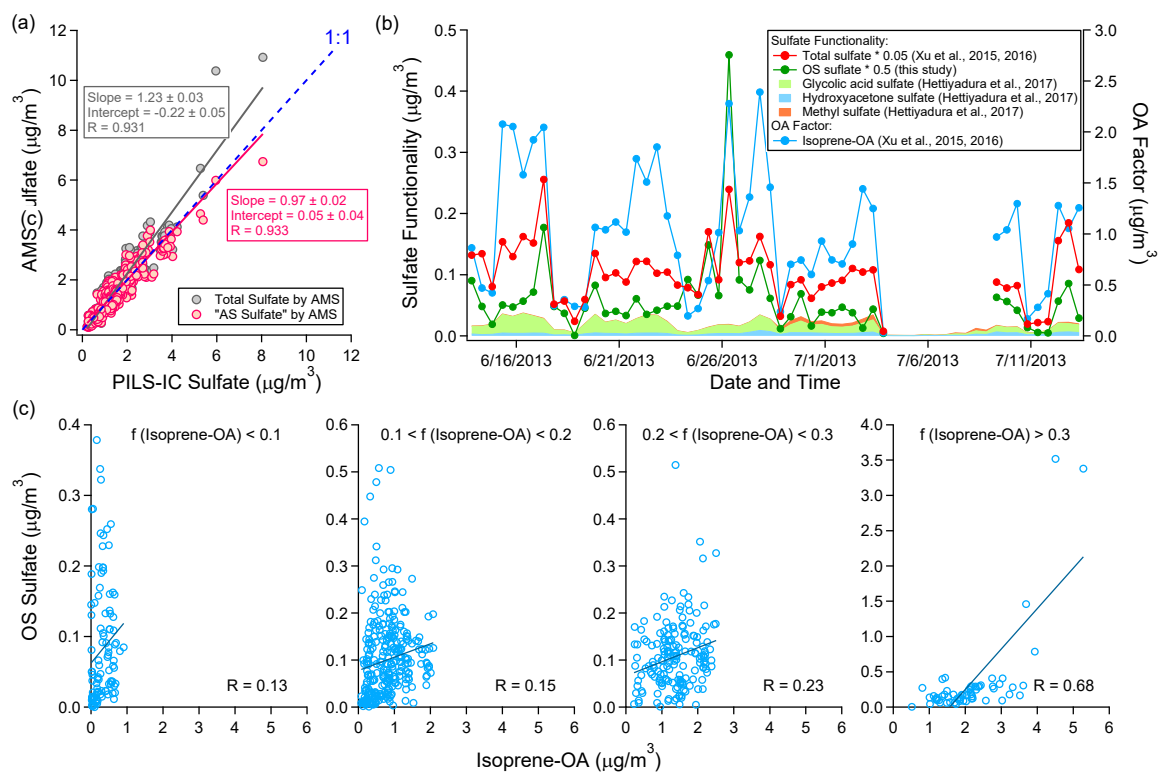


Figure A-11 (a) Comparison of AMS total sulfate and AMS "AS sulfate" (calculated by sulfate apportionment method) with PM₁ inorganic sulfate (measured by PILS-IC). (b) Time series of total sulfate (measured by the AMS), "OS sulfate" (calculated by sulfate apportionment method), sulfate functionality concentration of main organosulfur compounds (measured by offline HILIC-TQD), and isoprene-OA factor (resolved by PMF). (c) Comparison of "OS sulfate" with isoprene-OA. The Pearson's R is obtained by linear least-squares fit.

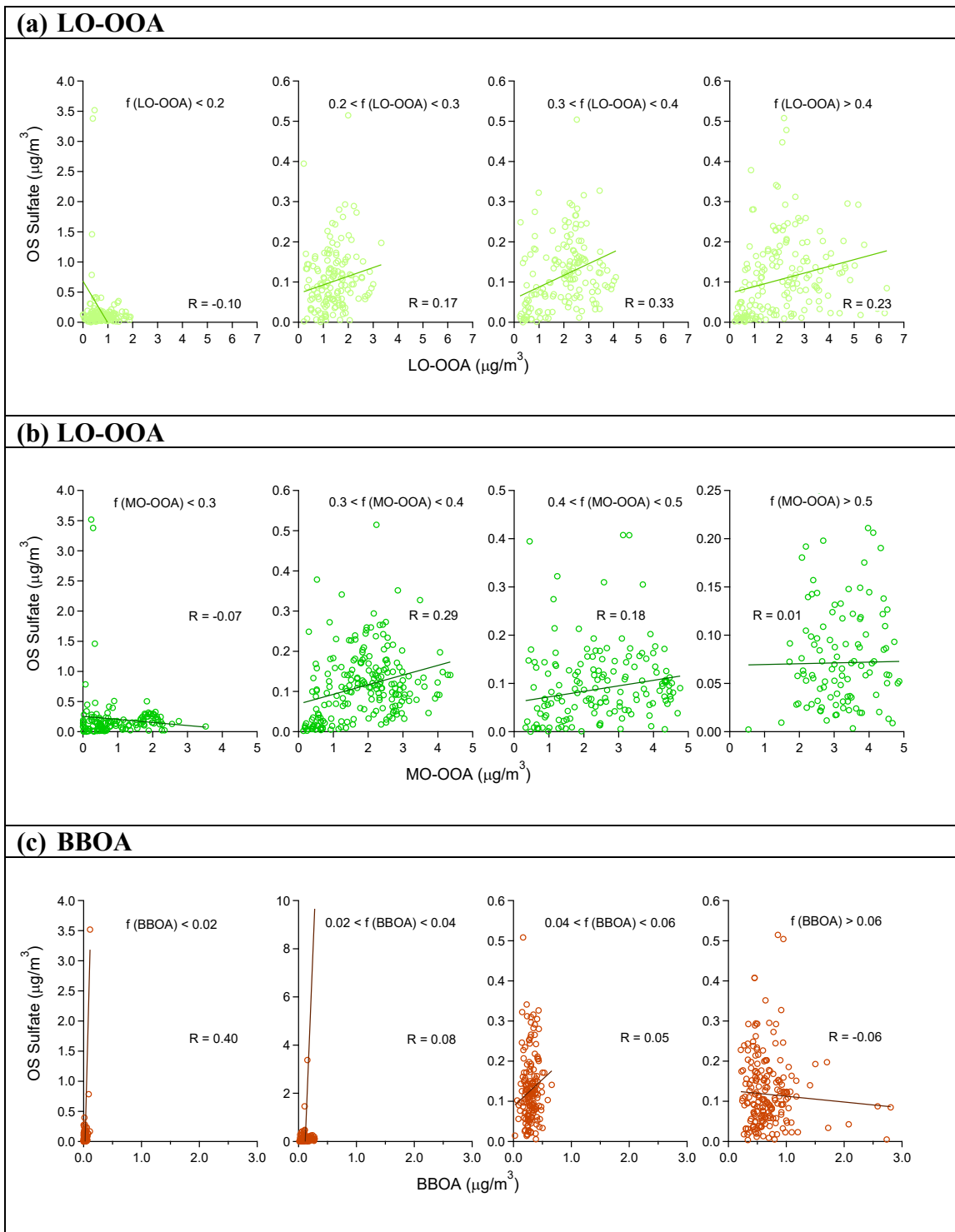


Figure A-12 Comparison of “OS sulfate” with (a) LO-OOA factor; (b) MO-OOA factor; (c) BBOA factor for Centreville measurements. The AMS factor time series are from (Xu et al., 2015a; Xu et al., 2015b) The Pearson’s R is obtained by linear

least-squares fit.

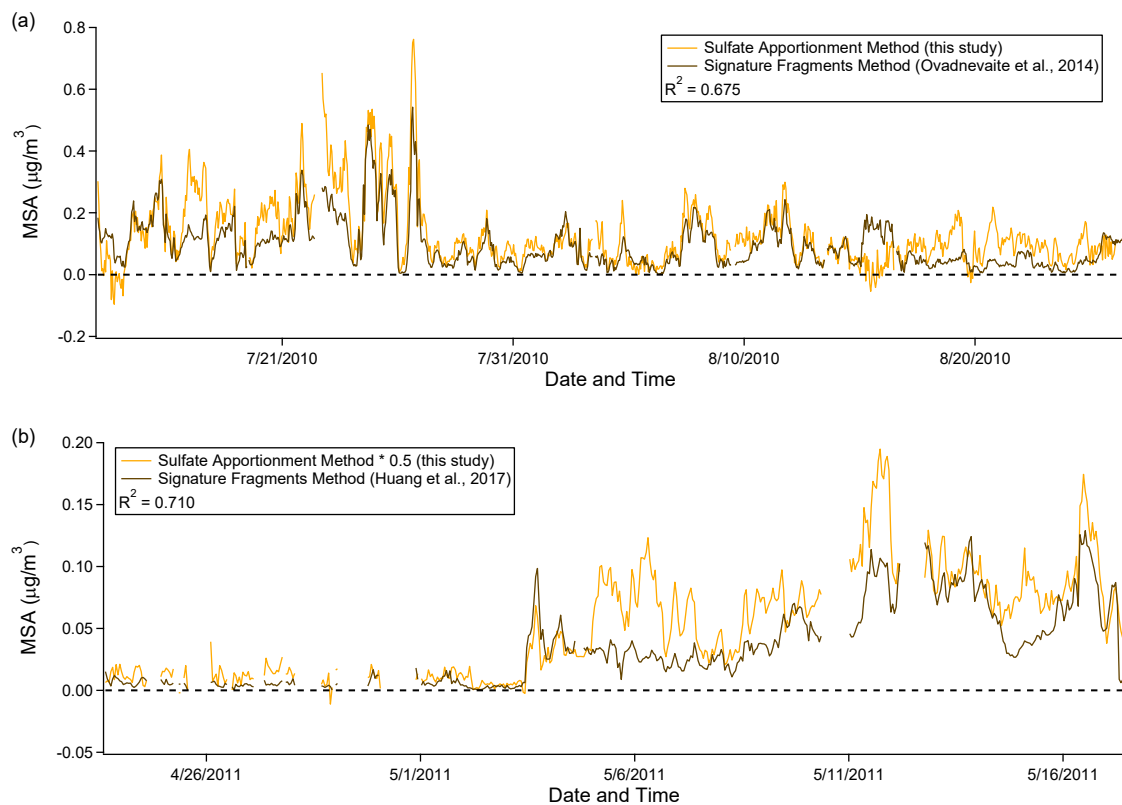


Figure A-13 Comparison of MSA mass concentration estimated by sulfate apportionment method and signature fragments method for (a) Mace Head measurements and (b) Polarstern measurements. The Pearson's R is obtained by linear least-squares fit.

REFERENCES

- Aiken, A. C., DeCarlo, P. F., and Jimenez, J. L.: Elemental Analysis of Organic Species with Electron Ionization High-Resolution Mass Spectrometry, *Analytical Chemistry*, 79, 8350-8358, 10.1021/ac071150w, 2007.
- Aiken, A. C., DeCarlo, P. F., Kroll, J. H., Worsnop, D. R., Huffman, J. A., Docherty, K. S., Ulbrich, I. M., Mohr, C., Kimmel, J. R., Sueper, D., Sun, Y., Zhang, Q., Trimborn, A., Northway, M., Ziemann, P. J., Canagaratna, M. R., Onasch, T. B., Alfarra, M. R., Prevot, A. S. H., Dommen, J., Duplissy, J., Metzger, A., Baltensperger, U., and Jimenez, J. L.: O/C and OM/OC Ratios of Primary, Secondary, and Ambient Organic Aerosols with High-Resolution Time-of-Flight Aerosol Mass Spectrometry, *Environmental Science & Technology*, 42, 4478-4485, 10.1021/es703009q, 2008.
- Aljawhary, D., Zhao, R., Lee, A. K. Y., Wang, C., and Abbatt, J. P. D.: Kinetics, Mechanism, and Secondary Organic Aerosol Yield of Aqueous Phase Photo-oxidation of α -Pinene Oxidation Products, *The Journal of Physical Chemistry A*, 120, 1395-1407, 10.1021/acs.jpca.5b06237, 2016.
- Allan, J. D., Bower, K. N., Coe, H., Boudries, H., Jayne, J. T., Canagaratna, M. R., Millet, D. B., Goldstein, A. H., Quinn, P. K., Weber, R. J., and Worsnop, D. R.: Submicron aerosol composition at Trinidad Head, California, during ITCT 2K2: Its relationship with gas phase volatile organic carbon and assessment of instrument performance, *Journal of Geophysical Research: Atmospheres*, 109, n/a-n/a, 10.1029/2003JD004208, 2004a.
- Allan, J. D., Delia, A. E., Coe, H., Bower, K. N., Alfarra, M. R., Jimenez, J. L., Middlebrook, A. M., Drewnick, F., Onasch, T. B., Canagaratna, M. R., Jayne, J. T., and Worsnop, D. R.: A generalised method for the extraction of chemically resolved mass spectra from Aerodyne aerosol mass spectrometer data, *Journal of Aerosol Science*, 35, 909-922, <http://dx.doi.org/10.1016/j.jaerosci.2004.02.007>, 2004b.
- Allen, H. M., Draper, D. C., Ayres, B. R., Ault, A., Bondy, A., Takahama, S., Modini, R. L., Baumann, K., Edgerton, E., Knote, C., Laskin, A., Wang, B., and Fry, J. L.: Influence of crustal dust and sea spray supermicron particle concentrations and acidity on inorganic NO_3^- aerosol during the 2013 Southern Oxidant and Aerosol Study, *Atmos. Chem. Phys.*, 15, 10669-10685, 10.5194/acp-15-10669-2015, 2015.
- Altieri, K. E., Seitzinger, S. P., Carlton, A. G., Turpin, B. J., Klein, G. C., and Marshall, A. G.: Oligomers formed through in-cloud methylglyoxal reactions: Chemical composition, properties, and mechanisms investigated by ultra-high resolution FT-ICR mass spectrometry, *Atmospheric Environment*, 42, 1476-1490, <https://doi.org/10.1016/j.atmosenv.2007.11.015>, 2008.

Andreae, M. O.: Emission of trace gases and aerosols from biomass burning – an updated assessment, *Atmos. Chem. Phys.*, 19, 8523-8546, 10.5194/acp-19-8523-2019, 2019.

Aplincourt, P., and Ruiz-López, M. F.: Theoretical Investigation of Reaction Mechanisms for Carboxylic Acid Formation in the Atmosphere, *Journal of the American Chemical Society*, 122, 8990-8997, 10.1021/ja000731z, 2000.

Baasandorj, M., Millet, D. B., Hu, L., Mitroo, D., and Williams, B. J.: Measuring acetic and formic acid by proton-transfer-reaction mass spectrometry: sensitivity, humidity dependence, and quantifying interferences, *Atmos. Meas. Tech.*, 8, 1303-1321, 10.5194/amt-8-1303-2015, 2015.

Bahreini, R., Keywood, M. D., Ng, N. L., Varutbangkul, V., Gao, S., Flagan, R. C., Seinfeld, J. H., Worsnop, D. R., and Jimenez, J. L.: Measurements of Secondary Organic Aerosol from Oxidation of Cycloalkenes, Terpenes, and m-Xylene Using an Aerodyne Aerosol Mass Spectrometer, *Environmental Science & Technology*, 39, 5674-5688, 10.1021/es048061a, 2005.

Bahreini, R., Ervens, B., Middlebrook, A. M., Warneke, C., de Gouw, J. A., DeCarlo, P. F., Jimenez, J. L., Brock, C. A., Neuman, J. A., Ryerson, T. B., Stark, H., Atlas, E., Brioude, J., Fried, A., Holloway, J. S., Peischl, J., Richter, D., Walega, J., Weibring, P., Wollny, A. G., and Fehsenfeld, F. C.: Organic aerosol formation in urban and industrial plumes near Houston and Dallas, Texas, *Journal of Geophysical Research: Atmospheres*, 114, doi:10.1029/2008JD011493, 2009.

Bates, K. H., and Jacob, D. J.: A new model mechanism for atmospheric oxidation of isoprene: global effects on oxidants, nitrogen oxides, organic products, and secondary organic aerosol, *Atmos. Chem. Phys. Discuss.*, 2019, 1-46, 10.5194/acp-2019-328, 2019.

Bikkina, S., Kawamura, K., and Sarin, M.: Secondary Organic Aerosol Formation over Coastal Ocean: Inferences from Atmospheric Water-Soluble Low Molecular Weight Organic Compounds, *Environmental Science & Technology*, 51, 4347-4357, 10.1021/acs.est.6b05986, 2017.

Bougiatioti, A., Stavroulas, I., Kostenidou, E., Zarrmpas, P., Theodosi, C., Kouvarakis, G., Canonaco, F., Prévôt, A. S. H., Nenes, A., Pandis, S. N., and Mihalopoulos, N.: Processing of biomass-burning aerosol in the eastern Mediterranean during summertime, *Atmos. Chem. Phys.*, 14, 4793-4807, 10.5194/acp-14-4793-2014, 2014.

Bougiatioti, A., Nikolaou, P., Stavroulas, I., Kouvarakis, G., Weber, R., Nenes, A., Kanakidou, M., and Mihalopoulos, N.: Particle water and pH in the eastern Mediterranean: source variability and implications for nutrient availability, *Atmos. Chem. Phys.*, 16, 4579-4591, 10.5194/acp-16-4579-2016, 2016.

Boyd, C. M., Sanchez, J., Xu, L., Eugene, A. J., Nah, T., Tuet, W. Y., Guzman, M. I., and Ng, N. L.: Secondary organic aerosol formation from the β -pinene+NO₃ system: effect of humidity and peroxy radical fate, *Atmos. Chem. Phys.*, 15, 7497-7522, 10.5194/acp-15-7497-2015, 2015a.

Boyd, C. M., Sanchez, J., Xu, L., Eugene, A. J., Nah, T., Tuet, W. Y., Guzman, M. I., and Ng, N. L.: Secondary organic aerosol formation from the β -pinene+NO₃ system: effect of humidity and peroxy radical fate, *Atmos. Chem. Phys.*, 15, 7497-7522, 10.5194/acp-15-7497-2015, 2015b.

Brown, S. S., Degouw, J. A., Warneke, C., Ryerson, T. B., Dube, W. P., Atlas, E., Weber, R. J., Peltier, R. E., Neuman, J. A., Roberts, J. M., Swanson, A., Flocke, F., McKeen, S. A., Brioude, J., Sommariva, R., Trainer, M., Fehsenfeld, F. C., and Ravishankara, A. R.: Nocturnal isoprene oxidation over the Northeast United States in summer and its impact on reactive nitrogen partitioning and secondary organic aerosol, *Atmospheric Chemistry and Physics*, 9, 3027-3042, 10.5194/acp-9-3027-2009, 2009.

Bruns, E. A., Perraud, V., Zelenyuk, A., Ezell, M. J., Johnson, S. N., Yu, Y., Imre, D., Finlayson-Pitts, B. J., and Alexander, M. L.: Comparison of FTIR and Particle Mass Spectrometry for the Measurement of Particulate Organic Nitrates, *Environmental Science & Technology*, 44, 1056-1061, 10.1021/es9029864, 2010.

Budisulistiorini, S. H., Canagaratna, M. R., Croteau, P. L., Marth, W. J., Baumann, K., Edgerton, E. S., Shaw, S. L., Knipping, E. M., Worsnop, D. R., Jayne, J. T., Gold, A., and Surratt, J. D.: Real-Time Continuous Characterization of Secondary Organic Aerosol Derived from Isoprene Epoxydiols in Downtown Atlanta, Georgia, Using the Aerodyne Aerosol Chemical Speciation Monitor, *Environmental Science & Technology*, 47, 5686-5694, 10.1021/es400023n, 2013.

Budisulistiorini, S. H., Baumann, K., Edgerton, E. S., Bairai, S. T., Mueller, S., Shaw, S. L., Knipping, E. M., Gold, A., and Surratt, J. D.: Seasonal characterization of submicron aerosol chemical composition and organic aerosol sources in the southeastern United States: Atlanta, Georgia, and Look Rock, Tennessee, *Atmos. Chem. Phys.*, 16, 5171-5189, 10.5194/acp-16-5171-2016, 2016.

Canagaratna, M., Jayne, J., Jimenez, J., Allan, J., Alfarra, M., Zhang, Q., Onasch, T., Drewnick, F., Coe, H., and Middlebrook, A.: Chemical and microphysical characterization of ambient aerosols with the aerodyne aerosol mass spectrometer, *Mass Spectrometry Reviews*, 26, 185-222, 2007.

Canagaratna, M. R., Jimenez, J. L., Kroll, J. H., Chen, Q., Kessler, S. H., Massoli, P., Hildebrandt Ruiz, L., Fortner, E., Williams, L. R., Wilson, K. R., Surratt, J. D., Donahue, N. M., Jayne, J. T., and Worsnop, D. R.: Elemental ratio measurements of organic compounds using aerosol mass spectrometry: characterization, improved calibration, and implications, *Atmos. Chem. Phys.*, 15, 253-272, 10.5194/acp-15-253-2015, 2015.

Canonaco, F., Crippa, M., Slowik, J. G., Baltensperger, U., and Prévôt, A. S. H.: SoFi, an IGOR-based interface for the efficient use of the generalized multilinear engine (ME-2) for the source apportionment: ME-2 application to aerosol mass spectrometer data, *Atmos. Meas. Tech.*, 6, 3649-3661, 10.5194/amt-6-3649-2013, 2013.

Carlton, A. G., Turpin, B. J., Lim, H.-J., Altieri, K. E., and Seitzinger, S.: Link between isoprene and secondary organic aerosol (SOA): Pyruvic acid oxidation yields low volatility organic acids in clouds, *Geophysical Research Letters*, 33, 10.1029/2005gl025374, 2006a.

Carlton, A. G., Turpin, B. J., Lim, H.-J., Altieri, K. E., and Seitzinger, S.: Link between isoprene and secondary organic aerosol (SOA): Pyruvic acid oxidation yields low volatility organic acids in clouds, *Geophysical Research Letters*, 33, n/a-n/a, 10.1029/2005GL025374, 2006b.

Carlton, A. G., Turpin, B. J., Altieri, K. E., Seitzinger, S., Reff, A., Lim, H.-J., and Ervens, B.: Atmospheric oxalic acid and SOA production from glyoxal: Results of aqueous photooxidation experiments, *Atmospheric Environment*, 41, 7588-7602, <http://dx.doi.org/10.1016/j.atmosenv.2007.05.035>, 2007.

Chameides, W. L., and Davis, D. D.: Aqueous-phase source of formic acid in clouds, *Nature*, 304, 427, 10.1038/304427a0, 1983.

Chan, M. N., Zhang, H., Goldstein, A. H., and Wilson, K. R.: Role of Water and Phase in the Heterogeneous Oxidation of Solid and Aqueous Succinic Acid Aerosol by Hydroxyl Radicals, *The Journal of Physical Chemistry C*, 118, 28978-28992, 10.1021/jp5012022, 2014.

Chebbi, A., and Carlier, P.: Carboxylic acids in the troposphere, occurrence, sources, and sinks: A review, *Atmospheric Environment*, 30, 4233-4249, [http://dx.doi.org/10.1016/1352-2310\(96\)00102-1](http://dx.doi.org/10.1016/1352-2310(96)00102-1), 1996.

Chen, Y., Takeuchi, M., Nah, T., Xu, L., Canagaratna, M. R., Stark, H., Baumann, K., Canonaco, F., Prévôt, A. S. H., Huey, L. G., Weber, R. J., and Ng, N. L.: Chemical characterization of secondary organic aerosol at a rural site in the southeastern US: insights from simultaneous high-resolution time-of-flight aerosol mass spectrometer (HR-ToF-AMS) and FIGAERO chemical ionization mass spectrometer (CIMS) measurements, *Atmos. Chem. Phys.*, 20, 8421-8440, 10.5194/acp-20-8421-2020, 2020.

Cheng, C. T., Chan, M. N., and Wilson, K. R.: Importance of Unimolecular HO₂ Elimination in the Heterogeneous OH Reaction of Highly Oxygenated Tartaric Acid Aerosol, *The Journal of Physical Chemistry A*, 120, 5887-5896, 10.1021/acs.jpca.6b05289, 2016.

Claeys, M., Szmigielski, R., Kourtchev, I., Van der Veken, P., Vermeylen, R., Maenhaut, W., Jaoui, M., Kleindienst, T. E., Lewandowski, M., Offenberg, J. H., and Edney, E. O.: Hydroxydicarboxylic Acids: Markers for Secondary Organic Aerosol from the Photooxidation of α -Pinene, *Environmental Science & Technology*, 41, 1628-1634, 10.1021/es0620181, 2007.

Clegg, S. L., Brimblecombe, P., and Wexler, A. S.: Thermodynamic model of the system H⁺-NH₄⁺-SO₄²⁻-NO₃⁻-H₂O at tropospheric temperatures, *Journal of Physical Chemistry A*, 102, 2137-2154, 10.1021/jp973042r, 1998.

Clegg, S. L., Seinfeld, J. H., and Edney, E. O.: Thermodynamic modelling of aqueous aerosols containing electrolytes and dissolved organic compounds. II. An extended Zdanovskii-Stokes-Robinson approach, *Journal of Aerosol Science*, 34, 667-690, 10.1016/s0021-8502(03)00019-3, 2003.

Crippa, M., Canonaco, F., Lanz, V. A., Äijälä, M., Allan, J. D., Carbone, S., Capes, G., Ceburnis, D., Dall'Osto, M., Day, D. A., DeCarlo, P. F., Ehn, M., Eriksson, A., Freney, E., Hildebrandt Ruiz, L., Hillamo, R., Jimenez, J. L., Junninen, H., Kiendler-Scharr, A., Kortelainen, A. M., Kulmala, M., Laaksonen, A., Mensah, A. A., Mohr, C., Nemitz, E., O'Dowd, C., Ovadnevaite, J., Pandis, S. N., Petäjä, T., Poulain, L., Saarikoski, S., Sellegri, K., Swietlicki, E., Tiitta, P., Worsnop, D. R., Baltensperger, U., and Prévôt, A. S. H.: Organic aerosol components derived from 25 AMS data sets across Europe using a consistent ME-2 based source apportionment approach, *Atmos. Chem. Phys.*, 14, 6159-6176, 10.5194/acp-14-6159-2014, 2014.

Cubison, M. J., Ortega, A. M., Hayes, P. L., Farmer, D. K., Day, D., Lechner, M. J., Brune, W. H., Apel, E., Diskin, G. S., Fisher, J. A., Fuelberg, H. E., Hecobian, A., Knapp, D. J., Mikoviny, T., Riemer, D., Sachse, G. W., Sessions, W., Weber, R. J., Weinheimer, A. J., Wisthaler, A., and Jimenez, J. L.: Effects of aging on organic aerosol from open biomass burning smoke in aircraft and laboratory studies, *Atmos. Chem. Phys.*, 11, 12049-12064, 10.5194/acp-11-12049-2011, 2011.

Cui, T., Zeng, Z., dos Santos, E. O., Zhang, Z., Chen, Y., Zhang, Y., Rose, C. A., Budisulistiorini, S. H., Collins, L. B., Bodnar, W. M., de Souza, R. A. F., Martin, S. T., Machado, C. M. D., Turpin, B. J., Gold, A., Ault, A. P., and Surratt, J. D.: Development of a hydrophilic interaction liquid chromatography (HILIC) method for the chemical characterization of water-soluble isoprene epoxydiol (IEPOX)-derived secondary organic aerosol, *Environmental Science: Processes & Impacts*, 20, 1524-1536, 10.1039/C8EM00308D, 2018.

D'Ambro, E. L., Møller, K. H., Lopez-Hilfiker, F. D., Schobesberger, S., Liu, J., Shilling, J. E., Lee, B. H., Kjaergaard, H. G., and Thornton, J. A.: Isomerization of Second-Generation Isoprene Peroxy Radicals: Epoxide Formation and Implications for Secondary Organic Aerosol Yields, *Environmental Science & Technology*, 51, 4978-4987, 10.1021/acs.est.7b00460, 2017.

Darer, A. I., Cole-Filipiak, N. C., O'Connor, A. E., and Elrod, M. J.: Formation and Stability of Atmospherically Relevant Isoprene-Derived Organosulfates and Organonitrates, *Environmental Science & Technology*, 45, 1895-1902, 10.1021/es103797z, 2011.

DeCarlo, P. F., Kimmel, J. R., Trimborn, A., Northway, M. J., Jayne, J. T., Aiken, A. C., Gonin, M., Fuhrer, K., Horvath, T., and Docherty, K. S.: Field-deployable, high-resolution, time-of-flight aerosol mass spectrometer, *Analytical chemistry*, 78, 8281-8289, 2006.

DeRieux, W. S. W., Li, Y., Lin, P., Laskin, J., Laskin, A., Bertram, A. K., Nizkorodov, S. A., and Shiraiwa, M.: Predicting the glass transition temperature and viscosity of secondary

organic material using molecular composition, *Atmos. Chem. Phys.*, 18, 6331-6351, 10.5194/acp-18-6331-2018, 2018.

Docherty, K. S., Aiken, A. C., Huffman, J. A., Ulbrich, I. M., DeCarlo, P. F., Sueper, D., Worsnop, D. R., Snyder, D. C., Peltier, R. E., Weber, R. J., Grover, B. D., Eatough, D. J., Williams, B. J., Goldstein, A. H., Ziemann, P. J., and Jimenez, J. L.: The 2005 Study of Organic Aerosols at Riverside (SOAR-1): instrumental intercomparisons and fine particle composition, *Atmospheric Chemistry and Physics*, 11, 12387-12420, 10.5194/acp-11-12387-2011, 2011.

Docherty, K. S., Jaoui, M., Corse, E., Jimenez, J. L., Offenberg, J. H., Lewandowski, M., and Kleindienst, T. E.: Collection Efficiency of the Aerosol Mass Spectrometer for Chamber-Generated Secondary Organic Aerosols, *Aerosol Science and Technology*, 47, 294-309, 10.1080/02786826.2012.752572, 2013.

Dockery, D. W., Pope, C. A., Xu, X., Spengler, J. D., Ware, J. H., Fay, M. E., Ferris, B. G., and Speizer, F. E.: An Association between Air Pollution and Mortality in Six U.S. Cities, *New England Journal of Medicine*, 329, 1753-1759, 10.1056/nejm199312093292401, 1993.

Drewnick, F., Diesch, J. M., Faber, P., and Borrmann, S.: Aerosol mass spectrometry: particle-vaporizer interactions and their consequences for the measurements, *Atmos. Meas. Tech.*, 8, 3811-3830, 10.5194/amt-8-3811-2015, 2015.

Eatough, D. J., Wadsworth, A., Eatough, D. A., Crawford, J. W., Hansen, L. D., and Lewis, E. A.: A multiple-system, multi-channel diffusion denuder sampler for the determination of fine-particulate organic material in the atmosphere, *Atmospheric Environment. Part A. General Topics*, 27, 1213-1219, [https://doi.org/10.1016/0960-1686\(93\)90247-V](https://doi.org/10.1016/0960-1686(93)90247-V), 1993.

Eddingsaas, N. C., Loza, C. L., Yee, L. D., Chan, M., Schilling, K. A., Chhabra, P. S., Seinfeld, J. H., and Wennberg, P. O.: α -pinene photooxidation under controlled chemical conditions - Part 2: SOA yield and composition in low- and high-NO_x environments, *Atmos. Chem. Phys.*, 12, 7413-7427, 10.5194/acp-12-7413-2012, 2012a.

Eddingsaas, N. C., Loza, C. L., Yee, L. D., Seinfeld, J. H., and Wennberg, P. O.: α -pinene photooxidation under controlled chemical conditions – Part 1: Gas-phase composition in low- and high-NO_x environments, *Atmos. Chem. Phys.*, 12, 6489-6504, 10.5194/acp-12-6489-2012, 2012b.

Ehn, M., Thornton, J. A., Kleist, E., Sipila, M., Junninen, H., Pullinen, I., Springer, M., Rubach, F., Tillmann, R., Lee, B., Lopez-Hilfiker, F., Andres, S., Acir, I.-H., Rissanen, M., Jokinen, T., Schobesberger, S., Kangasluoma, J., Kontkanen, J., Nieminen, T., Kurten, T., Nielsen, L. B., Jorgensen, S., Kjaergaard, H. G., Canagaratna, M., Maso, M. D., Berndt, T., Petaja, T., Wahner, A., Kerminen, V.-M., Kulmala, M., Worsnop, D. R., Wildt, J., and Mentel, T. F.: A large source of low-volatility secondary organic aerosol, *Nature*, 506, 476-479, 10.1038/nature13032, 2014.

Elser, M., Huang, R. J., Wolf, R., Slowik, J. G., Wang, Q., Canonaco, F., Li, G., Bozzetti, C., Daellenbach, K. R., Huang, Y., Zhang, R., Li, Z., Cao, J., Baltensperger, U., El-Haddad, I., and Prévôt, A. S. H.: New insights into PM_{2.5} chemical composition and sources in two major cities in China during extreme haze events using aerosol mass spectrometry, *Atmos. Chem. Phys.*, 16, 3207-3225, 10.5194/acp-16-3207-2016, 2016.

Ervens, B., Feingold, G., Frost, G. J., and Kreidenweis, S. M.: A modeling study of aqueous production of dicarboxylic acids: 1. Chemical pathways and speciated organic mass production, *Journal of Geophysical Research: Atmospheres*, 109, n/a-n/a, 10.1029/2003JD004387, 2004.

Ervens, B., Carlton, A. G., Turpin, B. J., Altieri, K. E., Kreidenweis, S. M., and Feingold, G.: Secondary organic aerosol yields from cloud-processing of isoprene oxidation products, *Geophysical Research Letters*, 35, n/a-n/a, 10.1029/2007GL031828, 2008.

Ervens, B., Turpin, B. J., and Weber, R. J.: Secondary organic aerosol formation in cloud droplets and aqueous particles (aqSOA): a review of laboratory, field and model studies, *Atmospheric Chemistry and Physics*, 11, 11069-11102, 10.5194/acp-11-11069-2011, 2011.

Estillore, A. D., Hettiyadura, A. P. S., Qin, Z., Leckrone, E., Wombacher, B., Humphry, T., Stone, E. A., and Grassian, V. H.: Water Uptake and Hygroscopic Growth of Organosulfate Aerosol, *Environmental Science & Technology*, 50, 4259-4268, 10.1021/acs.est.5b05014, 2016.

Eugene, A. J., Xia, S.-S., and Guzman, M. I.: Aqueous Photochemistry of Glyoxylic Acid, *The Journal of Physical Chemistry A*, 120, 3817-3826, 10.1021/acs.jpca.6b00225, 2016.

Facchini, M. C., Fuzzi, S., Lind, J. A., Fierlinger - Oberlinninger, H., Kalina, M., Puxbaum, H., Winiwarter, W., Arends, B. G., Wobrock, W., Jaeschke, W., Berner, A., and Kruisz, C.: Phase - partitioning and chemical reactions of low molecular weight organic compounds in fog, *Tellus B*, 44, 533-544, doi:10.1034/j.1600-0889.1992.t01-3-00007.x, 1992.

Facchini, M. C., Decesari, S., Rinaldi, M., Carbone, C., Finessi, E., Mircea, M., Fuzzi, S., Moretti, F., Tagliavini, E., Ceburnis, D., and O'Dowd, C. D.: Important Source of Marine Secondary Organic Aerosol from Biogenic Amines, *Environmental Science & Technology*, 42, 9116-9121, 10.1021/es8018385, 2008.

Falkovich, A. H., Schkolnik, G., Ganor, E., and Rudich, Y.: Adsorption of organic compounds pertinent to urban environments onto mineral dust particles, *Journal of Geophysical Research: Atmospheres*, 109, 10.1029/2003jd003919, 2004.

Fang, T., Guo, H., Zeng, L., Verma, V., Nenes, A., and Weber, R. J.: Highly Acidic Ambient Particles, Soluble Metals, and Oxidative Potential: A Link between Sulfate and Aerosol Toxicity, *Environmental Science & Technology*, 51, 2611-2620, 10.1021/acs.est.6b06151, 2017.

Farmer, D. K., Matsunaga, A., Docherty, K. S., Surratt, J. D., Seinfeld, J. H., Ziemann, P. J., and Jimenez, J. L.: Response of an aerosol mass spectrometer to organonitrates and organosulfates and implications for atmospheric chemistry, *Proceedings of the National Academy of Sciences*, 107, 6670-6675, 10.1073/pnas.0912340107, 2010.

Faust, J. A., Wong, J. P. S., Lee, A. K. Y., and Abbatt, J. P. D.: Role of Aerosol Liquid Water in Secondary Organic Aerosol Formation from Volatile Organic Compounds, *Environmental Science & Technology*, 51, 1405-1413, 10.1021/acs.est.6b04700, 2017.

Faxon, C., Hammes, J., Le Breton, M., Pathak, R. K., and Hallquist, M.: Characterization of organic nitrate constituents of secondary organic aerosol (SOA) from nitrate-radical-initiated oxidation of limonene using high-resolution chemical ionization mass spectrometry, *Atmospheric Chemistry and Physics*, 18, 5467-5481, 10.5194/acp-18-5467-2018, 2018.

Fountoukis, C., and Nenes, A.: ISORROPIA II: a computationally efficient thermodynamic equilibrium model for K^+ - Ca^{2+} - Mg^{2+} - NH_4^+ - Na^+ - SO_4^{2-} - NO_3^- - Cl^- - H_2O aerosols, *Atmos. Chem. Phys.*, 7, 4639-4659, 10.5194/acp-7-4639-2007, 2007.

Fridlind, A. M., and Jacobson, M. Z.: A study of gas-aerosol equilibrium and aerosol pH in the remote marine boundary layer during the First Aerosol Characterization Experiment (ACE 1), *Journal of Geophysical Research: Atmospheres*, 105, 17325-17340, 10.1029/2000JD900209, 2000.

Froyd, K. D., Murphy, S. M., Murphy, D. M., de Gouw, J. A., Eddingsaas, N. C., and Wennberg, P. O.: Contribution of isoprene-derived organosulfates to free tropospheric aerosol mass, *Proceedings of the National Academy of Sciences*, 107, 21360-21365, 10.1073/pnas.1012561107, 2010.

Fry, J. L., Brown, S. S., Middlebrook, A. M., Edwards, P. M., Campuzano-Jost, P., Day, D. A., Jimenez, J. L., Allen, H. M., Ryerson, T. B., Pollack, I., Graus, M., Warneke, C., de Gouw, J. A., Brock, C. A., Gilman, J., Lerner, B. M., Dubé, W. P., Liao, J., and Welti, A.: Secondary organic aerosol (SOA) yields from NO_3 radical + isoprene based on nighttime aircraft power plant plume transects, *Atmos. Chem. Phys.*, 18, 11663-11682, 10.5194/acp-18-11663-2018, 2018.

Gäb, S., Hellpointner, E., Turner, W. V., and Kořte, F.: Hydroxymethyl hydroperoxide and bis(hydroxymethyl) peroxide from gas-phase ozonolysis of naturally occurring alkenes, *Nature*, 316, 535-536, 10.1038/316535a0, 1985.

Gao, Z., Vasilakos, P., Nah, T., Takeuchi, M., Tanner, D. J., Ng, N. L., Huey, L. G., Weber, R. J., and Russell, A.: Emissions or reactions? Gas Phase Organic acids in the atmosphere, in prep., 2020.

Ge, X., Zhang, Q., Sun, Y., Ruehl, C. R., and Setyan, A.: Effect of aqueous-phase processing on aerosol chemistry and size distributions in Fresno, California, during wintertime, *Environmental Chemistry*, 9, 221-235, <http://dx.doi.org/10.1071/EN11168>, 2012.

Goldstein, A. H., and Galbally, I. E.: Known and Unexplored Organic Constituents in the Earth's Atmosphere, *Environmental Science & Technology*, 41, 1514-1521, 10.1021/es072476p, 2007.

Guo, H., Xu, L., Bougiatioti, A., Cerully, K. M., Capps, S. L., Hite Jr, J. R., Carlton, A. G., Lee, S. H., Bergin, M. H., Ng, N. L., Nenes, A., and Weber, R. J.: Fine-particle water and pH in the southeastern United States, *Atmos. Chem. Phys.*, 15, 5211-5228, 10.5194/acp-15-5211-2015, 2015.

Guo, H., Liu, J., Froyd, K. D., Roberts, J. M., Veres, P. R., Hayes, P. L., Jimenez, J. L., Nenes, A., and Weber, R. J.: Fine particle pH and gas-particle phase partitioning of inorganic species in Pasadena, California, during the 2010 CalNex campaign, *Atmos. Chem. Phys.*, 17, 5703-5719, 10.5194/acp-17-5703-2017, 2017a.

Guo, H., Weber, R. J., and Nenes, A.: High levels of ammonia do not raise fine particle pH sufficiently to yield nitrogen oxide-dominated sulfate production, *Scientific Reports*, 7, 12109, 10.1038/s41598-017-11704-0, 2017b.

Häkkinen, S. A. K., McNeill, V. F., and Riipinen, I.: Effect of Inorganic Salts on the Volatility of Organic Acids, *Environmental Science & Technology*, 48, 13718-13726, 10.1021/es5033103, 2014.

Hallquist, M., Wenger, J. C., Baltensperger, U., Rudich, Y., Simpson, D., Claeys, M., Dommen, J., Donahue, N. M., George, C., Goldstein, A. H., Hamilton, J. F., Herrmann, H., Hoffmann, T., Iinuma, Y., Jang, M., Jenkin, M. E., Jimenez, J. L., Kiendler-Scharr, A., Maenhaut, W., McFiggans, G., Mentel, T. F., Monod, A., Prévôt, A. S. H., Seinfeld, J. H., Surratt, J. D., Szmigielski, R., and Wildt, J.: The formation, properties and impact of secondary organic aerosol: current and emerging issues, *Atmos. Chem. Phys.*, 9, 5155-5236, 10.5194/acp-9-5155-2009, 2009.

Hayes, P. L., Ortega, A. M., Cubison, M. J., Froyd, K. D., Zhao, Y., Cliff, S. S., Hu, W. W., Toohey, D. W., Flynn, J. H., Lefer, B. L., Grossberg, N., Alvarez, S., Rappenglueck, B., Taylor, J. W., Allan, J. D., Holloway, J. S., Gilman, J. B., Kuster, W. C., De Gouw, J. A., Massoli, P., Zhang, X., Liu, J., Weber, R. J., Corrigan, A. L., Russell, L. M., Isaacman, G., Worton, D. R., Kreisberg, N. M., Goldstein, A. H., Thalman, R., Waxman, E. M., Volkamer, R., Lin, Y. H., Surratt, J. D., Kleindienst, T. E., Offenberg, J. H., Dusanter, S., Griffith, S., Stevens, P. S., Brioude, J., Angevine, W. M., and Jimenez, J. L.: Organic aerosol composition and sources in Pasadena, California, during the 2010 CalNex campaign, *Journal of Geophysical Research-Atmospheres*, 118, 9233-9257, 10.1002/jgrd.50530, 2013.

Herndon, S. C., Onasch, T. B., Wood, E. C., Kroll, J. H., Canagaratna, M. R., Jayne, J. T., Zavala, M. A., Knighton, W. B., Mazzoleni, C., Dubey, M. K., Ulbrich, I. M., Jimenez, J. L., Seila, R., de Gouw, J. A., de Foy, B., Fast, J., Molina, L. T., Kolb, C. E., and Worsnop, D. R.: Correlation of secondary organic aerosol with odd oxygen in Mexico City, *Geophysical Research Letters*, 35, 10.1029/2008gl034058, 2008.

Hettiyadura, A. P. S., Stone, E. A., Kundu, S., Baker, Z., Geddes, E., Richards, K., and Humphry, T.: Determination of atmospheric organosulfates using HILIC chromatography with MS detection, *Atmos. Meas. Tech.*, 8, 2347-2358, 10.5194/amt-8-2347-2015, 2015.

Hettiyadura, A. P. S., Jayarathne, T., Baumann, K., Goldstein, A. H., de Gouw, J. A., Koss, A., Keutsch, F. N., Skog, K., and Stone, E. A.: Qualitative and quantitative analysis of atmospheric organosulfates in Centreville, Alabama, *Atmos. Chem. Phys.*, 17, 1343-1359, 10.5194/acp-17-1343-2017, 2017.

Hettiyadura, A. P. S., Xu, L., Jayarathne, T., Skog, K., Guo, H., Weber, R. J., Nenes, A., Keutsch, F. N., Ng, N. L., and Stone, E. A.: Source apportionment of organic carbon in Centreville, AL using organosulfates in organic tracer-based positive matrix factorization, *Atmospheric Environment*, 186, 74-88, <https://doi.org/10.1016/j.atmosenv.2018.05.007>, 2018.

Hinks, M. L., Montoya-Aguilera, J., Ellison, L., Lin, P., Laskin, A., Laskin, J., Shiraiwa, M., Dabdub, D., and Nizkorodov, S. A.: Effect of relative humidity on the composition of secondary organic aerosol from the oxidation of toluene, *Atmos. Chem. Phys.*, 18, 1643-1652, 10.5194/acp-18-1643-2018, 2018.

Hogrefe, O., Drewnick, F., Lala, G. G., Schwab, J. J., and Demerjian, K. L.: Development, operation and applications of an aerosol generation, calibration and research facility, *Aerosol Science and Technology*, 38, 196-214, 10.1080/02786820390229516, 2004.

Hu, W., Palm, B. B., Day, D. A., Campuzano-Jost, P., Krechmer, J. E., Peng, Z., de Sá, S. S., Martin, S. T., Alexander, M. L., Baumann, K., Hacker, L., Kiendler-Scharr, A., Koss, A. R., de Gouw, J. A., Goldstein, A. H., Seco, R., Sjostedt, S. J., Park, J. H., Guenther, A. B., Kim, S., Canonaco, F., Prévôt, A. S. H., Brune, W. H., and Jimenez, J. L.: Volatility and lifetime against OH heterogeneous reaction of ambient isoprene-epoxydiols-derived secondary organic aerosol (IEPOX-SOA), *Atmos. Chem. Phys.*, 16, 11563-11580, 10.5194/acp-16-11563-2016, 2016.

Hu, W., Campuzano-Jost, P., Day, D. A., Croteau, P., Canagaratna, M. R., Jayne, J. T., Worsnop, D. R., and Jimenez, J. L.: Evaluation of the new capture vapourizer for aerosol mass spectrometers (AMS) through laboratory studies of inorganic species, *Atmos. Meas. Tech.*, 10, 2897-2921, 10.5194/amt-10-2897-2017, 2017.

Hu, W. W., Campuzano-Jost, P., Palm, B. B., Day, D. A., Ortega, A. M., Hayes, P. L., Krechmer, J. E., Chen, Q., Kuwata, M., Liu, Y. J., de Sá, S. S., McKinney, K., Martin, S. T., Hu, M., Budisulistiorini, S. H., Riva, M., Surratt, J. D., St. Clair, J. M., Isaacman-Van Wertz, G., Yee, L. D., Goldstein, A. H., Carbone, S., Brito, J., Artaxo, P., de Gouw, J. A., Koss, A., Wisthaler, A., Mikoviny, T., Karl, T., Kaser, L., Jud, W., Hansel, A., Docherty, K. S., Alexander, M. L., Robinson, N. H., Coe, H., Allan, J. D., Canagaratna, M. R., Paulot, F., and Jimenez, J. L.: Characterization of a real-time tracer for isoprene epoxydiols-derived secondary organic aerosol (IEPOX-SOA) from aerosol mass spectrometer measurements, *Atmos. Chem. Phys.*, 15, 11807-11833, 10.5194/acp-15-11807-2015, 2015.

Huang, D. D., Li, Y. J., Lee, B. P., and Chan, C. K.: Analysis of Organic Sulfur Compounds in Atmospheric Aerosols at the HKUST Supersite in Hong Kong Using HR-ToF-AMS, *Environmental Science & Technology*, 49, 3672-3679, 10.1021/es5056269, 2015.

Huang, R. J., Cao, J. J., Chen, Y., Yang, L., Shen, J. C., You, Q. H., Wang, K., Lin, C. S., Xu, W., Gao, B., Li, Y. J., Chen, Q., Hoffmann, T., O'Dowd, C. D., Bilde, M., and Glasius, M.: Organosulfates in atmospheric aerosol: synthesis and quantitative analysis of PM_{2.5} from Xi'an, northwestern China, *Atmospheric Measurement Techniques*, 11, 3447-3456, 10.5194/amt-11-3447-2018, 2018.

Huang, S., Poulain, L., van Pinxteren, D., van Pinxteren, M., Wu, Z., Herrmann, H., and Wiedensohler, A.: Latitudinal and Seasonal Distribution of Particulate MSA over the Atlantic using a Validated Quantification Method with HR-ToF-AMS, *Environmental Science & Technology*, 51, 418-426, 10.1021/acs.est.6b03186, 2017.

Huang, W., Saathoff, H., Shen, X. L., Ramisetty, R., Leisner, T., and Mohr, C.: Chemical Characterization of Highly Functionalized Organonitrates Contributing to Night-Time Organic Aerosol Mass Loadings and Particle Growth, *Environmental Science & Technology*, 53, 1165-1174, 10.1021/acs.est.8b05826, 2019.

Huey, L. G., Hanson, D. R., and Howard, C. J.: Reactions of SF₆- and I- with Atmospheric Trace Gases, *The Journal of Physical Chemistry*, 99, 5001-5008, 10.1021/j100014a021, 1995.

Huey, L. G.: Measurement of trace atmospheric species by chemical ionization mass spectrometry: Speciation of reactive nitrogen and future directions, *Mass Spectrometry Reviews*, 26, 166-184, doi:10.1002/mas.20118, 2007.

Iinuma, Y., Müller, C., Berndt, T., Böge, O., Claeys, M., and Herrmann, H.: Evidence for the Existence of Organosulfates from β -Pinene Ozonolysis in Ambient Secondary Organic Aerosol, *Environmental Science & Technology*, 41, 6678-6683, 10.1021/es070938t, 2007a.

Iinuma, Y., Müller, C., Böge, O., Gnauk, T., and Herrmann, H.: The formation of organic sulfate esters in the limonene ozonolysis secondary organic aerosol (SOA) under acidic conditions, *Atmospheric Environment*, 41, 5571-5583, <http://dx.doi.org/10.1016/j.atmosenv.2007.03.007>, 2007b.

Jacob, D. J.: Chemistry of OH in remote clouds and its role in the production of formic acid and peroxymonosulfate, *Journal of Geophysical Research: Atmospheres*, 91, 9807-9826, doi:10.1029/JD091iD09p09807, 1986.

Jacob, D. J., and Wofsy, S. C.: Photochemistry of biogenic emissions over the Amazon forest, *Journal of Geophysical Research: Atmospheres*, 93, 1477-1486, doi:10.1029/JD093iD02p01477, 1988.

Jacobs, M. I., Burke, W. J., and Elrod, M. J.: Kinetics of the reactions of isoprene-derived hydroxynitrates: gas phase epoxide formation and solution phase hydrolysis, *Atmos. Chem. Phys.*, 14, 8933-8946, 10.5194/acp-14-8933-2014, 2014.

Jaoui, M., Szmigielski, R., Nestorowicz, K., Kolodziejczyk, A., Sarang, K., Rudzinski, K. J., Konopka, A., Bulska, E., Lewandowski, M., and Kleindienst, T. E.: Organic Hydroxy Acids as Highly Oxygenated Molecular (HOM) Tracers for Aged Isoprene Aerosol, *Environmental Science & Technology*, 10.1021/acs.est.9b05075, 2019.

Jimenez, J. L., Canagaratna, M. R., Donahue, N. M., Prevot, A. S. H., Zhang, Q., Kroll, J. H., DeCarlo, P. F., Allan, J. D., Coe, H., Ng, N. L., Aiken, A. C., Docherty, K. S., Ulbrich, I. M., Grieshop, A. P., Robinson, A. L., Duplissy, J., Smith, J. D., Wilson, K. R., Lanz, V. A., Hueglin, C., Sun, Y. L., Tian, J., Laaksonen, A., Raatikainen, T., Rautiainen, J., Vaattovaara, P., Ehn, M., Kulmala, M., Tomlinson, J. M., Collins, D. R., Cubison, M. J., Dunlea, J., Huffman, J. A., Onasch, T. B., Alfarra, M. R., Williams, P. I., Bower, K., Kondo, Y., Schneider, J., Drewnick, F., Borrmann, S., Weimer, S., Demerjian, K., Salcedo, D., Cottrell, L., Griffin, R., Takami, A., Miyoshi, T., Hatakeyama, S., Shimojo, A., Sun, J. Y., Zhang, Y. M., Dzepina, K., Kimmel, J. R., Sueper, D., Jayne, J. T., Herndon, S. C., Trimborn, A. M., Williams, L. R., Wood, E. C., Middlebrook, A. M., Kolb, C. E., Baltensperger, U., and Worsnop, D. R.: Evolution of Organic Aerosols in the Atmosphere, *Science*, 326, 1525-1529, 10.1126/science.1180353, 2009.

Jonsson, Å. M., Hallquist, M., and Ljungström, E.: Impact of Humidity on the Ozone Initiated Oxidation of Limonene, Δ^3 -Carene, and α -Pinene, *Environmental Science & Technology*, 40, 188-194, 10.1021/es051163w, 2006.

Kahnt, A., Iinuma, Y., Blockhuys, F., Mutzel, A., Vermeylen, R., Kleindienst, T. E., Jaoui, M., Offenberg, J. H., Lewandowski, M., Böge, O., Herrmann, H., Maenhaut, W., and Claeys, M.: 2-Hydroxyterpenylic Acid: An Oxygenated Marker Compound for α -Pinene Secondary Organic Aerosol in Ambient Fine Aerosol, *Environmental Science & Technology*, 48, 4901-4908, 10.1021/es500377d, 2014a.

Kahnt, A., Iinuma, Y., Mutzel, A., Böge, O., Claeys, M., and Herrmann, H.: Campholenic aldehyde ozonolysis: a mechanism leading to specific biogenic secondary organic aerosol constituents, *Atmos. Chem. Phys.*, 14, 719-736, 10.5194/acp-14-719-2014, 2014b.

Kanakidou, M., Seinfeld, J. H., Pandis, S. N., Barnes, I., Dentener, F. J., Facchini, M. C., Van Dingenen, R., Ervens, B., Nenes, A., Nielsen, C. J., Swietlicki, E., Putaud, J. P., Balkanski, Y., Fuzzi, S., Horth, J., Moortgat, G. K., Winterhalter, R., Myhre, C. E. L., Tsigaridis, K., Vignati, E., Stephanou, E. G., and Wilson, J.: Organic aerosol and global climate modelling: a review, *Atmospheric Chemistry and Physics*, 5, 1053-1123, 10.5194/acp-5-1053-2005, 2005.

Kawamura, K., Seméré, R., Imai, Y., Fujii, Y., and Hayashi, M.: Water soluble dicarboxylic acids and related compounds in Antarctic aerosols, *Journal of Geophysical Research: Atmospheres*, 101, 18721-18728, 10.1029/96jd01541, 1996.

Kawamura, K., and Bikkina, S.: A review of dicarboxylic acids and related compounds in atmospheric aerosols: Molecular distributions, sources and transformation, *Atmospheric Research*, 170, 140-160, <http://dx.doi.org/10.1016/j.atmosres.2015.11.018>, 2016.

Keene, W. C., and Galloway, J. N.: Organic acidity in precipitation of North America, *Atmospheric Environment* (1967), 18, 2491-2497, [https://doi.org/10.1016/0004-6981\(84\)90020-9](https://doi.org/10.1016/0004-6981(84)90020-9), 1984.

Keene, W. C., Pszenny, A. A. P., Maben, J. R., Stevenson, E., and Wall, A.: Closure evaluation of size-resolved aerosol pH in the New England coastal atmosphere during summer, *Journal of Geophysical Research: Atmospheres*, 109, n/a-n/a, 10.1029/2004JD004801, 2004.

Khare, P., Kumar, N., Kumari, K. M., and Srivastava, S. S.: Atmospheric formic and acetic acids: An overview, *Reviews of Geophysics*, 37, 227-248, 10.1029/1998RG900005, 1999.

Kleindienst, T. E., Jaoui, M., Lewandowski, M., Offenberg, J. H., Lewis, C. W., Bhave, P. V., and Edney, E. O.: Estimates of the contributions of biogenic and anthropogenic hydrocarbons to secondary organic aerosol at a southeastern US location, *Atmospheric Environment*, 41, 8288-8300, <https://doi.org/10.1016/j.atmosenv.2007.06.045>, 2007.

Kostenidou, E., Karnezi, E., Hite Jr, J. R., Bougiatioti, A., Cerully, K., Xu, L., Ng, N. L., Nenes, A., and Pandis, S. N.: Organic aerosol in the summertime southeastern United States: components and their link to volatility distribution, oxidation state and hygroscopicity, *Atmos. Chem. Phys.*, 18, 5799-5819, 10.5194/acp-18-5799-2018, 2018.

Krechmer, J. E., Coggon, M. M., Massoli, P., Nguyen, T. B., Crouse, J. D., Hu, W., Day, D. A., Tyndall, G. S., Henze, D. K., Rivera-Rios, J. C., Nowak, J. B., Kimmel, J. R., Mauldin, R. L., Stark, H., Jayne, J. T., Sipilä, M., Junninen, H., Clair, J. M. S., Zhang, X., Feiner, P. A., Zhang, L., Miller, D. O., Brune, W. H., Keutsch, F. N., Wennberg, P. O., Seinfeld, J. H., Worsnop, D. R., Jimenez, J. L., and Canagaratna, M. R.: Formation of Low Volatility Organic Compounds and Secondary Organic Aerosol from Isoprene Hydroxyhydroperoxide Low-NO Oxidation, *Environmental Science & Technology*, 49, 10330-10339, 10.1021/acs.est.5b02031, 2015.

Kroll, J. H., and Seinfeld, J. H.: Chemistry of secondary organic aerosol: Formation and evolution of low-volatility organics in the atmosphere, *Atmospheric Environment*, 42, 3593-3624, 2008.

Kroll, J. H., Donahue, N. M., Jimenez, J. L., Kessler, S. H., Canagaratna, M. R., Wilson, K. R., Altieri, K. E., Mazzoleni, L. R., Wozniak, A. S., Bluhm, H., Mysak, E. R., Smith, J. D., Kolb, C. E., and Worsnop, D. R.: Carbon oxidation state as a metric for describing the chemistry of atmospheric organic aerosol, *Nat Chem*, 3, 133-139, <http://www.nature.com/nchem/journal/v3/n2/abs/nchem.948.html#supplementary-information>, 2011.

Lanz, V. A., Alfarra, M. R., Baltensperger, U., Buchmann, B., Hueglin, C., and Prévôt, A. S. H.: Source apportionment of submicron organic aerosols at an urban site by factor analytical modelling of aerosol mass spectra, *Atmos. Chem. Phys.*, 7, 1503-1522, 10.5194/acp-7-1503-2007, 2007.

Lanz, V. A., Alfarra, M. R., Baltensperger, U., Buchmann, B., Hueglin, C., Szidat, S., Wehrli, M. N., Wacker, L., Weimer, S., Caseiro, A., Puxbaum, H., and Prevot, A. S. H.: Source Attribution of Submicron Organic Aerosols during Wintertime Inversions by Advanced Factor Analysis of Aerosol Mass Spectra, *Environmental Science & Technology*, 42, 214-220, 10.1021/es0707207, 2008.

Lee, A., Goldstein, A. H., Kroll, J. H., Ng, N. L., Varutbangkul, V., Flagan, R. C., and Seinfeld, J. H.: Gas-phase products and secondary aerosol yields from the photooxidation of 16 different terpenes, *Journal of Geophysical Research: Atmospheres*, 111, n/a-n/a, 10.1029/2006JD007050, 2006.

Lee, A. K. Y., Herckes, P., Leaitch, W. R., Macdonald, A. M., and Abbatt, J. P. D.: Aqueous OH oxidation of ambient organic aerosol and cloud water organics: Formation of highly oxidized products, *Geophysical Research Letters*, 38, doi:10.1029/2011GL047439, 2011.

Lee, B. H., Lopez-Hilfiker, F. D., Mohr, C., Kurtén, T., Worsnop, D. R., and Thornton, J. A.: An Iodide-Adduct High-Resolution Time-of-Flight Chemical-Ionization Mass Spectrometer: Application to Atmospheric Inorganic and Organic Compounds, *Environmental Science & Technology*, 48, 6309-6317, 10.1021/es500362a, 2014.

Lee, B. H., Mohr, C., Lopez-Hilfiker, F. D., Lutz, A., Hallquist, M., Lee, L., Romer, P., Cohen, R. C., Iyer, S., Kurtén, T., Hu, W., Day, D. A., Campuzano-Jost, P., Jimenez, J. L., Xu, L., Ng, N. L., Guo, H., Weber, R. J., Wild, R. J., Brown, S. S., Koss, A., de Gouw, J., Olson, K., Goldstein, A. H., Seco, R., Kim, S., McAvey, K., Shepson, P. B., Starn, T., Baumann, K., Edgerton, E. S., Liu, J., Shilling, J. E., Miller, D. O., Brune, W., Schobesberger, S., D'Ambro, E. L., and Thornton, J. A.: Highly functionalized organic nitrates in the southeast United States: Contribution to secondary organic aerosol and reactive nitrogen budgets, *Proceedings of the National Academy of Sciences*, 113, 1516-1521, 10.1073/pnas.1508108113, 2016.

Lee, B. H., Lopez-Hilfiker, F. D., D'Ambro, E. L., Zhou, P., Boy, M., Petäjä, T., Hao, L., Virtanen, A., and Thornton, J. A.: Semi-volatile and highly oxygenated gaseous and particulate organic compounds observed above a boreal forest canopy, *Atmos. Chem. Phys.*, 18, 11547-11562, 10.5194/acp-18-11547-2018, 2018.

Lee, S.-H., Murphy, D. M., Thomson, D. S., and Middlebrook, A. M.: Chemical components of single particles measured with Particle Analysis by Laser Mass Spectrometry (PALMS) during the Atlanta SuperSite Project: Focus on organic/sulfate, lead, soot, and mineral particles, *Journal of Geophysical Research: Atmospheres*, 107, AAC 1-1-AAC 1-13, 10.1029/2000jd000011, 2002.

Liao, J., Froyd, K. D., Murphy, D. M., Keutsch, F. N., Yu, G., Wennberg, P. O., St. Clair, J. M., Crouse, J. D., Wisthaler, A., Mikoviny, T., Jimenez, J. L., Campuzano-Jost, P., Day, D. A., Hu, W., Ryerson, T. B., Pollack, I. B., Peischl, J., Anderson, B. E., Ziemba, L. D., Blake, D. R., Meinardi, S., and Diskin, G.: Airborne measurements of organosulfates over the continental U.S, *Journal of Geophysical Research: Atmospheres*, 120, 2990-3005, 10.1002/2014JD022378, 2015.

Liggio, J., and Li, S.-M.: Organosulfate formation during the uptake of pinonaldehyde on acidic sulfate aerosols, *Geophysical Research Letters*, 33, L13808, 10.1029/2006GL026079, 2006.

Lim, H.-J., and Turpin, B. J.: Origins of Primary and Secondary Organic Aerosol in Atlanta: Results of Time-Resolved Measurements during the Atlanta Supersite Experiment, *Environmental Science & Technology*, 36, 4489-4496, 10.1021/es0206487, 2002.

Lim, H.-J., Carlton, A. G., and Turpin, B. J.: Isoprene Forms Secondary Organic Aerosol through Cloud Processing: Model Simulations, *Environmental Science & Technology*, 39, 4441-4446, 10.1021/es048039h, 2005.

Lim, Y. B., Tan, Y., Perri, M. J., Seitzinger, S. P., and Turpin, B. J.: Aqueous chemistry and its role in secondary organic aerosol (SOA) formation, *Atmos. Chem. Phys.*, 10, 10521-10539, 10.5194/acp-10-10521-2010, 2010.

Lin, Y.-H., Zhang, Z., Docherty, K. S., Zhang, H., Budisulistiorini, S. H., Rubitschun, C. L., Shaw, S. L., Knipping, E. M., Edgerton, E. S., Kleindienst, T. E., Gold, A., and Surratt, J. D.: Isoprene Epoxydiols as Precursors to Secondary Organic Aerosol Formation: Acid-Catalyzed Reactive Uptake Studies with Authentic Compounds, *Environmental Science & Technology*, 46, 250-258, 10.1021/es202554c, 2012.

Lin, Y.-H., Zhang, H., Pye, H. O., Zhang, Z., Marth, W. J., Park, S., Arashiro, M., Cui, T., Budisulistiorini, S. H., and Sexton, K. G.: Epoxide as a precursor to secondary organic aerosol formation from isoprene photooxidation in the presence of nitrogen oxides, *Proceedings of the National Academy of Sciences*, 110, 6718-6723, 2013.

Link, M. F., Nguyen, T. B., Bates, K. H., Müller, J.-F., and Farmer, D. K.: Can isoprene oxidation explain high concentrations of atmospheric formic and acetic acid over forests?, *ACS Earth and Space Chemistry*, 10.1021/acsearthspacechem.0c00010, 2020.

Liu, J., D'Ambro, E. L., Lee, B. H., Lopez-Hilfiker, F. D., Zaveri, R. A., Rivera-Rios, J. C., Keutsch, F. N., Iyer, S., Kurten, T., Zhang, Z., Gold, A., Surratt, J. D., Shilling, J. E., and Thornton, J. A.: Efficient Isoprene Secondary Organic Aerosol Formation from a Non-IEPOX Pathway, *Environmental Science & Technology*, 50, 9872-9880, 10.1021/acs.est.6b01872, 2016.

Liu, J. M., Zhang, X. L., Parker, E. T., Veres, P. R., Roberts, J. M., de Gouw, J. A., Hayes, P. L., Jimenez, J. L., Murphy, J. G., Ellis, R. A., Huey, L. G., and Weber, R. J.: On the gas-particle partitioning of soluble organic aerosol in two urban atmospheres with contrasting

emissions: 2. Gas and particle phase formic acid, *Journal of Geophysical Research-Atmospheres*, 117, 15, 10.1029/2012jd017912, 2012.

Liu, M., Song, Y., Zhou, T., Xu, Z., Yan, C., Zheng, M., Wu, Z., Hu, M., Wu, Y., and Zhu, T.: Fine particle pH during severe haze episodes in northern China, *Geophysical Research Letters*, 44, 5213-5221, 10.1002/2017GL073210, 2017.

Lopez-Hilfiker, F. D., Mohr, C., Ehn, M., Rubach, F., Kleist, E., Wildt, J., Mentel, T. F., Lutz, A., Hallquist, M., Worsnop, D., and Thornton, J. A.: A novel method for online analysis of gas and particle composition: description and evaluation of a Filter Inlet for Gases and AEROsols (FIGAERO), *Atmospheric Measurement Techniques*, 7, 983-1001, 10.5194/amt-7-983-2014, 2014.

Lopez-Hilfiker, F. D., Mohr, C., D'Ambro, E. L., Lutz, A., Riedel, T. P., Gaston, C. J., Iyer, S., Zhang, Z., Gold, A., Surratt, J. D., Lee, B. H., Kurten, T., Hu, W. W., Jimenez, J., Hallquist, M., and Thornton, J. A.: Molecular Composition and Volatility of Organic Aerosol in the Southeastern U.S.: Implications for IEPOX Derived SOA, *Environmental Science & Technology*, 50, 2200-2209, 10.1021/acs.est.5b04769, 2016.

Lukács, H., Gelencsér, A., Hoffer, A., Kiss, G., Horváth, K., and Hartyáni, Z.: Quantitative assessment of organosulfates in size-segregated rural fine aerosol, *Atmos. Chem. Phys.*, 9, 231-238, 10.5194/acp-9-231-2009, 2009.

Malecha, K. T., and Nizkorodov, S. A.: Photodegradation of Secondary Organic Aerosol Particles as a Source of Small, Oxygenated Volatile Organic Compounds, *Environmental Science & Technology*, 50, 9990-9997, 10.1021/acs.est.6b02313, 2016.

Maria, S. F., Russell, L. M., Turpin, B. J., Porcja, R. J., Campos, T. L., Weber, R. J., and Huebert, B. J.: Source signatures of carbon monoxide and organic functional groups in Asian Pacific Regional Aerosol Characterization Experiment (ACE-Asia) submicron aerosol types, *Journal of Geophysical Research: Atmospheres*, 108, n/a-n/a, 10.1029/2003JD003703, 2003.

Massoli, P., Stark, H., Canagaratna, M. R., Krechmer, J. E., Xu, L., Ng, N. L., Mauldin, R. L., Yan, C., Kimmel, J., Misztal, P. K., Jimenez, J. L., Jayne, J. T., and Worsnop, D. R.: Ambient Measurements of Highly Oxidized Gas-Phase Molecules during the Southern Oxidant and Aerosol Study (SOAS) 2013, *ACS Earth and Space Chemistry*, 10.1021/acsearthspacechem.8b00028, 2018.

Matthew, B. M., Middlebrook, A. M., and Onasch, T. B.: Collection Efficiencies in an Aerodyne Aerosol Mass Spectrometer as a Function of Particle Phase for Laboratory Generated Aerosols, *Aerosol Science and Technology*, 42, 884-898, 10.1080/02786820802356797, 2008.

McNeill, V. F., Woo, J. L., Kim, D. D., Schwier, A. N., Wannell, N. J., Sumner, A. J., and Barakat, J. M.: Aqueous-Phase Secondary Organic Aerosol and Organosulfate Formation in Atmospheric Aerosols: A Modeling Study, *Environmental Science & Technology*, 46, 8075-8081, 10.1021/es3002986, 2012.

- Middlebrook, A. M., Bahreini, R., Jimenez, J. L., and Canagaratna, M. R.: Evaluation of Composition-Dependent Collection Efficiencies for the Aerodyne Aerosol Mass Spectrometer using Field Data, *Aerosol Science and Technology*, 46, 258-271, 10.1080/02786826.2011.620041, 2012.
- Millet, D. B., Baasandorj, M., Farmer, D. K., Thornton, J. A., Baumann, K., Brophy, P., Chaliyakunnel, S., de Gouw, J. A., Graus, M., Hu, L., Koss, A., Lee, B. H., Lopez-Hilfiker, F. D., Neuman, J. A., Paulot, F., Peischl, J., Pollack, I. B., Ryerson, T. B., Warneke, C., Williams, B. J., and Xu, J.: A large and ubiquitous source of atmospheric formic acid, *Atmos. Chem. Phys.*, 15, 6283-6304, 10.5194/acp-15-6283-2015, 2015.
- Müller, L., Reinnig, M. C., Naumann, K. H., Saathoff, H., Mentel, T. F., Donahue, N. M., and Hoffmann, T.: Formation of 3-methyl-1,2,3-butanetricarboxylic acid via gas phase oxidation of pinonic acid – a mass spectrometric study of SOA aging, *Atmos. Chem. Phys.*, 12, 1483-1496, 10.5194/acp-12-1483-2012, 2012.
- Murphy, D. M.: The design of single particle laser mass spectrometers, *Mass Spectrometry Reviews*, 26, 150-165, doi:10.1002/mas.20113, 2007.
- Murphy, D. M., Cziczo, D. J., Hudson, P. K., and Thomson, D. S.: Carbonaceous material in aerosol particles in the lower stratosphere and tropopause region, *Journal of Geophysical Research: Atmospheres*, 112, doi:10.1029/2006JD007297, 2007.
- Nagori, J., Janssen, R. H. H., Fry, J. L., Krol, M., Jimenez, J. L., Hu, W., and Vilà-Guerau de Arellano, J.: Biogenic emissions and land-atmosphere interactions as drivers of the daytime evolution of secondary organic aerosol in the southeastern US, *Atmos. Chem. Phys.*, 19, 701-729, 10.5194/acp-19-701-2019, 2019.
- Nah, T., Sanchez, J., Boyd, C. M., and Ng, N. L.: Photochemical Aging of α -pinene and β -pinene Secondary Organic Aerosol formed from Nitrate Radical Oxidation, *Environmental Science & Technology*, 50, 222-231, 10.1021/acs.est.5b04594, 2016.
- Nah, T., Guo, H. Y., Sullivan, A. P., Chen, Y. L., Tanner, D. J., Nenes, A., Russell, A., Ng, N. L., Huey, L. G., and Weber, R. J.: Characterization of aerosol composition, aerosol acidity, and organic acid partitioning at an agriculturally intensive rural southeastern US site, *Atmospheric Chemistry and Physics*, 18, 11471-11491, 10.5194/acp-18-11471-2018, 2018a.
- Nah, T., Ji, Y., Tanner, D. J., Guo, H. Y., Sullivan, A. P., Ng, N. L., Weber, R. J., and Huey, L. G.: Real-time measurements of gas-phase organic acids using SF₆(-)chemical ionization mass spectrometry, *Atmospheric Measurement Techniques*, 11, 5087-5104, 10.5194/amt-11-5087-2018, 2018b.
- Neeb, P., Sauer, F., Horie, O., and Moortgat, G. K.: Formation of hydroxymethyl hydroperoxide and formic acid in alkene ozonolysis in the presence of water vapour, *Atmospheric Environment*, 31, 1417-1423, [https://doi.org/10.1016/S1352-2310\(96\)00322-6](https://doi.org/10.1016/S1352-2310(96)00322-6), 1997.

Ng, N. L., Kwan, A. J., Surratt, J. D., Chan, A. W. H., Chhabra, P. S., Sorooshian, A., Pye, H. O. T., Crounse, J. D., Wennberg, P. O., Flagan, R. C., and Seinfeld, J. H.: Secondary organic aerosol (SOA) formation from reaction of isoprene with nitrate radicals (NO₃), *Atmos. Chem. Phys.*, 8, 4117-4140, 10.5194/acp-8-4117-2008, 2008.

Ng, N. L., Canagaratna, M. R., Zhang, Q., Jimenez, J. L., Tian, J., Ulbrich, I. M., Kroll, J. H., Docherty, K. S., Chhabra, P. S., Bahreini, R., Murphy, S. M., Seinfeld, J. H., Hildebrandt, L., Donahue, N. M., DeCarlo, P. F., Lanz, V. A., Prévôt, A. S. H., Dinar, E., Rudich, Y., and Worsnop, D. R.: Organic aerosol components observed in Northern Hemispheric datasets from Aerosol Mass Spectrometry, *Atmos. Chem. Phys.*, 10, 4625-4641, 10.5194/acp-10-4625-2010, 2010.

Ng, N. L., Brown, S. S., Archibald, A. T., Atlas, E., Cohen, R. C., Crowley, J. N., Day, D. A., Donahue, N. M., Fry, J. L., Fuchs, H., Griffin, R. J., Guzman, M. I., Herrmann, H., Hodzic, A., Inuma, Y., Jimenez, J. L., Kiendler-Scharr, A., Lee, B. H., Luecken, D. J., Mao, J., McLaren, R., Mutzel, A., Osthoff, H. D., Ouyang, B., Picquet-Varrault, B., Platt, U., Pye, H. O. T., Rudich, Y., Schwantes, R. H., Shiraiwa, M., Stutz, J., Thornton, J. A., Tilgner, A., Williams, B. J., and Zaveri, R. A.: Nitrate radicals and biogenic volatile organic compounds: oxidation, mechanisms, and organic aerosol, *Atmos. Chem. Phys.*, 17, 2103-2162, 10.5194/acp-17-2103-2017, 2017.

Nguyen, T. B., Bateman, A. P., Bones, D. L., Nizkorodov, S. A., Laskin, J., and Laskin, A.: High-resolution mass spectrometry analysis of secondary organic aerosol generated by ozonolysis of isoprene, *Atmospheric Environment*, 44, 1032-1042, <https://doi.org/10.1016/j.atmosenv.2009.12.019>, 2010.

Nguyen, T. B., Roach, P. J., Laskin, J., Laskin, A., and Nizkorodov, S. A.: Effect of humidity on the composition of isoprene photooxidation secondary organic aerosol, *Atmospheric Chemistry and Physics*, 11, 6931-6944, 10.5194/acp-11-6931-2011, 2011.

Nguyen, T. B., Bates, K. H., Crounse, J. D., Schwantes, R. H., Zhang, X., Kjaergaard, H. G., Surratt, J. D., Lin, P., Laskin, A., Seinfeld, J. H., and Wennberg, P. O.: Mechanism of the hydroxyl radical oxidation of methacryloyl peroxyxynitrate (MPAN) and its pathway toward secondary organic aerosol formation in the atmosphere, *Physical Chemistry Chemical Physics*, 17, 17914-17926, 10.1039/C5CP02001H, 2015a.

Nguyen, T. B., Crounse, J. D., Teng, A. P., St. Clair, J. M., Paulot, F., Wolfe, G. M., and Wennberg, P. O.: Rapid deposition of oxidized biogenic compounds to a temperate forest, *Proceedings of the National Academy of Sciences*, 112, E392-E401, 10.1073/pnas.1418702112, 2015b.

Oae, S.: Organic sulfur chemistry: structure and mechanism, edited by: Doi, J. T., Boca Raton, Fla. : CRC Press, Boca Raton, Fla., 1991.

Olson, C. N., Galloway, M. M., Yu, G., Hedman, C. J., Lockett, M. R., Yoon, T., Stone, E. A., Smith, L. M., and Keutsch, F. N.: Hydroxycarboxylic Acid-Derived Organosulfates: Synthesis, Stability, and Quantification in Ambient Aerosol, *Environmental Science & Technology*, 45, 6468-6474, 10.1021/es201039p, 2011.

Orlando, J. J., Nozière, B., Tyndall, G. S., Orzechowska, G. E., Paulson, S. E., and Rudich, Y.: Product studies of the OH- and ozone-initiated oxidation of some monoterpenes, *Journal of Geophysical Research: Atmospheres*, 105, 11561-11572, 10.1029/2000JD900005, 2000.

Ovadnevaite, J., Ceburnis, D., Leinert, S., Dall'Osto, M., Canagaratna, M., O'Doherty, S., Berresheim, H., and O'Dowd, C.: Submicron NE Atlantic marine aerosol chemical composition and abundance: Seasonal trends and air mass categorization, *Journal of Geophysical Research: Atmospheres*, 119, 11,850-811,863, 10.1002/2013JD021330, 2014.

Paulot, F., Crounse, J. D., Kjaergaard, H. G., Kroll, J. H., Seinfeld, J. H., and Wennberg, P. O.: Isoprene photooxidation: new insights into the production of acids and organic nitrates, *Atmos. Chem. Phys.*, 9, 1479-1501, 10.5194/acp-9-1479-2009, 2009a.

Paulot, F., Crounse, J. D., Kjaergaard, H. G., Kürten, A., St. Clair, J. M., Seinfeld, J. H., and Wennberg, P. O.: Unexpected Epoxide Formation in the Gas-Phase Photooxidation of Isoprene, *Science*, 325, 730-733, 10.1126/science.1172910, 2009b.

Paulot, F., Wunch, D., Crounse, J. D., Toon, G. C., Millet, D. B., DeCarlo, P. F., Vigouroux, C., Deutscher, N. M., González Abad, G., Notholt, J., Warneke, T., Hannigan, J. W., Warneke, C., de Gouw, J. A., Dunlea, E. J., De Mazière, M., Griffith, D. W. T., Bernath, P., Jimenez, J. L., and Wennberg, P. O.: Importance of secondary sources in the atmospheric budgets of formic and acetic acids, *Atmos. Chem. Phys.*, 11, 1989-2013, 10.5194/acp-11-1989-2011, 2011.

Perri, M. J., Seitzinger, S., and Turpin, B. J.: Secondary organic aerosol production from aqueous photooxidation of glycolaldehyde: Laboratory experiments, *Atmospheric Environment*, 43, 1487-1497, <https://doi.org/10.1016/j.atmosenv.2008.11.037>, 2009.

Phinney, L., Richard Leaitch, W., Lohmann, U., Boudries, H., Worsnop, D. R., Jayne, J. T., Toom-Saunty, D., Wadleigh, M., Sharma, S., and Shantz, N.: Characterization of the aerosol over the sub-arctic north east Pacific Ocean, *Deep Sea Research Part II: Topical Studies in Oceanography*, 53, 2410-2433, <http://dx.doi.org/10.1016/j.dsr2.2006.05.044>, 2006.

Praplan, A. P., Hegyi-Gaeggeler, K., Barmet, P., Pfaffenberger, L., Dommen, J., and Baltensperger, U.: Online measurements of water-soluble organic acids in the gas and aerosol phase from the photooxidation of 1,3,5-trimethylbenzene, *Atmos. Chem. Phys.*, 14, 8665-8677, 10.5194/acp-14-8665-2014, 2014.

Pye, H. O. T., Luecken, D. J., Xu, L., Boyd, C. M., Ng, N. L., Baker, K. R., Ayres, B. R., Bash, J. O., Baumann, K., Carter, W. P. L., Edgerton, E., Fry, J. L., Hutzell, W. T., Schwede, D. B., and Shepson, P. B.: Modeling the Current and Future Roles of Particulate Organic Nitrates in the Southeastern United States, *Environmental Science & Technology*, 49, 14195-14203, 10.1021/acs.est.5b03738, 2015.

Qi, L., Chen, M., Stefenelli, G., Pospisilova, V., Tong, Y., Bertrand, A., Hueglin, C., Ge, X., Baltensperger, U., Prévôt, A. S. H., and Slowik, J. G.: Organic aerosol source apportionment in Zurich using an extractive electrospray ionization time-of-flight mass spectrometer (EESI-TOF-MS) – Part 2: Biomass burning influences in winter, *Atmos. Chem. Phys.*, 19, 8037-8062, 10.5194/acp-19-8037-2019, 2019.

Rattanavaraha, W., Chu, K., Budisulistiorini, S. H., Riva, M., Lin, Y. H., Edgerton, E. S., Baumann, K., Shaw, S. L., Guo, H., King, L., Weber, R. J., Neff, M. E., Stone, E. A., Offenberg, J. H., Zhang, Z., Gold, A., and Surratt, J. D.: Assessing the impact of anthropogenic pollution on isoprene-derived secondary organic aerosol formation in PM_{2.5} collected from the Birmingham, Alabama, ground site during the 2013 Southern Oxidant and Aerosol Study, *Atmos. Chem. Phys.*, 16, 4897-4914, 10.5194/acp-16-4897-2016, 2016.

Riedel, T. P., Lin, Y. H., Zhang, Z., Chu, K., Thornton, J. A., Vizuete, W., Gold, A., and Surratt, J. D.: Constraining condensed-phase formation kinetics of secondary organic aerosol components from isoprene epoxydiols, *Atmos. Chem. Phys.*, 16, 1245-1254, 10.5194/acp-16-1245-2016, 2016.

Riva, M., Tomaz, S., Cui, T., Lin, Y.-H., Perraudin, E., Gold, A., Stone, E. A., Villenave, E., and Surratt, J. D.: Evidence for an Unrecognized Secondary Anthropogenic Source of Organosulfates and Sulfonates: Gas-Phase Oxidation of Polycyclic Aromatic Hydrocarbons in the Presence of Sulfate Aerosol, *Environmental Science & Technology*, 49, 6654-6664, 10.1021/acs.est.5b00836, 2015.

Robinson, N. H., Hamilton, J. F., Allan, J. D., Langford, B., Oram, D. E., Chen, Q., Docherty, K., Farmer, D. K., Jimenez, J. L., Ward, M. W., Hewitt, C. N., Barley, M. H., Jenkin, M. E., Rickard, A. R., Martin, S. T., McFiggans, G., and Coe, H.: Evidence for a significant proportion of Secondary Organic Aerosol from isoprene above a maritime tropical forest, *Atmos. Chem. Phys.*, 11, 1039-1050, 10.5194/acp-11-1039-2011, 2011.

Sanderson, R. T.: *Chemical bonds and bond energy*, New York, Academic Press, New York, 1971.

Sato, K., Jia, T., Tanabe, K., Morino, Y., Kajii, Y., and Imamura, T.: Terpenylic acid and nine-carbon multifunctional compounds formed during the aging of β -pinene ozonolysis secondary organic aerosol, *Atmospheric Environment*, 130, 127-135, <https://doi.org/10.1016/j.atmosenv.2015.08.047>, 2016.

Schobesberger, S., D'Ambro, E. L., Lopez-Hilfiker, F. D., Mohr, C., and Thornton, J. A.: A model framework to retrieve thermodynamic and kinetic properties of organic aerosol from composition-resolved thermal desorption measurements, *Atmospheric Chemistry and Physics*, 18, 14757-14785, 10.5194/acp-18-14757-2018, 2018.

Schroder, J. C., Campuzano-Jost, P., Day, D. A., Shah, V., Larson, K., Sommers, J. M., Sullivan, A. P., Campos, T., Reeves, J. M., Hills, A., Hornbrook, R. S., Blake, N. J., Scheuer, E., Guo, H., Fibiger, D. L., McDuffie, E. E., Hayes, P. L., Weber, R. J., Dibb, J. E., Apel, E. C., Jaeglé, L., Brown, S. S., Thornton, J. A., and Jimenez, J. L.: Sources and

Secondary Production of Organic Aerosols in the Northeastern United States during WINTER, *Journal of Geophysical Research: Atmospheres*, 123, 7771-7796, 10.1029/2018jd028475, 2018.

Schwantes, R. H., Teng, A. P., Nguyen, T. B., Coggon, M. M., Crouse, J. D., St. Clair, J. M., Zhang, X., Schilling, K. A., Seinfeld, J. H., and Wennberg, P. O.: Isoprene NO₃ Oxidation Products from the RO₂ + HO₂ Pathway, *The Journal of Physical Chemistry A*, 119, 10158-10171, 10.1021/acs.jpca.5b06355, 2015.

Schwantes, R. H., Charan, S. M., Bates, K. H., Huang, Y., Nguyen, T. B., Mai, H., Kong, W., Flagan, R. C., and Seinfeld, J. H.: Low-volatility compounds contribute significantly to isoprene secondary organic aerosol (SOA) under high-NO_x conditions, *Atmos. Chem. Phys.*, 19, 7255-7278, 10.5194/acp-19-7255-2019, 2019.

Seinfeld, J. H., and Pandis, S. N.: *Atmospheric chemistry and physics : from air pollution to climate change*, 3rd ed., Hoboken, New Jersey : John Wiley & Sons, Incorporated, 2016.

Setyan, A., Zhang, Q., Merkel, M., Knighton, W. B., Sun, Y., Song, C., Shilling, J. E., Onasch, T. B., Herndon, S. C., Worsnop, D. R., Fast, J. D., Zaveri, R. A., Berg, L. K., Wiedensohler, A., Flowers, B. A., Dubey, M. K., and Subramanian, R.: Characterization of submicron particles influenced by mixed biogenic and anthropogenic emissions using high-resolution aerosol mass spectrometry: results from CARES, *Atmos. Chem. Phys.*, 12, 8131-8156, 10.5194/acp-12-8131-2012, 2012.

Shiraiwa, M., Li, Y., Tsimpidi, A. P., Karydis, V. A., Berkemeier, T., Pandis, S. N., Lelieveld, J., Koop, T., and Poschl, U.: Global distribution of particle phase state in atmospheric secondary organic aerosols, *Nature Communications*, 8, 7, 10.1038/ncomms15002, 2017.

Shrivastava, M., Cappa, C. D., Fan, J. W., Goldstein, A. H., Guenther, A. B., Jimenez, J. L., Kuang, C., Laskin, A., Martin, S. T., Ng, N. L., Petaja, T., Pierce, J. R., Rasch, P. J., Roldin, P., Seinfeld, J. H., Shilling, J., Smith, J. N., Thornton, J. A., Volkamer, R., Wang, J., Worsnop, D. R., Zaveri, R. A., Zelenyuk, A., and Zhang, Q.: Recent advances in understanding secondary organic aerosol: Implications for global climate forcing, *Reviews of Geophysics*, 55, 509-559, 10.1002/2016rg000540, 2017.

Sorooshian, A., Ng, N. L., Chan, A. W. H., Feingold, G., Flagan, R. C., and Seinfeld, J. H.: Particulate organic acids and overall water-soluble aerosol composition measurements from the 2006 Gulf of Mexico Atmospheric Composition and Climate Study (GoMACCS), *Journal of Geophysical Research: Atmospheres*, 112, n/a-n/a, 10.1029/2007JD008537, 2007.

Sorooshian, A., Murphy, S. M., Hersey, S., Bahreini, R., Jonsson, H., Flagan, R. C., and Seinfeld, J. H.: Constraining the contribution of organic acids and AMS m/z 44 to the organic aerosol budget: On the importance of meteorology, aerosol hygroscopicity, and region, *Geophysical Research Letters*, 37, 10.1029/2010gl044951, 2010.

Sorooshian, A., Crosbie, E., Maudlin, L. C., Youn, J.-S., Wang, Z., Shingler, T., Ortega, A. M., Hersey, S., and Woods, R. K.: Surface and Airborne Measurements of Organosulfur and Methanesulfonate Over the Western United States and Coastal Areas, *Journal of geophysical research. Atmospheres : JGR*, 120, 8535-8548, 10.1002/2015JD023822, 2015.

Stark, H., Yatavelli, R. L. N., Thompson, S. L., Kang, H., Krechmer, J. E., Kimmel, J. R., Palm, B. B., Hu, W. W., Hayes, P. L., Day, D. A., Campuzano-Jost, P., Canagaratna, M. R., Jayne, J. T., Worsnop, D. R., and Jimenez, J. L.: Impact of Thermal Decomposition on Thermal Desorption Instruments: Advantage of Thermogram Analysis for Quantifying Volatility Distributions of Organic Species, *Environmental Science & Technology*, 51, 8491-8500, 10.1021/acs.est.7b00160, 2017.

Staudt, S., Kundu, S., Lehmler, H.-J., He, X., Cui, T., Lin, Y.-H., Kristensen, K., Glasius, M., Zhang, X., Weber, R. J., Surratt, J. D., and Stone, E. A.: Aromatic organosulfates in atmospheric aerosols: Synthesis, characterization, and abundance, *Atmospheric Environment*, 94, 366-373, <http://dx.doi.org/10.1016/j.atmosenv.2014.05.049>, 2014.

Stavrakou, T., Müller, J. F., Peeters, J., Razavi, A., Clarisse, L., Clerbaux, C., Coheur, P. F., Hurtmans, D., De Mazière, M., Vigouroux, C., Deutscher, N. M., Griffith, D. W. T., Jones, N., and Paton-Walsh, C.: Satellite evidence for a large source of formic acid from boreal and tropical forests, *Nature Geoscience*, 5, 26, 10.1038/ngeo1354

<https://www.nature.com/articles/ngeo1354#supplementary-information>, 2011.

Stefenelli, G., Pospisilova, V., Lopez-Hilfiker, F. D., Daellenbach, K. R., Hüglin, C., Tong, Y., Baltensperger, U., Prevot, A. S. H., and Slowik, J. G.: Organic aerosol source apportionment in Zurich using extractive electrospray ionization time-of-flight mass spectrometry (EESI-TOF): Part I, biogenic influences and day/night chemistry in summer, *Atmos. Chem. Phys. Discuss.*, 2019, 1-36, 10.5194/acp-2019-361, 2019.

Stone, E. A., Yang, L., Yu, L. E., and Rupakheti, M.: Characterization of organosulfates in atmospheric aerosols at Four Asian locations, *Atmospheric Environment*, 47, 323-329, <http://dx.doi.org/10.1016/j.atmosenv.2011.10.058>, 2012.

Su, F., Calvert, J. G., and Shaw, J. H.: Mechanism of the photooxidation of gaseous formaldehyde, *The Journal of Physical Chemistry*, 83, 3185-3191, 10.1021/j100488a001, 1979.

Sullivan, R. C., and Prather, K. A.: Investigations of the Diurnal Cycle and Mixing State of Oxalic Acid in Individual Particles in Asian Aerosol Outflow, *Environmental Science & Technology*, 41, 8062-8069, 10.1021/es071134g, 2007.

Surratt, J. D., Kroll, J. H., Kleindienst, T. E., Edney, E. O., Claeys, M., Sorooshian, A., Ng, N. L., Offenberg, J. H., Lewandowski, M., Jaoui, M., Flagan, R. C., and Seinfeld, J. H.: Evidence for Organosulfates in Secondary Organic Aerosol, *Environmental Science & Technology*, 41, 517-527, 10.1021/es062081q, 2007a.

Surratt, J. D., Lewandowski, M., Offenberg, J. H., Jaoui, M., Kleindienst, T. E., Edney, E. O., and Seinfeld, J. H.: Effect of Acidity on Secondary Organic Aerosol Formation from Isoprene, *Environmental Science & Technology*, 41, 5363-5369, 10.1021/es0704176, 2007b.

Surratt, J. D., Gómez-González, Y., Chan, A. W. H., Vermeylen, R., Shahgholi, M., Kleindienst, T. E., Edney, E. O., Offenberg, J. H., Lewandowski, M., Jaoui, M., Maenhaut, W., Claeys, M., Flagan, R. C., and Seinfeld, J. H.: Organosulfate Formation in Biogenic Secondary Organic Aerosol, *The Journal of Physical Chemistry A*, 112, 8345-8378, 10.1021/jp802310p, 2008.

Surratt, J. D., Chan, A. W., Eddingsaas, N. C., Chan, M., Loza, C. L., Kwan, A. J., Hersey, S. P., Flagan, R. C., Wennberg, P. O., and Seinfeld, J. H.: Reactive intermediates revealed in secondary organic aerosol formation from isoprene, *Proceedings of the National Academy of Sciences*, 107, 6640-6645, 2010.

Szmigielski, R., Surratt, J. D., Gómez-González, Y., Van der Veken, P., Kourchev, I., Vermeylen, R., Blockhuys, F., Jaoui, M., Kleindienst, T. E., Lewandowski, M., Offenberg, J. H., Edney, E. O., Seinfeld, J. H., Maenhaut, W., and Claeys, M.: 3-methyl-1,2,3-butanetricarboxylic acid: An atmospheric tracer for terpene secondary organic aerosol, *Geophysical Research Letters*, 34, 10.1029/2007gl031338, 2007.

Takahama, S., Liu, S., and Russell, L. M.: Coatings and clusters of carboxylic acids in carbon-containing atmospheric particles from spectromicroscopy and their implications for cloud-nucleating and optical properties, *Journal of Geophysical Research: Atmospheres*, 115, 10.1029/2009jd012622, 2010.

Takegawa, N., Miyakawa, T., Kawamura, K., and Kondo, Y.: Contribution of Selected Dicarboxylic and ω -Oxocarboxylic Acids in Ambient Aerosol to the m/z 44 Signal of an Aerodyne Aerosol Mass Spectrometer, *Aerosol Science and Technology*, 41, 418-437, 10.1080/02786820701203215, 2007.

Takeuchi, M., and Ng, N. L.: Chemical composition and hydrolysis of organic nitrate aerosol formed from hydroxyl and nitrate radical oxidation of α -pinene and β -pinene, *Atmos. Chem. Phys.*, 19, 12749-12766, 10.5194/acp-19-12749-2019, 2019.

Talbot, R. W., Beecher, K. M., Harriss, R. C., and Cofer, W. R.: Atmospheric geochemistry of formic and acetic acids at a mid-latitude temperate site, *Journal of Geophysical Research: Atmospheres*, 93, 1638-1652, doi:10.1029/JD093iD02p01638, 1988.

Talbot, R. W., Mosher, B. W., Heikes, B. G., Jacob, D. J., Munger, J. W., Daube, B. C., Keene, W. C., Maben, J. R., and Artz, R. S.: Carboxylic acids in the rural continental atmosphere over the eastern United States during the Shenandoah Cloud and Photochemistry Experiment, *Journal of Geophysical Research: Atmospheres*, 100, 9335-9343, doi:10.1029/95JD00507, 1995.

Tan, Y., Lim, Y. B., Altieri, K. E., Seitzinger, S. P., and Turpin, B. J.: Mechanisms leading to oligomers and SOA through aqueous photooxidation: insights from OH radical

oxidation of acetic acid and methylglyoxal, *Atmospheric Chemistry and Physics*, 12, 801-813, 10.5194/acp-12-801-2012, 2012.

Tao, S., Lu, X., Levac, N., Bateman, A. P., Nguyen, T. B., Bones, D. L., Nizkorodov, S. A., Laskin, J., Laskin, A., and Yang, X.: Molecular Characterization of Organosulfates in Organic Aerosols from Shanghai and Los Angeles Urban Areas by Nanospray-Desorption Electrospray Ionization High-Resolution Mass Spectrometry, *Environmental Science & Technology*, 48, 10993-11001, 10.1021/es5024674, 2014.

Tolocka, M. P., and Turpin, B.: Contribution of Organosulfur Compounds to Organic Aerosol Mass, *Environmental Science & Technology*, 46, 7978-7983, 10.1021/es300651v, 2012.

Tuet, W. Y., Chen, Y., Xu, L., Fok, S., Gao, D., Weber, R. J., and Ng, N. L.: Chemical oxidative potential of secondary organic aerosol (SOA) generated from the photooxidation of biogenic and anthropogenic volatile organic compounds, *Atmos. Chem. Phys.*, 17, 839-853, 10.5194/acp-17-839-2017, 2017.

Ulbrich, I., Canagaratna, M., Zhang, Q., Worsnop, D., and Jimenez, J.: Interpretation of organic components from Positive Matrix Factorization of aerosol mass spectrometric data, *Atmospheric Chemistry and Physics*, 9, 2891-2918, 2009.

Wang, W.-F., Schuchmann, M. N., Schuchmann, H.-P., and von Sonntag, C.: The Importance of Mesomerism in the Termination of α -Carboxymethyl Radicals from Aqueous Malonic and Acetic Acids, *Chemistry – A European Journal*, 7, 791-795, 10.1002/1521-3765(20010216)7:4<791::Aid-chem791>3.0.Co;2-2, 2001.

Weber, R. J., Sullivan, A. P., Peltier, R. E., Russell, A., Yan, B., Zheng, M., de Gouw, J., Warneke, C., Brock, C., Holloway, J. S., Atlas, E. L., and Edgerton, E.: A study of secondary organic aerosol formation in the anthropogenic-influenced southeastern United States, *Journal of Geophysical Research: Atmospheres*, 112, n/a-n/a, 10.1029/2007JD008408, 2007.

Wexler, A. S., and Clegg, S. L.: Atmospheric aerosol models for systems including the ions H^+ , NH_4^+ , Na^+ , SO_4^{2-} , NO_3^- , Cl^- , Br^- , and H_2O , *Journal of Geophysical Research-Atmospheres*, 107, 14, 10.1029/2001jd000451, 2002.

Willis, M. D., Burkart, J., Thomas, J. L., Kollner, F., Schneider, J., Bozem, H., Hoor, P. M., Aliabadi, A. A., Schulz, H., Herber, A. B., Leaitch, W. R., and Abbatt, J. P. D.: Growth of nucleation mode particles in the summertime Arctic: a case study, *Atmospheric Chemistry and Physics*, 16, 7663-7679, 10.5194/acp-16-7663-2016, 2016.

Xia, S.-S., Eugene, A. J., and Guzman, M. I.: Cross Photoreaction of Glyoxylic and Pyruvic Acids in Model Aqueous Aerosol, *The Journal of Physical Chemistry A*, 122, 6457-6466, 10.1021/acs.jpca.8b05724, 2018.

Xu, L., Kollman, M. S., Song, C., Shilling, J. E., and Ng, N. L.: Effects of NO_x on the Volatility of Secondary Organic Aerosol from Isoprene Photooxidation, *Environmental Science & Technology*, 48, 2253-2262, 10.1021/es404842g, 2014.

Xu, L., Guo, H., Boyd, C. M., Klein, M., Bougiatioti, A., Cerully, K. M., Hite, J. R., Isaacman-VanWertz, G., Kreisberg, N. M., Knote, C., Olson, K., Koss, A., Goldstein, A. H., Hering, S. V., de Gouw, J., Baumann, K., Lee, S. H., Nenes, A., Weber, R. J., and Ng, N. L.: Effects of anthropogenic emissions on aerosol formation from isoprene and monoterpenes in the southeastern United States, *Proceedings of the National Academy of Sciences*, 112, 37-42, 10.1073/pnas.1417609112, 2015a.

Xu, L., Suresh, S., Guo, H., Weber, R. J., and Ng, N. L.: Aerosol characterization over the southeastern United States using high-resolution aerosol mass spectrometry: spatial and seasonal variation of aerosol composition and sources with a focus on organic nitrates, *Atmos. Chem. Phys.*, 15, 7307-7336, 10.5194/acp-15-7307-2015, 2015b.

Xu, L., Pye, H. O. T., He, J., Chen, Y. L., Murphy, B. N., and Ng, N. L.: Experimental and model estimates of the contributions from biogenic monoterpenes and sesquiterpenes to secondary organic aerosol in the southeastern United States, *Atmospheric Chemistry and Physics*, 18, 12613-12637, 10.5194/acp-18-12613-2018, 2018a.

Xu, W., Croteau, P., Williams, L., Canagaratna, M., Onasch, T., Cross, E., Zhang, X., Robinson, W., Worsnop, D., and Jayne, J.: Laboratory characterization of an aerosol chemical speciation monitor with PM_{2.5} measurement capability, *Aerosol Science and Technology*, 51, 69-83, 10.1080/02786826.2016.1241859, 2017a.

Xu, W., Han, T., Du, W., Wang, Q., Chen, C., Zhao, J., Zhang, Y., Li, J., Fu, P., Wang, Z., Worsnop, D. R., and Sun, Y.: Effects of Aqueous-Phase and Photochemical Processing on Secondary Organic Aerosol Formation and Evolution in Beijing, China, *Environmental Science & Technology*, 51, 762-770, 10.1021/acs.est.6b04498, 2017b.

Xu, W., Lambe, A., Silva, P., Hu, W., Onasch, T., Williams, L., Croteau, P., Zhang, X., Renbaum-Wolff, L., Fortner, E., Jimenez, J. L., Jayne, J., Worsnop, D., and Canagaratna, M.: Laboratory evaluation of species-dependent relative ionization efficiencies in the Aerodyne Aerosol Mass Spectrometer, *Aerosol Science and Technology*, 52, 626-641, 10.1080/02786826.2018.1439570, 2018b.

Yan, C., Nie, W., Äijälä, M., Rissanen, M. P., Canagaratna, M. R., Massoli, P., Junninen, H., Jokinen, T., Sarnela, N., Häme, S. A. K., Schobesberger, S., Canonaco, F., Yao, L., Prévôt, A. S. H., Petäjä, T., Kulmala, M., Sipilä, M., Worsnop, D. R., and Ehn, M.: Source characterization of highly oxidized multifunctional compounds in a boreal forest environment using positive matrix factorization, *Atmos. Chem. Phys.*, 16, 12715-12731, 10.5194/acp-16-12715-2016, 2016.

Yao, X., Fang, M., and Chan, C. K.: Size distributions and formation of dicarboxylic acids in atmospheric particles, *Atmospheric Environment*, 36, 2099-2107, [https://doi.org/10.1016/S1352-2310\(02\)00230-3](https://doi.org/10.1016/S1352-2310(02)00230-3), 2002.

Yatavelli, R. L. N., Stark, H., Thompson, S. L., Kimmel, J. R., Cubison, M. J., Day, D. A., Campuzano-Jost, P., Palm, B. B., Hodzic, A., Thornton, J. A., Jayne, J. T., Worsnop, D. R., and Jimenez, J. L.: Semicontinuous measurements of gas-particle partitioning of organic acids in a ponderosa pine forest using a MOVI-HRToF-CIMS, *Atmos. Chem. Phys.*, 14, 1527-1546, 10.5194/acp-14-1527-2014, 2014.

Yatavelli, R. L. N., Mohr, C., Stark, H., Day, D. A., Thompson, S. L., Lopez-Hilfiker, F. D., Campuzano-Jost, P., Palm, B. B., Vogel, A. L., Hoffmann, T., Heikkinen, L., Äijälä, M., Ng, N. L., Kimmel, J. R., Canagaratna, M. R., Ehn, M., Junninen, H., Cubison, M. J., Petäjä, T., Kulmala, M., Jayne, J. T., Worsnop, D. R., and Jimenez, J. L.: Estimating the contribution of organic acids to northern hemispheric continental organic aerosol, *Geophysical Research Letters*, 42, 6084-6090, doi:10.1002/2015GL064650, 2015.

Yu, J. Z., Huang, X.-F., Xu, J., and Hu, M.: When Aerosol Sulfate Goes Up, So Does Oxalate: Implication for the Formation Mechanisms of Oxalate, *Environmental Science & Technology*, 39, 128-133, 10.1021/es049559f, 2005.

Zhang, H., Yee, L. D., Lee, B. H., Curtis, M. P., Worton, D. R., Isaacman-VanWertz, G., Offenberg, J. H., Lewandowski, M., Kleindienst, T. E., Beaver, M. R., Holder, A. L., Lonneman, W. A., Docherty, K. S., Jaoui, M., Pye, H. O. T., Hu, W., Day, D. A., Campuzano-Jost, P., Jimenez, J. L., Guo, H., Weber, R. J., de Gouw, J., Koss, A. R., Edgerton, E. S., Brune, W., Mohr, C., Lopez-Hilfiker, F. D., Lutz, A., Kreisberg, N. M., Spielman, S. R., Hering, S. V., Wilson, K. R., Thornton, J. A., and Goldstein, A. H.: Monoterpenes are the largest source of summertime organic aerosol in the southeastern United States, *Proceedings of the National Academy of Sciences*, 10.1073/pnas.1717513115, 2018a.

Zhang, Q., Worsnop, D. R., Canagaratna, M. R., and Jimenez, J. L.: Hydrocarbon-like and oxygenated organic aerosols in Pittsburgh: insights into sources and processes of organic aerosols, *Atmospheric Chemistry and Physics*, 5, 3289-3311, 10.5194/acp-5-3289-2005, 2005.

Zhang, Q., Jimenez, J. L., Canagaratna, M. R., Allan, J. D., Coe, H., Ulbrich, I., Alfarra, M. R., Takami, A., Middlebrook, A. M., Sun, Y. L., Dzepina, K., Dunlea, E., Docherty, K., DeCarlo, P. F., Salcedo, D., Onasch, T., Jayne, J. T., Miyoshi, T., Shimono, A., Hatakeyama, S., Takegawa, N., Kondo, Y., Schneider, J., Drewnick, F., Borrmann, S., Weimer, S., Demerjian, K., Williams, P., Bower, K., Bahreini, R., Cottrell, L., Griffin, R. J., Rautiainen, J., Sun, J. Y., Zhang, Y. M., and Worsnop, D. R.: Ubiquity and dominance of oxygenated species in organic aerosols in anthropogenically-influenced Northern Hemisphere midlatitudes, *Geophysical Research Letters*, 34, doi:10.1029/2007GL029979, 2007a.

Zhang, Q., Jimenez, J. L., Worsnop, D. R., and Canagaratna, M.: A Case Study of Urban Particle Acidity and Its Influence on Secondary Organic Aerosol, *Environmental Science & Technology*, 41, 3213-3219, 10.1021/es061812j, 2007b.

Zhang, Q., Jimenez, J. L., Canagaratna, M. R., Ulbrich, I. M., Ng, N. L., Worsnop, D. R., and Sun, Y.: Understanding atmospheric organic aerosols via factor analysis of aerosol mass spectrometry: a review, *Analytical and Bioanalytical Chemistry*, 401, 3045-3067, 2011.

Zhang, X., Chen, Z. M., and Zhao, Y.: Laboratory simulation for the aqueous OH-oxidation of methyl vinyl ketone and methacrolein: significance to the in-cloud SOA production, *Atmospheric Chemistry and Physics*, 10, 9551-9561, 10.5194/acp-10-9551-2010, 2010a.

Zhang, Y., Chen, Y., Lambe, A. T., Olson, N. E., Lei, Z., Craig, R. L., Zhang, Z., Gold, A., Onasch, T. B., Jayne, J. T., Worsnop, D. R., Gaston, C. J., Thornton, J. A., Vizuet, W., Ault, A. P., and Surratt, J. D.: Effect of the Aerosol-Phase State on Secondary Organic Aerosol Formation from the Reactive Uptake of Isoprene-Derived Epoxydiols (IEPOX), *Environmental Science & Technology Letters*, 5, 167-174, 10.1021/acs.estlett.8b00044, 2018b.

Zhang, Y. Y., Müller, L., Winterhalter, R., Moortgat, G. K., Hoffmann, T., and Pöschl, U.: Seasonal cycle and temperature dependence of pinene oxidation products, dicarboxylic acids and nitrophenols in fine and coarse air particulate matter, *Atmos. Chem. Phys.*, 10, 7859-7873, 10.5194/acp-10-7859-2010, 2010b.

Zhao, R., Mungall, E. L., Lee, A. K. Y., Aljawhary, D., and Abbatt, J. P. D.: Aqueous-phase photooxidation of levoglucosan – a mechanistic study using aerosol time-of-flight chemical ionization mass spectrometry (Aerosol ToF-CIMS), *Atmos. Chem. Phys.*, 14, 9695-9706, 10.5194/acp-14-9695-2014, 2014.

Zorn, S. R., Drewnick, F., Schott, M., Hoffmann, T., and Borrmann, S.: Characterization of the South Atlantic marine boundary layer aerosol using an aerodyne aerosol mass spectrometer, *Atmos. Chem. Phys.*, 8, 4711-4728, 10.5194/acp-8-4711-2008, 2008.